HYDRODECHLORINATION OF CHLORINATED ORGANIC WASTES OVER PD SUPPORTED MIXED OXIDE CATALYSTS

Beteley Tekola Meshesha

Dipòsit Legal: T-207-2011

Doctoral thesis

Beteley Tekola Meshesha

Hydrodechlorination of chlorinated organic wastes over Pd supported mixed oxide catalysts

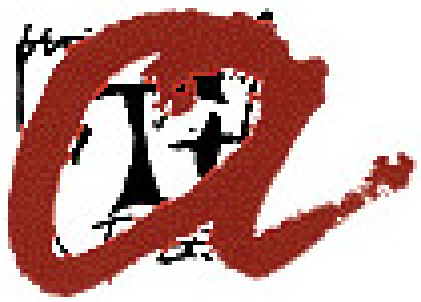

Universitat Rovira i Virgili

Universitat Rovira i Virgili

Departament d'Enginyería Química
Escola Técnica Superior d'Enginyería Química

Hydrodechlorination of chlorinated organic wastes over Pd supported mixed oxide catalysts

Presented by
Beteley Tekola Meshesha

To acquire the grade for
the European degree of Doctor
from
Universitat Rovira I Virgili

Supervised by
Dr. Francisco Medina
and co-supervised by
Dr. Jesús E. Sueiras and Dr. Ricardo J. Chimenton

Prof. Francesc Medina Cabello,

Prof. Jesús E. Sueiras

Dr. Ricardo J. Chimenton

Professors and researchers of the department of Chemical Engineering at the Universitat Rovira i Virgili, **certify t**hat the doctoral thesis entitled "Hydrodechlorination of chlorinated organic wastes over Pd supported mixed oxide catalysts" by Beteley Tekola Meshesha for the award of the European degree doctor has been carried out under our supervision in the Department of Chemical Engineering, Universitat Rovira i Virgili.

Tarragona, Spain, April 2011

Supervisor

F. Medina

Co-Supervisor

Jesús.E.Sueiras

Ricardo .J. Chimenton

THESIS TRIBUNAL

Prof. Bernard Coq

Institut Charles Gerhardt Montpellier UMR 5253 CNRS/ENSCM/UM2/UM1, 8, rue de l'Ecole Normale, 34296 Montpellier cedex 5, France

Prof. Francisco López Bonilla

Departament Enginyería Química, Universidad Rovira i Virgili, Spain

Dr. Jordi Llorca

Institut de Tècniques Energètiques, Universitat Politècnica de Catalunya, Barcelona, Spain

Dr. Karin Föttinger

Institute of Materials Chemistry, Vienna University of Technology, Vienna, Austria

Dr. Anton Dafinov

Department Enginyería Química, Universidad Rovira i Virgili, Tarragona, Spain

RESERVE

Dr. Sònia Abelló

L'Institut de Recerca en Energia de Catalunya, Bioenergy and Biofuels, Tarragona, Spain

Dr. Sandra Contreras

Department Enginyería Química, Universidad Rovira i Virgili, Spain

EXTERNAL REFEREES

Dr. Didier Tichet

Laboratoire de Materiaux Catalytiques et Catalysi en Chimie Organique, CNRS Montpelier (Francia)

Dr. Noelia Barrabés

Vienna University of Technology, Vienna, Austria

Acknowledgement

I am heartily thankful to my supervisor, Professor Francisco Medina, whose encouragement, guidance and support from the initial to the final level enabled me to develop an understanding. I would like to extend my gratitude to Professor Jesus E. Sueiras. I am grateful to my co-advisor, Dr. Ricardo J. Chimenton, whom I started to work with and received an endless help and support. Throughout my thesis-writing period, they provided encouragement, sound advice, good company, and lots of good ideas.

I would like to thank Professor G. Rupprechter and Dr. Karin Föttinger for making possible my research stay in the institute of material chemistry, Technical university of Vienna. Especial thank goes to Dr. Noelia Barrabes for her ideas and concepts that have had a remarkable influence on our joint research.

I am also indebted to many of my colleagues. I will never forget the good times, coffee breaks, conferences especially with Noe, Anton, Abel, Vero, Mayra, Sandra R., Biniam, and Kike which are my invaluable memories. Special thank goes to all my Ethiopian colleagues especially to Berhane, Nigus, Ashu, Belay, Asfaw, Fiteha, Messi and all the others. I also wish to express my special thank for Vienna's group, Karin, Katy, Christians, Andy, Andreas and Nikki. The time I spent together initiated and nurtured my maturity both as a researcher and person. Thank you for priceless experiences. My appreciation will also go to Urko and all my fortuny friends for the good times we have passed together. My humble gratitude also goes to my group mates Anna, Sandra C., Iuliana, Kaveh, Adriana and Alex for the time we had together in laboratories.

I would like to thank also Universitat Rovira I Virgili, Spanish ministry of education and AMIC for financial and material support throughout the thesis.

Finally I would like to offer my gratitude with respect to my father whose ideals and dedication in life has nourished my success in all the way. I also wish to thank my entire family for providing a loving and supportive environment.

Table of contents

Figure caption

1. *General introduction*

Fig. 1. Structure of some chlorinated organic compounds.

Fig. 2. Structure of some of toxic species produces after incineration of COCs.

Fig. 3. Schematic representation for HDC of 1,2,4-trichlorobenzene

Fig. 4. Idealized structure of a $Mg(OH)_2$ brucite structure.

Fig. 5. Structure of a layered double hydroxide with interlayer water and carbonate anions.

Fig. 6. Possible reaction pathway for hydrodechlorination of TCE.

2. *Aim and objectives*

3. *Experimental*

Fig. 1. The different radiation emitted during excitation of a solid surface.

Fig. 2. The five types of van der Waals adsorption isotherms.

Fig. 3. Typical hydrogen chemisorption at 373 K temperature on a Pd/HT catalyst containing 1 wt% palladium.

Fig. 4. 1,2,4-trichlorobenzene hydrodechlorination experimental setup.

Fig. 5. TCE Hydrodechlorination experimental setup.

4. *Results and Discussion*

4.1.Catalytic HDC of 1,2,4-trichlorobenzene over Pd/Mg(Al)Ox catalyst

Fig. 1. X-ray diffraction of the calcined hydrotalcite materials. (a) Different HT supports, (b) Pd-HT catalysts.

Fig. 2. TEM image of a representative sample: (a) Support material (HT-21), (b) Pd-HT-21 (c) Pd-HT-31 (d) Pd-HT-41 samples and (e, f) spent Pd-HT-21 catalyst (T of reaction 473 K).

Fig. 3. Energy-dispersive spectroscopy (EDS) analysis on the surface of the spent and fresh Pd-HT-21 catalyst.

Fig. 4. H_2-temperature-programmed reduction profile of the palladium catalysts. (a) Pd-HT-41, (b) Pd-HT-31 and (c) Pd-HT-21.

Fig. 5. TPO-MS profiles of the spent sample Pd-HT-21 showing: (a) Species evolved during the He-TPD and (b) Sequential analysis of TPO.

Fig. 6. Temperature programmed oxidation (TPO) of the spent Pd hydrotalcite catalysts. (a) Pd-HT-41, (b) Pd-HT-31 and (c) Pd-HT-21.

Fig. 7. Thermogravimetric analysis of the spent Pd-HT catalysts. (a), (b), (c), (d). Inset: Carbon content in the spent samples versus Mg/Al molar ratios.

Fig. 8. CO_2-TPD profiles of the Pd-HT-41 and Pd-HTR-41 samples.

Fig. 9. Selectivity of catalysts at 50% conversion versus Mg/Al molar ratio in the Mg(Al)O support. The reaction temperature was 433K

Fig.10. Conversion versus time of stream of the Pd hydrotalcite catalysts with a space velocity of 10 $ml.min^{-1}.g^{-1}$ at 473 K. (a) Pd-HT-41, (b) Pd-HT-31 and (c) Pd-HT-21.

Fig.11. Comparison in the catalytic performance between Pd-HT-41 and Pd-HTR-41 catalysts versus time of reaction using a space velocity of 40 $ml.min^{-1}.g^{-1}$.

4.2. Performance of alkali modified Pd/MgAlO catalysts for HDC of 1,2,4-trichlorobenzene

Fig. 1. SEM image of HT(a), Pd/HT(b) and representative of modified catalysts Pd/HT($NaNO_3$) (c) and, Pd/HT(NaOH) (d).

Fig. 2. XRD diffraction of freshly prepared catalysts a) Pd/HT(AOH), b) Pd/HT(ANO_3), Inset: Pd/HT($CsNO_3$) calcined at 723 K and 873 K respectively.

Fig. 3. TEM and HRTEM images of freshly prepared alkali hydroxide modified catalysts (a & d)-Pd/HT(NaOH), (b & c)-Pd/HT(LiOH), (e)-Pd/HT(CsOH) and (f)-Pd/HT($CsNO_3$).

Fig. 4. CO_2-Temperature programmed desorption profiles for Pd/HT, Pd/HT(AOH) and, Pd/HT(ANO_3) catalysts.

Fig. 5. Comparative HDC conversion through time of reaction at 373K of Pd/HT(AOH) (a), Pd/HT(ANO_3) (b) with the unmodified catalyst Pd/HT. (■) Pd/HT, (□) Li, (○) Na and (Δ) Cs.

Fig. 6. Comparative HDC study of Pd/HT(LiOH) (a) Pd/HT(CsOH) (b) catalysts prepared with different amount of basic additives at 373K.

Fig. 7. TCB reaction rate expressed by TCB consumed ($mmol.min^{-1}$) per exposed Pd surface (m^2/g) (a) vs. different alkaline metals and precursors (b) vs. number of basic sites in terms of μmol of CO_2/m^2 of the catalyst (c) vs. number of basic sites in terms of mmol of CO_2/g of the catalyst.

Fig. 8. Selectivity to benzene for Pd/HT, Pd/HT(AOH) and Pd/HT(ANO_3) catalysts Vs Pd dispersion (H/Pd) as obtained by H_2 chemisorption.

Fig. 9. TCB conversion (%) vs time on stream for fresh and regenerated Pd/HT($NaNO_3$) catalysts.

Fig. 10. ESEM image of used Pd/HT coupled with EDX spectra.

Fig.11. HRTEM images of (a & b) used Pd/HT catalyst (c) used Pd/HT($NaNO_3$) catalyst.

Fig.12. EDX spectra for used and reductively regenerated Pd/HT($NaNO_3$) catalyst.

4.3. *Catalytic HDC of 1,2,4-trichlorobenzene over Pd/Mg(Al)O catalysts: Effect of the calcination temperature of the support*

Fig. 1. Isotherm plots obtained from the N_2 physisorption analysis at 77K.

Fig. 2. X-ray diffraction patterns for hydrotalcite calcined at different temperatures, Spinel and MgO materials.

Fig. 3. SEM profiles of the mixed oxides calcined at different temperatures, Spinel and MgO.

Fig. 4. TPD-CO_2 profile for the prepared catalysts.

Fig. 5. Catalytic behavior of the prepared catalysts at 373 K.

4.4. *Gas-phase hydrodechlorination of trichloroethylene over Pd/NiMgAl catalyst*

Fig. 1. X-ray diffraction patterns for the different Pd/NiHT catalysts.

Fig. 2. HRTEM images of Pd/NiHT catalysts; a) TEM-Pd/NiHT3 b) Pd/NiHT1 c) Pd/NiHT2 d) Pd/NiHT3.

Fig. 3. TPR profiles for NiHT and Pd/NiHT catalysts.

Fig. 4. CO-FTIR profile for Pd/NiHT1 catalysts.

Fig. 5. UV-Vis diffuse reflectance spectroscopy of NiO and NiHT mixed oxide (a) and Ni and NiHT reduced (b).

Fig. 6. (a) Catalytic activity of Pd/NiHT catalysts (with different NiMgAl molar ratios reduced at 623K), (b) product distribution at end of reaction (c) selectivity at lower conversion level.

Fig.7. Effect of reduction temperature on the catalytic behavior of NiHT1 catalysts (a) conversion, (b) product distribution at steady state.

Fig.8. Effect of reduction temperature on the catalytic behaviour of Pd/NiHT1 catalysts reduced at 623 K and 723 K and product distribution.

Fig.9. X-ray diffraction patterns for the different rNiHT1-823 and Pd(*x*)/rNiHT1 catalysts where *x* represents Pd wt %.

Fig. 10. Low and high magnification of HRTEM images for Pd/rNiHT1 catalysts.

Fig. 11. Catalytic conversion Vs time of reaction for Pd/rNiHT1 and Pd/NiHT1-723 catalysts (a), product distribution at beginning o reaction (b), and product distribution at the end(c).

Fig. 12. Mechanism of ethylene conversion over Pd-Ni surfaces (dashed arrow represent less favoured pathway).

Fig. 13. Comparison of catalytic activities at the beginning of the reaction.

4.5. *Nanoparticle synthesis and application in HDC of trichloroethylene*

Fig. 1. Preparation of metal nanoparticles in homogeneous solution by chemical method.

Fig. 2. Different configurations of nanoparticles.

Fig. 3. XRD profile of copper nanoparticles synthesized using HDA and PVP (Stabilizer/Cu molar ratio of 3).

Fig. 4. UV-Vis spectra of HDA capped copper nanoparticles (HDA/Cu=3).

Fig. 5. FTIR spectra of HDA capped copper with HDA/Cu molar ratio 3.

Fig.6. Proton NMR spectra of HDA capped copper (Inset-pure HDA molecule with free NH_2 groups).

Fig. 7. TEM images of the alkylamine capped copper nanoparticles. The particle size distributions are shown in the form of histograms alongside the TEM images. (a) PVP/Cu molar ratio of 3. (b) HDA/Cu molar ratio of 3. (c) HDA/Cu molar ratio of 2.

Fig. 8a. TEM pictures of HDA stabilized palladium (a,b,c) and gold (d,e) nanoparticles, (HDA/Metal molar ratio of 3.

Fig. 8b. TEM pictures of HDA stabilized palladium Pd1Au1 (a and b), Pd5Au1(c and d) nanoparticles, (HDA/Metal molar ratio of 3.

Fig. 9. XRD profiles of γ-alumina supported Pd and PdCu nanoparticles (a) complete diffractogram (b) magnified (25-60^o), ■ PdO, ○-metallic Pd.

Fig. 10. H_2-TPR profiles for monometallic Pd and bimetallic $PdCu/Al_2O_3$ catalysts.

Fig. 11. TEM pictures of Pd/Al_2O_3 catalysts.

Fig. 12. HRTEM profile for $Pd1.6Cu1/Al_2O_3$ (a-d) and $Pd1Cu/Al_2O_3$ (e-h)samples.

Fig. 13. HDC activity of monometallic Pd and PdCu monometallic catalysts against time on stream.

Fig. 14. HDC activity of monometallic Pd and PdCu catalysts and product distribution (a) at initial catalytic activity (b) at 180 min of reaction.

Resumn

La contaminación ambiental mediante compuestos policlorados aromáticos y alifáticos es de gran preocupación. Este tipo de compuestos están presentes en todo el mundo debido a su diversidad de uso. No obstante, a pesar de dicha amplia aplicación, este tipo de productos son clasificados como productos químicos cancerígenos y mutagénicos que se someten a la bioacumulación en los tejidos grasos, presentando por ello graves problemas en la salud de los seres vivos. Debido a sus propiedades químicas y su utilización, estos compuestos pueden estar presentes en el agua, en el suelo y en el aire, principalmente de las instalaciones domésticas o industriales. Es por ello que se necesitan tecnologías que permitan la eliminación de este tipo de compuestos. Entre las tecnologías convencionales cabe destacar las relacionadas con la incineración, la pirólisis, el tratamiento biológico y la oxidación catalítica. No obstante todas ellas presentan una serie de inconvenientes asociados a altas emisiones de compuestos tóxicos como las dioxinas, o una baja tasa de eliminación, o un elevado coste energético. Es por todo ello que se necesitan nuevas tecnologías emergentes que permitan el tratamiento de este tipo de contaminantes.

En este sentido, la reacción de hidrodecloración catalítica selectiva (HDC) se presenta como una nueva tecnología eficaz para una eliminación segura de estos tipos de compuestos orgánicos clorados. La tecnología HDC está basada en la hidrogenación selectiva de los enlaces C-Cl, substituyendo el Cl por hidrógeno y obteniéndose de esta forma ácido clorhídrico y el compuesto orgánico declorado que puede ser aprovechado para otros fines.

Es por ello, que este trabajo de investigación se ha enfocado en el estudio de nuevos catalizadores activos, selectivos y estables en diferentes reacciones de hidrodecloración de dos familias de compuestos orgánicos clorados: 1,2,4-triclorobenceno (1,2,4-TCB-compuestos aromáticos clorados) y el tricloroetileno (representativo de un compuesto clorado alifático). La primera parte de la tesis relacionadas con el HDC de 1,2,4-TCB, tiene como objetivo la obtención de catalizadores activos y estables para la hidrogenación del enlace C-Cl en compuestos aromáticos y la obtención final del compuesto aromático orgánico declorado. Mientras que la segunda parte

tiene por objeto la obtención de catalizadores que permitan una gran selectividad a etileno y no hacia etano (hidrogenación profunda del tricloroetileno) durante la HDC de tricloroetileno. Por otra parte se ha realizado un estudio profundo en la síntesis de estos nuevos catalizadores, así como en la caracterización de los centros activos de dichos catalizadores, para su correlación con la actividad, selectividad y estabilidad de dichos catalizadores.

Como es bien conocido, en la reacción de HDC de compuestos cloroaromáticos la reacción de hidrogenación se produce a través de un ataque electrofílico del enlace C-Cl. Por ello, hemos estudiado diferentes materiales catalíticos que presentan una diferente basicidad combinando tanto el efecto de hidrogenación del metal (metal noble) como el efecto básico del soporte. Para ello se han preparado diferentes catalizadores a base de hidrotalcitas en las que se ha modificado sus propiedades básicas, variando la relación Mg/Al, así como sus protocolos de preparación. En dichas hidrotalcitas se ha incorporado como metal activo el Pd en un 1% en peso. Estos catalizadores fueron preparados, caracterizados y estudiados en la reacción hidrodecloración de 1,2,4-TCB. Los catalizadores frescos fueron caracterizados mediante ICP-OES, DRX, N_2-fisisorción, quimisorción de H2, TPR y TEM. Se ha observado que la actividad, la estabilidad y la selectividad de los catalizadores en la reacción de hidrodecloración de 1,2,4-triclorobenceno depende mucho de la relación Mg/Al en la hidrotalcita (soporte). Se ha demostrado que un catalizador de paladio soportado en hidrotalcitas calcinadas con elevada relación molar Mg/Al mostraron una conversión total de 1,2,4-TCB hacia benceno a 473K. La muestra con Mg/Al de 4 exhibió la más alta estabilidad y selectividad hacia la reacción de hidrodecloración teniendo una selectividad del 100% hacia benceno. La actividad catalítica y la selectividad siguen la siguiente tendencia Pd/HT41 > Pd/HT31 > Pd/HT21. Por otra parte, se estudió el proceso de rehidratación de los catalizadores de hidrotalcita calcinada conteniendo Pd (Pd/HT41), resultando en una mejora del rendimiento de la reacción de hidrodecloración. La rehidratación se relacionó con la generación de grupos básicos del tipo hidroxilo, centros básicos de Brønsted, lo que modificó el comportamiento catalítico de los catalizadores no rehidratados que contienen centros básicos del tipo Lewis. Los catalizadores usados se caracterizaron por TPO-MS, TGA y técnicas ESEM-EDS. El análisis de los catalizadores usados operados

a 473 K reveló que la desactivación se debe principalmente a la deposición de coque en la superficie y no del producto HCl. La estabilidad de los catalizadores dependen en gran medida la relación molar Mg/Al. Además la activación de la muestra Pd/Mg(Al)O (relación Mg/Al de 4) con rehidratación, mejora tanto la actividad catalítica como la estabilidad. Finalmente, estos resultados indican que los precursores catalíticos del tipo hidrotalcita y derivados son excelentes catalizadores en la reacción de hidrodecloración de 1,2,4-TCB.

Otra forma de inducir basicidad en el catalizador es mediante la promoción de la superficie del catalizador utilizando aditivos básicos, como los óxidos de metales alcalinos. Con este punto de vista, la mejor realización de catalizador de Pd/HT con una proporción Mg/Al de 4 se modificó de nuevo mediante la adición de diferentes metales alcalinos. Estos nuevos catalizadores fueron estudiados en la reacción de HDC de 1,2,4-TCB. La adición de alcalino se realizó con dos precursores de sales diferentes provenientes de nitratos e hidróxidos (ANO_3 y AOH). La presencia de estos precursores de metales alcalinos produjo una fuerte modificación en diferentes características físico-químicas de los catalizadores. No obstante, en general, los catalizadores modificados mostraron una mayor actividad, estabilidad y selectividad que el catalizador de Pd/HT sin la adición del metal alcalino. También se observó una fuerte influencia del tipo de precursor de la sal alcalina obtenida (nitrato o hidróxido). También se observó que entre los diferentes metales alcalinos utilizados (Li, Na, K y Cs), al aumentar las propiedades básicas intrínsecas del alcalino aumentó la actividad de los catalizadores. Los principales productos obtenidos fueron o-diclorobenceno y benceno. Se realizó una exhaustiva caracterización, tanto de los catalizadores frescos como usados mediante un gran número de técnicas entre ellas XPS, EDX y HRTEM, mostrando también el papel que juega la incorporación de especies cloruro en la superficie del catalizador usado. Se estudiaron también diferentes protocolos de regeneración de los catalizadores usados, mediante tratamientos de calcinación-reducción. La actividad catalítica inicial se recuperó cuando la muestra utilizada fue regenerado por un tratamiento directo de reducción. La regeneración de los catalizadores mediante estos protocolos recupera los centros activos del catalizador, removiendo las especies cloradas de la superficie del Pd.

También se estudió el efecto de la calcinación de la estructura hidrotalcitas sobre la actividad catalítica de los catalizadores. Con este punto de vista, se estudiaron varios catalizadores de Pd soportado Mg/Al óxido mixto (HT31), donde fue calcinado el soporte a 623K, 723K, 923k y 1123K. Los catalizadores obtenidos se caracterizaron y fueron probados en la reacción HDC de 1,2,4-triclorobenceno. Observaciones interesantes se han obtenido en este estudio. La segregación de fases obtenidas durante el proceso de calcinación de la hidrotalcitas permite modular y obtener catalizadores altamente activos y estables en este tipo de reacciones.

La segunda parte de la tesis, trata sobre la hidrodecloración de TCE. Aunque los catalizadores a base de metal noble presentan una buena actividad y estabilidad catalítica durante la reacción de HDC de TCE en condiciones suaves, el producto más importante obtenido es etano, que es un producto mucho menos deseado que el etileno. Para inducir una mejor selectividad hacia etileno en vez de etano, se ha estudiado la incorporación de un segundo metal no noble en los catalizadores. El metal elegido ha sido el níquel y para ello se han preparado diferentes hidrotalcitas de níquel en las que posteriormente a su proceso de calcinación se ha incorporado Pd. La promoción de los catalizadores de Ni con pequeñas cantidades de metales nobles como el paladio, aumenta su actividad catalítica para la reacción de HDC. Con este punto de vista, diferentes catalizadores a base de Pd/NiMgAl han sido preparados y estudiados en la reacción de hidrodecloración de TCE en fase gas. Los catalizadores fueron activados con diferentes temperaturas de reducción del catalizador. Nuestro trabajo demuestra que los catalizadores de NiMg(Al)O que incorporan paladio, son eficaces para la hidrodecloración en fase gaseosa del tricloroetileno. El rendimiento de los catalizadores para la hidrodecloración se ve afectada significativamente por la composición química del catalizador (relación molar entre Ni/Mg/Al), la temperatura de reducción y el método o protocolo de deposición del Pd en el catalizador final. Un ajuste fino entre las cantidades de Ni y Mg, así como la deposición de Pd, permiten obtener catalizadores altamente activos y totalmente selectivos hacia la obtención de etileno.

Otro tipo de catalizadores obtenidos han consistido en la obtención de nanopartículas de cobre con diferentes morfologías y posterior introducción de Pd en dichas nanopartículas. El objetivos es estudiar el efecto de dicha

morfología, así como la interacción del Pd con dichas nanopartículas de cobre en diferentes reacciones. En esta tesis se presenta un nuevo protocolo de síntesis de dichas nanopartículas. Para ello, se utiliza el proceso polyol al que se incorpora diferentes tipos de aminas y polivinilpirrolidona, permitiendo de esta forma controlar el tamaño y la morfología de dichas nanopartículas. También se han preparado nanopartículas de Pd y Au mediante dicho protocolo de síntesis. De nuevo se puede obtener un buen control del tamaño y de la morfología de estas nanopartículas. Estas nanopartículas han sido depositadas en alúmina y se han estudiado también en la reacción de hidrodecloración del tricloroetileno. La selectividad hacia el etileno depende de gran manera de la presencia de metal no noble. Estas nanopartículas han resultado ser más activas y selectivas en esta reacción que los mismos catalizadores pero preparados mediante técnicas más convencionales.

En resumen diferentes protocolos de síntesis se han estudiado en esta tesis, así como una profunda caracterización de los sistemas catalíticos obtenidos que han permitido obtener excelentes catalizadores activos, selectivos y estables en diferentes reacción de hidrodecloración selectiva de compuestos clorados tanto aromáticos como alifáticos. Las propiedades catalíticas de dichos catalizadores han sido bien correlacionadas con sus propiedades físico-químicas para lo que ha sido necesaria una profunda caracterización de los mismos.

Summary

Environmental pollution by chlorinated organic compounds, COCS, (polychlorinated aromatic (PCA) and aliphatic (PCAl)) is of great concern. They are distributed widely throughout the world due to their diverse application. Despite their wide application they are classified as carcinogenic and mutagenic chemicals that undergo bioaccumulation in fatty tissues. They can be released into water, soil and air from household or industrial facilities. The mounting evidence of adverse ecological and public health impacts has resulted in increasingly stricter legislation to limit such emissions, which leads to the necessity of developing cleaner disposing methodologies. A considerable effort is being directed at providing safe disposal methods for chemical wastes like COCs. Technologies should present high yield in contaminant removal and high selectivity to clean and useful products. The conventional treatment technologies include incineration, pyrolysis, biological treatment, and catalytic oxidation. However they all are associated with number of drawbacks associated like; high emissions of toxic compounds such as dioxins, or a low rate of elimination, or a high energy cost. As a result new and emerging technologies that enable the sound treatment of such contaminants are necessary. The search for an efficient and clean methodology to eliminate COCs gave birth to hydrodechlorination (HDC) reactions. Together with ecological safety, it often ensures complete regeneration of the initial raw material, which may open new avenues for the development of low-waste technologies. HDC technology is based on the selective hydrogenation of the C-Cl bond, H replacing chloride, and thereby obtaining hydrochloric acid and dechlorinated organic compound that can be used for other purposes. The hydrodechlorination can be promoted by metal catalysts and Pd is considered the best for this reaction. The selective removal of chlorine from organic compounds has been considered as a clean method and this interest is being experienced a rapid increase for environmental issues. The dechlorinated products are mostly non toxic hydrocarbons which can be recycled or easily destroyed with non-toxic emissions.

It is for this reason that this research has focused on the study of new catalyst that are active, selective and stable catalysts for HDC reaction of two

families of COCs: 1,2,4-trichlorobenzene and trichloroethylene. The first part of the work, related to the HDC of 1,2,4-TCB, is to obtain active and stable catalyst for the hydrodechlorination of C-Cl bond of aromatic compounds to dechlorinated organic aromatic compound (benzene). The second part of the thesis involves the HDC of trichloroethylene. This section has focused on the synthesis of active catalysts that allow high selectivity (yield) to ethylene (olefinic compounds) instead of ethane (product of TCE deep hydrogenation). On the other hand deep characterization of the active centers of the newly synthesized catalysts by different techniques was achieved in order to correlate the physical and chemical properties of the catalysts with the catalytic behavior for hydrodechlorination reaction.

It is well known that in HDC reaction of chloroaromatic compounds, the HDC reaction proceeds through an electrophilic attack of the C-Cl. The electrophilc attack can be promoted by an electron donating species like basic species that promotes the C-Cl scission. Therefore, we studied different catalytic materials that present different basicity combining both the effect of the hydrogenation metal (noble metal) and the basic effect of the support. For this reason basic Mg/Al hydrotalcite derived mixed oxides (HT) with different surface property were synthesized. They were investigated as support for Pd catalyst during gas-phase hydrodechlorination of 1,2,4-trichlorobenzene aiming higher catalytic activity and stability. The effect of rehydration-reconstruction of the supports together with Pd catalyst was investigated on the catalytic activity and stability. The HT mixed oxide was further promoted by alkali metals (Li, Na, Cs) using different precursors and the catalytic behavior towards hydrodechlorination of 1,2,4-trichloroethylene are discussed. On the way the effect of support calcination temperature was studied. The HDC reaction was found to be dependent on the support acid-basic property. Pd catalysts with higher Mg/Al ratio (higher basicity) resulted higher activity, stability and selectivity to benzene. The alkali metals modified the catalyst behavior at low operating temperature in which the Cs outmost the others. The support calcination temperature also affects the catalytic activity. The source and nature of deactivation on spent catalysts at higher reaction temperature (473 K) is mainly coking while at lower temperature (373 K) HCl poisoning is responsible for deactivation.

The second part of the thesis involves the HDC of trichloroethylene. This section has focused on the synthesis of active catalysts that allow high selectivity (yield) to ethylene (olefinic compounds) instead of ethane (product of TCE deep hydrogenation). Although catalysts based on noble metal exhibit good catalytic activity and stability during HDC reaction of TCE under mild conditions, the most important product obtained is ethane, which is a much less desirable than ethylene. To induce a better selectivity to ethylene instead of ethane, we have studied the incorporation of non-noble metal catalysts like Ni and Cu. In the first section, the metal that has been chosen was nickel. Different NiMgAl hydrotalcites have been prepared in which after its calcination process the noble metal, Pd, has been incorporated. Our findings demonstrate that NiMg(Al)O supported palladium catalysts are effective for the gas phase hydrodechlorination of trichloroethylene. The catalysts performance for the hydrodechlorination was significantly affected by the Ni/Mg/Al molar ratio, temperature of reduction, and method of noble metal deposition protocol in the support. It is found that, the higher Ni amount inside the mixed oxide, the higher catalytic activity and selectivity to ethylene in HDC of TCE. These materials are stable throughout the reaction. In general, a fine tuning between the composition of NiMgAl and prior treatment and Pd deposition protocol produce highly active catalysts and with higher selectivity to obtain ethylene.

Another type of metal introduced to induce a better selectivity to ethylene, contains copper nanoparticles together with Pd nanoparticles. The objective is to study the effect of the morphology as well as the interaction of Pd with the nanoparticles of copper. A novel method to synthesize bimetallic and monometallic Pd, PdCu and PdAu nanoparticles were designed. After deposition of the nanoparticles over alumina, the catalysts were studied for selective hydrodechlorination trichloroethylene to more valuable commercial product like ethylene. Comparison of the nanoparticle catalysts with the bulk ones showed that the former favors more ethylene formation while the later is associated with higher TCE conversion provided that the nanoparticle catalytsts exhibit lower metal loading.

In summary different catalyst synthesis protocols have been studied in this thesis, as well as a profound characterization of the catalytic systems obtained which have yielded excellent active catalysts, selective and stable in

different selective hydrodechlorination reaction of both aromatic and aliphatic chlorinated compounds. Characterization the fresh, spent and regenerated catalysts using different techniques was achieved in order to correlate the physical and chemical properties of the catalysts with activity, stability, and selectivity for hydrodechlorination reaction.

Background and motivation

Organic chemicals, chemicals in general, are an integral part of everyday life. Industries producing and using these substances have an enormous impact economic growth worldwide. There is hardly any industry where chemical substances are not implicated and there is no single economic sector where chemicals do not play an important role. Unfortunately besides their benefits it is increasingly recognized that they also have the potential to adversely impact human health and the environment if not managed properly. The health related effects range from acute poisoning to long term effects, such as cancers, birth defects, neurological disorders, and hormone-disruption. Environmental effects range from effects on sensitive species ecosystems, to large scale issues such as eutrophication of water bodies and stratospheric ozone depletion. Chemicals contamination is wide spread on air, land and in water. As a result, with the increased growth of industry, the disposable of wastes has become a problem. Of the hazardous chemicals, chlorinated organic wastes are one of the earliest environmental pollutants used widely during the industrial revolution as insecticides, refrigerants, solvents and anesthetic. They have been associated to adverse impact on human health and environment.

For some time now the Regulation on Hazardous Substances (RoHS) has been under review by the European Parliament with the environmental lobby calling for a ban on organochlorines, organobromides and PVC for use in electric appliances. “Now this may not immediately ring any alarm bells but it is not an isolated event. Earlier this year a restriction on the use of dichloromethane in paint strippers (except for industrial installations) was passed which signals that the full frontal attack on chlorine which occurred in the nineties may have diminished but chlorine containing substances are still the subject of attention today (Stockholm Convention on Persistent Organic Pollutants (POPs)”. Even though part of this family is controlled under different regulations and policies, persistent organic pollutants, part is regulated under REACH, TRI-Charter, Volatile organic carbons, their persistent nature still poses risks for the future [1].

Therefore, if their application and production are a growing fact, in addition to formulation of policies and regulations, a development of a technology for proper segregation, treatment and disposal these hazardous wastes are necessary. Technologies should present high yield in contaminant removal and high selectivity to clean and useful products [2]. The abatement of traces of pollutants from the industrial effluents (as gas or liquid) using 'environmental passive catalysis' is a new and exciting way to improve the quality of life [3]. Environmental catalysis is a promising technology which enables the development of catalysts to either safely decompose environmentally hazardous pollutants or transform it to non-toxic and recyclable products. Using catalysts, chlorinated organic wastes can selectively be transformed to hydrocarbon and HCl in hydrodechlorination reaction. However, the reactivity of the C-Cl bond decreases as the number of chloride species increases like in polychlorinated organic wastes. As a result the challenges in advancing catalytic hydrodechlorination (HDC) of polychlorinated organic wastes in real plants need new improvements due to the poor catalyst reactivity and rapid catalyst deactivation. Due to these challenges, HDC until now is limited only in laboratory scale when concerned about pollution abatement. Therefore, further efforts in the field of catalysis are needed to provide a new technology for the removal of chlorinated contaminants.

A systematic plan was executed to fulfill the overall and specific objectives. This thesis is composed of four main parts: introduction, experimental, results and discussion and conclusion. The Introduction part includes descriptions of chlorinated organic compound giving specific emphasis on two chlorinated organic compound (1,2,4-trichlorobenzene (1,2,4-TCB) and trichloroethylene (TCE)), which have been chosen as a model system to polychlorinated aromatic and non aromatic compounds. This part summarizes the impact of the molecules on human health and environment. The remediation technologies for disposal of these compounds are also discussed. Finally the past literatures concerning the HDC reaction related to the specific materials were reviewed in detail. In this section from respective mechanistic aspects, the chemical and physical behaviors that a HDC catalyst should possess were proposed. Finally the potential catalytic materials for HDC reaction were discussed. Based on this the aim and specific objectives of the thesis were stated accordingly in the second part. In

the third part, experimental methodologies related to catalyst preparation, catalyst characterization and HDC catalytic setup used were presented. In results and discussion part (fourth), characterization results of different newly synthesized catalytic materials and their catalytic behaviors towards HDC reaction are presented and discussed. Finally, conclusions are stated.

1.

General introduction

UNIVERSITAT ROVIRA I VIRGILI
HYDRODECHLORINATION OF CHLORINATED ORGANIC WASTES OVER PD SUPPORTED MIXED OXIDE CATALYSTS
Beteley Tekola Meshesha
DL: T.1347-2011

1.1. Chlorinated organic compounds (COCs)

1.1.1 Description, uses, classification and examples of Chlorinated organic compounds

Chlorinated organic compounds (COCs) are a large class of synthetic and natural organic molecules that contain one or more chlorine atoms. They are one of the most versatile and widely used classes of compounds in the industrial world. For instance, COCs are used in the composition of synthetic rubbers and shoes. They also create polymers used in packaging, and products like fluid pipes, furniture, fences, and so on. COCs can also be used as anesthetics, industrial solvents, and as precursors in the production of non-stick coatings like Teflon. COCs like DDT are some of the most potent and environmentally persistent insecticides. Its use in the control of insect-born disease has saved many millions of lives over the first half of the past century, chiefly through the dissemination of the *Anopheles* mosquito, the main carrier of the parasite that causes malaria. Furthermore, chlorfluorocarbons, composed of chlorine and fluorine molecules, have been used as refrigerants.

COCs can be categorized into two different groups: aliphatic and aromatic. They have distinct chemical and physical properties depending on the number of chlorine atoms and other functional groups they comprise. Chlorinated aliphatic compound refers to a substance containing an aliphatic chain of hydrocarbon in which at least one of the carbons bears a chlorine substituent rather than hydrogen. They are mainly used as starting materials in organic and pharmaceutical industries, solvents, refrigerants, monomers, etc. The most commonly used and widely distributed examples of chlorinated compounds include CFCs, vinyl chloride, trichloroethylene, Carbon tetra chloride etc. Chlorinated aromatic compound refers to a substance containing a mesomeric π-electron system in a carbocyclic framework in which at least one of the ring carbons bears a chlorine substituent rather than hydrogen. These compounds are recognized as important starting materials and additives in the production of high-quality insecticides, fungicides, herbicides, dyes, pharmaceuticals, disinfectants, rubbers, plastics, textiles, plant growth regulators, heat-transfer medium,

dielectric fluid, lubricants and solvents. The most common examples of chlorinated aromatic hydrocarbons include various chlorobenzenes, polychlorobisphenol (PCB), DDT.

The number of chlorine atoms or carbon atoms bonded to and how they are arranged strongly determines the chemical and physical properties of these molecules. Some of COCs are displayed below:

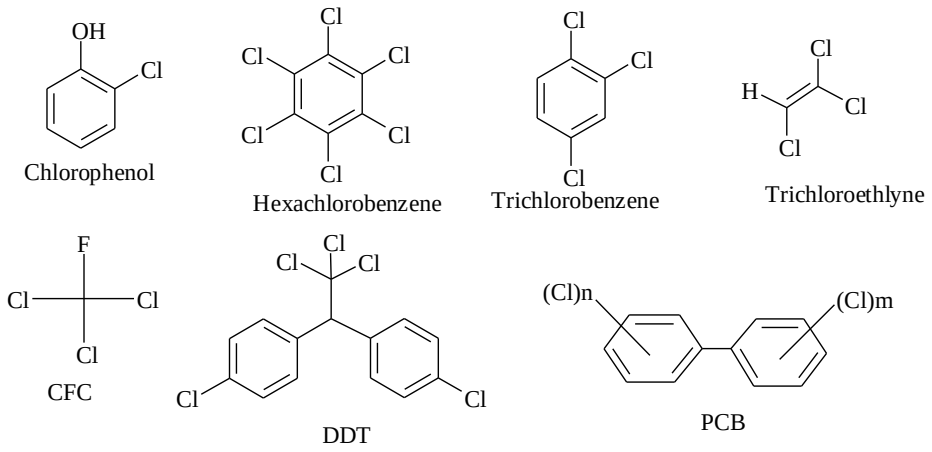

Fig. 1 Structures of some chlorinated organic compounds.

In particular of COCs groups, chlorinated ethylene and chlorinated benzenes will be discussed here due to their site of interest for in this dissertation.

Chlorinated benzene consist molecules like monochlorobenzene, 1,2-dichlorobenzene (1,2-DCB), 1,3-dichlorobenzene (1,3-DCB), 1,4-dichlorobenzene (1,4-DCB), 1,2,3-trichlorobenzene, 1,2,4-trichlorobenzene, 1,2,3,4,5,6-hexachlorobenzene. It is insoluble in water, slightly soluble in alcohol, and very soluble in benzene and solvents like petroleum ether, carbon disulfide, chlorinated aliphatic and aromatic hydrocarbons [4]. Trichlorobenzenes are produced by direct chlorination of benzene. Trichlorobenzenes were also produced in the lindane (hexachlorocyclohaxane) manufacturing process. Today, commercial production of 1,2,4-trichlorobenzene is 99.8% pure. Historically, trichlorobenzenes were produced as a mixture of 1,2,4-trichlorobenzene and

1,2,3-trichlorobenzene [5]. 1,2,4-TCB is used as a chemical intermediate, specifically for the production of herbicides, pigments, dye carries, heat transfer medium, dielectric fluid in transformers, degreaser, lubricant and solvent in chemical manufacturing [1, 4].

Chlorinated ethylene consist molecules like perchloroethylene (PCE), trichloroethylene (TCE), *cis*-1,2-dichloroethlyene (*cis*-DCE), *trans*-1,2-dichloroethylene (*trans*-DCE), 1,1-dichloroethylene (1,1-DCE), and vinyl chloride. In particular, trichloroethylene (TCE) is one of the most commonly used chlorinated ethylenes. TCE is a light, colorless liquid with a sweetish smell. It is miscible with most organic solvents and has a high solvency for natural and synthetic rubbers and various other polymers. E. Fischer first obtained trichloroethylene in 1864 from hexachloroethane by reductive dehalogenation with hydrogen. It was first commercially produced in Germany at the beginning 1900s. TCE is applied in vapor degreasing and cold cleaning. They are used in many industrial processes such as the manufacture of automobiles, electronics, paper, furniture, appliances, jewelry, and plumbing fixtures. They are also applied as a chain length modifier in the production of polyvinyl chloride (PVC). Other applications include solvent in adhesive formulations, in paints and coatings; and in miscellaneous chemical synthesis [1, 5]. Today 80% of TCE supply is mainly used as feedstock material to produce fluorinated hydrocarbons (for instance for use in refrigeration and air-conditioning systems) and fluorinated polymers, and the rest as an industrial solvent in various applications, among which the cleaning of storage tanks for liquid oxygen and hydrogen [1].

1.1.2 Environmental and Health implications

Over the last few decades, enormous quantities of COCs have been released into the environment. The primary environmental releases of COCs are due to air, water and soil from different industrial, agricultural and municipal facilities. Despite their wide spread industrial usage as described above, they have been recognized as high priority environmental pollutants. Due to their high persistency and mobility, they are detected even in regions where these synthetic chemicals had never been used such as Arctic and Mount Everest regions [6].

They are suspected to cause a number of health problems due to their toxicity and persistent nature. COCs are also potent carcinogen. The toxicity/persistency of COCs depends on the amount of chloride species they contain in which the removal of the chlorine atoms leads to their detoxification [6, 7]. Historically, one of the earliest examples of this problem was the pesticide DDT. It is an organic compound of chlorine, which imitates the action of certain hormones like estrogen. In 1950's populations of several bird species, dropped drastically [8]. The polychlorinated biphenyls (PCBs), has had similar effects in birds and fish. These compounds have been widely used as dielectric fluids at the industrial level due to their physical and chemical properties: low vapor pressure, low water solubility, high dielectric constant, and thermal stability [9]. However their persistency in environment led to concentrate in food chains undergoing bioaccumulation in animal tissues as detected in fish, foodstuffs, human blood, and mother milk [10]. Aliphatic chloro-carbons in the stratosphere tend to photo-dissociate and release chlorine atom into the atmosphere. Eventually the chlorine is responsible for destruction of ozone layer.

Chlorinated benzenes are also an important health risks. Derivatives of chlorobenzene are toxic (chloroanilines, chloronitrobenzenes), tratogenic (like chlorobenzene), lachrymatoric (like alpha-dichlorotolune), caricinogenic (like chlorbenzenes, 2-chloronitrobenzene, 4-chloronitrobenzene). Trichloroethylene is mainly emitted by industrial plants in the form of a vapour from degreasing and rubber industries. It is believed to cause photochemical smog and contribute to ozone depletion if oxidized photo-chemically. When inhaled trichloroethylene can cause headaches, dizziness, poor coordination, and potentially unconsciousness (similar effects as intoxication) [4].

1.1.3 European Union legislations and policies on regulation of COCs

Public concern over environmental problems has forced governments to pass regulations controlling the safe disposal, production and use of hazardous chemical wastes. These regulations attempt to protect human health and the environment while maintaining the nation's standard of living.

Trichloroethylene use is regulated under the Solvent Emissions Directive (1999/13/EC). ECSA (European Community Ship owners' Associations) welcomes the implementation of this directive, with its goals of reducing workplace exposures and environmental emissions. In July 2002, trichloroethylene has been classified in the EU as a category 2 carcinogen (R45). All products containing this solvent must carry the R45 hazard-warning label: “may cause cancer”.

According to EU Directive 90/415, emission of trichlorobenzenes to water is limited to 0.5 g/t capacity of chlorobenzene production from direct chlorination of benzene and 10 g/t production of trichlorobenzene from hexachlorocyclohexane pyrolysis. A surface water quality objective of 0.4 μg/l has been set by this Directive. A water quality objective of 0.1 μg/l has been proposed by EU scientific experts (CSTE, 1994). Trichlorobenzene according to Annex I of Directive 67/548/EEC and its 28 ATP, should be labeled harmful (Xn) by oral route (R22) and irritant for the skin (R38). The environmental classification is dangerous to the environment (N), very toxic to aquatic organisms and may cause long-term adverse effects on the aquatic environment (R50/53).

1.1.4 Remediation techniques

The mounting evidence of adverse ecological and public health impacts has resulted in increasingly stricter legislation to limit such emissions, which leads to the necessity of developing cleaner disposing methodologies. A considerable effort is being directed at providing safe disposal methods for chemical wastes like COCs. Technologies should present high yield in contaminant removal and high selectivity to clean and useful products.

1.1.4.1. Incineration

Incineration is one of the conventional methodologies, which has largely been used for disposing organic wastes from industries, hospitals and municipal hazardous organic wastes. Incineration is a technique that is placed in a larger class of thermal methods that have been developed and studied for pollutant degradation. It involved a complete oxidation of the

waste at elevated temperature (>800^{o}C). Ideal products during incineration of COCs are CO_2, H_2O and HCl products.

Although incineration is the primary method used to destroy hazardous chemical wastes, its application for COCs destruction has serious technical difficulties [11]. The three main problems include: (1) Expensive, COCs are thermally stable and their destruction requires high temperatures. (2) Many side reactions can take place, which produce by-products that are of much concern. Carcinogenic and mutagenic compounds are being formed during the incineration of COCs (i.e. polychlorinated dioxins, furans, biphenyls, and phosgene) [12-15]. Extracts from soot aerosols exhibited dioxin like response during incomplete combustion of trichloroethylene and pyrolisis of plastics [16]. Dioxins are probably the environmental contaminants with the worst reputation. In fact, 2,3,7,8-tetrachlorodibenzo-*p*-dioxin (2,3,7,8-TCDD) is considered as "the most toxic man-made chemical", 500 times more toxic than strichnine and 100,000 times more toxic than sodium cyanide [17-19].

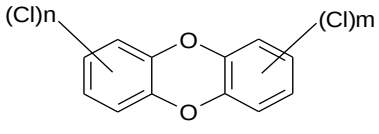

Dioxine

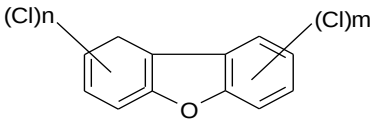

Dibenzofuran

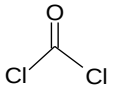

Phosgen

Fig. 2 Structures of some of toxic species produced after incineration of COCs

The problems associated with COCs waste incineration have prompted extensive research in developing new disposal methods. Biological degradation, critical water oxidation, Plasma technologies, catalytic oxidation and catalytic hydrodechlorination are some of the new technologies that have been and are extensively studied for COCs removal [20].

1.1.4.2. Biodegradation/ Biocatalysis

Bioremediation is a passive remedial approach that depends upon natural processes to degrade and dissipate contaminants in soil and groundwater. Bioremediation relies on bacteria, fungi, and plants to alter contaminants as these organisms carry out their normal life functions. Metabolic processes of these organisms are capable of using chemical contaminants as an energy source, rendering the contaminants harmless or less toxic products in most cases. The majority of chlorinated aromatic and aliphatic compounds can be readily degraded, either aerobically or anaerobically. Bioremediation can be used as a cleanup method for COCs contaminated soil and water. However, to achieve a successful bioremediation of chlorinated solvents, a sufficient population of microorganisms capable of degrading the compounds of interest should be established and maintained for prolonged periods. To create the "biological reactor" for destroying the chlorinated compounds, requires that an appropriate environment to be created or enhanced that sustains a viable population of the desired microorganisms. Creating an environment conducive to biodegradation of chlorinated solvents typically entails creation of an anaerobic environment, suppression of the redox potential, provision of a carbon (food) source, and even the provision of nutrients (minerals). They generally works well only at physiological p^H values in very dilute solutions of the substrate. In general, this process is associated with numerous limitations to be applied for real samples.

1.1.4.3. Hydrodechlorination of COCs

The search for an efficient and clean methodology to eliminate CoCs gave birth to hydrodechlorination reactions. Together with ecological safety, it often ensures complete regeneration of the initial raw material, which may open new avenues for the development of low-waste technologies. The selective removal of chlorine from organic compounds has been considered as a clean method and this interest is being experienced a rapid increase for environmental issues. Occasionally, it yields products of industrial interest.

A conceptual process is described 1978 for the hydrodechlorination of chlorinated pesticides (e.g. DDT, Aldrin, Dieldrin, and Toxaphene), and

other environmentally undesirable compounds (e.g. polychlorinated biphenyls, PCB). Experimental studies show that chlorines can in general be catalytically replaced by hydrogen to any desired extent [21]. It can operate in liquid or gas phase using different catalytic systems yielding none or partially chlorinated hydrocarbons and HCl as products. Some major advantages of HDC includes (1) non-destructive technology,(2) produce environmentally benign hydrocarbon compounds that can be recycled or easily eliminated, (3) ability to operate at mild conditions, (4) high rate of reaction, (5) No harmful side-products like dioxins, furans, phosgene (6) less sensitivity to pollutant concentrations and (7) allows selective removal of Chlorine from variety of chlorinated organic compounds or mixtures. HDC can be represented by the following chemical equation. It involves substitution of the chloride species by hydrogen molecule.

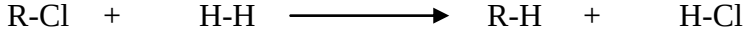

Fig. 3 Scheme of hydrodechlorination reaction

An example of HDC reaction is a Dow Chemical process in which waste 1, 2-dichloropropane is converted to reactant propylene [22]. Another example is the conversion of CCl_4, a by-product in many industrial chlorination processes and a potential ozone depletion agent, into valuable CH_2Cl_2, $CHCl_3$ that can be used as intermediates or solvents in organic synthesis. HDC processes can be performed in batch reactors for small and medium-scale processes (producing specialty chemicals, fine chemicals and pharmaceuticals), and/or continuous-flow reactors for large-scale processes (treating bulk hazardous chemicals).

In the HDC reaction the hydrogen source can be molecular hydrogen (H_2) or indeed any other hydrogen donor such as alcohol, formate salt, a hypophosphite salt, hydrazine etc [23-25]. The commonly used and preferred reducing agent in the metal-catalyzed hydrodechlorination is molecular hydrogen (H_2). Advantage of using this direct H_2 molecule involves clean process and high rate of reaction. However, the use of alternative hydrogen sources for HDC reactions, have been reported by different authors. For instance, formic acid, isopropanol and hydrazine were investigated as reducing agents for the Pd-catalyzed hydrodechlorination of chlorobenzene

in aqueous phase [23]. The next topic mainly reports on the catalytic HDC of COCs using molecular hydrogen as they attain a significant practical importance towards waste elimination. The hydrodechlorination can be promoted by thermal, catalytic, and reactive procedures ($NaBH_4$). Thermal (non-catalytic) dehalogenation has been successfully applied to a range of halogenated organic compounds but elevated temperatures (up to 1173K) are required to achieve near-complete conversion [26]. The final product is HCl as determined by thermodynamic analysis of gas-phase HDC reaction. Introduction of catalysts greatly lowers the reaction temperature providing a lower energy pathway for the reaction to occur [27].

1.2. Catalytic HDC of chlorinated organic wastes

Catalysis is an integral component in any green processing technology serving as an important tool to support sustainable development. The emergence of environmental catalysis as a discipline has focused in the development of catalysts as either decompose environmentally unacceptable compounds or provide alternative catalytic synthesis of important compounds without formation of environmentally unacceptable by products. Catalysis play a key role in the production of clean fuel, conversion of waste and green raw materials into energy, green combustion in terms of controlling NO_x and soot production and reducing green house gas emission [2]. Catalysis also plays an important role in hydrodechlorination reaction both for the purpose of synthesis of raw materials or waste treatment. Catalytic hydrodechlorination (HDC) is an attractive method for the treatment of chlorinated organic wastes [28-30]. HDC operates at low temperature and pressure, forms no harmful side-products and could eventually be selective towards chloride removal [31]. Unlike techniques such as pyrolysis and incineration, catalytic hydrodechlorination (HDC) enables hazardous chlorinated wastes to be transformed into null toxic commercial products or easily destructible compounds with non-toxic emissions [11, 18, 32, 33]. Moreover, HDC is simple and efficient. The HDC reaction can be catalyzed using homogeneous or heterogeneous catalysts.

Catalytic Hydrodechlorination by homogeneous catalysts take place in a uniform gas or liquid phase. Homogenous catalysts are a well-defined

chemical compounds or coordination complexes, which together with the reactant, are molecularly dispersed in the reaction medium. Most advances in industrial homogeneous catalysis are based on the development of organo-metallic catalysts. Thousands of organo-metallic complexes (i.e. compounds with metal–carbon bonds) have become known in the last few decades, and the rapid development of the organic chemistry of the transition metals has been driven by their potential applications as industrial catalysts. The chemistry of organo transition metal catalysis is explained in terms of the reactivity of organic ligands bound to the metal center. The d-orbitals of the transition metals allow ligands such as H (hydride), CO, and alkenes to be bound in such a way that they are activated towards further reaction. Catalytic hydrodechlorination is first established for homogeneous systems making it important in organic synthesis [6, 34]. Coenzymes like Vitamin B_{12} (Co), F_{430}(Ni) and hematin (Fe) have been used to promote homogeneous hydrodechlorination reactions. Polychlorinated benzenes were dechlorinated (90% conversion) with $NaBH_4$, using $PdCl_2$(dppf) (dppf=1,1-bis (diphenyl phospheno)-ferrocene) as catalyst. They showed that the catalytic activity was strongly dependent on the type of solvent. The addition of a base like TMEDA(N, N, N , N-tetramethyl-1,2-ethylenediammine) improved the yield in all cases [35, 36]. $NiCl_2$ promoted $NaBH_4$ and $NaBH_2(OCH_2CH_2OCH_3)_2$ dechlorinations were carried out on pentachlorophenol and 1,2,4-trichlorobenzene [37]. Zang *et.al.* also reported that the dechlorination of 1,2,4-$C_2H_3Cl_3$ in EtOH leading to 70% 1,2-$C_6H_4Cl_2$, 20% 1,3-$C_6H_4Cl_2$ and 10% 1,4-$C_6H_4Cl_2$ [38]. Others observed that 1,2,3,4-$C_6H_2Cl_4$ leads to 90% 1,2,4-$C_6H_3Cl_3$ and 10% 1,2,3-$C_6H_3Cl_3$ in ethanol/acetonitrile (6:1) and 1,2,4-$C_6H_3Cl_3$ gives (5%) 1,2-dichlorobenzene (20%) 1,3-dichlorobenzene and (75%) 1,4-dichlorobenzene in ethanol/acetonitrile by using Ni complex catalysts (4:1) [39].

The major disadvantage of homogeneous transition metal catalysts is the difficulty of separating the catalyst from the product. Although high turnovers have been achieved, application of homogeneous catalysts are not suitable for environmental protection purposes owing to the involvement of additional chemicals (such as solvents/ other hydrogen donors), difficult product/solvent/catalyst separation steps (such as distillation, liquid–liquid extraction, and ion exchange), high catalysts loss after reaction, low thermal stability, and high cost of catalyst [2].

Catalytic hydrodechlorination by heterogeneous catalysts is the most common method used now days especially in environmental processes. In this sense, heterogeneous catalysis (solids catalyst used to promote the conversion of reactants in the liquid or gas phase reaction) is of great interest for the development of new catalytic technologies able to work at mild operating conditions [2]. It usually takes place between several phases, where the catalyst is solid and the reactants are liquid or gases. Heterogeneously catalyzed reactions are composed of purely chemical and purely physical reaction steps. For the catalytic process to take place, the starting materials must be transported to the catalyst. Thus, apart from the actual chemical reaction, diffusion, adsorption, and desorption processes are of importance for the progress of the overall reaction. Heterogeneous catalysts are either automatically removed in the process (e. g., gas-phase reactions in fixed-bed reactors), or they can be separated by simple methods such as filtration or centrifugation. Even though heterogeneous catalysts are prefered in many industrial catalysis and particularly for environmental processes (also are the main site of interest from in this thesis), it can be stated that homogeneous and heterogeneous catalysts should be used to complement one another and not regarded as competitors, since each group has its special characteristics and properties [40]. Different metal catalysts like Ni [41-45][46], Ru [46, 47], noble metals are active for HDC reaction. Of this group, HDC is efficiently catalyzed by using noble metal catalysts on various supports under mild conditions. Palladium is considered the best catalyst to selectively replace chlorine atoms with hydrogen and is the least affected by the catalyst-poisoning properties of the halide ions released [30, 33, 47-49]. The common supports employed for HDC reaction are activated carbon, γ-Al_2O_3, MgO, SiO_2, and TiO_2.

The limitation of catalytic HDC reaction, like most catalytic systems, is associated with the challenges of practicality. These challenges are due to several factors but the most important factors include: rapid catalyst deactivation, poor reactivity of polychlorinated aromatic species and poor selectivity towards olefins during HDC of polychlorinated ethylene to ethylene. These factors should be investigated and studied in order to prepare stable, active and selective catalyst. In order to address the deactivation problems it is necessary to know the source of deactivation related to different conditions. The progress and knowledge of catalytic

hydrodehalogenation depends on the understanding of the reaction mechanism. The knowledge, then addresses a problem that are associated with the poor reactivity and selectivity of HDC catalysts. The mechanism aspect of the HDC reaction conditions widely vary depending on the aliphatic versus aromatic halides, gas-phase versus liquid-phase reaction, and hydrogen gas versus hydrogen donors as reducing agent so on. Furthermore the ease of C–Cl bond hydrogenolytic cleavage is dependent on the type and number of halogen involved the presence of other functional groups, the catalysts and conditions used for the reaction. Taking these into account one can modify the physico-chemical properties of a catalyst during selection, preparation and application, in order to modify the activity, selectivity and stability of the catalyst during hydrodechlorination reaction.

1.2.1. Catalyst deactivation during HDC reaction by heterogeneous catalyst

Catalysts active sites can lose or gain activity as the reaction progresses, because catalysts are often sensitive to changes in acidity/basicity, temperature, pressure, phase composition. Moreover, as the conversion increases, products and by-products can bind to the catalyst thereby changing the preferred reaction pathway. Such processes are known as deactivation. Some of the most important causes of catalysts deactivation in general are crystallite growth (particle sintering and agglomeration), carbon deposition, changes in physical properties (loss of porosity and surface area, active sites blockage), poisoning and leaching. The existence of fast deactivation of catalysts can be a considerable financial burden in the industrial implementation of the process. Batch process suffer more from deactivation than flow systems because of the local excess of poisons on the catalyst, which otherwise avoided through flow of the reactants in flow process [50, 51]. Therefore, a description of catalyst stability is recognized as integral part of catalytic studies.

One of the main drawbacks of catalytic hydrodehalogenation of organic halides is the catalyst deactivation. The nature and sources of deactivation depend not only on the type of reaction, but also the operating conditions. Catalytic decay in gas-phase hydrodechlorination has been linked to different phenomena such as poisoning of the active phase by the HCl

formed in the reaction [49, 52-54] particle sintering [55], and coke deposition [56, 57]. Active metal leaching is also responsible during aqueous phase HDC reaction. Particle sintering and coke formation are expected to be affected by the choice of the support. Moreover, an "electron-rich" metal site will be less prone to be deactivated by chlorine interaction. Catalyst deactivation, by chloride poisoning, can be minimized through the addition of a base compound to the reaction medium. The base compound can serve as a proton scavenger for hydrogen halide liberated in the reaction [38, 48]. Aramendia *et.al.* [58]reported that the added base does not influence the catalytic activity in a direct manner, but it clearly helps the reaction to complete by avoiding passivation of the catalysts. Coke deposition during the initial stages of the hydrogenolysis of CCl_2F_2 was reported by several researchers working with Pd/Al_2O_3 [59]. These carbonaceous species are responsible for the loss of activity detected with time on stream. Coke formation is cited to be promoted in acidic environment as a result basic systems can inhibit its formation to certain by indirectly neutralizing the acidic environment [60]. Active metal sintering and leaching during HDC reaction can be inhibited by employing thermal and chemically stable supports respectively.

1.2.2. HDC of polychlorobenzene (1,2,4-trichlorobenzene) over heterogeneous catalysts

One of the first studies dealing with the gas-phase HDC of chlorobenzene over Pd/Al_2O_3 catalysts was carried out by Coq *et.al.* [61]. After broad range of investigations regarding HDC of Chlorobenzene and its derivatives over different Pd supported catalysts both in gas [49, 62-66] and liquid phase [67, 68] were reported. Chlorobenzene and its derivatives are often chosen as model compounds for studying the HDC reaction since it represents the halogenated species found in many organic wastes. Trichlorobenzenes are also model molecules for hydrodechlorination reaction studies because they represent poly-chlorinated aromatic hydrocarbons [25, 46, 69-72]. Hydrodechlorination of poly chlorinated aromatics often proceeds through sequential removal of chlorines. In gas-phase hydrodechlorination of 1,2,4-trichlorobenzene the main products can be benzene, chlorobenzene, o-dichlorobenzene and p-dichlorobenzene as shown in Fig. 3. Various catalyst-support systems were employed for HDC of trichlorobenzene. Chary *et.al.* have reported the hydrodechlorination of

1,2,4-TCB over Niobia (Nb_2O_5) [70, 71] and ceria [72] supported Ni catalysts, Niobia supported Ru catalysts [46]. Cesteros *et.al*. have investigated in detail the HDC of 1,2,4-TCB by Ni supported catalysts which both observed similar product distribution [45, 73-75]. The hydrodechlorination of chlorobenzene over Pd surface is displayed below.

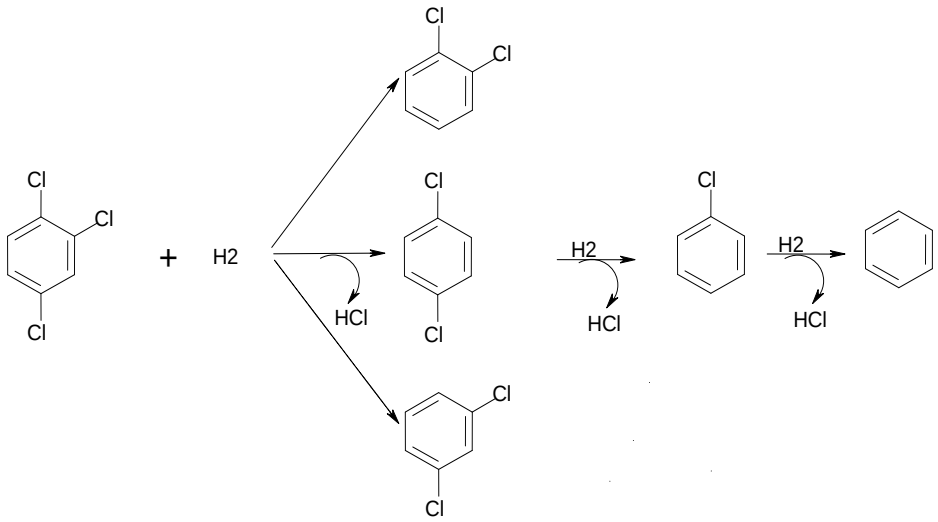

Fig. 3 Schematic representation for HDC of 1,2,4-trichlorobenzene

The mechanism of chlorination/dechlorination process for gas-phase hydrodechlorination of chlorobenzene over Pd catalysts was proposed by Coq et. al. [61]. It is based on a hypothesis that the hydrogen reacts in a dissociated form and the chlorobenzene and HCl competes for adsorption over the active sites. The surface reaction is displayed below:

$$Pd\text{-}H + C_6H_5Cl(g) \rightarrow Pd\text{-}Cl + C_6H_6(g) \quad (1)$$

$$Pd\text{-}H + HCl \rightarrow Pd\text{-}Cl + HCl \quad (2)$$

$$Pd\text{-}Cl + H_2 \rightarrow Pd\text{-}H + HCl \quad (3)$$

Step 1 and 2 describes the oxidation of Pd either by the chlorobenzene or HCl, which are adsorbed, on the Pd surface. Step 2 is considered as a self poisoning process by the HCl produced. Step 3 involves the self regeneration of the Pd surface by hydrogen. The global process

indicates that hydrodechlorination and deactivation occur simultaneously. Deactivation of the metal surface depends on the equilibrium between poisoning and regeneration of the Pd surface [51]. HDC reaction can also be activated by the spillover hydrogen from the support [76]. The mechanism of the HDC of chloroaromatic compounds has been associated with an electrophilic process for the gas-phase HDC over Ni and Pd catalysts [43, 44, 49, 75-77]. The electrophilic attack to the adsorbed aromatic substrate by surface dissociated hydrogen (probably involving "spillover hydrogen ") was proposed by Urbano [55] and Keane [44, 78] as the most possible mechanism for the supported Pd catalyzed liquid-phase HDC of *p*-substituted chloroarenes. As discussed by Keane et.al. an electrophilic mechanism presumes the involvement of a hydronium ion as the reactive species and spillover hydrogen has been variously characterized as H atoms [79] or H^+ ions [80]. There is however persuasive evidence [81, 82] for the co-existence of charged (H^+) and uncharged (H atoms) species. Once the molecular hydrogen has undergone homolytic dissociation on the supported nickel metal, the hydrogen radicals that are produced spill over onto the support where electron transfer yields a reservoir of surface hydronium ions and the probability of recombination to molecular hydrogen is reduced [81]. In addition to this behavior of the spillover hydrogen, it has been found that the electron-releasing *p*-substituent, like alkyl groups, activates the aromatic ring for the HDC reaction. This implies electron-withdrawing substituent's on the aromatic ring, eg. in polychlorinated arenes, can decrease the reactivity of the C-Cl bond. Generally, substituent like chlorine atom decreases the electron density in the aromatic ring by induction. Consequently, the higher number of chloride substituent in the ring, the more difficult the substitution to proceed [51]. Hence, electron donating agent is influential in stabilizing the active hydrogen and activating the aromatic ring for the HDC reaction to continue.

Electron donating property can be induced to the reaction through modification of the catalyst support. The influence of the support on the catalytic HDC reaction can hardly be overrated. The catalyst support determines the dispersion of the catalytically active metal particles, the catalyst's resistance to deactivation, coke resistance of the metal particles, the reactivity and may even participate in the catalytic reaction itself. Obviously, due to the nature of the chemical bonding between the support

and the metal atoms, the electronic properties and hence the reactivity of the metal is affected. There are several ways of inducing basicity in the catalytic system [47-49, 83, 84].

i. Direct utilization of basic catalyst supports and
ii. Promotion of support by basic species (alkaline oxides) [50, 85-87]

In conclusion, the low reactivity of polychlorinated arenes can be partially circumvented by the addition of electron donating species to the reaction medium. On his account, HDC activity may be promoted owing to the electron donor character of additives, promoters and supports that activate the aromatic compound, thus providing an electron-rich environment for hydrogen scission of the C-Cl bond.

Basic support and HDC reaction

The basic character of the support can influence on the catalytic behavior of the metal. Indeed a clear effect of basic supports has been reported on the catalytic properties for reactions involving arylchlorides, such as Heck reactions, in which the reactivity increases when hydrotalcites [88] or MgLa [89] mixed oxides are used as supports. Due to these characteristics, the basic supports and derived materials are widely applied in base catalyzed reaction as catalysts [90]. It is used in condensation reaction (such as cross-aldol condensation of aldehydes and ketones [91], Knoevenagel [92], Claisen–Schmidt [93]), Michael addition [94], transesterification and alkylation reactions [95]. Hashimoto *et.al* reported that a higher selectivity towards cyclohexane for Pd supported on chlorinated alumina and on silica-alumina was obtained showing the influence of the support in HDC reaction [96].

Surprisingly even though the HDC is promoted by electron donating species or basic conditions, basic supports have scarcely been used, probably because they were expected to be neutralized by the HCl produced by the reaction. As a result, utilization of common basic support, like hydrotalcite derived mixed oxide, could be interesting owing to its tunable basic property, high surface area and good chemical and thermal stability. Hydrotalcite and

hydrotalcite derived mixed oxides (HT) have been investigated as a catalysts and catalyst support for base catalyzed reaction. Hydrotalcite, a layered double hydroxide (LDH) with formula rhombohedral structure and formula of $Mg_6Al_2(OH)_{16}CO_3{\cdot}4H_2O$, is a natural anionic clay having interesting basic properties. The HT structure closely resembles that of brucite, $Mg(OH)_2$. In brucite, magnesium cations are octahedrally coordinated by hydroxyl ions, giving rise to edge-shared layers of octahedral (fig 4). The structure of an LDH may be derived by substitution of a fraction of the divalent cations (Mg^{2+}) in a brucite lattice by trivalent cations (Al^{3+}) such that the layers acquire positively charged cation, which is balanced by intercalation of anions and water between the layers [97]. Charge-balancing anions and water molecules are situated in the interlayer between the stacked brucite-like cation layers (fig 5).

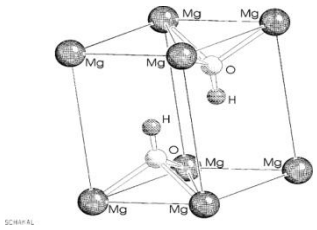

Fig. 4 Idealized structure of a $Mg(OH)_2$ brucite structure.

It is the possibility of varying the identity and relative proportions of the di and trivalent cations as well as the identity of the interlayer ions that gives rise to the large variety of materials having the general formula $[(M_{1-x}^{2+}M_x^{3+}{\cdot}(OH)_2]^{x+}(A_{x/n}^{n-})^{x-}{\cdot}mH_2O$, where M^{2+} and M^{3+} are di and trivalent metals, respectively, x is equal to the ratio $M^{3+}/(M^{2+}+M^{3+})$. A is an anion with charge n^- ($A^{n-}=CO_3^{2-}$, SO_4^{2-}, NO_3^-, Cl^-, etc.) which compensates the positive charge of the metal hydroxide layer [97, 98]. The bonding between octahedral layers and interlayer anions involve a combination of electrostatic effects and hydrogen bonding. Hydroxyl groups, particularly those bonded to trivalent cations are strongly polarized and interact with the interlayer anions.

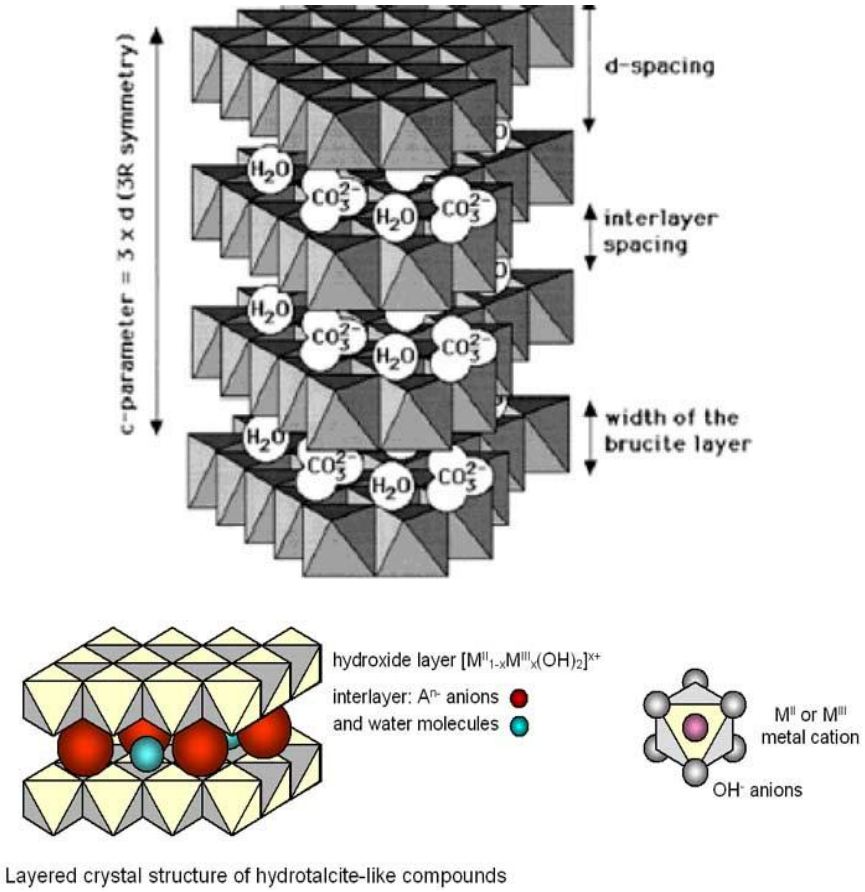

Fig.5 Structure of a layered double hydroxide with interlayer water and carbonate anions [99].

The hydrotalcites have been used in catalysis mainly after calcination (HT) or after rehydration of the calcined hydrotalcite (HTR) [97]. The mixed oxides obtained by the thermal calcination of as-synthesized hydrotalcite are homogeneous that cannot be achieved by mechanical means [98]. During calcination, the first process is the loss of physisorbed water, lamellar water molecules, and finally water from the dehydroxylation of the layers occurring at lower temperatures without collapse of the structure. Then at higher temperature the decomposition of the anions in the interlayer space as well as the hydroxyl groups from the brucite layer is performed. This leads the collapse of the layered structure forming mixed oxides with Lewis basic sites [97]. Some of important characteristics that make hydrotalcite derived mixed oxides interesting in catalysis are [97]:

- Tunable basic properties
- High surface area
- Memory effect that allows reconstruction of the original structure.
- Preparation of several reducible divalent (Ni, Cu, Co) and trivalent (Fe, Cr) cations in the structure together with the classical ones (Mg, Zn, Al)
- Good thermal and chemical stability

A relevant feature regarding catalytic applications is that the mixed oxides posses acid and basic sites whose nature, strength and relative amounts depend on the nature and molar ratio of cations, and of the calcination temperature. The acid character arises due to the presence of Mg^{2+} and Al^{3+} cations which generates acid sites of medium-high strength. On pure MgO, strong basic sites consisted predominantly of O^{2-} anions. However, the basic character of the mixed oxide arises due to three types of basic sites found in the mixed oxide: strong Lewis basic sites linked to isolated O^{2-} ions, medium basic sites belonging to M^{n+}- O^{2-} pairs, and weak Brønsted basic OH^- sites. The relative abundance of low and medium strength basic sites increased with the Al content. The addition of small amounts of Al to MgO diminished drastically the density of surface basic sites because of a significant Al surface enrichment [100]. As a result, increasing the divalent cation in the HT structure can be one way to enhance the basic property of the hydrotalcite. Formation of surface amorphous AlO_y structures in samples with low Al content (Mg/Al > 5) partially covered the Mg-O pairs and decreased the concentration of surface O^{2-}anions. At higher Al contents (5 > Mg/Al > 1), the basic site density increased because the Al^{3+} cations within the MgO lattice created a defect in order to compensate the positive charge generated, and the adjacent oxygen anions became coordinately unsaturated. In samples with Mg/Al < 1, segregation of bulk $MgAl_2O_4$ spinels occurred and caused the basic site density to diminish [100]. The basicity in layered double hydroxides can be also tuned by using specific divalent metal cations (Mg, Ca, Ba) or trivalent cation (La^{+3}) that have strong basic property.

It is also possible to induce basicity by intercalating specific basic anions like OH^- instead of CO_3^-. The calcined LDH is able to regenerate the layered structure back when it is exposed to water. The conversion of the

mixed metal oxide back to LDHs has been variously referred to as regeneration, reconstruction, restoration, rehydration or the "calcination-rehydration process", "structural memory effect" or simply "memory effect". The reconstructed hydrotalcite like material is called "meixenerite". This process makes it possible to intercalate different interlayer anions in the laminar structure depending once desire. The reconstruction of the meixenerite phase in water permits OH^- anions in the interlayer space with Brønsted basic property.

Moreover, hydrotalcite serve as precursors for the preparation of different reducible mixed oxides apart from Mg that are active for oxidation and hydrogenation/dehydrogenation reactions. Metal particles obtained in this way present homogeneous metal oxide particles, with very small crystallite size, stable to thermal and chemical treatments and good mechanical strength. Ni based catalysts prepared by using LDH precursors are widely used as catalysts for high temperature reactions like steam reforming.

Studies on the use of hydrotalcite mixed oxides as support have been reviewed by Tichit and Coq. It was explained that properties of supported catalysts could be fine-tuned by use of the metal-support interaction and cooperation; however interaction and cooperation between metals-basic supports have been scarcely investigated [101]. Metal-support interaction ("electron transfer [102] ") and metal-support cooperation (metal-base bi-functional catalysis) were put forward to interpret the highest selectivity in the hydrogenation of phenol to cyclohexanone on Pd/Mg(Al)O [103], or acetylene to ethylene on layered double hydroxides (LDH) [104], or acetonitrile to ethylamine [105]. Hence hydrotalcite derived mixed oxides could be very interesting to study as a support for HDC of chlorinated aromatic compounds due to their numerous advantages.

Alkali promotion and HDC reaction

An alternative approach for inducing basicity in the support is by the promotion using alkaline basic oxides [50, 85-87]. For example, the Na- and K-doped MgO showed a large increase in the generation of super base sites by an induction effect of the electron released from the alkali metal [106, 107]. The

effects of the modification of Pd/C by basic additives have been linked to chloroarene dissociation and surface charge effects [108]. A different charge at the Pd surface has been evidenced by the shift of the infrared band of CO in the case of Pd and Pt supported on hydrotalcites [102, 109, 110]. Aramendia *et.al.* reported that modification of aluminum *ortho*-phosphate support with NaOH not only modifies the initial activity but also resists the poisoning effect of HCl formed during the reaction [86]. Furthermore, it was also reported that the modification of the ZrO_2 with alkali metal carbonates improved the catalytic activity of the final palladium catalyst in the HDC reaction of 3-chloropyridine. This improvement depended on the ionic radii of the alkali metal added, i.e. the larger the ionic radii ($Li^+ < Na^+ < K^+$), the greater the catalytic activity of the palladium catalyst [50, 77].

1.2.3. HDC reactions of polychloroaliphatic (trichloroethylene) over heterogeneous catalysts

Hydrodechlorination of chloroaliphatic compounds has evolved from their destruction to production of valuable products that can be applied in other processes, by tailoring the catalysts property. Hydrodechlorination of polychlorinated ethylene unlike chloroaromatic compounds proceeds through multiple removals of chlorines. In gas-phase hydrodechlorination of TCE, wide variety products can be detected.

The presence of double bonds hinders the formation of radicals [111]. As a result the hydrodechlorination of olefinic chlorinated compounds would take place by means of a mechanism involving the chemisorption of both hydrogen and the chlorinated compound. The unsaturated molecules are easily adsorbed and hydrogenated onto metallic surfaces. Hence during HDC of chloroethylenes an emphasis should be given on understanding of the carbon-halogen bond dissociation and C-C double bond hydrogenation as a key step toward modifying activity and selectivity of a catalyst. During HDC reaction, trichloroethylene can undergo transformation by hydrogenation of double bond, hydrodechlorination of the C-Cl bond, and at higher operating temperature C-C cracking over the metallic surfaces. Ordónez *et.al.* proposed that the hydrogenation of double bond for the hydrogenation of TCE on noble metal catalysts, would take place catalytically, while the elimination of HCl would be essentially non-catalytic [111]. Similar mechanisms have been

suggested by Screier for tetrachloroethylene (TTCE) and TCE hydrodehalogenation in aqueous solution [112]. The hydrogenation of double bonds is favored as the number of substituent of the double bonds decreases, especially when the atoms are very electronegative (such as chlorine atoms) because it absorbs electron density from the π bond. Ethylene formed would be quickly hydrogenated on the surface of a very active hydrogenation catalyst such as Pd [113] forming less desired saturated hydrocarbon such as ethane. The hydrodechlorination of olefinic chlorinated compounds would take place by means of a mechanism involving the chemisorption of both hydrogen and the chlorinated compound, the addition of two hydrogen atoms to the double bond, and the elimination of hydrogen chloride [111, 112, 114] as is shown in fig. 6.

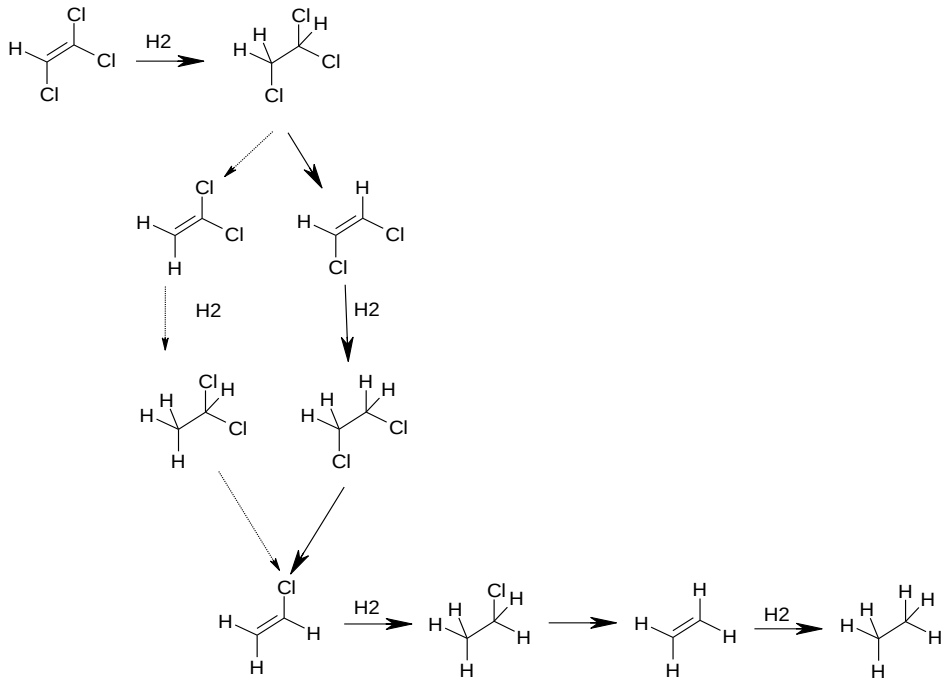

Fig. 6 Possible reaction pathway for hydrodechlorination of TCE [111].

The reaction pathway can be affected by the type of catalysts used, the state of the active phase (monometallic or bimetallic, particle size etc), operating conditions (temperature, pressure or H_2/TCE molar ratio etc), and type of metal-support interaction. One of the challenges faced during HDC of TCE is to design a catalyst that favors the formation of ethylene than

ethane. Olefinic product like ethylene is highly important compound both in industry and commerce. As a result from the HDC products a recyclable useful compound can be produced. The cleavage of the C-Cl bond has been extensively studied using Pd and Ni monometallic and bimetallic catalysts.

Pd metals have been suggested as excellent catalysts for hydrodechlorination of TCE. The reaction, catalyzed by noble metals, shows highly to moderately active/selective toward the formation of paraffin [18, 30]. Nishijima *et.al*., showed competitive HDC of chlorinated ethylene (TTCE, TCE and DCE) using Pd/C catalyst in organic solvents (liquid phase) at ambient condition in which addition of NaOH clearly increased in the degradation rate of PCE [115]. Ordoñez *et.al.*, studied the influence of several parameters (temperature, pressure, hydrogen flow rate, and nature of solvent) on both activity and stability of a 0.5% Pd/Al_2O_3, Pd/Graphite and Pd/C catalysts for tetrachloroethene (TTCE) hydrodechlorination. Although the carbon-supported catalyst yields higher initial conversion, the alumina-supported catalyst is more resistant to deactivation [52]. Pd supported on pure and modified graphite also showed enhanced activity and stability towards the HDC of TTCE by tuning the surface property [116]. Although supported monometallic noble metal catalysts, particularly Pd, exhibit good catalytic activities and stability during HDC of TCE at mild conditions, it mainly produces ethane [30, 117, 118]. Ethane is less desired commercial product when compared to ethylene. HDC over noble metal surfaces tend to rapidly hydrogenate the olefin formed as a primary product in the presence of H_2. Apart from the low selectivity towards ethylene, the main disadvantage of monometallic systems is the high degree of catalyst deactivation [119].

Other widely studied monometallic transition metal catalyst includes nickel, which is able to catalyze HDC of vicinal aliphatic chlorinated carbons. Some catalyst like Ni/Al_2O_3 [111, 120], Ni/Zeolite [42], Ni/SiO_2 [111], Ni/AC [57, 121] and Raney Ni [57, 111] have been tested for HDC of TCE. The effect of Ni precursor was investigated where the Ni-from sulphate catalyst experienced the lowest catalyst deactivation and showed the highest yield of vinyl chloride monomer (VCM) at large reaction time. Other Ni catalysts studied for HDC of various aliphatic chlorinated compounds include a hydro-processing catalyst $NiMo/Al_2O_3$ [111, 114, 122]. This works studied the influence of the catalyst pre-treatment (sulfidation), temperature, pressure and nature

of the solvent over the reaction yield. The results indicate that the conversions to nonchlorinated organics were found to be close to 100%, operating at 100 bar and 350^{o}C over a sulfided Ni/Mo-g-alumina catalyst. Kim Dae *et. al.* proposed a multiple chlorine removal steps that appear to be the dominant pathway for hydrodechlorination of olefins as opposed to sequential removal with desorption of intermediates. The Nickel-molybdenum hydrotreating catalysts possess low resistance to deactivation. In all the experiments, the reaction products were hydrogen chloride, and hydrocarbons (methane and ethane), some organochlorine byproducts, however with no ethylene product being detected. Unlike noble metal catalyst, supported Ni catalysts have been reported to be highly selective towards ethylene during HDC of vicinal chloro-carbons [121, 123, 124]. However, it requires high temperature (>473K) or high hydrogen pressure to reach significant conversion. Furthermore, similar to noble metal catalysts, Ni catalysts showed a rapid catalyst deactivation.

Monometallic Cu or Ag can also catalyze the reaction to form selectively ethylene; however these metals are associated with low activity [125]. In addition, according to the study of Fung and Sinfelt [126] concerning the hydrogenolysis of methyl chloride CH_3Cl on metals, metals from Group IB such as Ag and Cu, are able to form a metal–chlorine bond, as demonstrated by the existence of stable chloride showing rapid deactivation. Surface chlorine atoms could not be removed easily due to a lack of surface hydrogen. In this case, noble metals like Palladium, with high hydrogen chemisorption capacity, could be needed to provide an abundant source of dissociated hydrogen, to reduce surface CuCl species and form HCl. The modification of supported Pd noble metal catalyst by the addition of a second metal changes the catalytic performance for vicinal chloro-carbon dechlorination. Higher olefin selectivity can be attained as demonstrated by Pd catalysts doped with second transition metals like Ag [118], Cu [117, 127] or Sn [128]. Comparable catalytic activity can be obtained by Pd-Cu bimetallic alloys as monometallic noble metal catalysts, showing minimal deactivation. Several possible theories have been reported in the literature to explain the reasons for high olefin selectivity in hydrodechlorination using bimetallic catalysts from the point of view of the noble metal. The effect of an electronic modification of Pt on the ethylene selectivity of the Pt–Cu/SiO_2 catalysts in 1,2-dichloroethane hydrogen-assisted dechlorination has been

investigated [129]. The electronic state of Pt was probed by CO adsorption. It was shown that Pt in the Pt–Cu/SiO_2 catalysts is modified electronically, but this modification does not control the selectivity toward ethylene [117]. To explain the high ethylene selectivity of the Pt–Cu catalysts for the dechlorination of 1,2-dichloroethane, Vadlamannati *et. al.* suggested that the C–Cl bond dissociation on Pt is a structure-sensitive or size-demanding elementary step [119]. If the dissociative adsorption of 1,2-dichloroethane requires large ensembles, the dilution of Pt with Cu splits such ensembles and suppresses the activity of Pt in the dechlorination reaction. Kovalchuk *et. al.* [117] proposed that the governing factor for the high olefin selectivity of bimetallic catalysts in hydrogen-assisted dechlorination of chlorocarbons is the low adsorption energy for olefins on active sites, which consist of isolated noble metal atoms in a matrix of the modified catalyst's surface. Thus, adjusting the chlorocarbon to H_2 ratio in the reaction feed could be an effective means to control the hydrogenation activity of the catalysts for hydrogen-assisted dechlorination of vicinal chlorocarbons.

From the point of view of the modifiers (Cu and Ag), the mechanism of 1,2-dichloroethane hydrodechlorination studied by Heinrichs *et. al.* for Pd-Ag catalysts suggested that the mechanism over alloys is based on the sequence of elementary steps, which suggests a process of chlorination of the silver surface by 1,2-dichloroethane followed by a hydrodechlorination of that surface by hydrogen adsorbed on palladium. Used alone, silver deactivates rapidly due to its covering by chlorine atoms. However palladium present in the alloy supplies hydrogen atoms for the regeneration of the chlorinated silver surface into metallic silver [125, 130]. A study for 1,2-dichloroethane hydrodechlorination over Pt–Cu/SiO_2 catalysts also proved that the addition of CO into the $CH_2Cl–CH_2Cl + H_2$ reaction mixture at 200^oC to block Pt sites only results in an improvement in the ethylene selectivity of the bimetallic catalysts at the expense of ethane. These observations were consistent with the idea that with Pt–Cu catalysts, ethylene forms on Cu sites that were not blocked by carbon monoxide [131]. Barrabes *et.al.* [127] presented a reaction scheme similar to what was proposed by the groups of Heinrichs [125] and d'Itri [131] for hydrogen-assisted dechlorination of dichloroethane on PdCu catalysts where, adsorption of TCE on the Cu phase leading to dechlorination reaction producing ethene is proposed. The main role of the noble metal forming the alloy is the

regeneration of the Cu-Cl_x species by spillover of hydrogen. On the alloyed particles a high selectivity to ethene is obtained. However, on catalysts containing copper and the noble metal in separate phase, the dehalogenation reaction occurs on the copper surface whereas on the surface of the noble metal a deep hydrogenation to ethane is taking place [127]. The catalytic performance, however, depends on the modifier to noble metal ratio, and reaction condition [128]. Supported bimetallic Pd-Cu catalysts are one of the most widely studied for HDC of TCE to ethylene.

Promotion of Ni rich catalysts using small amount of noble metals like Pd also modifies its catalytic behavior for HDC reaction [132-134]. In this way, it is possible to design Pd-Ni bimetallic catalyst, which is selective for olefin formation. The catalytic performance, however, depends on the modifier to noble metal ratio [128]. Moreover, the selection of an appropriate catalyst structure as stated in the above topic is important to modify the catalytic behavior (activity, selectivity and stability) and limit the degree of deactivation [118]. For instance, the choice of catalyst support and method of preparation can play an important role in the development of hydrodechlorination catalysts [123, 135]. The effect of pretreatment and metal precursor salt for Pt/CeO_2 catalyst in the selective hydrodechlorination of trichloroethylene, has been studied by Barrabes et al [136]. They proposed that pretreatment the reduced 0.5% Pt/CeO_2 catalyst by alter oxidation, followed by reduction increased the selectivity to ethylene up to 85% at the same conversion level when compared to reduced catalyst. At the same time using chloride precursor salts for platinum favored the selectivity towards ethylene. The hydrotalcite can also serve as precursors for the preparation of different reducible mixed oxides apart from Mg that are active for oxidation and hydrogenation/dehydrogenation reactions. Metal particles obtained in this way present homogeneous metal and metal oxide particles, with very small crystallite size, stable to thermal and chemical treatments and good mechanical strength. Ni based catalysts prepared by using LDH precursors are widely used as catalysts for high temperature reactions like steam reforming. There are also reported studies on the application of these materials for HDC reaction. Previously in our group, Cesteros and et. al. have investigated in detail the HDC of 1,2,4-TCB by Ni supported on pure and mixed delta/alpha-alumina [45], $Ni/NiAl_2O_4$ [73], Ni spinel [137], Ni/MgAl mixed oxide [75], and Ni/Al-MCM-41 [74] catalysts. The influence of support

on the active metal phases and how it affects the HDC reaction were discussed in detailed. When the magnesium content in the Ni/MgAl catalysts increases, both the activity and selectivity to benzene greatly enhanced. Furthermore, deactivation of the catalysts becomes slower. This catalytic behavior was explained as the MgO modifies the electronic properties of the nickel particle causing the hydrogen desorption at lower temperatures and also adsorbs the HCl produced during the hydrodechlorination reaction.

In general the improvement of this technology in order to increase the selectivity towards valuable compounds is of great interest nowadays. All in all exploring Pd-Ni or Pd-Cu bimetallic catalysts by modifying the catalyst environment could be interesting to study for HDC of TCE to ethylene.

UNIVERSITAT ROVIRA I VIRGILI
HYDRODECHLORINATION OF CHLORINATED ORGANIC WASTES OVER PD SUPPORTED MIXED OXIDE CATALYSTS
Beteley Tekola Meshesha
DL: T.1347-2011

2.

Aim & Objectives

UNIVERSITAT ROVIRA I VIRGILI
HYDRODECHLORINATION OF CHLORINATED ORGANIC WASTES OVER PD SUPPORTED MIXED OXIDE CATALYSTS
Beteley Tekola Meshesha
DL: T.1347-2011

Aim and Objectives

The overall aim of this investigation is to study the hydrodechlorination of environmentally polluting polychlorinated organic wastes by using heterogeneous catalysts. The research has mainly focused on evaluation of the activity, selectivity and stability of newly synthesized Pd based catalysts for hydrodechlorination of 1,2,4-trichlorobenzene and trichloroethylene. The catalysts were prepared by considering the mechanistic behaviours of each reaction. Hydrotalcite derived mixed oxides were employed in this reaction owing to their diverse chemical and physical properties. The specific objectives of this thesis are stated below:

Section 4.1. The objective of this section is to investigate the activity of palladium supported on calcined Mg/Al hydrotalcite (HT) catalysts with for hydrodechlorination reaction of 1,2,4-trichlorobenzene. Different basic property was attained by preparing a hydrotalcite with Mg/Al molar ratio of 2, 3, and 4. The effect of rehydration-reconstruction of the supports together with Pd catalyst will be investigated on the catalytic activity and stability. Finally the source and nature of deactivation for each of spent catalysts were studied and final discussions and conclusions were made accordingly. Different reaction temperatures between 373 K-473K were employed.

Section 4.2. The section addresses the HDC of 1,2,4-TCB on Pd/HT catalysts promoted by Li, Na and Cs that comes from nitrates and hydroxides salts. The hydrotalcite was prepared with Mg/Al molar ratio of 4. The study focuses on studying the activity, selectivity and stability in relation with the basic properties of the promoted mixed oxides. A low reaction temperature (373K) has been chosen to study the deactivation and the regeneration of the catalysts. Finally characterizations of spent catalysts were achieved using different techniques to determine the source of deactivation and the state of the active metal.

Section 4.3. The objective of this section is to study the influence of calcination temperature of hydrotalcite, as a support towards HDC reaction of 1.2.4-Trichlorobenzene. Various $MgAlO_x$ mixed oxide calcined at different temperatures were used as support. The Pd supported over these mixed oxide species were comparatively investigated for HDC reaction of

1,2,4-TCB. The effect of different crystalline phases and influence of support basicity on Pd activity and selectivity were discussed. The structure influence of hydrotalcite (HT) support by changing the calcination temperature was evaluated.

Section 4.4. The main objective of this section is to study the catalytic behaviour of Pd/Ni(Mg)Al catalysts for gas-phase HDC of trichloroethylene. In this section different Ni(Mg)Al hydrotalcite derived mixed oxides (NiHT) with varying compositions were synthesized and consequently promoted by Pd. The catalysts were characterized using different techniques to investigate Pd-Ni interactions and the effect of the support. These catalysts were studied for gas-phase hydrodechlorination of trichloroethylene using a stoichiometric amount of [H_2/Cl] at 573 K. The influence of support composition and catalyst reduction temperature was studied. Previously, it was reported that immobilization of Pd over reduced CuMgAl catalyst showed Pd/Cu interaction enhancing the catalytic behavior [127]. This protocol was also studied for Pd supported on reduced NiMgAl catalysts. Several characterization techniques were employed in order to correlate physical-chemical properties of the surface by changing Ni/Mg/Al molar ratios in the hydrodechlorination reaction.

Section 4.5. This section deals with a development of a procedure for synthesis of 1-hexadecylamine (HDA) capped metal Cu nanoparticles (HDA-M) using polyol method. The metal nanoparticle complex can be recovered from the solution by polyol-organic phase-transfer techniques. In addition, using this technique several HDA protected Pd, Cu, Au monometallic and bimetallic nanoparticles were synthesized by polyol process and characterized using different techniques. The nanoparticles prepared were then applied for gas-phase HDC of trichloroethylene. As a result the above protocol was adopted to prepare several monometallic Pd and bimetallic Pd-Cu nanoparticles with different Pd/Cu molar ratios and Pd1Au1 catalysts were also prepared and employed for HDC of trichloroethylene

Detailed characterization of the fresh and spent and regenerated catalysts using different techniques was attained in order to correlate the physical and chemical properties of the catalyst with activity, selectivity and stability for hydrodechlorination catalyst.

3.

Experimental

UNIVERSITAT ROVIRA I VIRGILI
HYDRODECHLORINATION OF CHLORINATED ORGANIC WASTES OVER PD SUPPORTED MIXED OXIDE CATALYSTS
Beteley Tekola Meshesha
DL: T.1347-2011

3.1. Catalyst preparation

Introduction

Methods of catalyst preparation are very diverse and each catalyst may be produced via different routes. Preparation usually involves several successive steps. Many heterogeneous catalysts consist of an active component or components deposited on a support (such as silica, alumina, and carbon). The role of the support may be to improve the properties (e.g. stability) of the active component(s), or to participate directly in the catalytic reaction (e.g. by providing acid or basic sites). The properties of heterogeneous catalysts depend on all their previous history. Many supported metal and oxide catalysts arc prepared by the succession of impregnation, drying, calcination, activation; zeolite catalysts are prepared by precipitation of gel, crystallisation, washing, ion exchange, drying. Three fundamental stages of heterogeneous catalyst preparation may be distinguished:

I. Preparation of the primary solid associating all the useful components (e.g. by impregnation, co-precipitation, or crystallization),

II. Processing of that primary solid to obtain the catalyst precursor, for instance by heat treatment;

III. Activation of the precursor to give the active catalyst: reduction of metal precursor (hydrogenation catalysts), formation of sulfides (hydrodesulfurisation). Activation may take place spontaneously at the beginning of the catalytic reaction (selective oxidation catalysts).

There are several ways to prepare oxide support material and deposit the active component. Precipitation/co-precipitation techniques are commonly employed to prepare bulk catalysts and supports. Impregnation is one of the simple and common techniques applied to deposit active components over the support surfaces.

1.1. Support preparation by precipitation (coprecipitation)

Bulk materials (catalyst or catalyst supports) are mainly produced when the active components are cheap. Bulk materials are typically made by precipitation (coprecipitation), hydrothermal synthesis, or fusion. They are

(mixed) metal oxides and, as their name suggests, the entire catalyst can be made of active or support material. Precipitation and co-precipitation are mainly used for the production of oxidic catalysts and for the manufacture of pure support materials. The process involves co-precipitation of one or more components as hydroxides or carbonates. An amorphous or crystalline precipitate or a gel obtained is then aged through time and which is washed thoroughly to remove any precipitant agents. Further steps like drying, shaping, calcination, and activation are necessary. The silica/alumina hydrocracking catalysts, zeolites, the ammonia synthesis catalyst, hydrotalcite and the Raney metals are usually prepared using this method.

There are several ways to carry out the precipitation process. The simplest implementation of the precipitation reaction is the batch operation where the simultaneous addition of both the metal salts and a precipitating agent (usually a base) under strict control of pH. Different parameters influence the final product of the precipitation. pH, solution composition, concentration, aging time, presence of additives, temperature, mixing sequence, solvent, super saturation and precipitating agent are some of the parameter that control phase purity, crystallintiy, textural property, homogeneity, particle size of the product produced. The dawn stream process include, drying, calcining at higher temperature, shaping.

The layered double hydroxides (LDHs) have been known for over 150 years since the discovery of the mineral hydrotalcite, and a large class of minerals with closely related structures that are usually known by the mineralogists as the sjöenite-hydrotalcite group [97]. Conventional synthesis of the Hydrotalcite like materials is via coprecipitation of the aqueous mixture of divalent and trivalent metal salts with NaOH solution at optimal pH. After precipitation, the solution is aged overnight. The resulting precipitate is washed thoroughly to obtain alkali and nitrate free solid and then dried at 393K. This material often has a low surface area and has to be activated by thermal decomposition to obtain a high-surface area and well-dispersed Mg(Al)O mixed oxide. The specific preparation of catalyst support will be discussed in the respective topics.

1.2. Impregnation

One of the best-known methods for producing heterogeneous catalysts is the impregnation of porous support materials with solutions of active components. Especially, catalysts with expensive active components such as noble metals are obtained in this way. In the impregnation process, active components with thermally unstable anions (e.g., nitrates, acetates, carbonates, hydroxides) or previously prepared nanoparticles are used. The nanoparticle precursors are previously prepared from the metal salt, oxide or hydroxides and dispersed in a solvent before impregnation. It follows that nanoparticle atoms have lower coordination numbers than in the bulk and as a consequence are expected to exhibit greatly enhanced activity to all manner of substrates. Greater accessibility to all constituent (surface) atoms and enhanced activity because of the low coordination number they exhibit make nanoparticles interesting in catalysis. The support is immersed in a solution of the active component under precisely defined conditions (concentration, mixing, temperature, time). In this process, the liquid penetration into the pellets is hindered by air trapped in the pellet pores. Various techniques like pressurizing, vacuum treatment, acoustic activation etc. are used to facilitate the impregnation process. They, however, are expensive and allow only limited control of absorption and penetration depth. During impregnation many different processes take place with different rates like:

- Selective adsorption of species (charged or not) by Coulomb force, van der Waals forces or H-bonds;
- Ion exchange between the charged surface and the electrolyte;
- Polymerization/depolymerisation of the species (molecules, ions) attached to the surface;
- Partial dissolution of the surface of the solid.

The main parameters affecting the liquid are the pH, the nature of the solvent, the nature and concentrations of the dissolved substances. The first parameter affects ionisation and, in many cases, the nature of the ions containing the active elements. The second and third influence solvation. The main properties of the solid are the texture, the nature of functional groups (e.g., the number and strength of the acidic and basic centres, the isoelectric

point), the presence of exchangeable ions, and the reactivity (surface dissolution in acidic or basic solution, etc.).

Methods of impregnation

Impregnation by soaking, or with an excess of solution:- excess liquid is eliminated by evaporation or by draining. Deposition of the active element is never quantitative. The quantity deposited depends on the solid-liquid ratio. Deposition is slow, requiring several hours or days. Extensive restructuring of the surface (loss of surface area, dissolution of surface, etc) may occur. However, the method allows the distribution of the species to be very well controlled and high dispersions may be obtained. *Co-impregnation*:-two or several active components are introduced in a single step. Co-impregnation with uniform distribution and without segregation of species is extremely difficult to achieve. *Successive impregnation* :-two or several active components are introduced sequentially. Pretreatments like drying, reducing (and often calcination) can take place between the impregnations. For the second impregnation the properties of the surface to take into account are those of the solid obtained after the previous impregnation. The specific preparation of impregnated catalysts will be discussed in the respective topics in detail.

3.2. Characterization techniques

Catalysis is still very much a black box discipline, and catalyst characterization tools help us look inside this box. Both the physical and the chemical structure of a catalyst must be known if relationships between the material structure of the catalyst and activity, selectivity, and lifetime are to be revealed. The discussion under this topic is focused mainly on the fundamental of basic principles of characterization techniques used throughout the thesis.

3.2.1. Spectroscopic characterization techniques

When electrons are accelerated up to high energy levels (few hundreds keV) and focused on a catalyst surface, they can scatter or

backscatter elastically or inelastically, or produce many interactions, source of different signals such as X-rays, Auger electrons or light as shown in Fig. 1. These signals include secondary electrons (that produce SEM images), backscattered electrons (BSE), diffracted backscattered electrons (EBSD that are used to determine crystal structures and orientations of minerals), photons (characteristic X-rays that are used for elemental analysis and continuum X-rays), visible light (cathodoluminescence and Photoluminescence), and heat. Some of them are used in transmission electron microscopy (TEM).

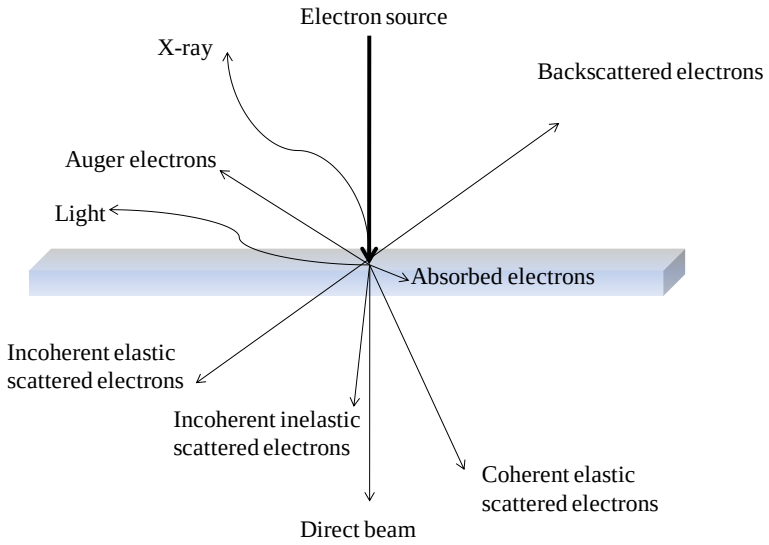

Fig. 1 The different radiation emitted during excitation of a solid surface.

3.2.1.1. X-ray diffraction spectroscopy

X-ray diffraction (XRD) is a versatile, non-destructive technique that reveals detailed information about the chemical composition and crystallographic structure of natural and manufactured materials. This technique had its beginnings in von Laue's discovery in 1912 that crystals diffract x-rays, the manner of the diffraction revealing the structure of the crystal. At first, x-ray diffraction was used only for the determination of crystal structure. Later on, however, other uses were developed, and today the method is applied, not only to structure determination, but to such diverse

problems as chemical analysis and stress measurement, to the study of phase equilibria, the measurement of particle size and distributions using scherrer equation, and to determine of the orientation of one crystal or the ensemble of orientations in a polycrystalline aggregate. Scherrer equation (shown below) relates the size of sub-micrometer particles, or crystallites, in a solid to the broadening of a peak in a diffraction pattern:

$$\tau = \frac{k\lambda}{\beta\cos\theta}$$

Where k is the shape factor, λ is the x-ray wavelength, β is the line broadening at half the maximum intensity (FWHM) in radians, and θ is the Bragg angle; τ is the mean size of the ordered (crystalline) domains, which may be smaller or equal to the grain size. Other applications of XRD include characterization of crystalline materials, identification of fine-grained minerals such as clays and mixed layer clays that are difficult to determine optically, determination of unit cell dimensions and measurement of sample purity. With specialized techniques, XRD can also be used to determine crystal structures using Rietveld refinement. It can determine of modal amounts of minerals (quantitative analysis), characterize thin films samples [138-140].

X-ray diffraction is based on constructive interference of monochromatic X-rays and a crystalline sample. X-rays are generated in a cathode ray tube by heating a filament to produce electrons, accelerating the electrons toward a target by applying a voltage, and bombarding the target material with electrons. When electrons have sufficient energy to dislodge inner shell electrons of the target material, characteristic X-ray spectra are produced. These spectra consist of several components, the most common being K_α and K_β. The specific wavelengths are characteristic of the target material (Cu, Fe, Mo, Cr). Copper is the most common target material for single-crystal diffraction, with CuK_α radiation = 1.5418Å. These X-rays generated by a cathode ray tube are filtered to produce monochromatic radiation, collimated to concentrate, and directed toward the sample [138]. The geometry of an X-ray diffractometer is such that the sample rotates in the path of the collimated X-ray beam at an angle θ while the X-ray detector is mounted on an arm to collect the diffracted X-rays and rotates at an angle of

2θ. The instrument used to maintain the angle and rotate the sample is termed a *goniometer*. The interaction of the incident rays with the sample produces constructive interference (and a diffracted ray) according to Braggs law:

$$n\lambda = 2dsin\theta$$

Where "d" is the spacing between atomic planes in the crystalline phase and "λ" is the x-ray wavelength. This law relates the wavelength of electromagnetic radiation to the diffraction angle θ and the lattice spacing in a crystalline sample. These diffracted X-rays are then detected, processed and counted. By scanning the sample through a range of 2θ-angles, all possible diffraction directions of the lattice should be attained due to the random orientation of the powdered material. Conversion of the diffraction peaks to d-spacing allows identification of the mineral because each mineral has a set of unique d-spacing. Typically, this is achieved by comparison of d-spacing with standard reference patterns [138, 140, 141].

Instrumentation

The XRD analysis of the catalysts was recorded using a Siemens D5000 diffractometer (Bragg-Bentano for focusing geometry and vertical θ-θ goniometer) with an angular 2θ-diffraction range between 3º and 90º. The samples were dispersed on a Si (510) sample holder. The data were collected with an angular step of 0.03º at 5 s per step and sample rotation. Cu Kα radiation (λ=1.54056 Å) was obtained from a copper X-ray tube operated at 40 kV and 30 mA. The crystalline phases were identified using the JCPDS files.

3.2.1.2. *X-ray Photoelectron spectroscopy*

X-ray photoelectron spectroscopy (XPS) is a quantitative spectroscopic technique that measures the elemental composition, empirical formula, chemical state and electronic state of the elements that exist within a material by measuring the binding energies. XPS spectra are obtained by irradiating a material with a beam of X-rays while simultaneously measuring the kinetic energy and number of electrons that escape from the top 1 to 10 nm of the material being analyzed. XPS requires ultra high vacuum (UHV)

conditions. XPS is a surface chemical analysis technique that can be used to analyze the surface chemistry of a material in its "as received" state, or after some treatment, for example: surfaces after chemical reaction, fracturing, cutting or scraping in air or UHV to expose the bulk chemistry, ion beam etching to clean off some of the surface contamination, exposure to heat to study the changes due to heating, exposure to reactive gases or solutions, exposure to ion beam implant, exposure to ultraviolet light. XPS is also known as ESCA, an abbreviation for Electron Spectroscopy for Chemical Analysis. Because the energy of an X-ray with particular wavelength is known, the electron binding energy of each of the emitted electrons can be determined by using an equation that is based on the work of Ernest Rutherford (1914):

$$E_{binding} = E_{photon} - (E_{kinetic} + \emptyset)$$

Where $E_{binding}$ is the binding energy (BE) of the electron, E_{photon} is the energy of the X-ray photons being used, $E_{kinetic}$ is the kinetic energy of the electron as measured by the instrument and φ is the work function of the spectrometer (not the material).

Instrumentation

The XPS analysis of the catalysts was performed with a SPECS system equipped with a dual anode XR50 source operating at 150 W and a Phoibos 150 MCD-9 detector. Sample powders were pressed to pellets and then fixed into a special sample holder (no glue was used). Spectra were recorded with pass energy of 25 eV at a pressure below 6 10^{-9} mbar; binding energies were referred to the adventitious C 1s signal. The apparatus was equipped with an additional high pressure cell (HPC-20) for in-situ reduction (H_2, 1 bar and 623 K). Temperature was provided with an infrared source and was measured directly on the sample holder by a thermocouple. After each in-situ treatment, samples were transferred from the reaction cell to the analysis chamber under high vacuum (less than 10^{-8} mbar).

3.2.1.3. Electron microscopy (EM)

Electron microscopy in catalysis is mainly used for determining the size, shape, topography, morphology and if integrated composition of supported particles. Transmission electron microscopy (TEM) and scanning

electron microscopy (SEM) are indeed outstanding tools in textural analysis of solids. The information given by these techniques is generally very useful for the critical discussion of the data coming from adsorption isotherms and XRD analysis. Examples of applications of electron microscopy include; dispersion measurements with good agreement with chemisorption measurements, sintering, segregation, and re-dispersion of metal particles as a result of oxidative treatment, study of coking processes and detection of surface impurities and surface poisoning.

i. *Scanning Electron Microscopy (SEM)*The scanning electron microscopy is one of the most versatile instruments available for examination and analysis of the micro structural characteristics of solid surfaces. In catalysis, the main interest of SEM lies in studying topography, morphology and chemical composition of the active component on supported catalysts. In typical scanning electron microscopy (SEM), a high-energy (typically 10-50 keV) electron beam is scanned over a small rectangular area of the sample. When the energetic electrons hit the surface under investigation, secondary electrons are emitted (SE), and/or some incident electrons are being backscattered (BSE). The secondary electrons are detected by attracting them onto a phosphor screen, and measuring the light intensity with a photomultiplier. Some of the beams electrons strike atomic nuclei, and bounce back. These electrons, known as back-scattered primaries, give information on the surface topography and on the average atomic number in the scanned area. The microscope records the secondary and back-scattered electrons as a function of the beams position. The surfaces that face the detector appear brighter than those set at an angle, creating contrast in the image [142, 143]. Magnification is achieved through the electron beam scanning an increasing smaller area of the same specimen and most modern scanning electron microscopes have a magnification range of x 720, up to more than × 300,000, and resolution in the order of 2-4 nm or better. The great depth of focus of the microscope (>500 times that of light microscopy) is achieved by the convergence angle of the primary electron beam and the relatively long working distance between the final lens and the specimen. This depth of focus enables production of images that appear to be three-dimensional.One major advantage of the SEM (in comparison to a TEM) is the ease of specimen preparation, a result of the fact that the specimen does not have to be made thin. In fact, many conducting specimens require no special

preparation before examination in the SEM. On the other hand, specimens of insulating materials do not provide a path to ground for the specimen current and may undergo electrostatic charging when exposed to the electron probe. Therefore, the local charge on the specimen can be positive or negative. Negative charge presents a more serious problem, as it repels the incident electrons and deflects the scanning probe, resulting in image distortion or fluctuations in image intensity [142]. One solution to the charging problem is to coat the surface of the SEM specimen with a thin film (thickness 10-20 nm) of metal like gold or chromium or conducting carbon. SEM can also provide the detailed information of chemical composition and distribution if integrated with other techniques.

Instrumentation

The morphologies of the catalysts prepared were observed by SEM with a JEOL JSM-35C scanning microscope operated at an acceleration voltage of 15 KV. A small portion of each sample powder was coated on a metallic disk holder and covered with a thin gold layer before SEM analysis.

ii. Environmental electronic scanning microscopy (ESEM-EDX)

An alternative approach to overcoming the specimen-charging problem is to surround the specimen with a gaseous ambient rather than high vacuum. The modified equipment is called environmental SEM. In this situation, the primary electrons ionize gas molecules before reaching the specimen. If the specimen charges negatively, positive ions are attracted toward it, largely neutralizing the surface charge. In an environmental SEM (also called a low-vacuum SEM), primary electrons encounter gas molecules only during the last few mm of their journey, after being focused by the objective lens. Of course, there must still be a good vacuum within the SEM column in order to allow the operation of a thermionic or field emission source, to enable a high voltage to be used to accelerate the electrons and to permit the focusing of electrons without scattering from gas molecules. A small-diameter aperture in the bore of the objective allows the electrons to pass through but prevents most gas molecules from travelling up the SEM column. Those that do so are removed by continuous pumping. The environmental chamber extends the range of materials that can be examined

by SEM and avoids the need for coating the specimen to make it conducting. The main drawback to ionizing gas molecules during the final phase of their journey is that the primary electrons are scattered and deflected from their original path. This effect adds an additional skirt (tail) to the current-density distribution of the electron probe, degrading the image resolution and contrast. Therefore, an environmental SEM would usually be operated as a high-vacuum SEM (by turning off the gas supply) in the case of conductive specimens that do not have a high vapour pressure.

iii. *Energy Dispersive X-Ray Spectroscopy (EDS or EDX)*

Energy Dispersive X-Ray Spectroscopy (EDS or EDX) is a chemical microanalysis technique used in conjunction with scanning electron microscopy (SEM). The EDS technique detects x-rays emitted from the sample during bombardment by an electron beam to characterize the elemental composition of the analyzed volume. The excited atom will decay to its ground state by emitting either a characteristic X-ray photon or an Auger electron. The x-ray energy is characteristic of the element from which it was emitted. The EDS x-ray detector measures the relative abundance of emitted x-rays versus their energy. The detector is typically a lithium-drifted silicon, solid-state device. The spectrum of x-ray energy versus counts is evaluated to determine the elemental composition of the sampled volume. The minimum detection limits vary from approximately 0.1 to a few atom percent, depending on the element and the sample matrix. Quantitative results can be obtained from the relative x-ray counts at the characteristic energy levels for the sample constituents. Semi-quantitative results are readily available without standards by using mathematical corrections based on the analysis parameters and the sample composition. Elemental Mapping characteristic x-ray intensity is measured relative to lateral position on the sample. Variations in x-ray intensity at any characteristic energy value indicate the relative concentration for the applicable element across the surface. Analysis of the x-ray energy spectrum at each position provides plots of the relative elemental concentration for each element versus position along the line.

Instrumentation

Environmental scanning electron microscopy analysis (ESEM) combined with energy dispersive spectroscopy (EDS) analysis of the catalysts placed on metallic support was carried out in a FEI QUANTA 6000 scanning microscope operating at an accelerating voltage of 20 kV with 10 mm of working distance (WD) sample.

iv. Transmission electron Microscopy

A transmission electron microscope (TEM) is like an optical microscope in which the optical lenses have been replaced by electromagnetic ones. An electron beam hits the sample, and the transmitted electrons are magnified by the electromagnetic lenses. The optics brings the scattered electrons from the same point in the sample to the same point in the image (the so-called bright-field image). Higher-energy electrons with an accelerating potential of 50 kV can penetrate distances of several microns into a solid. If the solid is crystalline, the electrons are diffracted by atomic planes inside the material as in the case of x-rays. It is therefore possible to form a transmission electron diffraction patterns from electrons that have passed through a thin specimen, as first demonstrated by G.P. Thomson (1927). Modern TEMs use an electron accelerating voltage between 100 kV and 300 kV, a few high-voltage instruments (HVEMs) have been constructed with accelerating voltages as high as 3 MV. However, technical problems of voltage stabilization have prevented HVEMs from achieving their theoretical resolution. Later it was realized that if these transmitted electrons could be focused, their very short wavelength would allow the specimen to be imaged with a spatial resolution much better than the light-optical microscope. As a result, TEM is well known technique for imaging supported catalysts with an atomic size resolution. Catalytic samples can be prepared first by suspending the supported catalysts in any of volatile solvents like methanol, ethanol or toluene. Ultra-sonication of the suspended catalyst can also be used to achieve fine particles, with thin layers. A drop of this suspension is deposited in a carbon coated copper grid and the solvent is evaporated.

It determines the size, distribution and shape of metal particles (supported or unsupported) to the level of atomic resolution. A conventional

TEM can magnify ×300,000 with a resolution of 0.5nm, whereas as high-resolution apparatus can magnify ×1,000,000 giving atomic resolution. The contrasts in the image reflect the different scattering processes and the interactions between the transmitted electrons and different atoms in the sample (typically, the metal has a much higher electron density than the support, and appears darker in the TEM image). Thus, supported metal particles appear as dark spots, while the support itself appears as a lighter background [141, 143].

Since electrons are very small and easily deflected by hydrocarbons or gas molecules, it is necessary to use the electron beam in a vacuum environment. A series of pumps are used to accomplish an adequate vacuum for this purpose. One limitation of the TEM is that, unless the sample is made very thin, electrons are strongly scattered within the specimen, or even absorbed rather than transmitted. Therefore, sample preparation of the TEM analysis should be done carefully.

Instrumentation

High-Resolution Transmission Electron Microscopy (HRTEM) was carried out at 200 kV with a JEOL JEM 2100 instrument equipped with a LaB_6 source. The point-to-point resolution of the microscope was 0.20 nm. Samples were deposited on holey-carbon-coated Cu grids from alcohol suspensions. For each sample, particle-size distribution histograms were obtained. Transmission electron microscopy (TEM), operated at 80kV (JEOL JEM-2000EX II) was taken to analyze the morphology and dispersion of our catalysts. Samples were dispersed in alcohol in an ultrasonic bath and a drop of supernatant suspension was poured onto a holey carbon-coated grid and dried completely before the measurements were taken. About 90–250 individual particles were used in each sample for particle size distribution study.

3.2.1.4. Atomic absorption spectroscopy

Atomic absorption analysis involves measuring the absorption of light (ultraviolet or visible) radiation by vaporized ground state atoms and relating the absorption to concentration. These free atoms are produced by

nebulizing a solution in a flame (acetylene/oxygen) and are detected when they absorb light from a hollow cathode discharge lamp. The lamp emits discrete wavelengths (lines), which are specifically absorbed by a particular atom; *thus*, one needs a different hollow cathode lamp for each species to be monitored. This gives the AA process a great deal of specificity, but at the expense of acquiring many lamps and changing them when a different atom is to be studied. The sample should be in a liquid phase in order to atomize completely the given metals. Solid samples (inorganic catalysts) thus first digested by using concentrated nitric acid and microwave digester to obtain a homogeneous and total dilution of the metal to the solution can be achieved.

Instrumentation

The chemical composition of the samples was determined by ICP-OES with a Perkin-Elmer Plasma 400 instrument and by atomic absorption spectroscopy (AAS) with a Perkin-Elmer Plasma 400 instrument.

3.2.1.5. Fourrier transform Infrared spectroscopy

Infrared (IR) spectroscopy is the most widely used technique for studying the surface chemistry of heterogeneous catalysts. It can give information about the catalyst structure, as well as about the species adsorbed on the catalyst surface. By using probe molecules like CO, NO and NH_3, information is obtained about the nature and environment of atoms and ions exposed on the surface. The method is based on the absorption, transmission, or reflection by a catalyst of infrared radiation; this excites molecular vibrations. IR spectroscopy of solid catalysts can be performed either by transmission of the IR beam through a thin section of the solid, or by its reflection from the surface. The energy of these vibrations depends on the nature and bonding of the molecules. The vibrational frequencies of surface groups and probe molecules are identified by comparing their "fingerprints" with literature databases. IR spectroscopy has two important advantages: It is non-destructive and non-invasive, and it can be adapted to measurements at high temperatures and pressures. This means that IR studies can be done under real process conditions, and even, with today's advanced computers, using on-line analysis. By using reactive probe molecules, you can qualify and quantify the type and number of active sites. For example,

pyridine vapour is used for titrating Brønsted acid sites on solids, and the changes in the acid absorption bands are easily monitored using diffuse-reflectance infrared Fourier-transform spectroscopy (DRIFTS). IR spectroscopy can even be used for detecting the way that molecules are adsorbed on the catalyst surface. CO, for example, can form different adcomplexes on metal surfaces: linear (M-CO, μ_1, 2000–2130 cm^{-1}); bridged between two metal atoms ((M_2)-CO, μ_2, 1860–2000 cm^{-1}); triply bridged ((M_3)-CO, μ_3,1800–1920 cm^{-1}); and even quadruple bridged ((M_4)-CO, μ_4, 1650–1800 cm^{-1}). The linear configuration is common for most group VII metals, while bridged configurations are found more with group VIII metals.

Instrumentation

The Fourier transformed infrared (FT-IR) spectra were recorded on a Bruker IFS 28 instrument with a resolution of 4cm^{-1}. The spectrometer cell is connected to a vacuum system working in the 10-6 mbar range and to a heating system. The cell can be used for in situ pre-treatments of samples and adsorption of gases. The samples were pressed into self-supporting wafers that were placed inside a ring furnace in the vacuum cell. The catalysts were reduced in situ using 500 mbar of pure H_2. The catalysts were heated until 573 K in hydrogen atmosphere using a temperature ramp of 10ºC/min and kept at that temperature for 30 min. After the reduction, the cell was evacuated for 30 min. The CO adsorption measurements were carried out using 5mbar of pure CO.

3.2.1.6. Photoluminescence spectroscopy (PL)

When light of sufficient energy is incident on a material, photons are absorbed and electronic excitations are created. Eventually, these excitations relax and the electrons return to the ground state. If radiative relaxation occurs, the emitted light is called Photo luminescence. This light can be collected and analyzed to yield a wealth of information about the photo-excited material [144-147]. The PL spectrum provides the transition energies, which can be used to determine electronic energy levels. The PL intensity gives a measure of the relative rates of radiative and non-radiative recombination. Variation of the PL intensity with external parameters like temperature and applied voltage can be used to characterize further the

underlying electronic states and bands [147]. In catalysis, Because PL often originates near the surface of a material; PL analysis is an important tool in the characterization of surfaces. The utility of PL for this purpose is derived from its unique sensitivity to discrete electronic states, many of which lie near surfaces and interfaces at low metal loading. Using the techniques noted above, the nature of these states can be probed in detail. The energy distribution and density of interface states can be ascertained by studying the excitation intensity dependence of the PL spectrum. The presence of surface adsorbate alters the intensity of the PL signal. As a result, PL techniques can be used to characterize acidic and basic sites by means of probe molecules, as well as various materials used in catalysis and electroluminescence, including a consideration of future directions of research involving PL spectroscopy [145-147].

Instrumentation

Photoluminescence and UV diffuse reflectance measurements were carried out at room temperature using quartz glass cells kept under vacuum ($p < 10^{-5}$mbar). The UV diffuse reflectance spectra were acquired using a Edinburgh instruments spectrometer (FSP920) with a Xenon arc-lamp, double grating monochromators and a photomultipliers tube.

3.2.2. Adsorption techniques

Adsorption method can be used to provide information about the total surface area of the catalysts, the surface area of the phase carrying the active sites or possibly even the type and number of active sites. The interaction between the adsorbate and the adsorbent may be chemical (chemisorption) or physical (physisorption) in nature and ideally should be a surface specific interaction [148].

3.2.2.1. Physisorption Techniques

This technique is widely used to determine the surface physical properties. Porosity, surface area, Pore size distribution, average pore volume are the main parameters that can be determined using N_2-physisorption analysis [148-151]. Physisorption (physical adsorption) is

adsorption in which the forces involved are intermolecular forces of the same kind as those responsible for the imperfection of real gases and the condensation of vapours, and which do not involve a significant change in the electronic orbital patterns of the species involved. The forces responsible for the physisorption depend on the molecule in question and on the chemical nature of the surface. But they are of the some kind as those that hold molecules together in liquids, and are collectively described as Van der Waals forces, comprising dipole-dipole interactions, induced dipole charges, London forces due to mutually-induced fluctuating dipoles and nuclear quadruple forces [150-152]. Molecules of gas adsorbed to solid surface are a function of their partial pressure of the bulk. The measurement of the amount of gas adsorbed over a range of partial pressures at a single temperature results a graph known as an adsorption isotherm.

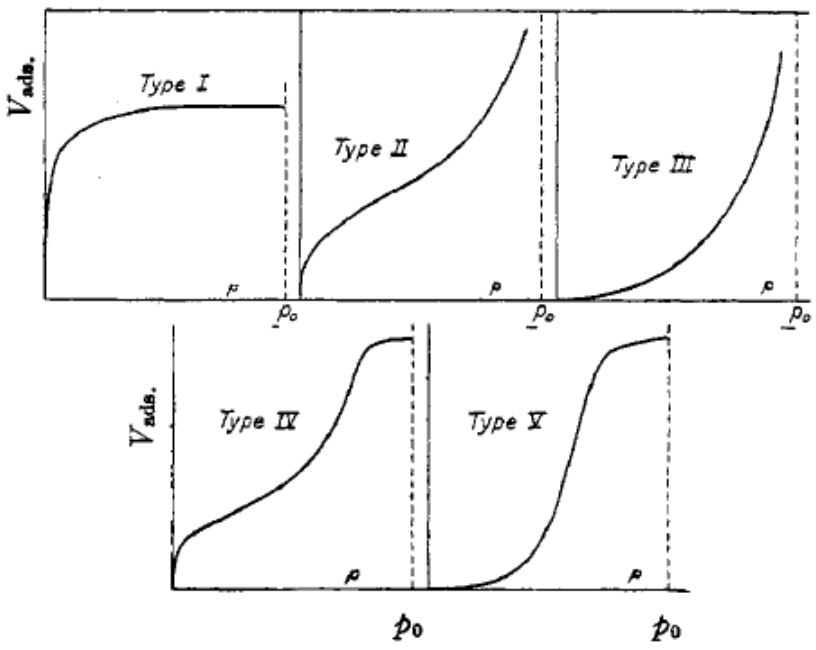

Fig. 2 The five types of Van der Waals adsorption isotherms [152].

In 1940, Brunauer et.al.[152] *p*roposed to classify the physical adsorption isotherms in five different groups numbered from type *I* to type *V* as shown in Fig 2. To give an example of each type we may mention the adsorption of oxygen on charcoal at -183^{o}C (Type I), nitrogen on iron

catalysts at -195 ^{o}C (Type II), bromine on silica gel at 79^{o}C (Type III), benzene on ferric oxide gel at 50^{o}C (Type IV), and water vapour on charcoal at 100^{o}C (Type V). Type I is the well-known Langmuir adsorption isotherm, Type II is the S-shaped or sigmoid isotherm. Types II and III are closely related to Types IV and V, only in the former cases the adsorption increases as the vapour pressure P*a* of the adsorbed gas is approached, whereas in the latter cases the maximum adsorption is attained, or almost attained, at some pressure lower than the vapour pressure of the gas. Many other types of adsorption isotherms are observed by different literatures afterwards. These isotherms can have different shapes depending on the type of adsorbents, the type of adsorbate and the intermolecular interactions among the gas and the solid surface. Sometimes, however, an isotherm cannot be related to one definite group of this classification because different types of pores are present in the adsorbent. These "mixed" isotherms are also indicative of the general porosity of the solid. Another easy way to get information on the porous texture of the adsorbent is to look the shape of the hysteresis loop. The presence of a hysteresis loop into five main groups has been proposed by Boer [153]. Each group is related to the general shape of the pores present in the solid, as illustrated.

- ✓ *Type A hysteresis* is associated with "cylinder shaped" pores of rather constant cross section.
- ✓ *Type B hysteresis* points to the presence of slit-shaped pores.
- ✓ *Type C and D hysteresis* derive from the type *A* and *B* respectively and formed the non-parallel plates (type *D*). These two types of hysteresis loops are rather unusual.
- ✓ *Type E hysteresis* very frequently occurs. It corresponds to "inkbottle" pores, spherical cavities or voids between close-packed spherical-like particles.

The main reason for these differences in the isotherms is the existence of real solids of a more and less broad pore size distribution whereas the models used are based on ideal solids where all pores have the same size. In general, the broader pore size distribution the wider the hysteresis loops [151]. Furthermore, "mixed" hysteresis loop may often observed if different pore shapes are present in the same solid. Since the publication, in 1938, by Brunauer, Emmett and Teller [149] of their famous

model for physical adsorption of vapours on solid, the BET theory and its use as a toll for determination of specific surface area of solids have formed the subject of many papers, reviews and books. Several authors have critically discussed the limitations and the range of applicability of the BET model [151]. The BET equation is more conveniently written in the following form:

$$\frac{X}{V_a(1-x)} = \frac{1}{V_m C} + \frac{C-1}{V_m C}$$

Where V_a is the adsorbed volume of the adsorbate per unit mass of adsorbent, V_m is the volume of adsorbate just sufficient to cover the surface developed by unit of mass of adsorbent, x is the relative pressure P/P_0, c is a constant varying with the adsorbent-adsorbate interactions. The V_m value is directly proportional to the specific surface area of the adsorbent, because V_m is, by definition, the amount of adsorbate just sufficient to cover with a complete monolayer the whole surface developed by the unit mass of adsorbent. The specific surface are thus can be calculated using the following equation:

$$s = a_m v_m \frac{N_a}{V_m}$$

Where s is the specific surface area, v_m is the monolayer capacity of unit mass of solid, N_a is the Avogadro constant, V_m is the molar volume of adsorbate and a_m is the part of surface occupied by one molecule of adsorbate in a closed layer. In the case of nitrogen adsorption at liquid nitrogen temperature (77 K) the most widely admitted and used value of the area occupied by a nitrogen molecule is: $a_m(N_2)=16.2 \times 10^{-20}$ m^2. Pore size distribution can be calculated using the Barrett-Joyner-Halenda (BJH) equation method. BJH calculating pore size distributions is based on a model of the adsorbent as a collection of cylindrical pores. The theory accounts for capillary condensation in the pores using the classical Kelvin equation, which in turn assumes a hemispherical liquid-vapour meniscus and a well-defined surface tension [150, 154].

Instrumentation

N_2 physisorption adsorption-desorption isotherms at 77K was measured using Micromeritics ASAP 2000 surface analyzer and Specific

surface areas and pore volume were calculated using the BET method. Prior to the physisorption measurements, all the samples were degassed in vacuum (10^{-4}Pa) at 393K.

3.2.2.2. *Chemisorption Techniques*

Many heterogeneous catalysts comprise an active component deposited on a support. In order to investigate relationships between catalytic properties and the amount of active sites, it is necessary to have means of determining the surface area of the phase carrying the active sites (active phase). The main purpose of the chemisorption methods is to evaluate the number of active sites that can be reached or that can interact with a substrate. These techniques are based on a chemical reaction between a suitable reactive gas and the surface reactive site. A wide variety of adsorbates have been used, the choice depending on the nature of the surface to be examined and the type of information being pursued. For instance, for metals H_2, CO, O_2, N_2O, for sulfides NO, CO, O_2, H_2S and for oxides NH_3, CO_2, and various organic compounds, have been performed. [148]

There are different methods to perform the above operation: the static volumetric, the static gravimetric or the flow methods. In the volumetric method, the sample is kept under high vacuum before the analysis. The analytical instrument then introduces known doses of reactive gas into the sample holder, measuring afterwards the equilibrium pressure that will be established between the sample and the gaseous phase. The pressure range should be chosen in order to complete the adsorption isotherm covering a monolayer of reacted molecules over the sample. The pressure range therefore depends on the catalyst/adsorbate nature and the analysis temperature. Most of catalytic systems analyzed around room temperature show the monolayer covering below 100 torr equilibrium pressure. The advantage of the static method is that the system catalyst/adsorbate reaches the real equilibrium conditions. Furthermore, it is possible to distinguish in a quantitative way the amount of gas strongly bound to the active sites and weakly bound to the support. On the contrary, the static volumetric method requires high vacuum system, long lasting measurements, and generally higher instrumentation costs. What is measured is the total number of accessible surface atoms, which not necessarily equal to the number of

catalytic sites in a given reaction. The dispersion *D* of the metal ($D \leq 1$) is defined as the ratio of the number of surface metal atoms to the total number of metal atoms in the sample. Dispersion is also expressed as percentage. According to IUPAC rules, the expression "*percentage exposed*" should be preferred over the word dispersion. The most common adsorptive used in the selective chemisorption are H_2, CO, O_2, and N_2O. From the catalysis point of view, the percentage exposed is the most direct and pertinent measurement. If part of the metal surface is poisoned, the percentage exposed may correlate directly the catalytic activity although particle size translated into dispersion would not be a useful quantity. In typical hydrogen adsorption, experiment the metallic catalyst is first contacted with flowing hydrogen in the adsorption cell at appropriate temperature to ensure thorough reduction. The cell is then evacuated and cooled to room temperature for the determination of total adsorption. When this isotherm is completed, the weakly adsorbed hydrogen is removed from the sample by evacuating the adsorption cell at room temperature to a pressure approximately 10^{-6} torr. A second isotherm is then run at room temperature. This isotherm constitutes the weakly adsorbed hydrogen. The difference between the total adsorption and the weakly adsorbed hydrogen is strongly chemisorbed hydrogen. From the volume of the total hydrogen adsorption and the irreversible adsorption one can determine the dispersion, D. In hydrogen chemisorption on the Group VIII metals, it is generally accepted that the hydrogen molecule dissociates, so that hydrogen atoms are adsorbed on the surface. Typical data on the chemisorption of hydrogen on room temperature on platinum on alumina catalyst are show in Figure.

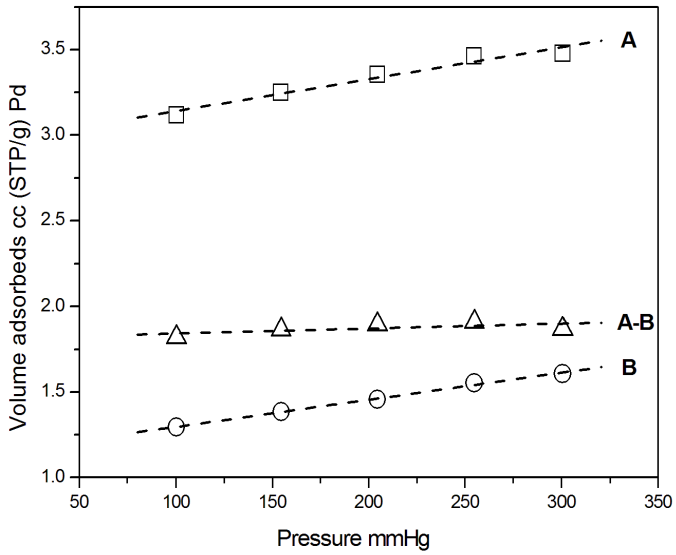

Fig. 3 Typical hydrogen chemisorption at 373 K temperature on a Pd/HT catalyst containing 1 wt% palladium.

Isotherm A represents the total chemisorption, and isotherm B represents the weakly chemisorbed fraction, since it is removed by simple evacuation at room temperature. Isotherm B includes adsorption on the alumina carrier. The difference isotherm, labeled A-B, is obtained by subtracting isotherm B from A and is independent of pressure over the range of pressures used in obtaining the isotherm. It represents the strongly chemisorbed fraction, that is, the amount that cannot be removed by evacuation at room temperature. The quantity *H/M* represents the ratio of the number *H* of hydrogen atoms adsorbed to the number *M* of metal atoms in the catalyst. If we assume a stoichiometry of one hydrogen atom per surface metal atom in the case of strongly chemisorbed fraction, the value of H/M determined from the difference isotherm A-B corresponds to the ratio of surface platinum atoms to total platinum atoms in the catalyst. If a comparison with results from physical techniques is wanted, or just out of habit of dealing with particle size, a handy conversion between dispersion *D* and particle size *d*, in nm, is given by: $D \approx 0.9/d$ or more simply $D = 1/d$, (d in nm). More rigorous determination of the particle size should take into

account the shape of the particle. In this case, the average particle size *d* is obtained by means of:

$$d = \frac{f v_{sp}}{s_m}$$

Where S_m is the specific surface area of the metal obtained from the selective chemisorption data by assuming an average number density, V_{sp} is the specific volume of the metal and *f* is the shape factor of small particles of metal on supports.

Instrumentation

The chemisorption analysis was performed under static volumetric conditions with a Micromeritics ASAP 2010 apparatus. Prior to the measurement, the sample was evacuated at 373 K for 1 hour, treated in flow pure hydrogen (30 cm^3min^{-1}) at 623 K for 3 hours, evacuated at 623 K for 1 hour, cool down to 373 K and evacuated 30 minutes. Finally the chemisorption analysis was performed at 373 K. The double isotherm method was used to determine the amount of irreversible adsorbed hydrogen which allows calculating the apparent metallic dispersion (H/Pd) assuming an adsorption stoichiometry of H:Pd = 1:1. From the first isotherm the total volume of hydrogen adsorbed was obtained. The sample was evacuated (about 10^{-6} Torr) again at the chemisorption analysis temperature for 10 minutes for back sorption measurements in order to obtain the volume of hydrogen reversibly adsorbed. The linear zone of each isotherm was extrapolated to zero pressure in order to estimate the volume of the strong hydrogen adsorbed.

3.2.2.3. Temperature programmed desorption (TPD)

Temperature programmed desorption (TPD), which is also referred to us thermal desorption spectroscopy (TDS), can be used in technical catalysis but is particularly used on surface science. TPD was reported by Amonomiya and Cvetanovic [144, 155] in 1963 called the flash desorption technique to the study ethene-alumina and propylene-alumina systems as a continuation in the series of studies of olefin-alumina systems by this technique. Nowadays,

Temperature-programmed desorption (TPD) is extensively applied for catalyst characterization. Unlike temperature programmed reaction technique, TPD detects molecules physically adsorbed over surfaces. In TPD studies, a solid previously equilibrated with an adsorbing gas is submitted to a programmed temperature rise and the amount of desorbing gas is continuously monitored, i.e. diluted reactive gases CO_2/He or NH_3/He are adsorbed over the oxide surfaces and subsequently desorbed by an inert gas at constant rate of temperature. Commonly used probing molecules are NH_3, H_2, and CO_2. Acidity of a certain oxide surface can be easily probed using NH_3 while CO_2 can be used to determine the basic sites. H2 can also adsorb physically over hydrogenation metal. From the desorption pattern much useful information can be obtained. TPD is used to characterize adsorption states and to determine the kinetics of desorption. Qualitatively TPD can be interpreted simply because the higher the desorption temperature the more strongly is the adsorbate bonded to the surface. Since the area under a TPD curve is proportional to the coverage, TPD spectra allow determination of relative coverage. TPD is used to determine:

a) type, strength and number of surface active sites like acidity and basicity
b) Temperature range of adsorbate release, temperatures of rate maxima
c) Total desorbed amount, adsorption capacity, metal surface area and dispersion
d) Surface energetic heterogeneity, binding states and energies of adsorbed molecules
e) Mechanism and kinetics of adsorption and desorption

Instrumentation

The basic properties of the materials were characterized by TPD of CO_2 using a ThermoFinnigan (TPORD 110) apparatus equipped with a programmable temperature furnace and a TCD detector. Typically, 20 mg of catalyst was placed between plugs of quartz wool in a quartz reactor. The sample was first purged using pure He (flowing at 20 cm^3/min^{-1}) at 393 K for 30 min. After the temperature was cooled to room temperature, CO_2/He (3/97, vol/vol%) mixture was contacted with the sample (flowing at 20 cm^3 min^{-1}). The temperature was raised to 353K with a rate of 20 K/min and kept at 353 K for 60 min. Then the weakly adsorbed CO_2 was then purged using

He at 353 K for 30 min. The CO_2 desorption was then started by heating the sample from 300 to 1123 K at 10 K min^{-1} in He flow (20 cm^3 min^{-1}). Magnesium perchlorate was used as a trap for water. The amount of basic sites i.e. total CO_2 desorbed (cm^3/g) was calculated from the CO_2 peaks by deconvolution using the TPD/R/O software of the equipment, and the equipment was calibrated using different known amounts of $CaCO_3$.

3.2.3. Temperature programmed technique

Temperature-programmed (TP) techniques measure the reactivity of a solid as a function of the temperature under controlled conditions. The temperature at which species interact, physically or chemically, on the surface reflects the bond strength of this species. Different chemical species interact at different temperatures, displaying distinct maxima in the Temperature programmed profile. The most common temperature programmed techniques are Temperature Programmed Desorption (TPD), Temperature Programmed Reduction (TPR), and Temperature Programmed Oxidation (TPO).

Diluted reactive gases like H_2/Ar, O_2/He, CO_2/He, NH_3/He depending on the method, is pumped over the catalyst while the temperature is increased. As the temperature rises, the reactant consumption and/or the product formation, reactant desorption are measured. This is often done, by comparing the thermal conductivity of the gas before and after the reactor, using a thermal conductivity detector (TCD). Alternatively, one can determine the composition of the gas phase at the reactor exit using gas chromatography, mass spectrometry (MS), or other methods.

3.2.3.1. Temperature programmed reaction

Temperature programmed reaction methods include Temperature Programmed Reduction (TPR), and Temperature Programmed Oxidation (TPO). They are techniques in which a chemical reaction is monitored while the temperature is increased linearly in time. The equipment for these investigations is relatively simple. The catalyst is placed in a tubular reactor, for example in case of TPR, the oxide supported catalyst is reduced in a flow of inert gas, usually Ar or N_2 containing a few percentage (5%) of H_2. The

off-gases are continuously monitored by a thermal conductivity detector or mass spectrometer and the consumption of hydrogen is recorded as a function of the reaction temperature. The complete reduction of a catalyst can be determined by TPR method. Integration of the H_2 consumption signal allows the determination of the total amount of hydrogen used to titrate the reactive oxygen in the catalyst and is expressed in moles of H_2 per g of metal atoms. TPO is an equally valid technique to determine the amount of reduced species in catalyst material. The experimental setup of TPO equipment is identical to that of a TPR. Therefore, both techniques can easily be combined. TPR measurement can give information such as:

a) Redox properties of materials, "fingerprint" of sample
b) Temperature range of consumption of reducing agent, rate maxima
c) Total consumption of reducing agent
d) Interaction between metal oxide and support
e) Indication of alloy formation in bimetallic catalysts
f) Mechanism and kinetics of reduction

TPO profile can give information like

a) Redox properties of metals and metal oxides
b) Characterization of coke species in deactivated catalysts
c) Total coke content in deactivated catalysts
d) Mechanism and kinetics of oxidation reactions

Instrumentation

The reducibility of fresh catalysts was determined by TPR. The temperature programmed reduction studies were performed in a ThermoFinnigan (TPORD 110) apparatus equipped with a thermal conductivity detector (TCD). The samples were then purged with argon flow before the TPR analysis. The analysis was carried out using a 3% H_2/Ar gas flowing at 20 ml min^{-1} by heating from room temperature to 1173K with a ramp of 10 K min^{-1}. Water produced during TPR was trapped in CaO + Na_2O (Soda lime) before reaching the TCD.

Temperature programmed desorption and oxidation (TPDO/MS) was performed for used catalysts in order to observe adsorbed species. It was carried out for spent catalysts (washed with ethanol) in ThermoFinnigan (TPORD 110) apparatus equipped with a thermal conductivity detector (TCD). Previously we have seen that no effect in reactivation of the spent catalyst by washing with ethanol. Before analysis the catalysts were pretreated using He-TPD/MS heating from room temperature to 623 K at 20 K min-1 and maintained for 30 minutes at this temperature to remove ethanol and other species. Then the sample was cooled to room temperature and TPO/MS analysis was carried out.

3.2.3.2. Thermogravimetric analysis

Thermoanalytical techniques can be considered as transient response techniques, in which some characteristic property of a solid sample is related to its temperature in a process of programmed heating. In particular, thermogravimeteric analysis involves the amount or the rate of weight change in a material as a function of temperature or time in a controlled atmosphere. Thermogravimetric Analysis (TGA) is a widely used analytical method for determining changes in the mass of a material as a function of temperature. It provides a measure of the reaction kinetics associated with structural decomposition, oxidation, corrosion, and moisture adsorption/desorption, and gas evolution. One application include for the characterization of used catalysts in order to determine for example amount of coke, or hydration or carbonation etc.

Instrumentation

Thermogravimetric Analysis (TGA), were performed in order to quantify the amount of carbonaceous deposits for the spent catalysts after hydrodechlorination reaction at 473 K. Thermogravimetric analyses (TGA) was carried out on a Perkin-Elmer TGA 7 microbalance with an accuracy of ±1 μg which was equipped an automatically programmed temperature controller. Prior to analysis the catalysts were treated with Argon (20 ml min^{-1}) heating at 5 $Kmin^{-1}$ from room temperature to 1173 K and then cooled down again to room temperature. This step was adopted to eliminate all inorganic carbon (carbonate) species. In the sequence the sample was heated

up to 1173 K in oxygen flow (5 $Kmin^{-1}$, 20 ml min^{-1}) and the weight loss was recorded

3.3. Catalytic test

The catalytic activities were employed using a plug flow reactor. The plug flow reactor was made of a glass (Pyrex or quartz) tube with a sintered disc or quartz wool for supporting the solid catalyst, either alone or mixed with an inert diluents solid. One or several thermo wells are located in the reactor to monitor the catalyst bed temperature. It is convenient to use thermocouples sliding inside thermo wells to monitor axial or longitudinal temperature gradients. The reactants and any diluents gas are brought to a temperature close to that of the catalyst before passing through the catalyst bed. At the outlet of the reactor the reaction products are sampled, either as gases, liquids, or combinations of the two and analyzed, usually by gas chromatography and/or by mass spectrometry.

The suitability of a catalyst for an industrial process depends mainly on the following three properties: Activity, Selectivity, Stability (deactivation behaviour). One of the parameters used to determine the activity of catalysts is called conversion. The conversion is the ratio of the amount of reactant that has reacted to the amount that was introduced into the reactor. It is expressed as

$$Conversion(\%) = \left(\frac{N_{reacted}}{N_{feed}}\right) \times 100$$

Where $N_{reacted}$ is assigned to number of moles of reacted substrate and N_{feed} expresses number of moles of the substrate. The space velocity (τ) is the volume flow rate, relative to the catalyst mass:

$$\tau = \frac{v}{m}$$

Where *v* is the liquid substrate flow rate (ml/min) and *m* represent the amount of catalyst (g). The selectivity towards a certain product (*S*p) of a reaction is the fraction of the starting material that is converted to the desired

product p. It is expressed by the ratio of the amount of desired product to the reacted quantity of a reaction partner and therefore gives information about the course of the reaction.

$$Sp = \left(\frac{N_{p1}}{N_{p1} + N_{p2} + N_{p3} \ldots + N_{pn}} \right) \times 100$$

Where N_{p1} is number of moles of the specific product *p1*. The chemical, thermal, and mechanical stability of a catalyst determines its lifetime in industrial reactors. Catalyst stability is influenced by numerous factors, including decomposition, coking, and poisoning. Catalyst deactivation can be followed by measuring activity or selectivity as a function of time. Catalysts that lose activity during a process can often be regenerated before they ultimately have to be replaced. The total catalyst lifetime is of crucial importance for the economics of a process. Alternative parameters also also used to express the the catalytic activity. For instance, the activity of a catalyst was expressed in terms of mol of the 1,2,4-TCB converted per exposed Pd surface area (from hydrogen chemisorption results), or total basic sites (CO_2-temperature programmed desorption experiment) in the support.

$$TOF = \frac{X_{TCB}(mmol\ of\ TCB)}{Hydrogen\ uptake\ (\frac{cm^3}{g})}$$

3.3.1. Catalytic setup for HDC of 1,2,4-trichlorobenzene

The sample feed contains 4 v/v% solution of 1,2,4-trichlorobenzene (98.5%, Sdl) in hexadecane (99%, Sigma Aldrich). Hydrodechlorination of 1,2,4-trichlorobenzene was carried out in 50 ml continuous glass micro reactor (Afora, V-53255), which was connected to the continuously flowing hydrogen gas and the liquid, feed on the top and a product collector at the bottom. The molar ratio of H_2/1,2,4-trichlorobenzene was maintained constant at 180 for all reaction. The catalyst (250 mg) used in each experiment was reduced in situ with hydrogen gas at 623 K prior to the reaction. Reactions were studied in temperature range of 323-523 K and a pressure of 1bar. The space velocity used was varied according to the

materials compared. The product collector was located at the bottom of the reactor with two containers assigned, one to collect the liquid products and the other, contains NaOH solution, to trap the HCl produced. The products were subjected to a GC (schimadzu) equipped with flame ionization detector and capillary column (I.D. of 30 m×0.032 mm operating between 353-573 K). In addition GC/MS was used to determine the obtained products. The set up is displayed in Fig. 4.

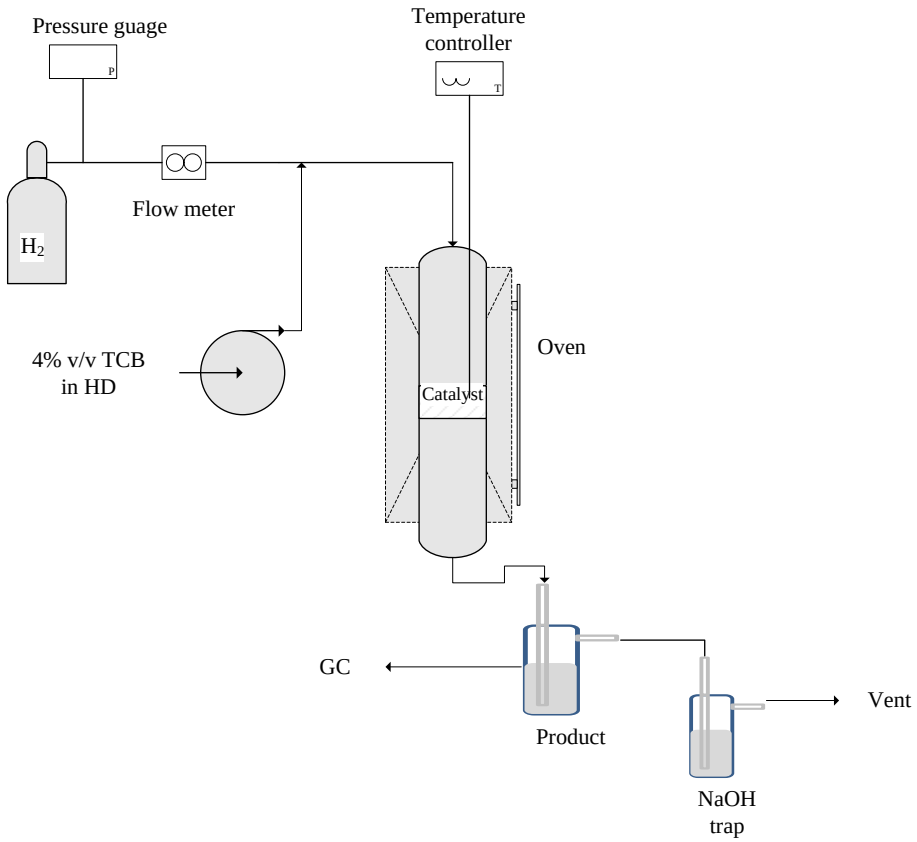

Fig. 4 1,2,4-trichlorobenzene hydrodechlorination experimental setup.

3.3.2. Catalytic setup for HDC of trichloroethylene

The catalysts were tested for gas-phase hydrodechlorination reaction of trichloroethene (TCE) using a continuous fixed-bed glass reactor at appropriate temperature and atmospheric pressure as stated in [127]. The gas

feed is obtained by flowing an inert gas (He) and hydrogen through a saturator kept at 298K by a thermostat, containing trichloroethylene (TCE) in liquid phase. The TCE partial pressure of 92 mbar was achieved. The molar ratio of H_2/TCE was maintained at stoichiometric amount. The gas flows are adjusted by mass flow controllers (Brooks Instrument 0154) and introduced into the reactor, which is placed in a furnace coupled with a temperature controlling system. The outlet of the reactor is connected by a six-way valve to a gas chromatograph (HP 5890 series II, HP Poraplot column, FID). Catalytic conversion and selectivity were calculated by analyzing the peak areas of TCE and the respective products. For some catalysts, different space velocity was used to achieve lower conversion levels maintaining similar H_2/TCE molar ratio. The set up is displayed in Fig. 5.

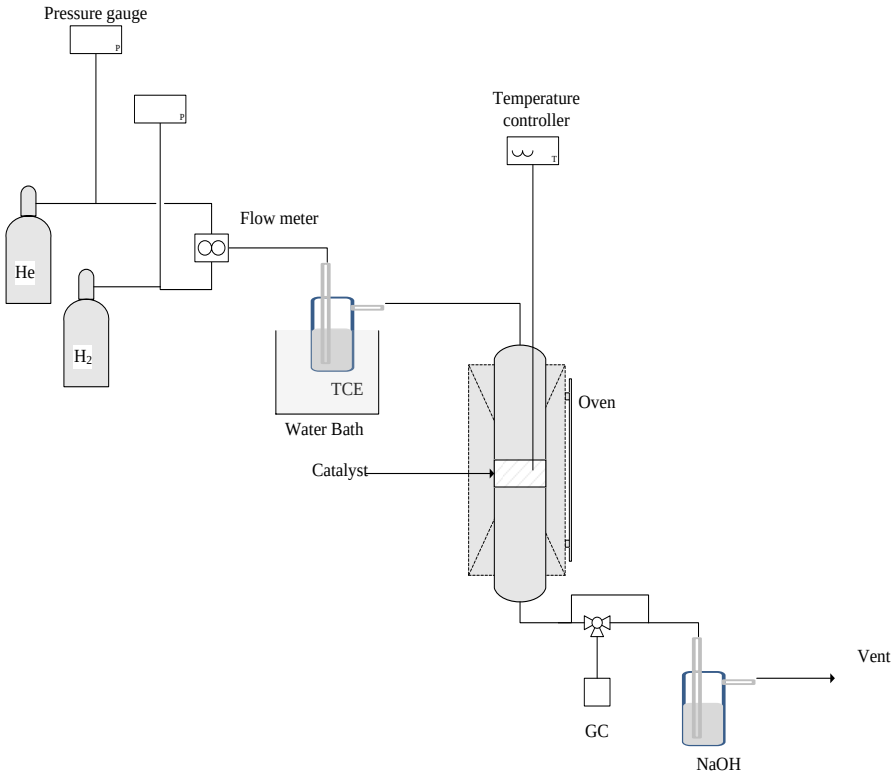

Fig. 5 TCE Hydrodechlorination experimental setup.

4.

Results and Discussion

UNIVERSITAT ROVIRA I VIRGILI
HYDRODECHLORINATION OF CHLORINATED ORGANIC WASTES OVER PD SUPPORTED MIXED OXIDE CATALYSTS
Beteley Tekola Meshesha
DL: T.1347-2011

4.1.

Catalytic HDC of 1,2,4-trichlorobenzene over Pd/Mg(Al)O catalysts

Catalytic hydrodechlorination is a promising technology for removal of chlorinated organic wastes. It can be effectively catalyzed using noble metal catalysts. Particularly Pd has been regarded as the most active and less prone to deactivation. The characteristic of catalytic HDC reaction is the occurrence of fast deactivation, observed with most substrates. Catalytic decay in gas-phase hydrodechlorination has been linked to different phenomena such as poisoning of the active phase by the HCl formed in the reaction [49, 53, 54, 156], particle sintering [55], and coke deposition [56, 57]. Particle sintering and coke formation are expected to be affected by the choice of the support. Basic supports have scarcely been used for dechlorination, probably because they were expected to be neutralized by the HCl produced by the reaction. An increase of the electron density at the surface induced by the support should decrease the adsorption of chloride which is an electro-donor. Moreover, coke formation catalyzed by acid-base mechanisms should also be

affected. In general, the effect on deactivation is also expected to change by utilization of basic supports. Another characteristic of catalytic HDC reaction is the low reactivity of C-Cl bond on polychlorinated aromatic compounds. This is due to existence of another electron withdrawing chloride substituent that decreased the reactivity of the aromatic ring. From mechanistic point of view the reactivity can be modified by introduction of an electron donating species. By utilization of basic catalyst supports the electron donating property of the catalysts can be modified, hence increase the reactivity of the C-Cl bond. One of the commonly used basic materials includes hydrotalcite. Owing to its tunable basic property, high surface area of the calcined mixed oxide, good thermal and chemical stability, these materials are good candidate support for hydrodechlorination reaction.

In this in view, we report the hydrodechlorination reaction of 1,2,4-trichlorobenzene over hydrotalcite-like supported Pd. The activity of palladium supported on calcined Mg/Al hydrotalcites with different basic character was studied. The effect of rehydration-reconstruction of the supports together with Pd catalyst was investigated on the catalytic activity and stability. Finally the source and nature of deactivation on spent catalysts were studied. The activity and stability of the catalyst was also assessed with the meixenerite-like phase obtained by rehydration of calcined hydrotalcite.

1. Experimental

1.1. Preparation of the support

The hydrotalcite-like (HT) compound was prepared by coprecipitation of suitable amounts of $Mg(NO_3)_2\ 6H_2O$ and $Al(NO_3)_3 \cdot 9H_2O$ (Mg/Al molar ratio of 2, 3 and 4) with solutions of NaOH (2.0 M) as stated elsewhere [157]. HT was prepared with constant stirring maintaining the pH at 10. The addition of the alkaline solution and pH were controlled by p^H-STAT Titrino (Metrohm). The suspension was stirred overnight at room temperature. The resulting gel was centrifuged and washed several times thoroughly with distilled water (Na<100 ppm) until the pH of the centrifuged material is neutral and also to remove any free sodium ions. The sample was dried in an oven overnight at 393 K and then heat-activated in air flow at 723 K for 6 h (heating rate: 1 K min^{-1}) to yield the Mg(Al)O mixed

oxide. Calcined hydrotalcites with different Mg/Al molar ratios of 2, 3 and 4 prepared were labeled as HT-21, HT-31 and HT-41 respectively. The chemical compositions of the samples were determined by ICP-OES in a Perkin-Elmer Plasma 400.

1.2. Catalyst preparation

The palladium Mg(Al)O catalysts were prepared by two procedures. Pd (II) acetylacetonate ($Pd(C_5H_7O_2)_2$) was used as Pd precursor. In the first one, the calcined solid was introduced in a toluene solution of palladium (II) acetylacetonate for 12 h, dried at 398 K under vacuum, and calcined in air flow at 673 K for 2 h. The calcined material was reduced at 623 K under hydrogen flow for 2 h before reaction. The palladium catalysts were denoted as Pd-HT-41, Pd-HT-31 and Pd-HT-21. In the second procedure 250 mg of calcined Pd-HT-41 catalyst was first reduced at 623 K under hydrogen flow (60 cm^3min^{-1}) and then rehydrated in gas phase at 373 K using argon (flow 40 ml min^{-1}) saturated with de-ionized water for 18 h in situ. This catalyst hereafter was named as Pd-HTR-41.

1.3. Catalyst characterization

ICP-OES. The chemical composition of the samples was determined by ICP-OES with a Perkin-Elmer Plasma 400 instrument. The XRD analysis of the materials were recorded after the samples were dispersed on Si (510) sample holder. The angular 2θ diffraction range was between 5º and 90º. N_2 physisorption analysis at 77 K was measured after the samples were degassed in vacuum at 393 K for 6 h. Hydrogen-Chemisorption analysis was performed under static volumetric conditions. Prior to the measurement, the sample was evacuated at 373 K for 1 hour, treated in flow pure hydrogen (30 cm^3min^{-1}) at 623 K for 3 hours, evacuated at 623 K for 1 hour, cool down to 373 K and evacuated 30 minutes. Finally the chemisorption analysis was performed at 373 K. Transmission electron microscopy (TEM), operated at 80 kV (JEOL JEM-2000EX II) was taken to analyze the morphology and dispersion of our catalysts. H_2-TPR studies were performed in a ThermoFinnigan (TPORD 110) apparatus equipped with a thermal conductivity detector (TCD). The catalysts were treated in O_2 for 1 h at 573 K before TPR analysis. The samples were then purged with argon flow before the TPR analysis. The basic properties of the materials were also

determined by TPD of CO_2. The catalysts (150mg) were first purged using He 373 K for 45 minutes. The CO_2/He (3%) adsorption was carried out by heating the sample from 303 K to 373 K flowing at 20 ml/min and kept at 373 K for 60 min. Finally the weakly adsorbed CO_2 were purged using He flowing at 373 K for 45min. Typically, ca. 150 mg of sample were placed between plugs of quartz wool in a quartz reactor, and the desorption of CO_2 was measured by heating the sample from room temperature to 1123 K at 10 K min^{-1} under a He gas flow (20 cm^3 STP min^{-1}). Temperature programmed desorption and oxidation (TPDO/MS) analysis for spent catalysts (washed with ethanol) was carried out in ThermoFinnigan (TPORD 110) apparatus equipped with a thermal conductivity detector (TCD). Previously we have seen that no effect in reactivation of the spent catalyst by washing with ethanol. Before analysis the catalysts were pretreated using He-TPD/MS heating from room temperature to 623 K at 20 K min^{-1} and maintained for 30 min at this temperature to remove ethanol and other species. Then the sample was cooled to room temperature and TPO/MS analysis was carried out. Thermogravimetric Analysis (TGA), were performed in order to quantify the amount of carbonaceous deposits for the spent catalysts after hydrodechlorination reaction at 473 K. Thermogravimetric analyses (TGA) was carried out on a Perkin-Elmer TGA 7 microbalance with an accuracy of ±1 μg which was equipped an automatically programmed temperature controller. The spent catalysts for Pd-HT-21 and Pd-HT-31 were analyzed after 20 hours of reaction whereas after 60 hours for Pd-HT-41 and Pd-HTR-41 catalysts. Prior to analysis the spent catalysts were treated with Argon (20 $mlmin^{-1}$) heating at 5 $Kmin^{-1}$ from room temperature to 1173 K and then cooled down again to room temperature. In the sequence the sample was heated up to 1173 K in oxygen flow (5 K min^{-1}, 20 ml min^{-1}) and the weight loss was recorded. Environmental scanning electron microscopy (ESEM) analysis combined with energy dispersive spectroscopy (EDS). Analysis of the spent catalysts placed on metallic support was carried out in a FEI QUANTA 6000 scanning microscope operating at an accelerating voltage of 20 kV with 10 mm of working distance (WD) sample.

1.4. Catalytic activity

The hydrodechlorination of 1,2,4-trichlorobenzene was studied in a fixed-bed flow tubular reactor (10 mm i.d., 200 mm long) using 0.25 g of

catalyst at atmospheric pressure and at different temperatures ranging from 323 to 523 K. The catalyst sample was packed at the center of the reactor between to plugs of wool. Prior to reaction the catalyst was reduced insitu by hydrogen flow at 632 K for 2 h. 1,2,4-trichlorobenzene was injected continuously with help of a pump and H_2 (> 99.9% pure) and the molar ratio of H_2/1,2,4-trichlorobenzene was maintained 180 to favor 1,2,4-trichlorobenzene transport at room temperature [73]. The stabilities of the catalysts were studied over a period of 18 hours of reaction at 473 K. Two space velocities were used to compare their stability.Space velocity of 10 ml $min^{-1}.g^{-1}$ was used for comparing the catalytic activities of Pd-HT-21, Pd-HT-31 and Pd-HT-41 and 40 ml. $min^{-1}.g^{-1}$ for comparing the catalytic activities of Pd-HT-41 and Pd-HTR-41. The space velocities were calculated by deviding the total liquid flow rate ($ml.min^{-1}$) by mass of the catalysts (g). The product mixture was collected in an ice-cold trap and analyzed by gas-chromatograph (CG-17A, MS Shimadzu instruments) equipped with flame ionization detector (FID) and capillary column. Before characterization, the spent catalysts were washed with ethanol to remove the solvent hexadecane and dried at 323 K for 48 hours.

2. Results

2.1. Catalyst Characterization

Table 1 shows the magnesium and aluminum loading in the samples as determined by ICP-OES. The nominal Mg and Al species contents analyzed in the solids were very similar indicating the efficiency of the preparation. Hereafter we have referred to nominal Mg/Al molar ratio to describe the experimental results and the discussion along the manuscript. The nominal loading of Pd was maintained 1 wt % in all catalysts. Specific surface areas of the supported palladium catalysts (Pd-HT) are given in Table 1. All samples are mesoporous. Calcined hydrotalcite supports (HT) have surface areas in the range of 169 and 196 m^2g^{-1}. A slight decrease in surface area of the catalysts was observed when the Mg/Al ratio increases. Similar trend was observed for Pd-HT catalysts with surface area range of 165 and 185 m^2g^{-1}. When the corresponding Pd-HT-41 was rehydrated in a flow of argon saturated with water the BET surface area dropped, as expected, from 169 to 100 m^2g^{-1}.

Table 1. Some characteristics of the catalysts

Sample	Mg/Al[a]	$S_{BET}(m^2/g)$[b]	H/Pd[c]	Pd particle size (nm) [d]
HT-21	1.9	196	-	-
HT-31	2.8	187	-	-
HT-41	3.7	169	-	-
Pd-HT-21	1.9	185	0.19	4.8
Pd-HT-31	2.8	179	0.06	3.8
Pd-HT-41	3.7	165	0.04	3.6
Pd-HTR-41	3.7	104	-	3.6

[a]ICP-OES

[b] Specific surface area

[c]Weight percentage of Pd exposed at the surface obtained by hydrogen chemisorption

[d] From TEM

X-ray diffraction patterns of the different calcined hydrotalcite (HT) supports, and fresh palladium catalysts (Pd-HT) are shown in Fig. 1. The XRD profiles of the support materials calcined at 723 K are shown in Fig. 1a. In general the XRD patterns of the calcined materials are characteristic of well defined crystallized mixed oxide with periclase ($MgAlO_x$) structure shown at (1,1,1), (2,0,0) and (2,2,0), (3,1,1) and (2,2,2) (JCPDS file: 87-0653).

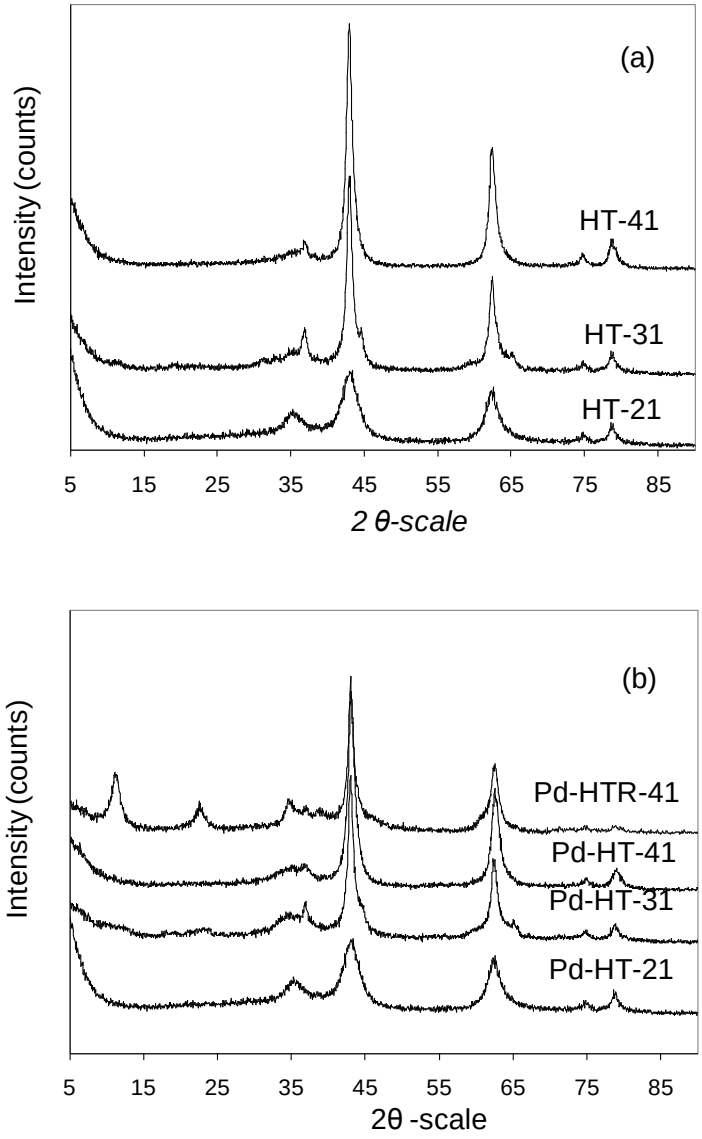

Fig. 1 X-ray diffraction of the calcined hydrotalcite materials. (a) Different HT supports, (b) Pd-HT catalysts.

Diffraction patterns of calcined HT samples showed no residual hydrotalcite or hydroxide phase, confirming that heating at 723 K leads to complete decomposition of hydrotalcite samples. The XRD profile for the Pd-HT (Fig. 1b) samples did not reveal distinct peaks corresponding to palladium species. As the Pd loading was rather low, the absence of diffraction line of Pd species may be due to the fact that the corresponding

Pd particles are too small to be detected by the XRD instrument. It is worth noting that the impregnation of palladium species on the support material did not change the periclase phase.

The TEM technique was subsequently used to evaluate the size of the reduced palladium particles. The TEM images for HT-21, Pd-HT-21 and spent Pd-HT-21 catalysts are shown in Fig. 2a, 2b, and 2c respectively. Fig. 2a shows the TEM image for the support material with a platelet morphology characteristic of derived hydrotalcite materials. Fig. 2b shows the typical morphology of a Pd crystallite. Palladium particles are clearly visible as dark dots uniformly dispersed on the surface of support. TEM was used to determine the crystal size of palladium particles. The diameter of a crystallite was taken as an average of the longest and shortest diameter, and over 200 individual crystallites were measured. The mean diameter values of the Pd particles in the catalysts are reported in Table 1.

The TEM micrographs of the Pd-HT-21 catalysts revealed the appearance of relatively narrow size distribution (Fig. 2b) showing Pd crystallites with mean diameter of 4.7 nm and only few particles over this size were observed. For Pd-HT-31 and Pd-HT-41 the size distribution was also narrow and the overall crystallite dimensions were similar as shown in fig. 2c and fig. 2d. It follows that the Pd particles may be considered as fairly mono dispersed for all samples supporting the fact that no Pd crystalline phase was detected in the XRD analysis. The TEM images obtained for the spent Pd-HT-21 catalyst (temperature of reaction was 473 K) are shown in the fig. 2e and fig. 2f. This material seems to be covered by some fouling species.

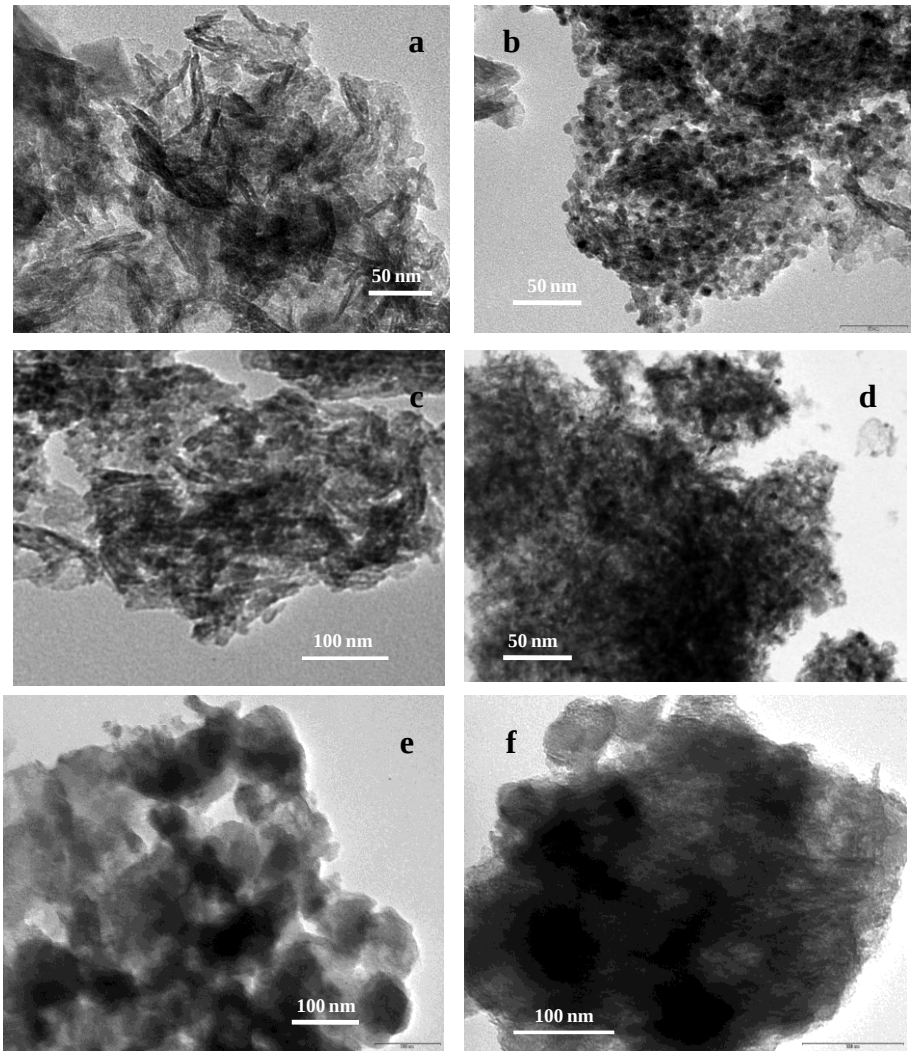

Fig. 2 TEM image of a representative sample: (a) Support material (HT-21), (b) Pd-HT-21 (c) Pd-HT-31 (d) Pd-HT-41 samples and (e, f) spent Pd-HT-21 catalyst (T of reaction 473 K).

By energy-dispersive spectroscopy (EDS) analysis carbon was detected on the surface of the spent catalyst as observed in Fig. 3. The presence of carbonaceous species in the spent samples may suggest that the deactivation originated from coking during hydrodechlorination.

The ability of a catalyst to dissociate molecular hydrogen into its hydrogen atoms so that it can easily attack C-Cl bond is an important property for the reaction of hydrodechlorination. As a result, hydrogen

chemisorption was measured for the three catalysts Pd-HT-41, Pd-HT-31, Pd-HT-21. The H_2-chemisorption results are shown in Table 1 in terms of the percentage of Pd exposed at the surface. Based on these results, it appears that as the amount of magnesium species in the support increases, the uptake of hydrogen decreases.

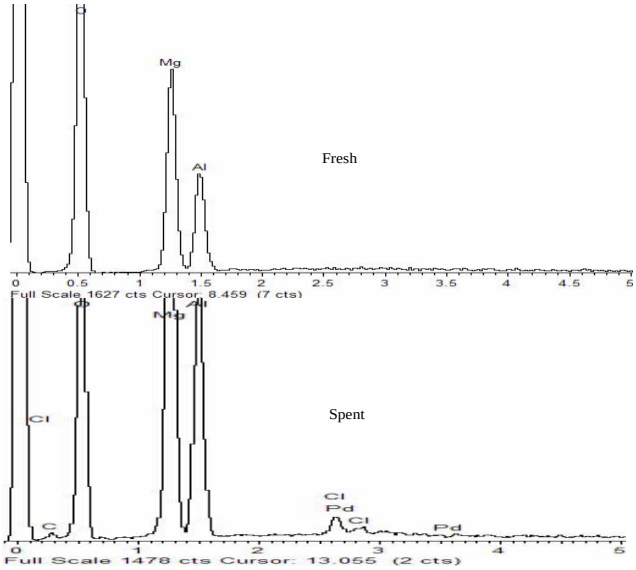

Fig. 3 Energy-dispersive spectroscopy (EDS) analysis on the surface of the spent and fresh Pd-HT-21 catalyst.

TPR profiles of palladium catalysts Pd-HT-41, Pd-HT-31 and Pd-HT-21 are shown Fig.4. They show a major reduction peak at temperature around 600 K. The reduction temperature depends on the degree of interaction between the active species and the support. The small peaks at 300-420 K can be assigned to reduction of PdO crystallites to Pd^o metal [158]. The second peak between 593 and 603 K indicated further consumption of hydrogen on all the catalysts, and corresponds to palladium strongly interacting with the support, for instance as cations. A peculiar behavior of Pd concerns its ability to form a Pd hydride species (β-H_xPd) at ambient temperature. No peak corresponding to β-H_xPd hydride decomposition was observed in the samples. This can be ascribed to the rather small size of palladium particles, since Hwang and Boudart [159] reported that the solubility of hydrogen decreased with Pd particle size.

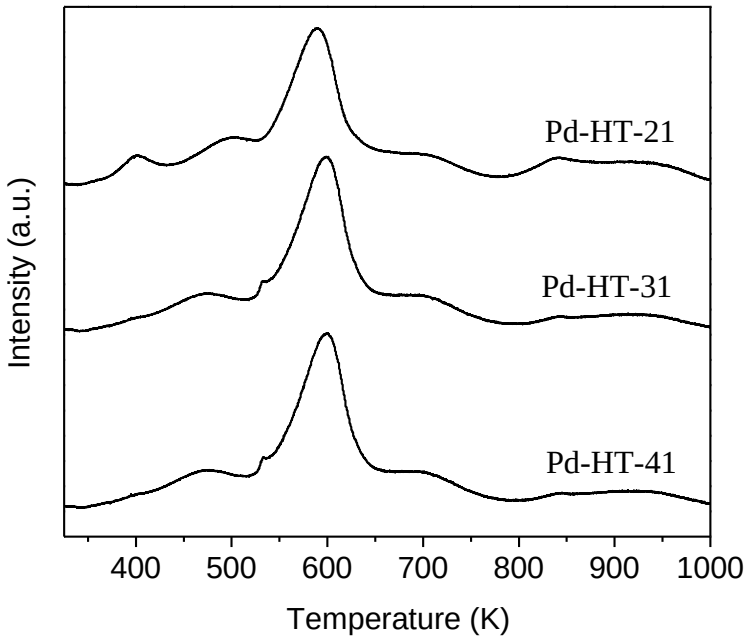

Fig. 4 H_2-temperature-programmed reduction profile of the palladium catalysts. (a) Pd-HT-41, (b) Pd-HT-31 and (c) Pd-HT-21.

TPD-TPO/MS analyses for the spent catalysts are reported on Fig. 5. The spent catalysts Pd-HT-21, Pd-HT-31, Pd-HT-41 and Pd-HTR-41 were analyzed first using the He-HTPD/MS, followed by TPO/MS in order to investigate the nature of the species retained at the surface. The MS profiles of He-TPD for all the spent catalysts showed no signal in the mass spectroscopy (MS) presenting no evolution of deposited species on the used catalysts as depicted in Fig. 5. It can be pointed out that no Cl evolution was observed. By contrast, TPO/MS profiles show the presence of signals corresponding to CO_2, CO, and C, with consumption of oxygen. This is a clear evidence of the formation of "coke" at the surface.

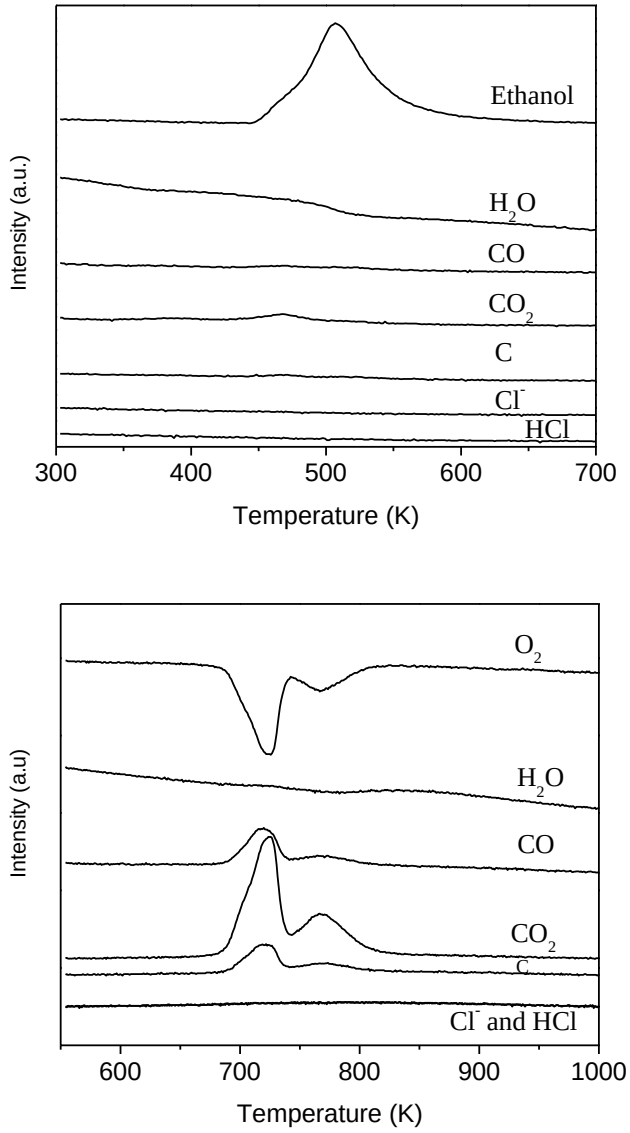

Fig. 5 TPO-MS profiles of the spent sample Pd-HT-21 showing: (a) Species evolved during the He-TPD and (b) Sequential analysis of TPO.

The TPO profiles of the used catalysts are depicted in Fig. 6. The profile for Pd-HT-21 catalyst exhibits two peaks at 629 K and 729 K suggesting two different sites for deactivation. The TPO profiles for the other

catalysts are characterized by a single peak. These results suggest that the species deposited on the spent catalysts is coke.

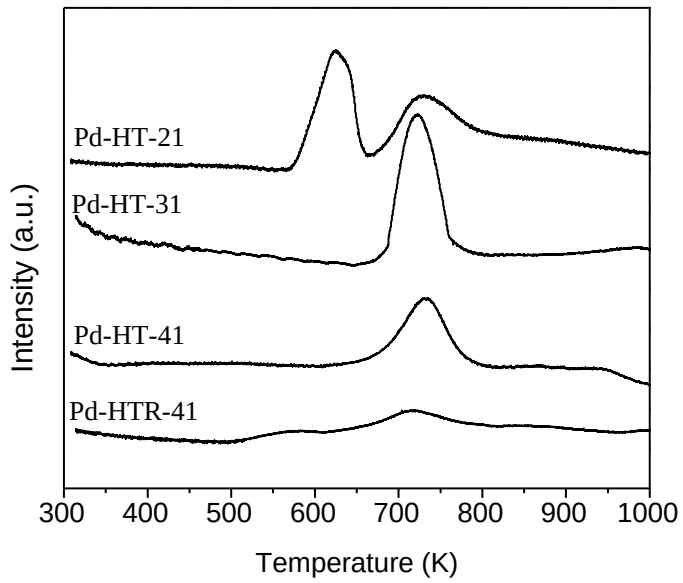

Fig. 6 Temperature programmed oxidation (TPO) of the spent Pd hydrotalcite catalysts. (a) Pd-HT-41, (b) Pd-HT-31 and (c) Pd-HT-21.

The results of TGA measurements are reported in Fig. 7, and show two distinct weight losses dependent on the Mg-Al molar ratios. The total weight loss after heating the sample from room temperature to 1173 K for Pd-HT-21, Pd-HT-31, Pd-HT-41 and Pd-HTR-41 were, 6%, 3%, 2% and 1% respectively. In view of the results of MS analysis, these weight losses are attributed to carbonaceous deposits.

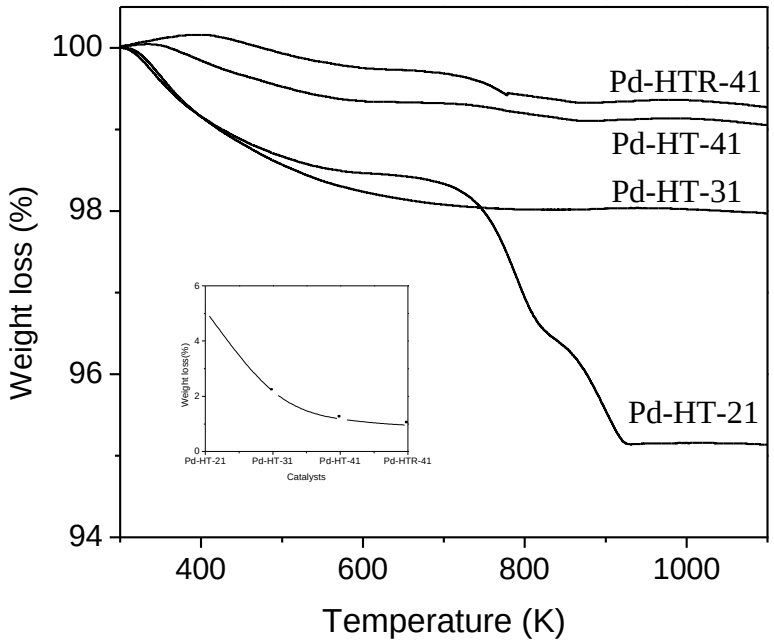

Fig. 7 Thermogravimetric analysis of the spent Pd-HT catalysts. (a), (b), (c), (d). Inset: Carbon content in the spent samples versus Mg/Al molar ratios.

The inset of the Fig. 7 shows the amount of carbon in the Pd-HT catalysts, determined by TGA as a function of the Mg/Al in the catalyst. These TGA results clearly demonstrate that the Mg/Al molar ratio plays a strong role in the extent of carbon deposition in the catalysts. An increase in the Mg content is beneficial to the suppression of carbonaceous deposits. Particularly the Pd-HTR-41 catalyst showed the lowest weight loss. The rehydration of the Pd-HT-41 sample induced a decrease of the carbon deposits.

The basic properties of the Pd-HT-41 and Pd-HTR-41 were determined by CO_2-TPD. Fig. 8 shows the TPD trace for two representative samples (Pd-HT-41 and Pd-HTR-41). From the quantification of the amount of the CO_2 evolved by integration of the corresponding peaks indicated that Pd-HT-41 and Pd-HTR-41 presented values of 1.43 and 5.03 mmol g^{-1} respectively. A small shift of the peak is also observed from 674 K to 705 K which would be indicative of a higher basic strength on the rehydrated sample.

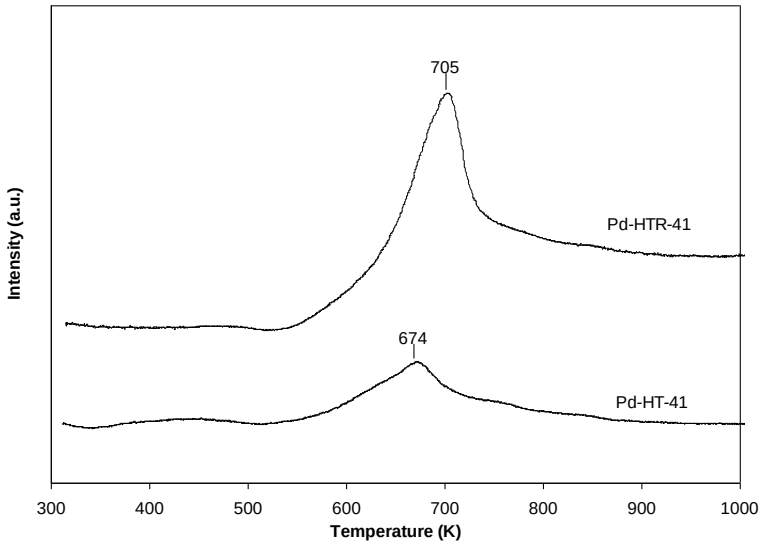

Fig. 8 CO_2-TPD profiles of the Pd-HT-41 and Pd-HTR-41 samples.

Table 2 Product distribution in function of temperature over the Pd-HT catalysts

Catalyst	T (K)	X(%)[a]	Selectivity (%) [b]			
			Bz	*Chl*	*o-Dichl*	*p-Dichl*
Pd-HT-21	373	25.8	30.3	6.1	50.4	13.2
	433	48.1	46.4	5.1	39.4	9.1
	473	69.4	61.1	4.4	25.2	9.3
Pd-HT-31	373	52.1	61.3	3.6	29.4	5.7
	433	72.6	70.8	2.0	23.2	4.0
	473	84.6	85.0	2.2	11.5	2.3
Pd-HT-41	373	74.6	79.2	5.8	11.9	3.1
	433	88.0	92.0	2.2	4.2	2.7
	473	100.0	100.0	0	0	0

[a] X(%): conversion of 1,2,4-trichlorobenzene

[b] *Bz*: benzene, *Chl*: chlorobenzene, *o-Dichl*: -dichlorobenzene, *p-Dichl*: *p*-dichlorobenzene.

2.2. Catalytic activity

The hydrodechlorination of 1,2,4-trichlorobenzene over Pd-HT catalysts was studied in a temperature range of 323-573 K. The main products detected were benzene, chlorobenzene, o-dichlorobenzene and p-dichlorobenzene. The products obtained in this study are in line with previous results obtained for hydrodechlorination of 1,2,4-trichlorobenzene on Ni/Niobia [70], Ni/Al_2O_3 [160], and Ni/Mg/Al hydrotalcite catalysts [75, 161]. A blank test run with the different oxide supports showed no conversion of 1,2,4-trichlorobenzene at the same reaction conditions.

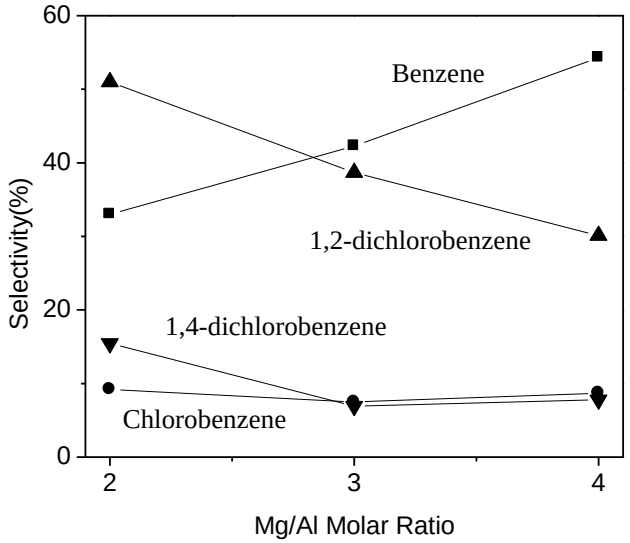

Fig. 9 Selectivity of catalysts at 50% conversion versus Mg/Al molar ratio in the Mg(Al)O support. The reaction temperature was 433K.

The comparison of the different palladium-supported catalysts was performed at a constant mol ratio of H_2/1,2,4-trichlorobenzene of 182 for all the catalysts. Table 2 shows the conversion and product distribution as a function of the temperature, for the conversion of 1,2,4 -trichlorobenzene. As temperature increased, the production of benzene increased, whereas chlorobenzene, o-dichlorobenzene and p-dichlorobenzene decreased. In all cases chlorobenzene and p-dichlorobenzene were minor products. Fig. 9

shows the product distribution of Pd-HT catalysts at the same conversion. It clearly shows that an increase of the Mg/Al molar ratio in the support material induced an increase in the selectivity to benzene and a decrease in the selectivity toward the other products. According to these results it is tempting to conclude that the basic character of the catalyst is beneficial for the catalytic performance in the 1,2,4-trichlorobenzene hydrodechlorination reaction. Hydrodechlorination (HDC) is a stepwise process for the elimination of chlorine species, and the lower rates to *o*-dichlorobenzene and p-dichlorobenzene formation observed in our experiments may then be related to the inductive and steric effects induced by the Ph-Cl bonds.

The effect of time on stream was studied at 473 K over Pd-HT catalysts. The space velocity of 1,2,4-trichlorobenzene was maintained at 15.6 $mg.min.mmol^{-1}$. The study was carried out for 18 hours on stream. Conversion decreased with time on stream over all catalysts, as illustrated on Fig. 10. The deactivation of the Pd catalysts for the hydrodechlorination of the 1,2,4-trichlorobenzene appeared to be greatly dependent on the Mg/Al molar ratio of the support. In particular, a comparison between the catalyst Pd-HT-41 and Pd-HT-21 showed that the higher initial activity is associated with a higher Mg content. Pd-HT-21 catalyst showed the highest rate of decay, and Pd-HT-41 was the most stable with time. The selectivity to benzene decreased whereas o-dichlorobenzene showed an increase with time. This selectivity to o-dichlorobenzene increased probably due to deactivation of the catalyst by blockage of the active sites.

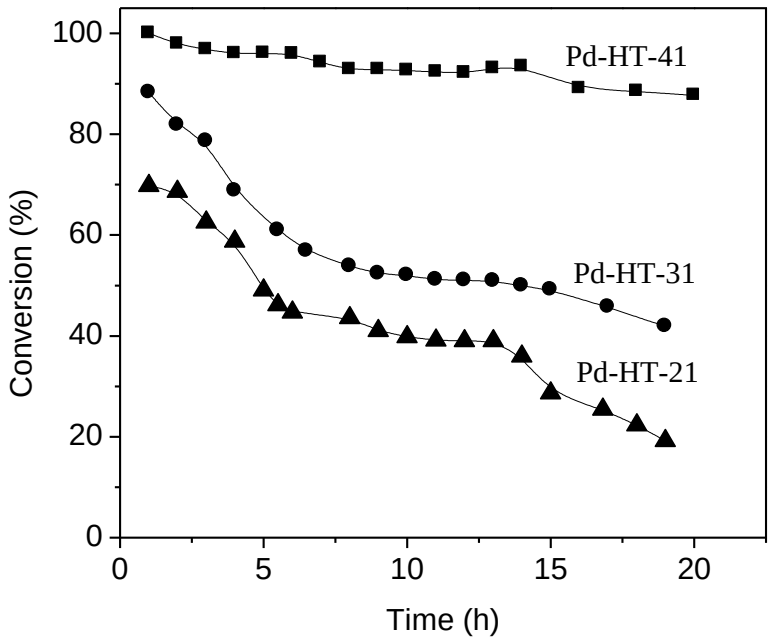

Fig. 10 Conversion versus time of stream of the Pd hydrotalcite catalysts with a space velocity of 10 ml. $min^{-1}.g^{-1}$ at 473K. (a) Pd-HT-41, (b) Pd-HT-31 and (c) Pd-HT-21.

Deactivation with time on stream was studied at 473 K over Pd-HT-41 and Pd-HTR-41 catalysts as shown in Fig. 11, using a space velocity of 1,2,4-trichlorobenzene increased by four times (61.6 $mg.min.mmol^{-1}$). It appears that the rehydrated catalyst Pd-HTR-41 possesses higher catalytic activity than Pd-HT-41 and a good stability. This is related to the introduction of Brönsted basic sites that influence the hydrodechlorination activity.

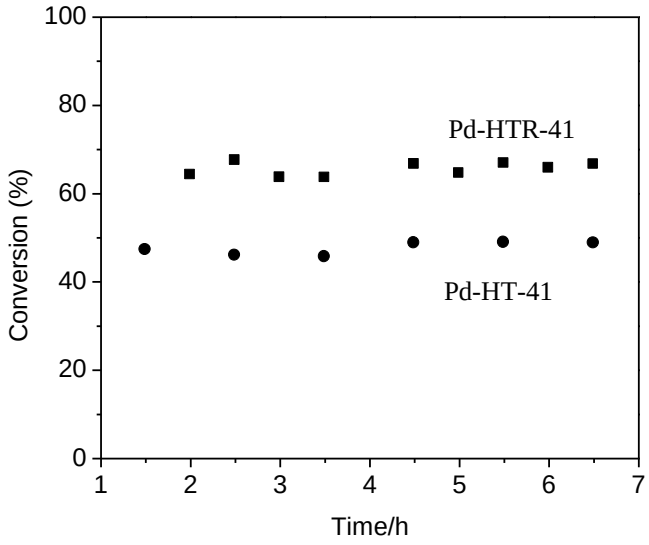

Fig. 11 Comparison in the catalytic performance between Pd-HT-41 and Pd-HTR-41 catalysts versus time of reaction using a space velocity of 40 ml. $min^{-1}.g^{-1}$.

3. Discussion

These catalysts supported by hydrotalcites show good activities, reach nearly full selectivity for benzene, and most surprisingly deactivate very little. The cause of the activity loss was investigated by several means: the presence of carbon in the spent catalysts was confirmed by TPO/MS and TGA shown in Fig. 6 and 7. Both analyses confirmed that carbonaceous species had been adsorbed on the spent catalysts suggesting deactivation by coking. As a result the observed loss in activity can be linked to a blockage of active sites by carbonaceous deposits. By contrast, the contribution of deactivation due to HCl produced in the hydrodechlorination reaction might be negligible when compared with the carbon species. ESEM/energy dispersive X-ray (EDS) analysis of the spent samples, as depicted in Fig. 3, revealed residual chlorides and carbon species. However no chlorine was found in the effluents in the mass spectroscopy analysis of the He-TPD and

TPO in a given range of temperature as shown the Fig. 5, therefore the main poison seems to be coke.

The Mg content played a role in the decrease of the carbon content in the samples. The analyses showed that lower amounts of carbon were detected as the Mg/Al molar ratio in our Pd-HT catalysts increased. Different TPO features were observed depending on the Mg/Al molar ratio: the Pd-HTR-41, Pd-HT-41 and Pd-HT-31 sample presented only one peak at about 730 K, while decreasing the Mg content (Pd-HT-21), a second peak appeared at lower temperature with its maximum located around 629 K. It has to be emphasized that two different steps are also observed by thermo gravimetric analysis of the combustion of carbonaceous species. An appreciable amount of carbon of about 6% was detected in the spent Pd-HT-21 sample from TGA analysis. The Pd-HT-41 and Pd-HTR-41 samples showed the lowest carbon deposition level with value around 2% and 1%.

The analysis of spent catalysts by TPO coupled to MS gives an evaluation of HCl, CO_2, O_2 and CO in the outlet gas. The results for CO_2 signal for a representative sample (Pd-HT-21), reported in Fig. 5 confirm that the peaks detected in the TPO measurements correspond to the combustion of carbonaceous deposits. Marecot et al [162]investigated the deactivation of Pd/SiO_2 deactivated by coke formed by the conversion of cyclopentane. Two peaks were observed in the TPO profiles of coked catalysts, corresponding to coke deposition on the metallic function, since silica has no acidity: the first one near 523 K, was attributed to coke deposited on palladium atoms of high coordination number, and a second TPO peak near 673 K involving palladium atoms of low coordination number. In this hypothesis, the deactivation would be related to the distribution of particles sizes, but since this distribution is only slightly altered by the change of the support, while clear changes of deactivation do occur, it appears difficult to favour this interpretation.

The most stable catalysts show only one peak, which has then to be attributed to carbon deposited on the metallic surface. The comparison of basicities of fig. 8 suggests that there exists a correlation between basicity and coke deposition on the metallic surface. Indeed as discussed above, an effect of the basicity of the support on the adsorptive and catalytic properties of Pd have been evidenced [89, 109]. A basic support acts as a basic additive,

introduced from the liquid phase.[13] A faster rate of dechlorination of 1,2,4-trichlorobenzene increases the concentration in di-chloro intermediates which can react faster, which accounts for the higher selectivity to benzene. The observation that benzene is not hydrogenated on the most basic catalyst is also consistent with the report that the activity for benzene hydrogenation on Pd increased on acid supports [163, 164]. The mechanism of coke formation is still not clear but could involve reactions of alkylation of aromatics in which Pd is known to be active [60, 165]. These reactions are considered to involve oxidized species of Pd [60] which should be unfavoured on basic supports.

4. Conclusion

A series of palladium catalysts supported on several Mg/Al hydrotalcite materials were prepared and studied in the hydrodechlorination of 1,2,4-trichlorobenzene. The results were correlated with the basic character of the Mg(Al)O mixed oxide support. It has been shown that palladium catalyst supported on calcined hydrotalcites with higher Mg/Al ratio showed a total conversion of 1,2,4-trichlorobenzene toward benzene at 473 K. Instrumental characterizations of the spent catalysts operated at 473K revealed that the deactivation is mainly due to coke deposition on the surfaces and not from the HCl product. The stabilities of the catalysts were also strongly dependent on the Mg/Al of the support. Additionally activation of the Pd-Mg(Al)O sample with Mg/Al molar ratio of 4 by rehydration enhanced both the catalytic activity and stability. Finally these results indicated the feasibility of hydrotalcite-like and derived materials as catalyst support in the hydrodechlorination reaction of 1,2,4-trichlorobenzene.

4.2.

Performance of alkali modified Pd/MgAlO catalysts for HDC of 1,2,4-trichlorobenzene

In previous section it has been reported that the HDC of 1,2,4-trichlorobenzene (124-TCB) on a series of Pd catalysts supported on several basic $MgAlO_x$ mixed oxides, that the palladium catalyst with higher basicity of the support gave the uppermost activity and stability [135]. The best HDC performances were obtained for a Mg/Al molar ratio of 4. The $MgAlO_x$ supports were derived from hydrotalcite precursors (HT). It was also shown that catalyst deactivation at high temperature reaction (473 K) was mainly due to coke formation, which decreased as the basic character of the support increased.

The basic properties of an inorganic oxide can be boosted by using alkaline additives. For instance, the Na- and K-doped MgO showed a large increase in the generation of super base sites by an induction effect of the electron released from the alkali metal [106, 107]. On that account, the enhancement of the basic properties of Mg(Al)O mixed oxides may be expected upon addition of alkaline promoters. Indeed, a clear effect of alkaline-doping agents on the catalytic activity of hydrotalcite-like compounds has been observed for the aldol condensation reaction [91]. One may thus anticipate that the same effect should be beneficial for the HDC catalytic properties of alkaline-promoted $Pd/MgAlO_x$ catalysts. With this view the present work will address the HDC of 1,2,4-TCB as a model reaction on $Pd/MgAlO_x$ promoted by Li, Na and Cs from nitrates and

hydroxides precursors. The study focuses on activity, selectivity and stability in relation with the basic properties of the promoted mixed oxides. A low reaction temperature (273 K) has been chosen to study the deactivation and the regeneration of the catalysts.

1. Experimental

1.1 Preparation of the supports and catalysts

Full details of the support synthesis were given previously [135]. In brief, the hydrotalcite-like compound was prepared by co-precipitation of suitable amounts of $Mg(NO_3)_2 \cdot 6H_2O$ and $Al(NO_3)_3 \cdot 9H_2O$ (Mg/Al molar ratio of 4) with NaOH 2 M at pH 10. The resulting gel was washed thoroughly several times with deionized water to remove any remaining free sodium ions. The sample was dried and calcined in flowing air at 723 K for 12 h (heating rate: 1 K min^{-1}) to yield the $MgAlO_x$ mixed oxide (HT). For the alkali-doped HT, 1 g of this $MgAlO_x$ was impregnated with the appropriate amount of an aqueous solution of the alkali hydroxides or nitrates to obtain the desired alkali loading (see Table 1). The solids were dried and calcined at 723 K (for alkali hydroxides) or 873 K (for alkali nitrates) for 12 h, the supports thus obtained were labelled HT(AOH) and HT(ANO_3) (A = Li, Na and Cs; and OH and NO_3 indicate the type of alkali precursor).

These supports were used to prepare the metal catalysts by depositing palladium by the incipient wetness impregnation method [135]. The metal precursor used was Pd(II) acetylacetonate ($Pd(acac)_2$). A solution of $Pd(acac)_2$ in toluene was used to impregnate the corresponding alkali-doped mixed oxide support. The nominal Pd content in all samples was 1%wt. The samples were then dried and calcined in air at 623 K for 3 h. The catalysts were reduced in situ at 623 K for 2 h before starting the reaction. The final catalysts were labelled Pd/HT(AOH) and Pd/HT(ANO_3).

1.2 Characterization of catalysts

1.2.1. Textural, structural and morphological characterizations

The chemical composition of the samples was determined by atomic absorption spectroscopy with a Perkin-Elmer Plasma 400 instrument. Textural properties of the solids were obtained from N_2 adsorption-

desorption isotherms at 77 K using a Micromeritics ASAP 2000 surface analyzer. The XRD analysis of the materials was recorded using a Siemens D5000 diffractometer (Bragg-Bentano for focusing geometry and vertical θ-θ goniometer) with an angular 2θ-diffraction range between 5º and 90º. The morphologies of the catalysts were observed by SEM with a JEOL JSM-35C scanning microscope operated at an acceleration voltage of 15 kV.

1.2.2. Characterization of the basic properties

The basic properties of the materials were characterized by TPD of CO_2 using a ThermoFinnigan (TPDRO110) apparatus equipped with a programmable temperature furnace and a TCD detector. The amount of basic sites displayed in Table 1 was calculated from the CO_2 peaks by deconvolution using the TPD/R/O software of the equipment, and the equipment was calibrated using different known amounts of $CaCO_3$.

1.2.3. Metal phase Characterization

High-Resolution Transmission Electron Microscopy (HRTEM) was carried out at 200 kV with a JEOL JEM 2100 instrument equipped with a LaB_6 source. The metallic dispersion of the palladium catalyst was determined by hydrogen chemisorption at 373 K, carried out in a static volumetric apparatus (Micromeritics ASAP 2010). The Pd/HT($NaNO_3$) spent and regenerated catalysts were further characterized by X-ray photoelectron spectroscopy (XPS) technique. It was performed with a SPECS system equipped with a dual anode XR50 source operating at 150 W and a Phoibos 150 MCD-9 detector.

1.3 Hydrodchlorination of 1,2,4-Trichlorobenzene

The hydrodechlorination (HDC) of 1,2,4-trichlorobenzene (1,2,4-TCB) in hexadecane (4/96, vol/vol%) (Sigma-Aldrich) was studied in a tubular fixed-bed flow reactor (10 mm i.d., 200 mm long) using 0.25 g catalyst at atmospheric pressure. The catalyst sample was packed at the center of the reactor on the surface of porous silica. Before the reaction, the catalyst was reduced in situ by H_2 flow at 623 K for 2 h. 1,2,4-Trichlorobenzene was injected continuously with help of a pump together with H2 (>99.9% pure). The molar ratio of H_2/[Cl] was maintained at 60. The product mixtures (scheme 1) were collected in an ice-cold trap and analyzed by a gas chromatograph (GC-17A, MS Shimadzu instruments)

equipped with a flame ionization detector (FID) and a capillary column. Hydrogen chloride formation was evaluated by passing the effluent gas through an aqueous solution of NaOH (2M) trap. Selected spent catalysts were recovered from the reactor for further characterization study. The catalysts were cooled to room temperature and washed in-situ several times by pumping liquid ethanol through the reactor in order to eliminate the organic substrates from the surfaces. Then, the spent catalysts were dried by flowing Ar at room temperature for 4 hours.

2. Results and discussion

2.1. *Properties of the catalysts*

The main properties of the catalysts are presented in Table 1. The parent Pd/HT exhibits a surface area of 151 m^2 g^{-1} and a pore volume of 0.40 cm^3 g^{-1}. After alkali modification of the support, significant decreases in surface area and pore volume were observed. This indicates some modifications of the textural and chemical properties of the Mg-Al mixed oxide (obtained after the calcination of hydrotalcite) during the addition of alkali promoters. This fact could be due to several factors. It is well known that Mg-Al mixed oxide, obtained from hydrotalcite calcination, can be reconstructed in contact with water forming a meixnerite-like phase that usually shows lower surface area than the mixed oxide [91]. Furthermore, the presence of the alkali metal precursors could destroy the porous system decreasing the surface area of the support probably by the partial dissolution of the mixed oxide. Besides, the alkaline oxide obtained after the calcination of the sample could produce pore blockage of the support decreasing the surface area of the mixed oxide. The detrimental effect on structural properties is much larger for Na and Cs promoted catalyst than for Li. This is probably due to the higher basic properties of these species compared with Li, as well as the high amount in weight composition presented in the catalysts (1.2 wt% for Li, 4.0 wt.% for Na and 22.8 wt% for Cs, these weight percentage are equimolar and represents 1.7 mmol of alkali per gram of support). Furthermore, this detrimental effect on structural properties is much larger with hydroxides than for nitrates precursors. This could be explained by the strong alkaline medium of the aqueous solutions of alkali

hydroxides, which leads to partial dissolution of the support and therefore a loss of surface area and pore volume. Moreover, it was found that the BET surface area in alkaline-modified smectites decreases as a result of the surface contraction associated with electrostatic forces [166]. Alkali addition on HT should produce a similar effect by decreasing the repulsion and initiating more close packing/stacking of the fragments. This effect depends strongly on the pH of the impregnating solution and is more pronounced for alkali hydroxide-impregnated catalysts.

Table 1 Some characteristics of the catalysts

Sample	Composition (wt/wt%)		BET surface ($m^2\ g^{-1}$)	Pore volume ($cm^3\ g^{-1}$)	CO_2 desorption[a]		Pd H_2-uptake (H/Pd%)	Pd size (nm) from TEM
	Pd	Alkali			(mmol g^{-1})	(μmol m^{-2})		
Pd/HT	1.1	-	151	0.40	3.7	25	18	4.8
Pd/HT(LiOH)	1.0	1.2	115	0.20	8.3	72	19	4.9
$Pd/HT(LiOH)_{0.24}$	1.0	0.24	118	0.21	-	-	18	5.0
$Pd/HT(LiOH)_{0.12}$	1.0	0.12	117	0.20	-	-	17	4.9
Pd/HT(NaOH)	0.98	4.9	21	0.06	6.7	320	5.5	5.0
Pd/HT(CsOH)	0.97	23	12	0.04	6.0	500	2.3	5.1
$Pd/HT(CsOH)_{4.6}$	1.0	4.6	25	0.06	-	-	5	5.0
$Pd/HT(CsOH)_{2.3}$	1.1	2.3	28	0.09	-	-	7	4.9
$Pd/HT(LiNO_3)$	1.2	1.2	92	0.33	3.8	29	24	5.0
$Pd/HT(NaNO_3)$	1.0	5.0	70	0.20	5.1	73	16	4.9
$Pd/HT(CsNO_3)$	0.99	22.8	70	0.18	5.8	83	6.4	4.8

[a] Obtained by deconvolution of CO_2-TPD profiles

Fig. 1 shows the representative SEM images of HT, Pd/HT, Pd/HT($NaNO_3$) and Pd/HT(NaOH). The typical morphology for the hydrotalcite-derived mixed oxide phase (Fig. 1a) was maintained after Pd impregnation (Fig. 1b). However, a significant change in morphology was observed for the alkali-impregnated catalysts (Fig. 1c and 1d). The alkali-doped Pd/HT catalyst showed a more agglomerated material, thus resulting in a decrease in surface area. This indicates that the dissolution of some part of the mixed oxide structure by the strong basic character is the determinant factor for the final textural properties of the catalysts as has been also suggested by BET.

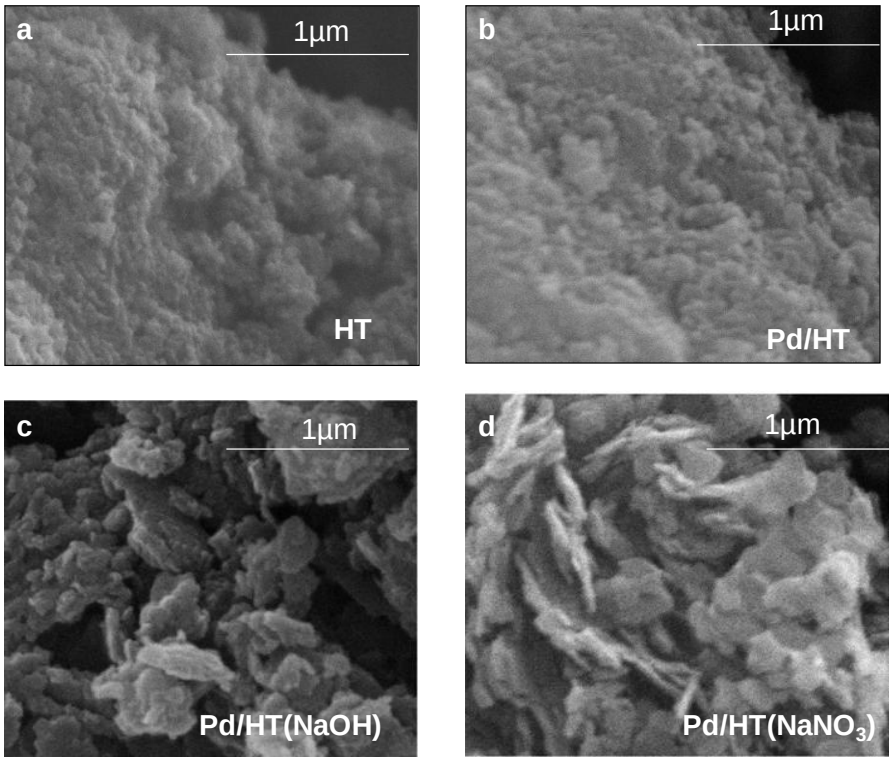

Fig. 1 SEM image of HT(a), Pd/HT(b) and representative of modified catalysts Pd/HT($NaNO_3$) (c) and, Pd/HT(NaOH) (d) .

The X-ray diffraction patterns of the catalysts are shown in Fig. 2. In general, these patterns are characteristic of well-defined crystallized mixed oxide with periclase phase ($MgAlO_x$, JCPDS 87-0653). As in a previous

study [135], the XRD profile for the palladium-impregnated catalysts revealed no distinct peaks corresponding to palladium species. This is probably due to the low Pd loading (1%) which is below the detection limit of the XRD instrument. Na- and Li-doped catalysts did not show any new peaks corresponding to alkali metal species regardless of the source of the alkaline metal (AOH or ANO_3). However, the XRD profile of Pd/HT($CsNO_3$) catalysts showed some additional peaks of $CsNO_3$. This shows how difficult it is to completely remove the nitrate species from the $CsNO_3$-impregnated catalyst even at high temperature (723 K). The calcination temperature for Pd/HT(ANO_3) catalysts was therefore 873 K rather than 723 K. On the other hand, the addition of alkali caused a significant decrease in the crystallinity of the mixed oxide support following the trend as: Cs > Na > Li. From these results, it is tempting to conclude that as the basicity of the alkaline additive increases, the crystallinity of the periclase phase decreases. This may be caused by the interaction between the alkali metals and the acidic sites of aluminum species, which affects the periclase phase of the $MgAlO_x$ support. Moreover, the marked loss of crystallinity for alkali-nitrate-modified catalysts could be due to the high calcination temperature (873 K) applied to remove traces of nitrates from the surface (see inset in Fig. 2b).

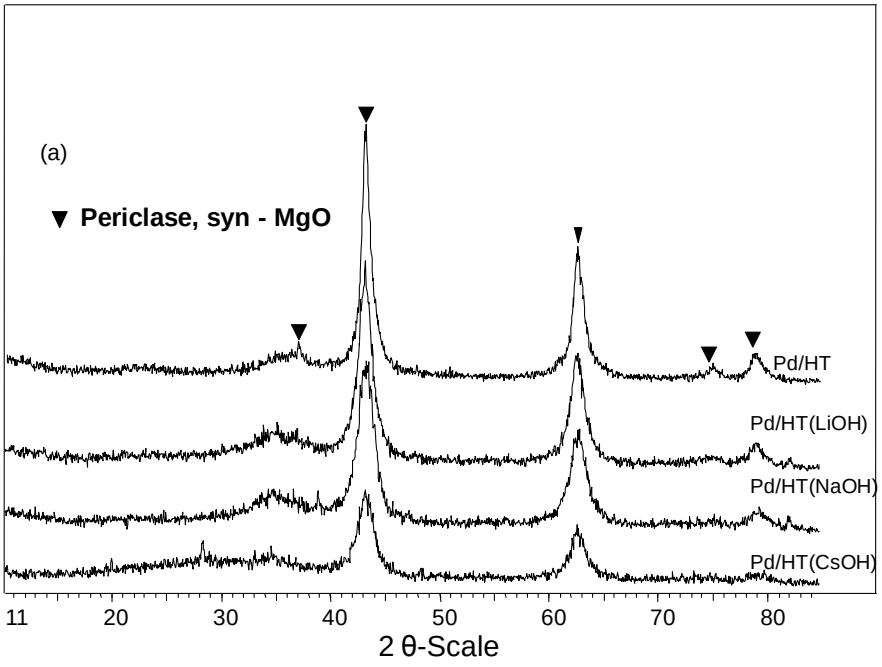

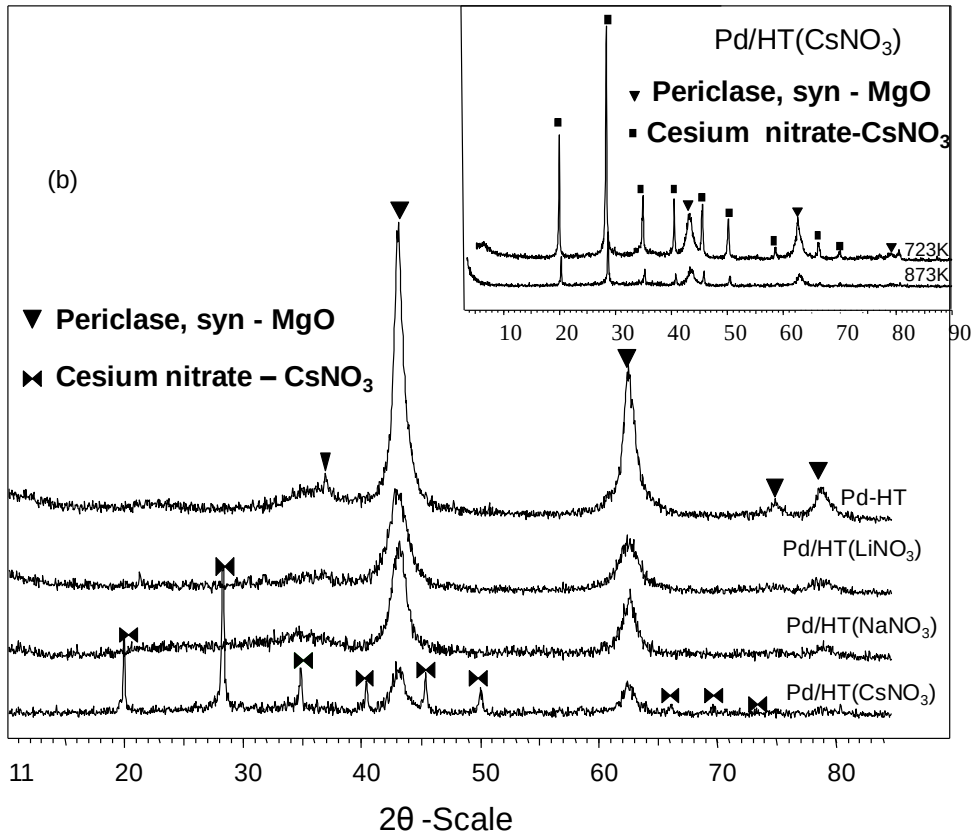

Fig. 2 XRD diffraction of freshly prepared catalysts a) Pd/HT(AOH), b) Pd/HT(ANO_3), Inset: Pd/HT($CsNO_3$) calcined at 723 K and 873 K respectively.

TEM pictures for alkali-doped catalysts showed no significant differences between samples Pd/HT(LiOH), Pd/HT(NaOH), and Pd/HT(CsOH). In all cases, the samples contained small metallic Pd particles supported over larger grains with a platelet-like morphology; This is exemplified in Fig. 3a, which corresponds to Pd/HT(NaOH) sample. More than 90 Pd particles were used in order to determine the particle size distribution. The size distribution is similar for all samples with an average particle size of around 5 nm. The microstructure of Pd particles was inspected by high-resolution transmission electron microscopy (HRTEM). Fig. 3c shows a representative HRTEM image of Pd/HT(LiOH); an individual Pd particle with lattice fringes at 2.24 Å is highlighted, which corresponds to Pd(111). We drew the same conclusions for all the samples.

An HRTEM image of Pd/HT(NaOH) is shown in Fig. 3d. Two Pd particles are indicated by arrows, their lattice fringes at 2.24 Å again correspond to Pd(111). Similarly, Fig. 3e shows an individual Pd particle for Pd/HT(CsOH) sample, with no evidence of any alkali metal oxide layer. However, it is worth noting that HRTEM can only detect oxide layer if a minimum number of ordered atomic rows are present. Therefore, HRTEM cannot completely rule out the possibility of patches or thin layer of alkali oxide onto the Pd surface, however, the thickness of such species could not exceed ca 0.5 nm. As suggested previously, the Cs nitrate appears in the XRD pattern indicating relatively big and crystalline particles of such species. Another HRTEM image, corresponding to the Pd/HT($CsNO_3$) sample, is included in Fig. 3f. Fourier Transform Analysis of the particle enclosed by the square (see inset) indicates that the particle is an individual Pd metal crystallite oriented along the [112] crystallographic direction. Once again, the Pd particles show clean facets without any evidence of an alkali metal oxide layer.

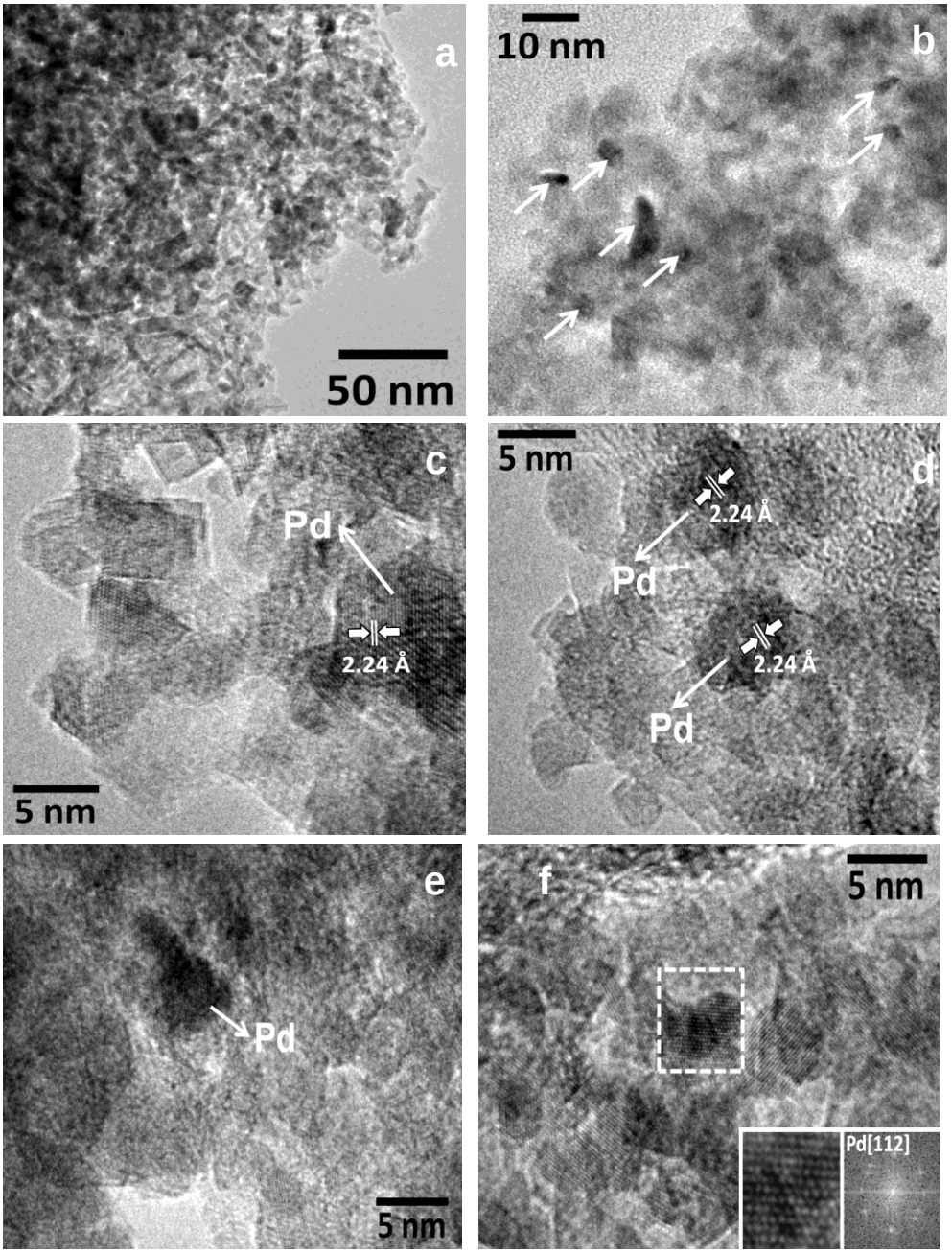

Fig. 3. TEM and HRTEM images of freshly prepared alkali hydroxide modified catalysts (a & d)-Pd/HT(NaOH), (b & c)-Pd/HT(LiOH), (e)-Pd/HT(CsOH) and (f)-Pd/HT($CsNO_3$).

The dispersion of palladium in the catalysts, obtained by hydrogen chemisorption, was expressed in terms of H/Pd ratio (fraction of exposed Pd atoms, see Table 1). The Pd/HT catalyst exhibits a Pd dispersion of 0.18, which is consistent with the average size estimated from TEM. The impregnation of HT with Na or Cs induces a decrease of the Pd dispersion, being the largest for Cs (Table 1). This phenomenon can be related to some embedding of Pd into the support surface, or by a decoration effect with some oxide species (Na, Cs) onto the Pd particles, thus decreasing the fraction of Pd exposed. However, for Li-modified HT, practically no significant changes of Pd dispersion were observed. On the one hand, TEM did not put in evidence any great difference in the average Pd size between the various catalysts. The Pd dispersion for catalysts prepared with different weight amounts of CsOH are shown in Table 1. For Pd/HT(CsOH)$_x$ catalysts the Pd dispersion decreased as Cs loading increased. On the other hand, the alkali hydroxide precursors produce a higher dispersion decrease than nitrate precursors.

The basic properties of the materials were examined using TPD of CO_2 as a probe molecule. Comparisons of the TPD profiles and the amount of basic sites of the catalysts are shown in Fig. 4 and Table 1, respectively. The CO_2 adsorbs selectively on basic sites, and the desorption temperature is an indication of the strength of the basic sites. From Fig. 4, a CO_2 desorption peak of around 658 K is observed for Pd/HT catalyst. A shift to lower desorption temperature was observed for LiOH modified catalyst (643 K). However, a shift to higher desorption temperature was observed for NaOH and CsOH (668K and 683 K, respectively). The shift to higher temperature for CsOH and NaOH modified catalysts is maybe due to the strong basic character of these alkaline metals compared to Li and Mg-Al mixed oxide species. When comparing catalysts obtained from alkali nitrate precursors calcined at 873 K, the Li catalyst showed a CO_2 desorption peak at similar temperature as the Mg-Al mixed oxide support (660 K). However, for Na nitrate precursor the desorption temperature of CO_2 increased up to 683K. However, for Cs nitrate precursor the CO_2 is desorbed at lower temperature (around 656K that is similar as the mixed oxide). The decrease of CO_2 desorption temperature observed for this Cs catalyst is probably due to the low decomposition of the alkali nitrate precursors during the calcination process (performed at 873K). This was confirmed by XRD.

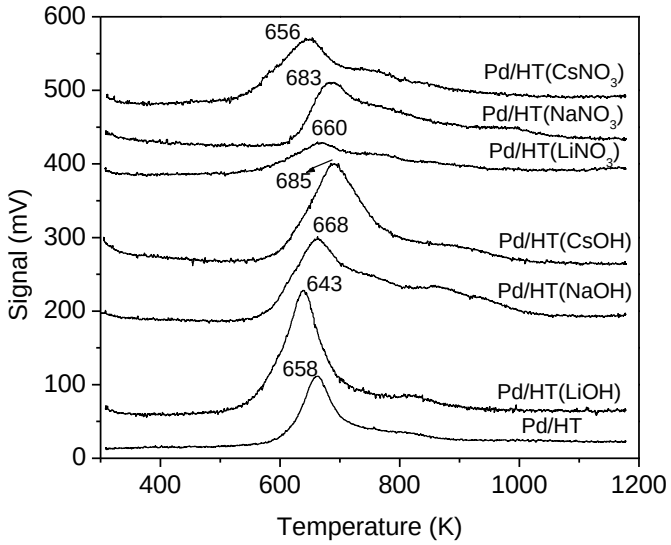

Fig. 4 CO_2-Temperature programmed desorption profiles for Pd/HT, Pd/HT(AOH) and, Pd/HT(ANO_3) catalysts.

The amounts of basic sites of the different catalysts are shown in Table 1. The CO_2 amount for Pd/HT catalyst was 3.7 mmol g^{-1}. The addition of alkaline hydroxides produces an increase in the amount of basic sites. When compare equimolar amount of alkali, the catalyst containing Li showed the highest number of basic sites (8.3 mmol g^{-1}). Furthermore, the addition of alkali using nitrate precursors produced a decrease in the amount of basic sites compared to those obtained by the hydroxide precursors. All catalysts doped with alkali metals showed higher amount of basic sites than non-doped catalysts.

2.2. Catalytic hydrodechlorination reaction

The modified Pd/HT catalysts were studied for HDC of 1,2,4-trichlorobenzene using a continuous reactor at atmospheric pressure and 373 K. The influence of type of alkaline metal and type of precursor on the activity, selectivity and stability of the HDC reaction were analyzed. The source of deactivation and different regeneration methods were also studied.

2.2.1. Effect of alkaline metals on the catalytic activity.

The comparative study of the modified palladium catalysts in the

HDC reaction of 1,2,4-trichlorobenzene was conducted at 373 K (Fig. 5). Pd/HT unmodified catalyst showed significant initial conversion of 65%. Catalysts modified by $NaNO_3$, $LiNO_3$, and LiOH showed high conversions (up to 85%), while the $CsNO_3$-doped catalyst showed moderate activity (77%). However, the catalysts based on Pd/HT(AOH), where A = Na and Cs, showed the lowest conversions (20 % and 30 %, respectively) at the same conditions. Additionally, Pd/HT(LiOH), Pd/HT($LiNO_3$) and Pd/HT($NaNO_3$) catalysts also showed the highest stability.

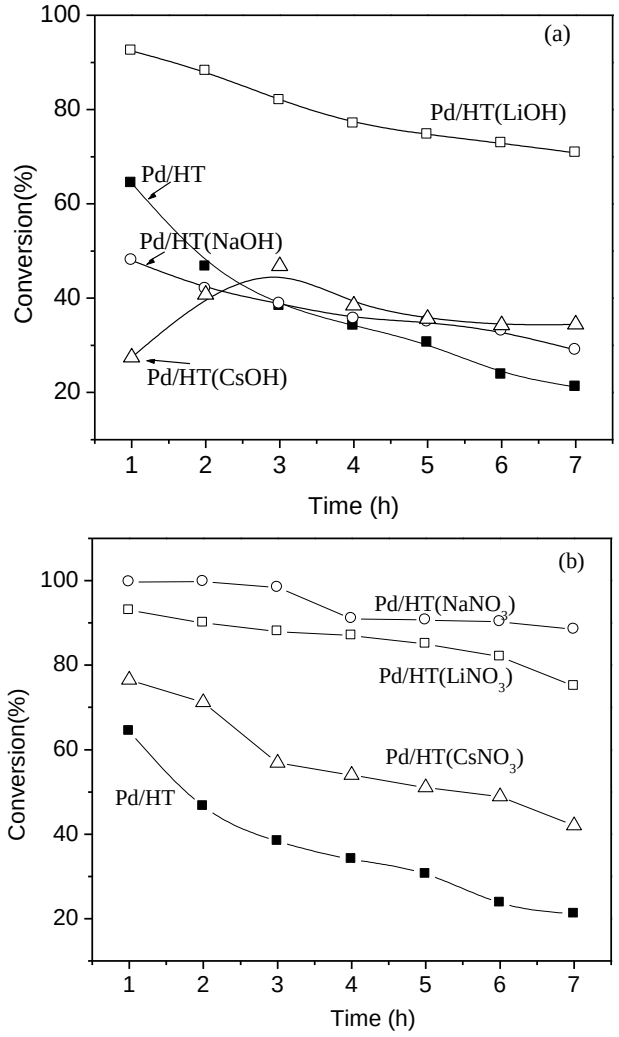

Fig. 5 Comparative HDC conversion through time of reaction at 373K of Pd/HT(AOH) (a), Pd/HT(ANO_3) (b) with the unmodified catalyst Pd/HT. (■) Pd/HT, (□) Li, (○) Na and (Δ) Cs.

From characterization results, it seems that two main factors could affect the catalytic activity: the basic properties and metal dispersion of the catalysts. For Pd/HT(LiOH) catalysts the metal dispersion is quite similar as the obtained for Pd/HT catalyst (around 20%). However, the addition of NaOH or CsOH decreases considerably the Pd dispersion (between 2% and 7%). So, a strong dependence between the number of Pd atoms exposed on the surface and the catalytic behaviour is inferred. The addition of alkali produces a decrease in the H_2 uptake capacity of the Pd particles and consequently a decrease in the metal dispersion [166]. However, the average size of Pd particles obtained by TEM showed similar values for all the catalysts (around 5 nm). Consequently, a decoration effect of palladium due to the addition of alkali metal ions seems to be responsible for the decrease in H_2 uptake. However, we have no detected any alkali metal oxide layer on the Pd surface by HRTEM. This is probably due to the low resolution of the HRTEM equipment that can only detect layers when a minimum number of ordered atomic rows are present. However, as it has been mentioned in the HRTEM discussion we cannot completely rule out some decoration effect of the alkali metals or the support due to their dissolution by the addition of the alkaline metals. Furthermore, the effect of the decrease in the H_2 uptake capacity of the catalysts may be explained in terms of alkali sizes. Li practically has not any effect in the Pd dispersion while Cs produces the highest dispersion decrease. Furthermore, the use of alkali hydroxide precursors caused a more pronounced decrease in dispersion compared to alkali nitrate precursors affecting the catalytic conversion (Fig.5).

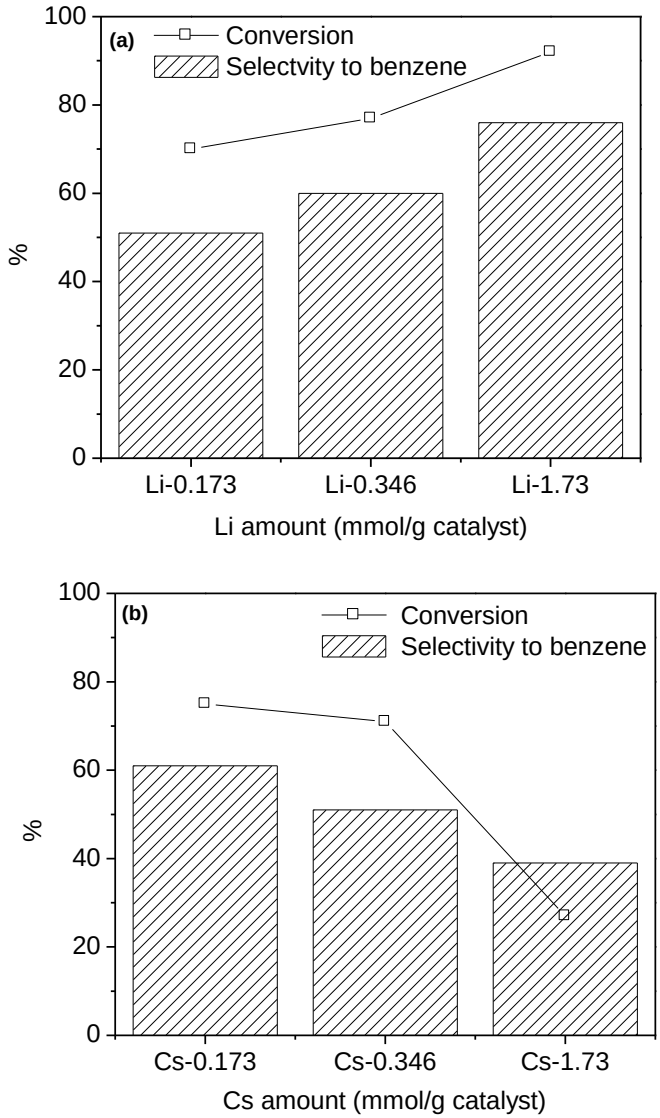

Fig. 6 Comparative HDC study of Pd/HT(LiOH) (a), Pd/HT(CsOH) (b) catalysts prepared with different amount of basic additives at 373K.

On the other hand, the different molecular weight of the alkaline hydroxide precursors generates an important difference in weight quantity, which could influence the catalytic activity. For this reason, we prepared different LiOH- and CsOH-doped catalysts based on different weight % of

alkali, Pd/HT (LiOH)x (where x = 1.2, 0.24 and 0.12 wt/wt% of Li) and Pd/HT(CsOH)x (where x= 22.8, 4.6 and 2.3 wt/wt % of Cs). The amount of alkali for LiOH and CsOH of these catalysts are equimolar and represent 0.17, 0.34 and 1.7 mmol of alkaliper gram of support, respectively. The initial conversion for the HDC of 1,2,4-TCB at 373 K over the above mentioned catalysts are shown in Fig. 6. The catalytic activity of $Pd/HT(LiOH)_x$ catalysts showed an increasing trend with increasing lithium content. The initial conversion achieved for the $Pd/HT(LiOH)_x$ catalysts was between 58% (for x=0.12) up to 96% (for x=1.2) (Fig. 6a). The same trend was observed in the selectivity towards the benzene formation. However, the $Pd/HT(CsOH)_x$ catalysts showed inverse behaviour in terms of both activity and selectivity to benzene. As the amount of Cs increased, the conversion and selectivity decreased significantly (Fig. 6b) which could be attributed to progressively covering of the active sites. This drop in HDC catalytic activity may be due to the fact that the harsh alkaline pH affected both the morphology of the support and the H_2 uptake capacity of metallic Pd.

However, we found that the catalytic behaviour of the alkali-doped catalysts does not depend only on the amount of alkaline species. The type of alkaline and the precursor used (hydroxide or nitrate salts) during the synthesis of the modified catalyst have also an important effect on the activity and selectivity in the HDC reaction.

A more rigorous comparison of intrinsic reactivity is required in order to understand the effect of the addition of alkaline. Fig. 7a indicates the catalytic activity expressed as the consumption of 1,2,4-trichlorobenzene per exposed area of Pd (expressed as $mmol.min^{-1}.m^{-2}$). The Pd/HT unmodified catalyst showed the lowest HDC activity (1.08 $mmol.min^{-1}.m^{-2}$), whereas the Cs doped catalysts showed the highest activity independently of the alkali precursor (around 3.6 $mmol.min^{-1}.m^{-2}$). The activity for Pd catalysts modified by Na and Li lies in between the Cs modified and unmodified catalysts as is shown in Fig. 7a. In general the HDC catalytic activity of 1,2,4-trichlorobenzene over these catalyst was Pd-HT(Cs) > Pd-HT(Na) > Pd-HT(Li) > HT regardless of the used precursor.

Furthermore, the activity correlates with the basicity of the doped support. The total basicity (expressed as $\mu mol.CO_2.m^{-2}$) versus the catalytic activity is plotted in fig. 7b. A clear correlation between the basicity and the

catalytic activity is observed. This implies that Pd can specifically be promoted by increasing the basic properties of the catalytic support [135].

Additionally, there is a relationship between the activity and the total basic sites (mmol CO_2 g^{-1} of catalyst) as shown in Fig 7c. It represents the total TCB consumed per exposed Pd surface vs the total basic sites. All alkali modified catalysts presented higher catalytic activity than unmodified Pd/HT catalyst. This is in agreement with the higher total basic sites for the alkali modified catalysts which follows a trend as PdHT(AOH) > PdHT(ANO_3) > PdHT. Furthermore the alkali hydroxide precursors showed higher amount of basic sites compared to those obtained by the nitrate precursors. This property is reflected clearly on the catalytic activity results where, in general, catalyst with hydroxide precursors scored higher catalytic activity than the nitrate counterpart. This is much more clearly observed for Li and Na modified catalysts where the hydroxide precursor scored higher catalytic activity than nitrate precursor.

Considering the activity of alkali nitrate modified catalysts, when the total basic site increase the activity also increases following a trend; Pd/HT($CsNO_3$)> Pd/HT($NaNO_3$)> Pd/HT($LiNO_3$). This is also in agreement with the intrinsic basic strength of the alkali metals which follows the tendency Cs> Na> Li. This indicates that catalytic activity can exclusively be promoted by increasing both number of basic sites and its strength at the same time. In contrast, Pd/HT catalysts modified with alkali hydroxide precursors showed higher catalytic activity as the total basic sites decreases. As shown in Table 1, the total basic site increases following a trend Pd/HT(LiOH) > Pd/HT(NaOH) > Pd/HT(CsOH). This result is in contra to the intrinsic basic strength of the alkaline metals (Cs>Na>Li). The decrease in total basic sites for Cs and Na modified catalysts may be accounted due to the surface dissolution of the support by the harsh alkaline solution of Na and Cs (Vida infra) which limits the distribution of basic site over the surface. Hence, in this case, the HDC catalytic activity is highly dependent in the intrinsic property of alkali metal species. The hydroxide precursor lead to a higher density of surface basic sites while nitrate lead to much lower density. However both cesium hydroxide and nitrate present the same activity since they possess comparable total basic sites. This indicates that the alkali metal is the main factor altering the activity.

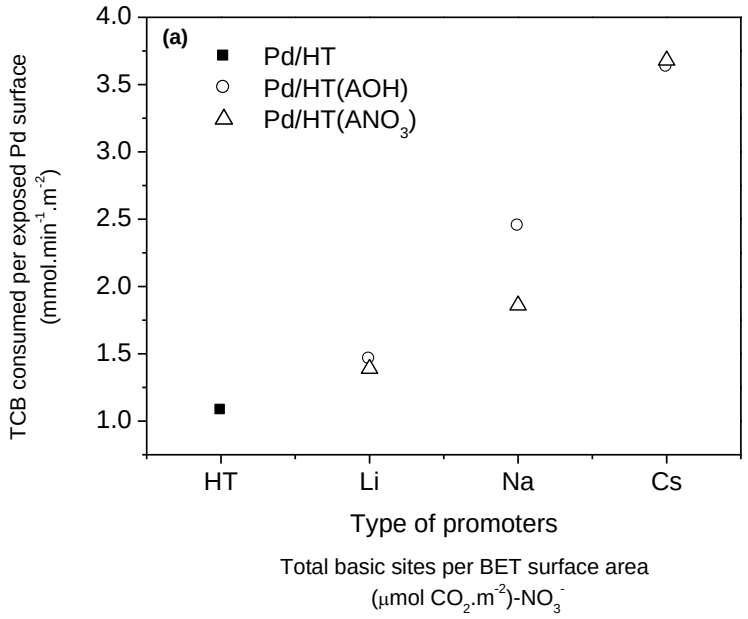
(a)
Pd/HT
Pd/HT(AOH)
Pd/HT(ANO3)
TCB consumed per exposed Pd surface
(mmol.min-1.m-2)
4.0
3.5
3.0
2.5
2.0
1.5
1.0
HT
Li
Na
Cs
Type of promoters
Total basic sites per BET surface area
(μmol CO2.m-2)-NO3-

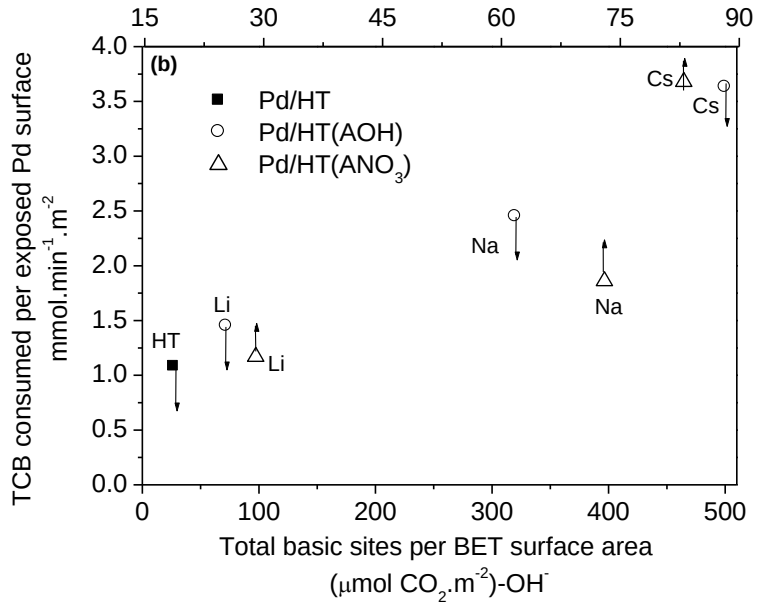
(b)
Pd/HT
Pd/HT(AOH)
Pd/HT(ANO3)
TCB consumed per exposed Pd surface
mmol.min-1.m-2
15
30
45
60
75
90
4.0
3.5
3.0
2.5
2.0
1.5
1.0
0.5
0.0
0
100
200
300
400
500
HT
Li
Li
Na
Na
Cs
Cs
Total basic sites per BET surface area
(μmol CO2.m-2)-OH-

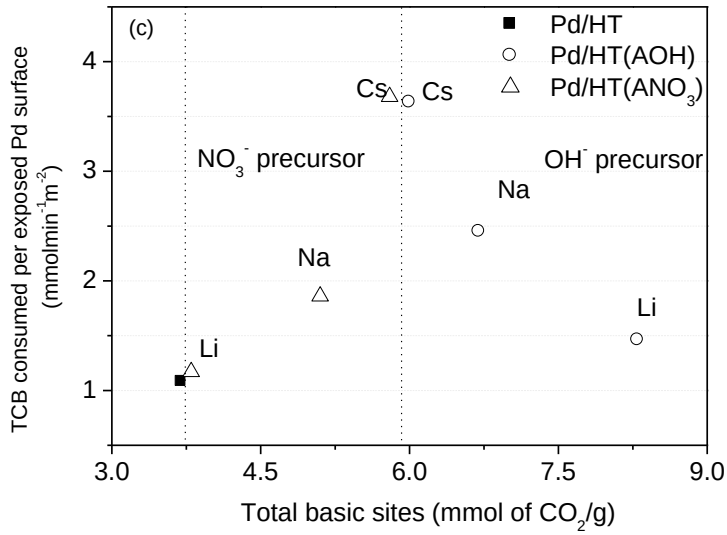

Fig. 7 TCB reaction rate expressed by TCB consumed (mmol.min^{-1}) per exposed Pd surface (m^2) (a) vs. different alkaline metals and precursors (b) vs. number of basic sites in terms of μmol of CO_2/m^2 of the catalyst (c) vs. number of basic sites in terms of mmol of CO_2/g of the catalyst.

2.2.2. Effect of the alkaline metals on the selectivity.

The HDC of 1,2,4-trichlorobenzene is a sequential reaction that produces dichlorobenzenes, chlorobenzene or benzene as products (Scheme 1). The detected products were benzene, chlorobenzene, *o*-dichlorobenzene and *p*-dichlorobenzene. We did not observe the production of *m*-dichlorobenzene during the reaction. A blank test with the support (Mg-Al mixed oxide) showed no conversion of 1,2,4-trichlorobenzene at the reaction conditions. The mixture of products was mainly formed by benzene and *o*-dichlorobenzene. In general, throughout the reaction, the production of *o*-dichlorobenzene was favoured for all catalysts, which suggests that the HDC of *o*-dichlorobenzene to chlorobenzene or benzene is the rate-limiting step. On the other hand, the difference in the product distribution of the dichlorobenzene compounds may also be related to the inductive and steric effects induced by the Ph-Cl bonds [49]. The chloride situated in the *p*-

position (position 4) is likely to be easily substituted since it is less influenced by the steric effect from the neighboring chlorides. This favours the higher rate of *o*-dichlorobenzene production. Bearing in mind the steric effect, the substitution of the chloride in the *o*-position (Position 2) seems more difficult. This contradicts with our results in which the rate of formation of *p*-dichlorobenzene was higher than that of *m*-dichlorobenzene. This is explained by the electronic effects rather than by steric hindrance. The electrophilic attack on the *o*- position (position 2) therefore seems to be preferred. In general, the steric effect dominates and can explain the high rate of *o*-dichlorobenzene formation, whereas the electronic effect supports the formation of *p*-dichlorobenzene rather than *m*-dichlorobenzene.

Fig 8 shows, the effect of the type of alkaline metal used (1.7 mmol per gram of catalyst) and its precursors (AOH or ANO_3) on the selectivity towards benzene. The modified palladium catalysts presented higher selectivity than their unmodified counterparts, particularly the Pd/HT(ANO_3) and Pd/HT(LiOH) catalysts. CsOH and NaOH modified catalysts showed similar selectivity to benzene as compared to the unmodified Pd/HT catalyst.

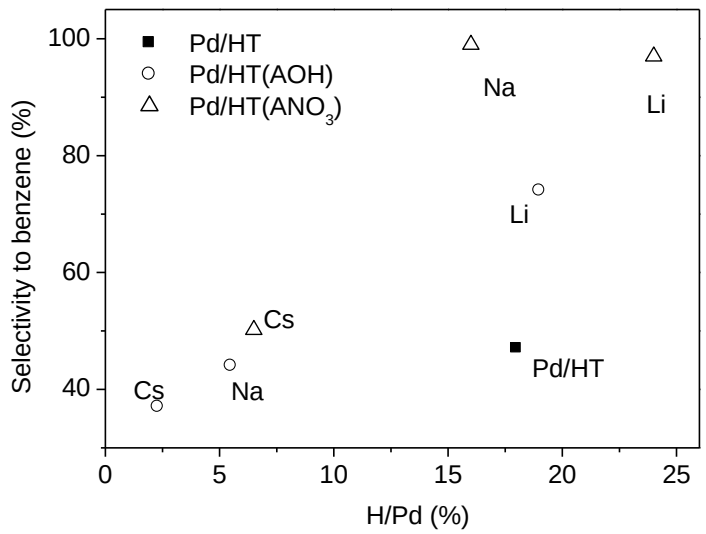

Fig. 8 Selectivity to benzene for Pd/HT, Pd/HT(AOH) and Pd/HT(ANO_3) catalysts Vs Pd dispersion (H/Pd) as obtained by H_2 chemisorption.

Fig. 8 also relates the selectivity of the catalyst to benzene versus (H/Pd) ratio determined by hydrogen chemisorption, in order to assess the effect of Pd dispersion on the selectivity. The H/Pd ratio also revealed a clear relationship for the selectivity to benzene. In fact, as the dispersion of the catalyst increases the selectivity to benzene also increases. The presence of higher dispersion of Pd in the catalyst favours the formation of high amount of active hydrogen species that are necessary to achieve a higher hydrodechlorination degree. In this case, catalysts containing higher dispersion like Li doped catalyst possess higher selectivity towards benzene with respect to Cs catalysts. This fact could be explained by the low H_2 uptake capacity of the Pd particles for Cs-doped catalysts as determined by H_2-chemisorption. In this case, it is assumed that the large ionic radius of Cs covers the Pd particles, which, to a certain extent, hinders the diffusion of the molecular hydrogen or the chloroaromatic compound. However it seems that the selectivity of the catalysts did not consisted of a merely effect of the dispersion Pd clusters. From Fig. 8 we can also observe, when compare with the non promoted catalysts (Pd/HT) that shows a higher Pd dispersion, that the modification of the catalyst by basic additives is influential for increasing the selectivity to benzene.

Furthermore, the alkali nitrate doped catalysts presented a higher selectivity to benzene when compared with the alkali hydroxide modified catalysts. This behaviour can be explained in two ways. The first is related to the morphology of the catalysts. In this case, Pd/HT(ANO_3) catalysts presented a moderate decrease in surface areas probably because of the lower basic property of the impregnating precursor solution. In contrast the surface area of Pd/HT(AOH) catalysts (except for Pd(LiOH)) drastically decreased by the strong alkaline hydroxide solution resulting into a low catalytic selectivity to benzene.

The second explanation involves the hydrogen adsorption capacity. In this case the Pd/HT(AOH), (where A represents Na or Cs) presented a significant decrease of hydrogen uptake capacity than the Pd-HT(ANO_3) catalysts. This could be due to a lower decoration effect of metallic Pd sites by alkali metal or the support species.

2.2.3. Stability and regeneration of catalysts

The source of deactivation during the HDC reaction could be related to the presence of chloride species, cocking or metal sintering. The deactivation behaviour is usually related to the operation conditions. It is well known that, during the hydrodechlorination reaction of chlorinated compounds using supported metal catalysts, the chloride species formed during the reaction can interact with the metal and basic sites of the catalyst leading to its deactivation [167, 168].

Fig. 5 revealed a conversion decrease for all the catalysts with time on stream. The Pd/HT catalyst showed the rapid deactivation as compared to the alkali modified catalysts at a given time of reaction. The Cs and Na modified catalyst have shown best stability for HDC of 1,2,4-TCB than the Li modified ones. This suggests that the basicity of the catalysts, apart from the promoting the catalytic activity, it is also influential for promoting stability of the catalyst. The extra-stability of the doped catalysts can be explained for the greater affinity of the chloride, produced during the reaction, to the strong basic alkali surface than to the accessible Pd particles. In general, the chloride affinity towards the alkali surface increases with increase in basicity of the alkali metal impregnated.

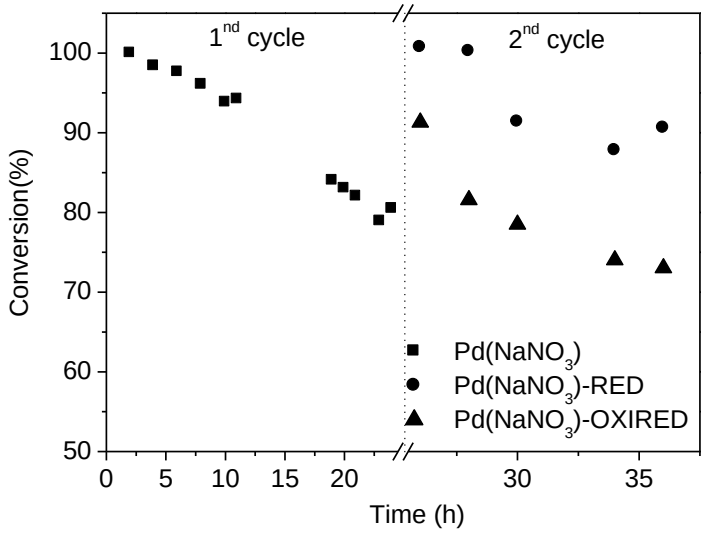

Fig. 9 TCB conversion (%) vs time on stream for fresh and regenerated Pd/HT($NaNO_3$) catalysts.

In order to study the stability and regeneration of the catalysts a reaction test for 24 hours was performed for the Pd/HT ($NaNO_3$) sample (see Fig. 9). This catalyst has been chosen owing to its high stability during the seven hours of catalytic test. From Fig. 9 a decrease of conversion from 100% to around 80% was observed after 24 hours on stream. Two in situ procedures of catalyst regeneration were employed. The first one involved calcination step at 573K for 2 hours by flowing O_2 at 20 ml/min followed by reduction with H_2 flow (20ml/min) for 2 hours at 573K. In the second type of regeneration method only the reduction treatment was employed.

Catalytic tests of the regenerated samples compared to the fresh one are presented in Fig. 9. Taking in account the behaviour of the fresh sample at the end of its run (at 24 hours) it is clear the improvement promoted by both regeneration procedures. This improvement can be explained by elimination of chloride and organic species on the surface of the used catalyst by the regeneration methods. Particularly for the sample treated by the reductive regeneration process we observed a slight increase in the activity compared to the oxidative-reductive procedure. Under oxidative-reductive condition, the oxygen treatment step may result in a more pronounced sintering of the palladium exhibiting low metal dispersion [169] explaining the lower activity improvement compared to the reductive regeneration procedure.

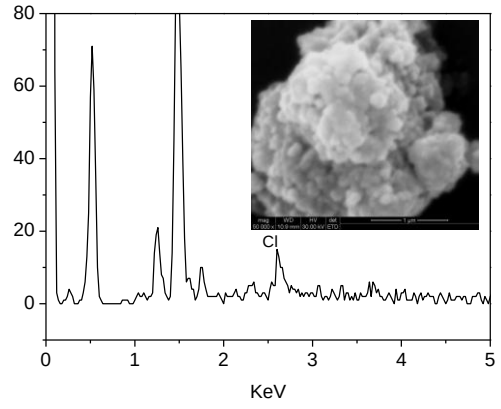

Fig. 10 ESEM image of used Pd/HT coupled with EDX spectra.

The used catalysts were characterized by ESEM-EDX, N_2-physisorption, HRTEM, and XPS techniques. The results suggested that there is surface modification most probably by the chloride species produced during reaction. Characterization of used Pd/HT by ESEM-EDX shows that the texture of the catalyst shows a more agglomerated structured as is shown in Fig.10. Furthermore the EDX spectrum has revealed the existence of chloride species. The N_2 physisorption analysis for used Pd/HT showed a BET surface area of (32 m^2/g) and a pore volume of (0.19 $cm^3.g^{-1}$) indicating a significant lost in the textural properties during the HDC reaction. Furthermore, Fig. 11a shows a representative HRTEM image of Pd/HT used sample. Pd particles of about 5.0-5.2 nm in diameter are well distributed over the support. In the image, lattice spacing at 1.94 Å is ascribed to (200) plane of fcc Pd. Concerning the support, lattice fringes at 2.10 Å are ascribed to (200) of MgO. As a general rule, the support contains mainly well-defined MgO crystallites with sharp edges along with less crystalline phase, which is probably aluminum oxide. Fig. 11b corresponds to a HRTEM image of the support only and its corresponding Fourier Transform (FT) image. In the FT image there are only rings at 1.49 and 2.10 Å, which are ascribed to (220) and (200) planes of MgO. No spacings corresponding to $MgCl_2$ have been detected in any case, suggesting that $MgCl_2$ is not present in the sample or, if it does, should be in the form of an amorphous phase that escape HRTEM detection. The HRTEM of the used Pd/HT($NaNO_3$) sample is indicated in Fig. 11 c. Again, Pd particles of about 5.1-5.3 nm in diameter are well distributed on the support (see particle labeled “b” in the Fig. 11c). The FT image of particle “b” shows lattice fringes at 1.94 Å corresponding to Pd (200). The support, labeled “a” in the image, shows lattice fringes only at 2.10 Å, which are ascribed to MgO (200). Again, no evidence for the presence of magnesium chloride has been found.

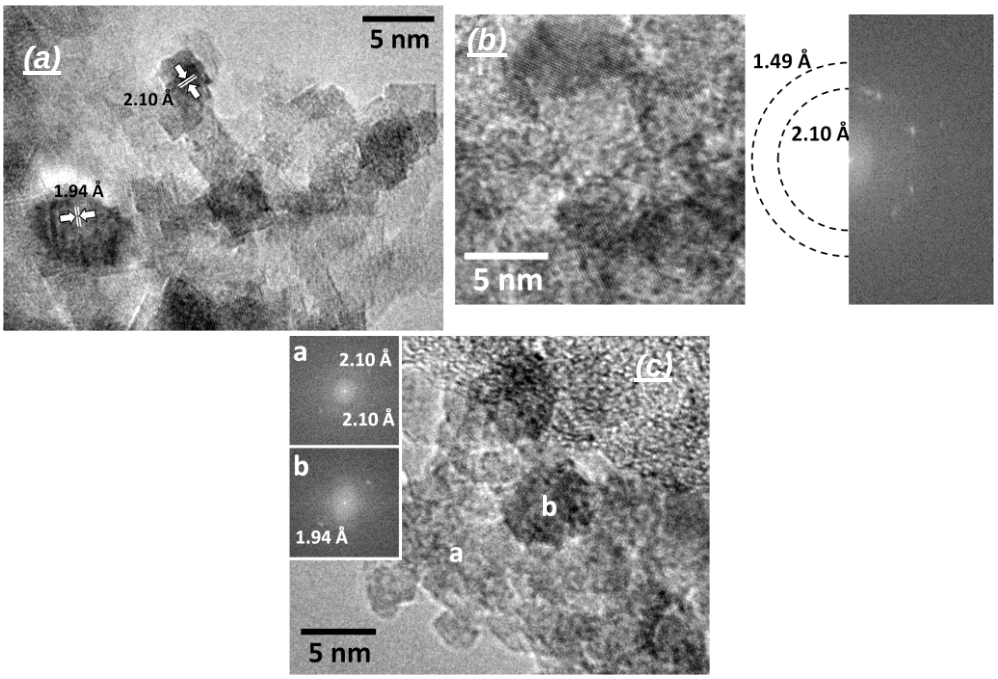

Fig. 11 HRTEM images of (a & b) used Pd/HT catalyst (c) used Pd/HT($NaNO_3$) catalyst.

The binding energy values from XPS of Pd/HT($NaNO_3$) for fresh, used and regenerated by reduction samples are compiled in Table 2. The binding energy of Al 2s is located in a narrow range between 119.1 and 119.5 eV. Concerning the Mg 2s signal, the binding energy for fresh and used catalysts showed very similar values (88.9 and 88.8 eV, respectively). However, it is interesting to note that the binding energy for regenerated catalyst presented a value of 89.6 eV, which is higher than for the fresh and used catalysts. This value of binding energy can be ascribed to the presence of $MgCl_2$ species [170]. These $MgCl_2$ chloride species on the surface of the catalyst were formed during the regeneration protocol. Probably, the chloride species, on the surface of Pd of the used catalyst, are removed by H_2 during the regeneration process forming HCl. Then the HCl produced reacts with the magnesium oxide near the Pd particle forming the $MgCl_2$.

Table 2:- XPS results of fresh, used and regenerated Pd/HT ($NaNO_3$) catalysts.

Pd/HT($NaNO_3$) Catalyst	XPS binding energy (BE, eV)					
	Al2s	Mg2s	Na1s	Pd3d	Cl2p	
	BE	BE	BE	BE	BE	%[a]
F	119.5	88.9	1073.0	337.0	-	-
U	119.3	88.8	1072.8	336.3	198.8	5.2
R	119.1	89.6	1074.6	336.6	198.6	10.6

F-fresh, U- used, R-used regenerated by reduction

[a]-percentage composition

Concerning the Na 1s core level, again similar binding energy values were obtained for fresh and used samples (around 1073.0 eV), whereas a remarkable increase of the Na 1s binding energy is observed for regenerated sample (1074.6 eV). This fact could be ascribed to the formation of NaCl species [57] in the same way as the formation of $MgCl_2$. Concerning the Pd, the binding energy values for fresh, used and regenerated catalysts were 337.0, 336.3 and 336.6 eV, respectively. It is known that Pd^o shows a binding energy value of around 335 eV [171]. Furthermore, by HRTEM we have observed that Pd for fresh, used and regenerated is as Pd^o. The explanation of the high binding energies observed for these catalysts could be ascribed to an electron transfer of Pd to the Mg^{2+} and Na^+ that are located on the support near the Pd, and by the presence of chloride species for the used and regenerated catalysts [57, 171]. Furthermore the XPS also shows the presence of chloride species for used and regenerated catalysts that appears between 199.6- 199.8 eV. Moreover, the presence of chloride species detected by XPS is higher for the regenerated catalyst than for the used one (10.6 and 5.2 %, respectively). Additional support for the distribution of chloride on the surface of the catalyst was also given by EDX analysis of the used and regenerated material (Fig 12). Chloride species were detected in

both used and regenerated catalysts. However, for the regenerated one the level of the chloride species is lower. This is reasonable since EDX is bulk technique while XPS is a surface technique. It seems that significant amounts of the chloride species removed after hydrogen treatment are trapped on the surface. This correlates with the presence of high binding energy values for Mg and Na only observed by XPS for the regenerated sample. This may suggest that the HDC reaction and reductive regeneration may result in a change of environment of active metal site, alkaline promoter and support material probable due to the chloride species.

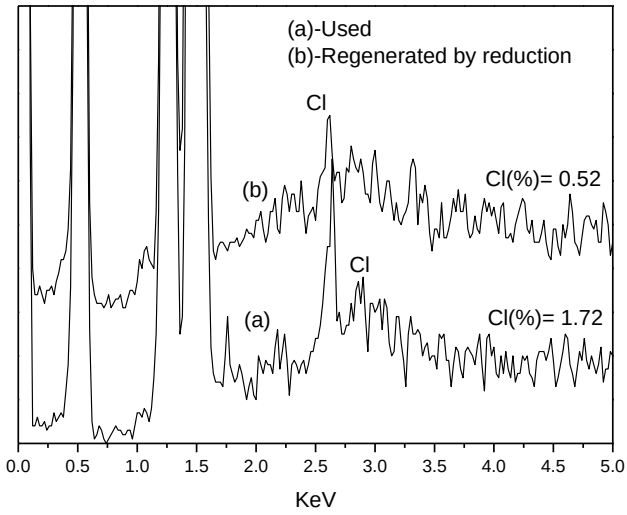

Fig. 12 EDX spectra for used and reductively regenerated Pd/HT($NaNO_3$) catalyst.

Conclusion

Alkaline-metal-modified Pd/HT catalysts were synthesized for the HDC reaction of 1,2,4-trichlorobenzene. The catalysts were modified by addition of alkaline nitrates and alkaline hydroxides precursors. The alkaline-metal-modified Pd/HT catalysts showed lower BET surface area, H_2-uptake capacity (mainly for Cs and Na catalysts) and crystallinity than the unmodified Pd/HT catalyst. However, the average size of Pd particles was quite similar for all the catalysts. On the other hand, depending on the alkali

precursor Pd/HT-modified catalysts presented some differences in basic strength with respect to the Pd/HT catalyst. The total number of basic sites followed the trend: Pd/HT(AOH) > Pd/HT(ANO_3) > Pd/HT.

In general, the modified catalysts showed higher activity, stability and selectivity than the Pd/HT unmodified catalyst. However, differences in catalytic behaviour depended on the type of alkaline metal or alkaline precursor used. The basicity of the alkaline metals is considered responsible for the higher activity of the modified catalyst. The main products obtained were *o*-dichlorobenzene and benzene. In general, higher selectivity to benzene was recorded for the alkali-modified catalysts, particularly for alkali nitrate modified catalysts. However, the poor selectivity to benzene of the CsOH and NaOH modified catalysts than the nitrate may be due to the harsh alkaline impregnating solution, which affects their textural and metallic properties. The used catalysts can be regenerated by calcination-reduction and reduction treatments. However, reductive regeneration resulted in a change of environment of active metal site, alkaline promoter and support material probable due to the chloride species.

4.3.

Catalytic HDC of 1,2,4-trichlorobenzene over Pd/Mg(Al)O catalysts: Effect of the calcination temperature of the support

From the above sections it has been demonstrated that the catalysts performance (activity and stability) problem can be minimized by employing a suitable catalyst-support system. Basic layered hydrotalcite (Mg-Al precursor) derived mixed oxides have been explored as viable support in HDC of 1,2,4-TCB. The effect of basic supports or basic additives during HDC reactions have been clearly seen to enhance the catalytic activity.

As explained in the introduction section, the thermal decomposition of hydrotalcite leads to the formation of $MgAlO_x$ mixed metal oxides, which are characterized by high specific surface areas, homogeneous dispersion of metals and unique acid–base properties[101]. During calcination it progressively loses physisorbed water, interlamellar water molecules and finally water from the dehydroxylation of the layers along with the charge-compensating anions leading to the collapse of the layered structure forming homogeneous Mg/Al mixed oxide. Further calcination of the $MgAlO_x$ mixed

oxide at higher temperature results a segregated MgO and spinel ($MgAl_2O_4$) like phases. As a result depending on the calcination temperature the surface properties progressively changes allowing for the preparation of a target material with specific applications. For instance the spinel phase possesses a good combination of features like good mechanical strength, low dielectric constant and high chemical resistance against both alkali and acids [172]. Different metal dispersion, acid-base property can be obtained depending on the calcination temperature of the Mg/Al supports. As a result the effect of calcination temperature was worth of studying for HDC reaction owing to these properties.

With this regard various $MgAlO_x$ mixed oxide calcined at different temperatures were used as support in catalytic HDC reaction of 1,2,4-TCB. The Pd supported over these mixed oxide species were comparatively investigated for HDC reaction of 1,2,4-TCB. The effect of different crystalline phases and influence of support basicity on Pd activity and selectivity were discussed. The structure influence of hydrotalcite (HT) support by changing the calcination temperature was evaluated.

1. Experimental

1.1. Preparation of catalysts

Full details of the support synthesis were given previously. In brief, the hydrotalcite-like compound was prepared by co-precipitation of suitable amounts of $Mg(NO_3)_2 \cdot 6H_2O$ and $Al(NO_3)_3 \cdot 9H_2O$ (Mg/Al molar ratio of 3) with NaOH 2 M at pH 10. The resulting gel was washed several times thoroughly with distilled water (Na<100 ppm) to remove any presence of free sodium ions. The sample was dried and calcined under air flow at different calcination temperatures (523, 723, 923, 1123 K) for 12 h (heating rate: 20 K min^{-1}). These supports were used to prepare the metal catalysts by depositing palladium by the incipient wetness impregnation method. The used metal precursor was Pd(II) acetylacetonate ($Pd(acac)_2$) instead of $PdCl_2$ to avoid any residual chlorine in the final catalyst. A solution of Pd $(acac)_2$ and toluene was impregnated over the corresponding mixed oxide supports. The nominal Pd content in all samples was kept at 1 wt%. The samples were dried and again calcined in air at 673 K for 3h. The catalysts were reduced *in situ* at 623 K for 2 hours prior to the reaction. The palladium catalysts were

denoted as Pd/HT523, Pd/HT623 Pd/HT923 and Pd/HT1123, where the number represents the calcination temperature (K) of the support.

1.2. Characterization of catalysts

Textural properties of the solids were obtained from N_2 adsorption-desorption isotherms at 77 K using a Micromeritics ASAP 2000 surface analyzer. The XRD analysis of the materials was recorded similar as section 4.2. The morphologies of the catalysts were observed by SEM with a JEOL JSM-35C scanning microscope as explained in section 4.2. The basic properties of the materials were characterized by TPD of CO_2 as mentioned in section 4.2 but without prior desorption of the weakly adsorbed CO_2.

1.3. Catalytic activity

The hydrodechlorination (HDC) of 1,2,4-trichlorobenzene (124TCB) in hexadecane (4/96, vol/vol) (Sigma-Aldrich) was studied in a tubular fixed-bed flow reactor (10 mm i.d., 200 mm long) using 0.25 g catalyst at atmospheric pressure as mention in section 4.2.

2. Result and discussion

2.1. Catalyst characterization

The BET surface area and pore volumes of the catalysts were analyzed by the N_2-physisorption results and are displayed in Table 1. As the calcination temperature increases both the BET surface area and pore volume of the catalysts decreases. As shown in Table 1 HT623 catalyst is associated BET surface area and pore volume of with 94 m^2/g and 0.25 cm^3/g respectively. The lower surface area and pore volume exhibited by this catalyst is due to the existence of different surface and interlayer molecules in the mixed oxide structure occupying pores. Under calcination at 723K the surface area and pore volume increased dramatically to 210 m^2/g and 0.48cm^3/g respectively. This increase shows that the surface and interlayer components (water in layer, dehydroxilation, and carbonate) are removed completely from the catalyst creating craters in the metal oxide sheet. As the catalyst was further calcined at higher temperature 923 K both the surface area and the pore volume started to decline progressively. Finally 111 m^2/g

and 0.35 cm^3/g of BET surface area and pore volume was recorded for catalyst calcined at 1123 K respectively. This shows that the high temperature calcination destroys the porous structure. The pure spinel calcined at 1123 K show also lower BET surface area of 78 m^2/g and pore volume around 0.35 cm^3/g. While the pure MgO catalysts calcined at 1123 K scored lowest BET surface around 58 m^2/g and pore volume of 0.1 cm^3/g which shows good thermal resistance property of spinel than the MgO. The pore volumes of each catalyst are displayed in table 1. When the calcination temperature increased to 723 K an increase in pore volume was observed (0.48 cm^3/g). While further aumenting the temperature, a decrease in pore volume values were noticed probably due to the collapse of the pores. The isotherms of the mixed oxides calcined at different temperatures are also shown in fig 1. The isotherm closely resembles a type II isotherm, where the N_2 uptake increases with the P/Po values due to the sorption by the mesoporous.

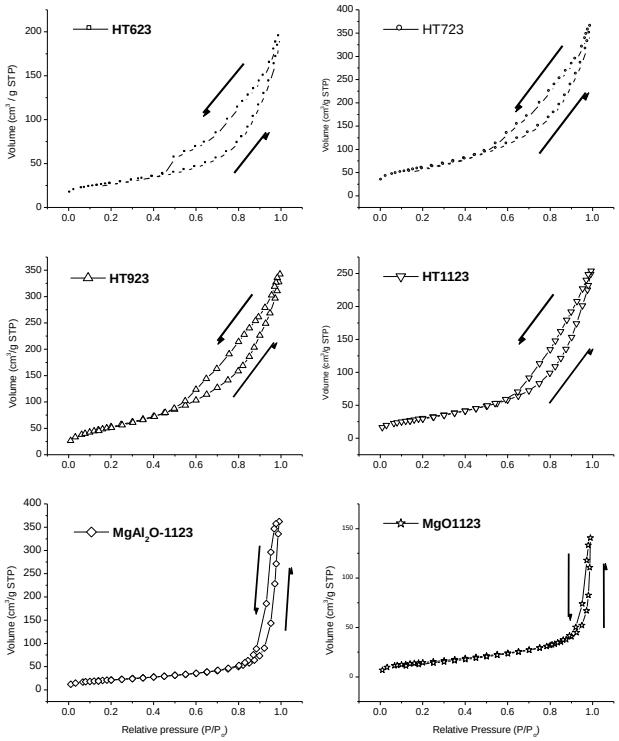

Fig. 1 Isotherm plots obtained from the N_2 physisorption analysis at 77K.

Table 1 Some characteristics of the catalysts

Sample	BET surface ($m^2\ g^{-1}$)	Pore volume ($cm^3\ g^{-1}$)	Total CO_2 desorbed (mmol of CO_2/g)[a]
HT623	94	0.25	1.6
HT723	210	0.48	1.1
HT923	170	0.40	0.33
HT1123	111	0.35	0.08
SP1123	78	0.35	0.05
Pd-MgO-1123	52	0.10	0.18

[a] Obtained by deconvolution of CO_2-TPD profile.

X-ray diffraction analysis conducted for the Pd supported catalysts is comparatively displayed in Fig. 2. Decomposition of the hydrotalcite with temperature has resulted transformation of the hydrotalcite like structure. The obtained results reveal that the layered structure of hydrotalcite disappeared for catalysts calcined at 623K. The positions of diffraction lines correspond to the (111), (200) and (220) diffractions of mixed cubic MgO-like oxide. The formation of an intense mixed oxide phase with periclase structure (JCPDS file 087-0653) can be observed as the calcination temperature is raised up to 723 K, which the intense periclase phase was observed. Apparently the mixed oxide is MgO phase, where the Al cations are evenly distributed throughout the structure, creating a solid solution. The periclase structure of the mixed oxide is still conserved during calcination at 923K. However, calcination at higher temperature (1123K) leads to segregation of mixed oxide to MgO and $MgAl_2O_4$ (spinel) structure as shown in the Fig.2 This results a significant change in the textural property of the support as shown from the BET and Pore volume results. Furthermore as the calcination temperature increases the crystallinity of the materials also increases. This can also justify for the decrease in surface area and pore volume in addition to the destruction of the porous system and segregation during calcination. Pure spinel ($MgAl_2O_4$) and periclase (MgO) phases were

analyzed after calcination at 1123K for comparison.

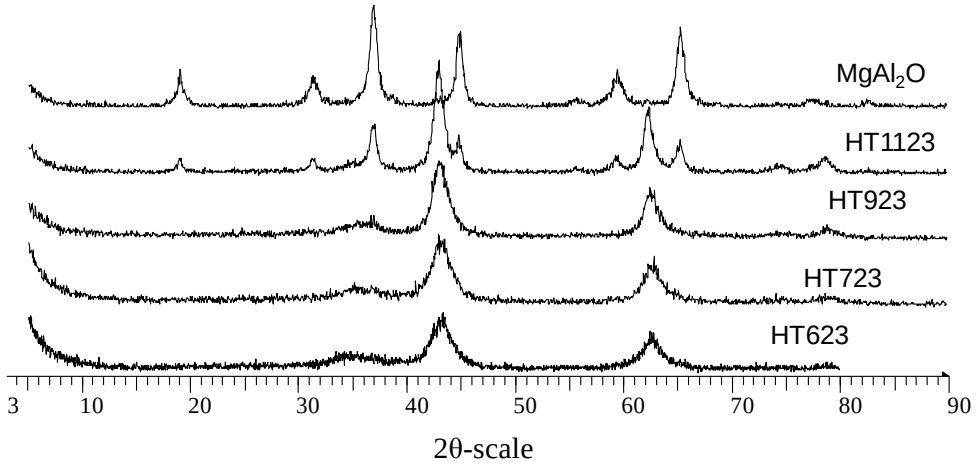

Fig. 2 X-ray diffraction patterns for hydrotalcite calcined at different temperatures, Spinel and MgO materials.

Thermal decomposition of hydrotalcite precursors leads to the formation of the corresponding Mg/Al mixed oxides, and spinel like phases, whose textural properties depend on the calcination temperatures. The SEM profiles shown in Fig. 3 were used in order to investigate the surface morphological evolution of hydrotalcite structure with calcination temperature. Distinct surfaces were obtained depending on the calcination temperature used. Typical platelet like morphology was observed for the hydrotalcite materials as shown in Fig. 3. MgO surface was characterized as layer like structures with big grain size similar to hydrotalcite structure. The platelate like structure was destroyed by calcination at 723 K and uniformly distributed surfaces with small particles were observed. Almost similar surface morphology was observed for Pd/HT calcined at 923 K. Further calcination of the Pd/HT at 1123K resulted in different morphology. It consists of aggregated small particles with irregular shapes, which may be a result of the structural collapse caused by incomplete filling of the metal sources. This structure was similar to the pure $MgAl_2O_4$ spinel prepared as shown in the Fig. 3.

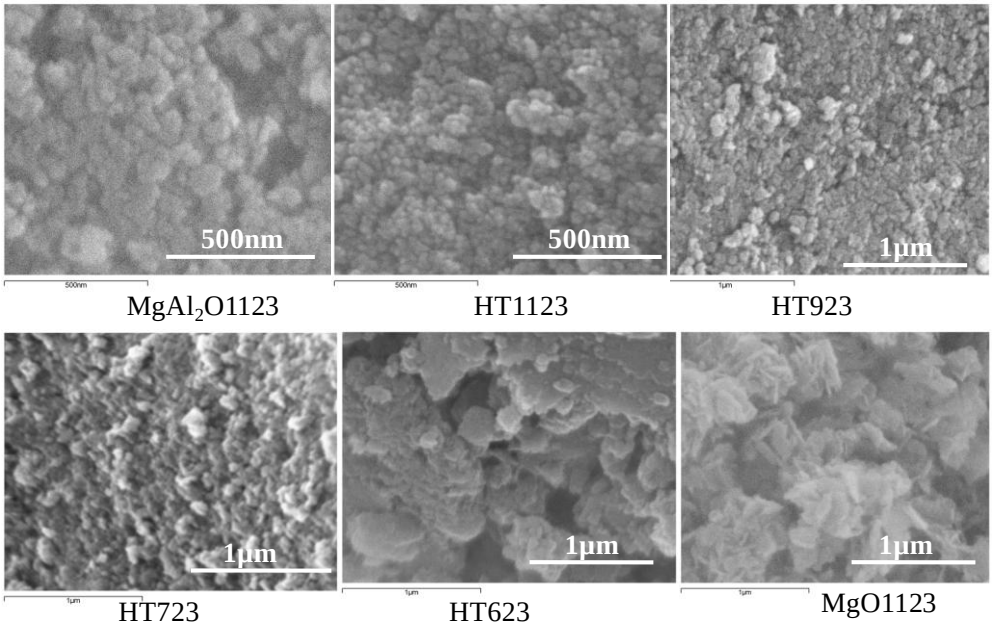

Fig. 3 SEM profiles of the mixed oxides calcined at different temperatures, Spinel and MgO.

The basicity of an oxide surfaces is generally related to the electro donating properties of the combined oxygen anions (Lewis) or adsorbed OH^- groups (Brønsted) so that the higher the partial negative charge on the combined oxygen anions, the more basic oxide [100]. The nature, strength and relative amounts of these sites depend essentially on the nature and molar ratio of cations, and the calcination temperature, as extensively shown from several physico-chemical characterizations and reaction tests. Probing the basic sites by acidic CO_2 is the conventional way to study the basicity of a solid.

The total amount of the CO_2 was determined by integration of the relative peak areas. Calcined hydrotalcite generally has been characterized to have three types of basic sites which have interact with the CO_2 different degree. The bicarbonates are formed over Brønsted OH^- groups and represent weak basic sites, the bidentate and monodentate carbonates are attached probably to the M-O pairs and monodentate carbonates formed on low coordinated oxygen anions which are strong basic sites [100, 173].

The CO_2-Temperature programmed desorption profiles for calcined samples are presented comparatively in fig 4. The CO_2-TPD profile in all

samples contains a low temperature peak around 370-400 K. This peak can be assigned to the bidentate and monodentate carbonates desorbed from the M-O pairs. The intensity of this peak decrease as the calcination temperature increases. The lowest is recorded for the HTO1123 support. As shown in the Fig. 4 higher desorption peaks was recorded for HT723 sample followed by HT923, HT623, respectively. The CO_2-TPD profile for HT623 samples possess another peak located at around maximum of 814K. This CO_2 desorption peak could be related to bicarbonate groups formed by the interaction of CO_2 with hydroxyl groups in the mixed oxide.

The HT723 has additional CO_2 desorption peak centered at maximum 633K. Apparently the desorption peak is associated with CO_2 adsorbed in relatively stronger basic sites of the O^-. From this profiles we can understand that the HT723 support possess much weaker basic site as compared to the HT623 support. Further calcination of the hydrotalcite at higher temperature progressively reduces the stronger basic sites that are associated to the high temperature desorption peaks. As shown for HT923 support, it is characterized by a unique broad CO_2 desorption peak located at around maximum of 449K. This desorption peak is assigned to the CO_2 adsorbed on the weaker basic sites of the mixed oxide as explained above. The HT1123 is associated with small peak located 440K. The spinel property is similar to that of alumina, which is influential for enhancing metal dispersion. It has low basicity when compared to $MgAlO_x$ mixed oxide (periclase) and higher than Alumina. In general as the temperature increases the basicity due to the Brønsted type of basic sites (characterized by high temperature CO_2 desorption peaks) gradually disappears leaving the Lewis type of basic sites. The amount of CO_2 desorbed was calculated from the integration of CO_2-TPD profiles and are displayed in table 1. It can be seen that increasing the calcination temperature diminishes the number of strong basic sites due to the O^- groups of the support. In contrast the Lewis type of week basic sites are favored with increasing temperature. The total basic site follows a trend as HT623>HT723>HT923>HT1123

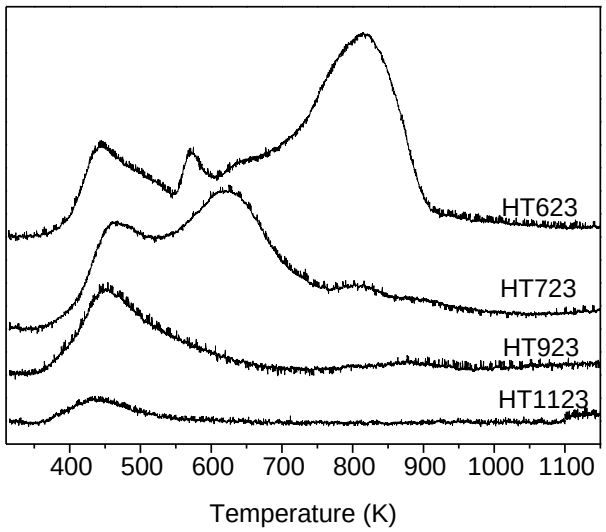

Fig. 4 TPD-CO_2 profile for the prepared catalysts.

2.2. Catalytic activity

The effect of support calcination temperature was investigated for the HDC reaction of 1,2,4-trichlorobenzene. The initial catalytic activities and selectivity towards benzene and O-Dichlorobenzene of the catalysts was comparatively displayed in Fig. 5. The catalytic activities follow a trend Pd/HT623 > Pd/HT723 ≈ Pd/HT923 > Pd/HT1123. The catalytic behaviors can be explained taking account the number, strength and probably type of basic sites over the catalysts. Consequently the higher number of basic site and strength of Pd/HT623 catalyst resulted in higher catalytic activity. The higher catalytic activity achieved by the Pd/HT623 catalyst can be related to its higher basicity, probably due to the existence of some OH^- groups, as observed from the TPD-CO_2 profile. In contrast, the Pd/HT1123 catalysts with low basic property resulted in lower catalytic activity. In general as the basicity of the support increases the catalytic behavior tend to increase for the mixed oxides supported catalysts. However it is important to note both Pd/HT723 and Pd/HT923 catalysts, which the later possess higher number basic site and strength, achieved similar catalytic activity. The similar

catalytic behavior observed for these catalysts despite basicity difference could be explained in terms of the type of basic sites observed.

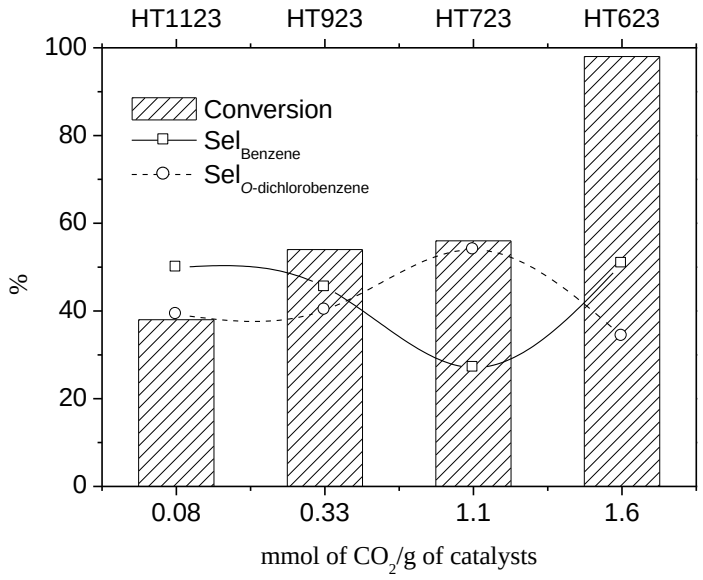

Fig. 5 Catalytic behavior of the prepared catalysts at 373 K.

The selectivity of the catalysts towards formation of benzene and dichlorobenzene at the respective conversions are shown in Fig 5. The HDC of 1,2,4-trichlorobenzene is a consecutive reaction that produces dichlorobenzenes, chlorobenzene or benzene as final products. The detected products were benzene, chlorobenzene, *o*-dichlorobenzene and *p*-dichlorobenzene. We also observed traces of *m*-dichlorobenzene during the reaction. A blank test with the support (Mg-Al mixed oxide) showed no conversion of 1,2,4-trichlorobenzene at the reaction conditions. The mixture of products was mainly formed by benzene and *o*-dichlorobenzene. The presence of higher dispersion of Pd in the catalyst can favour the formation of high amount of active hydrogen species that are necessary to achieve a higher hydrodechlorination degree. Most of the catalysts have comparable selectivity results. The highest selectivity towards benzene was observed for Pd/HT1123 and Pd/HT623 catalysts. As shown in the figure the least selectivity was scored by the Pd/HT723 catalyst despite its higher surface

area and total basicity. The selectivity of catalysts towards benzene is correlated to Pd dispersion and its ability to dissociate hydrogen in the previous section. S. Narayanan et. al. [174] deeply investigated the effect of calcination temperature of HT on dispersion and catalytic activity of Pd. Two maxima in dispersion were seen when support is calcined in the region of room temp to 573 K and at 973–1173 K. The dispersion of Pd slightly increases when the support is dried at 373 K and calcined at 473 K compared to the support dried at room temperature and calcined at 573 K. There is an abrupt decrease in CO uptake when the support is calcined between 673 K and 773 K, and CO uptake progressively increases up to a calcination temperature of 1173 K and again decreases thereafter. Despite a large surface areas observed for HT calcined between 723-923 K, the dispersion of Pd is low on these supports. They suggested that there is no direct relationship between surface area of the support, which exists in different phases, and Pd dispersion indicating that the structural properties are playing a major role in metal dispersion. We believe that and specific metal interaction with surface groups over the HT calcined at different temperatures also influence the Pd dispersion. As a result the slight increase of selectivity observed for Pd/HT623 and Pd/HT1123 catalysts can be associated with relatively higher dispersion.

Conclusion

Interesting observations have been made in this study. Pd catalytic behavior towards HDC of 1,2,4-trichlorobenzene depends on the HT structure. The highest surface area was observed for Pd/HT723 and Pd/HT923 catalysts. While at calcination > 923K results a decrease in surface are due to pore destruction and increase in crystallinity. Upon calcination of HT support, different structural evolution was observed by the XRD analysis. Calcination at 1123 K results in segregation of the mixed oxide into MgO and spinel phases, increasing its crystalline nature. It was demonstrated that the basicity of the mixed oxide support decreases as the calcination temperature increases. Pd/HT623 catalysts possess higher basicity due to the existence of some OH^- groups. The calcination mainly affects the catalytic conversion while slight difference was observed for the

selectivity. Pd impregnated over HT calcined at lower temperature resulted in higher activity and stability for HDC of 1,2,4-trichlorobenzene. In summary HTs are an attractive alternative supports for noble metals.

4.4.

Gas-phase hydrodechlorination of trichloroethylene over Pd/NiMgAl catalyst

Trichloroethylene (TCE) is one of the most widely distributed halogenated organic pollutants throughout the world. It is a volatile organic compound that has been used extensively as degreasing agent (in metals and rubber industry), dry cleaning agent and as a polymer precursor [51, 117]. Catalytic hydrodechlorination (HDC) is a promising reductive technology that converts the organochlorinated pollutants into non-toxic, easily degradable or useful raw materials. Most studies of HDC of TCE compounds have been carried out using noble metal catalyst [18, 30]. Although supported noble metal catalysts specifically Pd exhibit better catalytic activities and stability during HDC of TCE at mild conditions, they mainly produce ethane, which is much less desired product, than ethylene [30, 117, 118]. Higher olefin selectivity is attained by doping the noble metal catalysts with different transition metals like Ag [118], Cu [117, 127] or Sn [128]. For instance, supported bimetallic Pd-Cu or Pd-Ag catalysts are cited to selectively hydrodechlorinate TCE to ethylene [117, 118, 127, 175]. Other cheaper but active

transition metal includes nickel, which is able to catalyze HDC of vicinal aliphatic chlorinated carbons. Some of Ni catalysts studied for HDC of various aliphatic chlorinated compounds include; $NiMo/Al_2O_3$ [111, 114, 122], Ni/Al_2O_3[111, 120], Ni/Zeolite [42], Ni/SiO_2 [111], Ni/AC [57, 121] and Raney Ni [57, 111]. Unlike noble metal catalyst, supported Ni catalysts have shown to be selective to ethylene during HDC of vicinal chlorocarbons [121, 123, 124]. The major disadvantages of using Ni catalysts are that it requires high temperature (>473K) or high hydrogen pressure to reach significant activity and their rapid catalyst deactivation. Promotion of Ni rich catalysts using small amount of noble metals like Pd, increases its catalytic activity for HDC reaction [132-134]. In this way, it is possible to design cheap Pd-Ni bimetallic catalyst, which is selective for olefin formation.

Moreover, the selection of an appropriate catalyst structure is important to modify the catalytic behavior (activity, selectivity and stability) and limit the degree of deactivation [118]. For instance, the choice of catalyst support and method of preparation can play an important role in the development of hydrodechlorination catalysts [123, 135]. Lately, mixed oxides from hydrotalcite-like precursors containing noble metals are receiving attention for HDC reaction due to their numerous catalytic advantages. This new catalytic materials inhibit deactivation by metal sintering, cocking or poisoning by HCl produced during the HDC reaction [135]. Moreover, a clear effect of the basic properties of the supports has been reported on the catalytic properties for HDC reactions in which the Pd reactivity increases when the Mg content in the Mg/Al hydrotalcite derived mixed oxide increased [135]. Gas-phase HDC of TCE over Pd or Pt modified Cu/Mg/Al hydrotalcite derived mixed oxide has also shown improved catalytic activity, enhanced selectivity to ethylene and good stability [127]. HDC of 1,2,4-trichlorobenzene by Ni/Mg/Al hydrotalcite derived mixed oxide, show higher activities [75]. In general, incorporation of an active metal like Ni inside the hydrotalcite structure, can favour the HDC activity since the metal and the basic sites of Mg are in close proximity. Based on this, in the present work a hydrotalcite derived NiMgAl mixed oxides with different Ni/Mg/Al molar ratios were prepared and consequently promoted by Pd. The catalysts were characterized using different techniques to investigate Pd-Ni interactions and the effect of the support. These catalysts were studied for gas-phase hydrodechlorination of trichloroethylene using a stoichiometric

amount of [H_2/TCE] at 573K. The influence of support composition and catalyst reduction temperature was also investigated. Previously, it was reported that immobilization of Pd over reduced CuMgAl catalyst showed Pd/Cu interaction enhancing the catalytic behavior [127]. This protocol was also studied for Pd supported on reduced NiMgAl catalysts. Several characterization techniques were employed in order to correlate physical-chemical properties of the surface by changing Ni/Mg/Al molar ratios in the hydrodechlorination reaction.

1. Experimental

1.1. Catalysts synthesis

The Ni/Mg/Al (NiHT) hydrotalcite was prepared by co-precipitation as described previously [75]. Aqueous solutions of an appropriate amounts of $Ni(NO_3)_2.6H_2O$, $Mg(NO)_2.6H_2O$ and $Al(NO_3)_2.9H_2O$ salts and 3M NaOH alkaline solution were separately prepared. These two solutions were then simultaneously added drop-wise into 100 ml of deionized water maintaining a constant pH (10±0.5) under vigorous mechanical stirring. After the co-precipitation, the suspension was aged overnight under stirring room temperature, filtered, and thoroughly washed with deionized water. The resulting solid was then dried overnight at 373K and calcined at 723 K for 15 h to obtain the hydrotalcite derived NiHT mixed oxides. In such a way, three different mixed oxides (NiHT) with different molar ratios were synthesized. The Ni/Mg molar ratios were 2:1, 1:1 and 1:3; and the molar ratio between bivalent and trivalent cations was 2:1. These catalysts were labelled as NiHT1, NiHT2 and NiHT3, respectively.

Pd supported NiHT catalysts were prepared by the impregnation of the HT mixed oxide with a toluene solution of Pd acetylacetonate, (Pd = 0.5 wt/wt %). The resulting catalysts were dried at 373 K and calcined at 623K for 2 hours. These catalysts were designated as Pd/NiHT1, Pd/NiHT2, Pd/NiHT3.

The effect of the reduction temperature of the samples was also studied and the samples were labelled indicating the reduction temperature as Pd/NiHT-723 showing that the Pd/NiHT1 catalyst was reduced at 723 K.

For the introduction of Pd, another protocol was also studied. In this protocol, the NiMgAlOx mixed oxide was previously reduced at 823 K for 2 h. Then, the reduced sample (labelled as rNiHT1) was introduced into a toluene solution containing $Pd(AcAc)_2$. These steps were carried out under argon atmosphere in order to avoid re-oxidation of Nickel. The solvent was then evaporated in vacuum, dried in 373 K and finally calcined at 623 K for 2h. In this way, three Pd(*x*)/rNiHT1 catalysts where *x* represents different Pd weight percentage (0.5, 0.3, 0.1 wt/wt %) were prepared and the catalysts were designated as Pd(0.1)/rNiHT1, Pd(0.3)/rNiHT1 and Pd(0.5)/rNiHT1, respectively.

Catalysts characterization

The chemical composition of the samples was determined by atomic absorption spectroscopy with a Perkin-Elmer Plasma 400 instrument. The N_2 physisorption adsorption-desorption isotherms at 77 K as well as the BET surface area of the samples were measured using Micromeritics ASAP 2000. The XRD of the materials were recorded using Siemens D5000 diffractometer (Bragg-Bentano para focusing geometry and vertical θ-θ goniometer) fitted with a grazing incident (ω: 0.52º) attachment for thin film analysis and scintillation counter as a detector. The Hydrogen-Chemisorption analysis was performed under static volumetric conditions with a Micromeritics ASAP 2010 apparatus. Prior to the measurement, the sample was evacuated at 373 K for 1 hour, treated in flow pure hydrogen (30 cm^3min^{-1}) at 623 K for 3 hours, evacuated at 623 K for 1 hour, cool down to 373 K and evacuated 30 minutes. Finally, the chemisorption analysis was performed at 373 K. High-resolution transmission electron microscopy (HRTEM) was carried out with a JEOL 2010F instrument equipped with a field emission source. The temperature programmed reduction studies were performed in a ThermoFinnigan (TPORD 1100) apparatus equipped with a thermal conductivity detector (TCD). Photoluminescence and UV diffuse reflectance measurements were carried out at room temperature using quartz glass cells kept under vacuum ($p < 10^{-5}$mbar). The UV diffuse reflectance spectra were acquired using an Edinburgh instruments spectrometer (FSP920) with a Xenon arc-lamp, double grating monochromators and a photomultipliers tube.

1.2. Catalytic activity

The catalysts were tested for gas-phase hydrodechlorination reaction of trichloroethene (TCE) at 573 K using a continuous fixed-bed glass reactor described previously as well as the reaction conditions [127]. The gas feed is obtained by flowing an inert gas (He) and hydrogen through a saturator kept at 298 K by a thermostat, containing trichloroethylene (TCE) in liquid phase. The TCE partial pressure of 92 mbar was achieved. The molar ratio of H_2/TCE was maintained at stoichiometric amount related to the three chloride species. The gas flows were adjusted by mass flow controllers (Brooks Instrument 0154) and introduced into the reactor, which is placed in a furnace coupled with a temperature controlling system. The products were analyzed on-line using a gas chromatograph (HP 5890 series II, HP Poraplot column, FID). Catalytic conversion and selectivity were calculated by analyzing the peak areas of TCE and the respective products. For some catalysts, different residence times were used to achieve lower conversion levels maintaining similar H_2/TCE molar ratio.

2. Results

2.1. Characterization of the catalyst

Atomic composition and textural properties of the mixed oxide catalysts are summarized in Table 1. The atomic compositions of Ni, Mg and Al, showed little differences with respect to the initial molar ratios introduced during the preparation. The textural properties were displayed in terms of S_{BET} and pore volume of the catalysts. Table 1 clearly demonstrates that the BET surface area of the NiHT catalysts is highly affected by the chemical composition of the sample. Pd/NiHT2 catalysts scored higher BET surface area of 151 m^2/g. As the Ni content increased, the surface area lowers to 115 m^2/g as is shown for Pd/NiHT1 sample. This is probably due the higher crystalline of the NiO species. In addition, increasing the Mg content as for Pd/NiHT3 catalyst moderately lowers the BET surfaces area to 146 m^2/g.

Table 1 Some properties of the catalysts

Catalysts	Pd (%)	Ni/Mg/Al molar ratio (AAS result)	BET (m^2/g)	Pore diameter (nm)	D [a] (%)	H_2 uptake (cm^3/g)	dp [b] (nm)
Pd-NiHT1	0.5	$Ni_{1.37}Mg_{0.7}Al_1$	115	9.9	19	0.1	4.1
Pd-NiHT2	0.54	$Ni_{0.75}Mg_1Al_1$	151	8.7	14	0.075	4.0
Pd-NiHT3	0.5	$Ni_{0.75}Mg_{3.1}Al_1$	146	10.3	5	0.026	4.3

[a] Pd dispersion obtained from H_2 chemisorption data,

[b] Pd particle size obtained from HRTEM

X-ray diffraction patterns of hydrotalcite derived mixed oxide catalysts (Pd/NiHT1, Pd/NiHT2, Pd/NiHT3) are shown in Fig 1. After calcination of the samples at 723 K the lamellar structure disappears and crystalline NiO phase is observed. The XRD profile for the Pd/NiHT samples did not reveal peaks correspondent to palladium species or $NiAlO_x$ spinel phase. As the Pd loading was rather low, the absence of diffraction line of Pd species may be due to the fact that the corresponding Pd particles are too small or highly dispersed to be detected by the XRD instrument. The crystallinity of the catalysts was affected by the molar composition of NiMgAl support. Pd/NiHT2 and Pd/NiHT3 catalyst showed a decrease in crystallinity, as compared to Pd-NiHT1 catalyst. In case of Pd/NiHT1, the higher crytallinity is probably due to the higher amount of Ni in the mixed oxide phase.

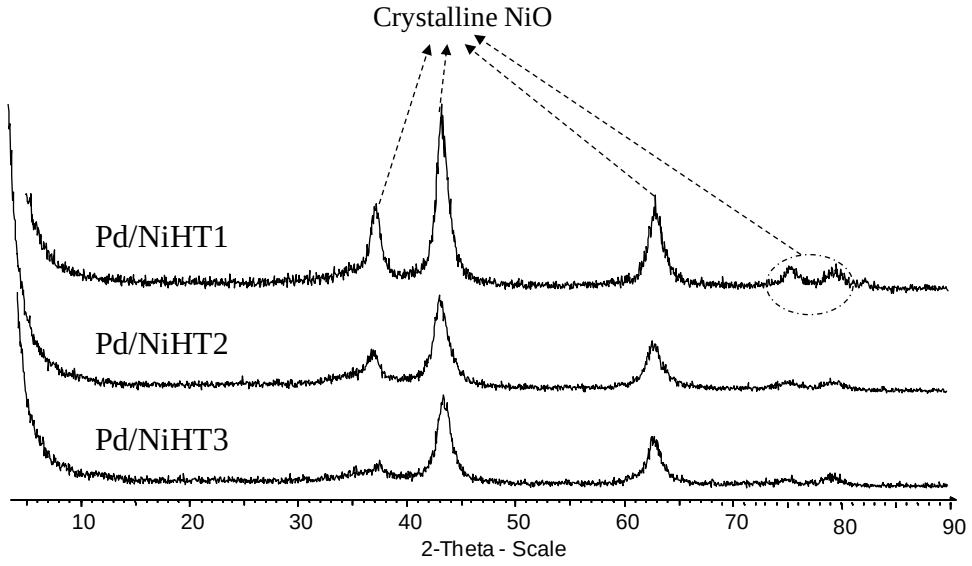

Fig. 1 X-ray diffraction patterns for the different Pd/NiHT catalysts.

The hydrogen chemisorption analysis for Pd/NiHT1, Pd/NiHT2 and Pd/NiHT3 catalysts was performed after reduction at 623 K. The hydrogen uptake results are shown in table 1. The higher hydrogen uptake was recorded for Pd/NiHT1 catalysts (0.1 cm^3/g) while the lowest was observed for Pd/NiHT3 (0.026 cm^3/g) catalyst. The hydrogen uptake capacity for the catalyst follows a trend: Pd/NiHT1>Pd/NiHT2>Pd/NiHT3. As demonstrated by different authors, the higher the Pd-Ni concentration on the surface the higher will be the hydrogen uptake capacity. As a result, as shown for Pd/NiHT1 catalyst, the presence of higher quantity of Pd-Ni in the mixed oxide support is beneficial for improving the H_2 uptake capacity. On the other hand the lower Pd-Ni concentration in the surface of Pd/NiHT3 catalyst results in poor hydrogen uptake. As also demonstrated in the first section of the thesis, increasing the basicity by increasing the Mg/Al molar ratio favours more metal-support interaction decreasing the hydrogen uptake capacity. Hence, apart from the lower in Ni content, the increase in Mg content can be responsible for decrease in hydrogen uptake capacity of the Pd/NiHT3 catalyst.

The Pd/NiHT catalysts were further characterized using HRTEM and TEM techniques. At low-magnification, general TEM view of sample Pd/NiHT3 is shown in Fig. 2a. Hydrotalcite derived nickel mixed oxide

support is comprised by homogeneous particles of about 5-10 nm in size. The support crystallites are well faceted and exhibit sharp edges, as deduced by the representative HRTEM image shown in Fig. 2d, which corresponds to the Pd/NiHT3 sample. In addition to support crystallites, the sample also contains round-shaped particles with a high electron contrast, which correspond to metallic Pd, as indicated in Fig. 2d. The distribution of Pd particles in this sample is very homogeneous and centered at about 4.3 nm, being most of them (> 90%) comprised in the very narrow interval of 3-5 nm. The microstructure of the other two samples, Pd/NiHT1 and Pd/NiHT2, is very similar. Fig. 2b shows a representative image of sample Pd/NiHT1. Again, well-faceted support crystallites are homogeneously distributed in the sample along with smaller, round-shaped Pd particles. For this sample, the mean particle size of Pd particles is centered at about 4.1 nm. A similar situation is encountered in sample Pd/NiHT2 (Fig. 2c), where both the mixed oxide support and Pd particles exhibit virtually the same particle distribution. In all cases, from HRTEM analysis of lattice spacing no evidence for the existence of Pd-Ni alloy or Pd covered by Ni has been encountered, although the groundmass of the support particles prevents an exhaustive and accurate analysis. However, in all cases where Pd lattice fringes are observed for instance in Fig. 10 at 2.24 Å for Pd(111), no evidence for covering has been observed. In addition, the spacing values determined correspond to pure Pd metal, thus suggesting that no alloy with Ni occurs.

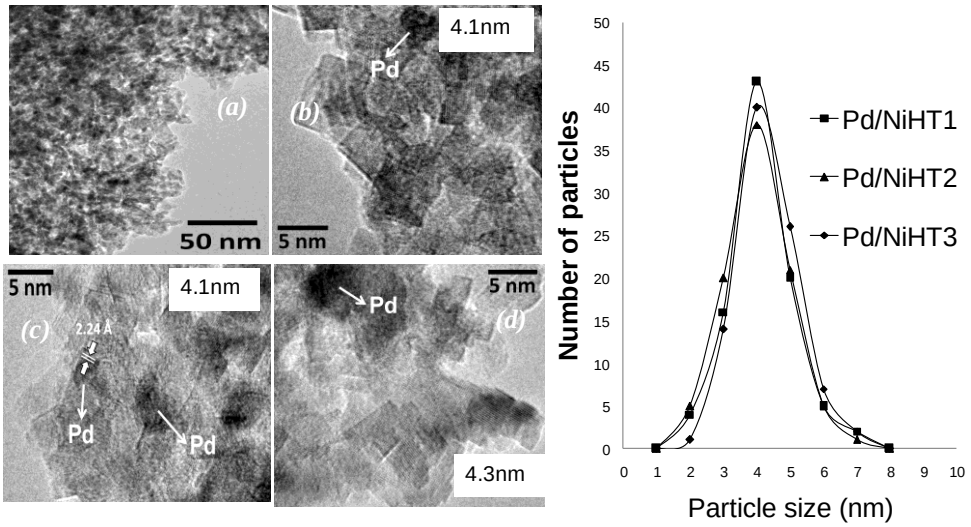

Fig. 2 HRTEM images of Pd/NiHT catalysts; a) TEM-Pd/NiHT3 b) Pd/NiHT1 c) Pd/NiHT2 d) Pd/NiHT3.

TPR experiments were used to investigate reducibility, metal-support and metal-metal interactions for NiHT and Pd-NiHT catalysts. It is well known that supported metal catalysts show different reduction patterns depending on the nature of interaction with the support. The TPR profile of NiHT catalysts are represented by dotted line as shown in Fig 3. For NiHT catalysts, it is shown that reduction peak of NiO occurs at a relatively higher temperature (TPR peak at > 798 K). They can be reasonably associated with the reduction of NiO that are incorporated into the framework or partially covered by a surface of mixed oxide. The broad NiO reduction peaks for NiHT1, NiHT2, and NiHT3 are centered at 1013K, 1058K, and 1118K, respectively. The comparison of the TPR profiles obtained for different NiMgAl samples showed that upon increasing Mg amount a shift of the NiO reduction peak towards higher temperatures and lower hydrogen consumption was observed. Increasing the Ni content increased both the reducibility of NiO at lower temperature and the hydrogen uptake as shown for NiHT1 catalysts.

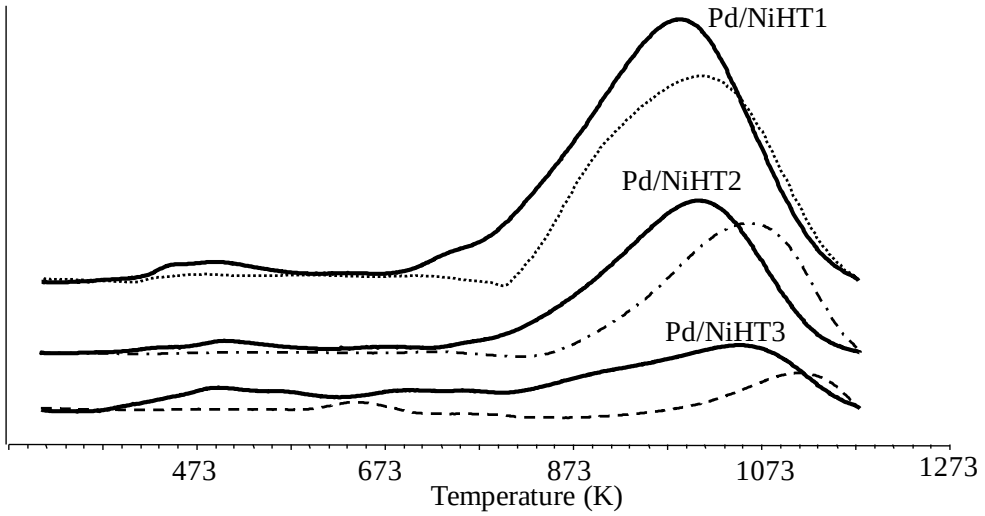

Fig. 3 TPR profiles for NiHT and Pd/NiHT catalysts.

The TPR profile for Pd impregnated NiMgAl catalysts on the other hand are represented in solid line as shown in Fig 3. Separate reduction peaks of PdO at lower temperature and NiO at higher temperatures were observed. The TPR peaks between at 373-573K are attributed to the reduction of PdO species with different interaction with the mixed oxide surface as shown in the inset of fig 3. In Pd/NiHT3 catalyst, the Pd reduction peaks shifted to the higher temperature. While increasing the Ni content inside the mixed oxide facilitates the reducibility of Pd at lower temperature as shown for Pd/NiHT1 catalyst. In general the reducibility of Pd over the NiMgAl mixed oxide depends on the strength of Pd interaction with different sites of the mixed oxide support. TPR profile depicted that the presence of Pd affects the reducibility of NiO in all catalysts, which is demonstrated by the respective shift of the reduction peak of the NiO to the lower reduction temperature upon the addition of Pd. Moreover, the hydrogen consumption of the NiO species increases as observed by increase in the peak intensities. Even though, the HRTEM study revealed no Pd-Ni alloy formation in all catalysts. However, it seems that there is some type of surface interaction and cooperation between Pd-Ni as is demonstrated by the shift in reduction peaks and area of the peaks in the TPR.

The state of the noble metal for NiHT1 and Pd/NiHT1 catalyst was further investigated using FTIR spectroscopy by using CO as a probe

molecule. Fig. 4 shows a comparison of the spectra of Pd/NiHT1 reduced at 523 K and after adsorption of CO. It revealed different adsorption bands corresponding for hydroxyl stretching band- ions (3000-4000 cm^{-1}) and strong carbonate (1413, and 1579 cm^{-1}) bands that were not removed during calcination at 723K or introduced during pellet preparation for FTIR measurement. The band at 1007 cm^{-1} is associated with 'Al'–OH translation modes. CO molecule could adsorb on the surface Ni and Pd species. The FTIR bands at 2061, 1979 and 1904 cm^{-1} can be assigned for both Ni-CO and Pd-CO adsorption bands arranged linear M-CO, bridged $(M)_2$-CO and multi centered (M)x-CO species, respectively [75]. Ni-CO vibration bands can also interfere with the FTIR profile despite lower catalysts reduction temperature.

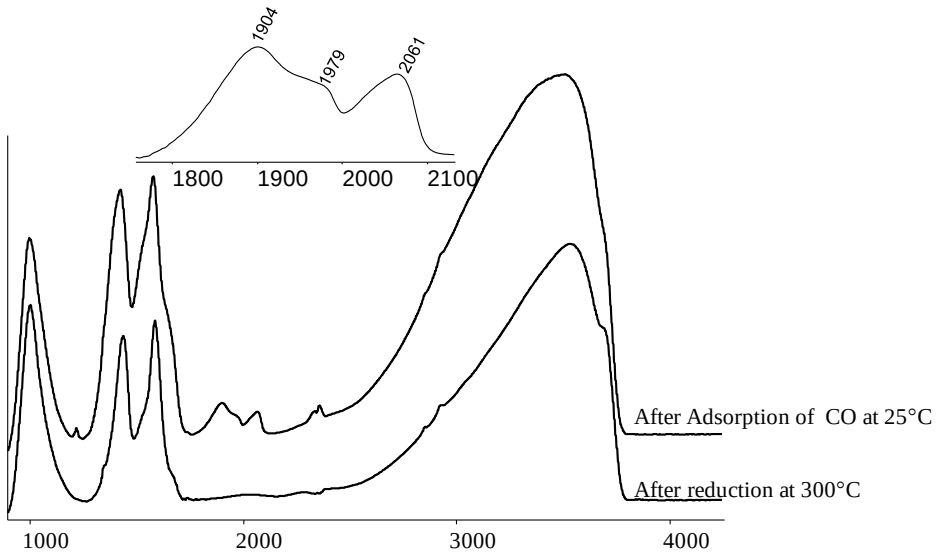

Fig. 4 CO-FTIR profile for Pd/NiHT1 catalysts

Diffuse reflectance spectra of NiHT1 oxide and reduced were obtained with a Edinburgh spectrophotometer. The measurements were made in the wavelength range 200 to 800 nm at room temperature. The NiHT1 profile was compared with pure NiO, obtained from calcination of commercially available $Ni(OH)_2$ at 723 K and reduced 773 K for 2 h. Fig 5a shows the UV-Vis diffuse reflectance absorption spectra of pure NiO and NiHT1 oxides. The spectrum of NiO as expected contains three bands due to spin-allowed transitions located at 1140, 650 and 420 nm. These ligand field transitions has been assigned to $^3A_{2g}(F) \rightarrow {}^3T_{2g}(F)$, $^3A_{2g}(F) \rightarrow {}^3T_{1g}(F)$ and

$^3A_{2g}(F) \rightarrow {}^3T_{1g}(P)$ transition of the O^{-3} band ($^3A_{2g}$ –> $^3T_1(P)$) of Ni^{+2} ions in an octahedral environment respectively [176]. Four additional bands observed at 725, 465, 385 and 337 nm are assigned to spin-forbidden transitions. Absorption peak at 385 nm assigned to the $^3A_{2g}(F) \rightarrow {}^3T_{1g}(F)$ transition [177]. The absorption band at 725 nm is not due to a distortion of the crystal field indeed, a similar spin-forbidden transition has been previously reported for a nickel fluorosilicate in which Ni^{+2} ions are submitted to a perfectly octahedral crystal field.

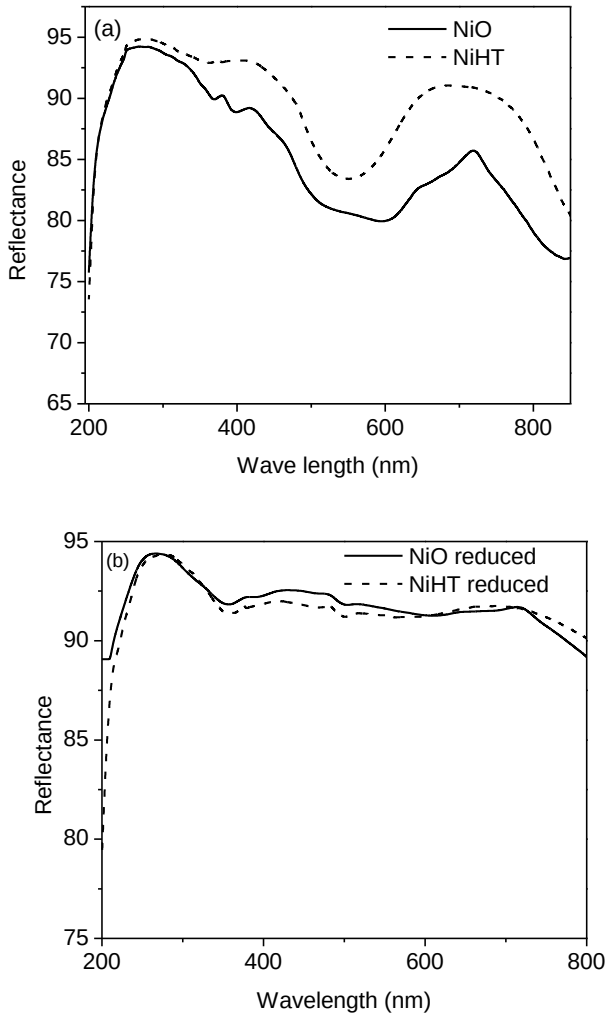

Fig. 5 UV-Vis diffuse reflectance spectroscopy of NiO and NiHT mixed oxide (a) and Ni and NiHT reduced (b)

Similar absorption peaks as the bulk NiO but broadened was observed in mixed oxide samples. In comparison to bulk, NiO the diffuse reflectance curve of NiHT1 surfaces shows additional increase in absorbance, which results from the presence of $MgAlO_x$. This increase may be due to spin-forbidden electronic transitions or because of the severe distortion away from Oh symmetry for coordination geometry of the Ni^{2+} ions in an octahedral field. In addition, the absorption observed in the UV region of 200-300 nm is ascribed to a charge transfer process. Upon reduction of the NiO the d-orbital's are fully occupied. As a result no or limited d-d transitions will be observed. Fig. 5b shows the UV-Vis absorption spectra of the reduced bulk NiO and NiHT1 samples that decreased in intensity possibly due to completion of the d-orbital's. However, traces of d-d transition occur for samples reduced at 823 K possibly due to existence of Ni^{2+} or Ni^{+1} species or some charge transfer processes. Both the bulk reduced Ni and mixed oxide samples possess similar profile depicting the surface of NiHT mixed oxide possess similar spectral property as the pure NiO surfaces.

2.2. Catalytic activity-Hydrodechlorination of TCE

2.2.1. Effect of support composition

The gas-phase HDC of TCE over Pd/NiHT catalysts (reduced at 623 K) was performed at 573 K, maintaining a stoichiometric molar ratio of H_2/TCE. The hydrodechlorination of TCE over these catalysts produces various products such as chlorinated hydrocarbons, hydrocarbons, and HCl. The catalytic behaviors of Pd/NiHT catalysts are shown in Fig. 6. The results of catalytic conversion as a function of time on stream are displayed in Fig 6a. It is observed that the catalytic activity is strongly dependent on the molar compositions of the support. The Pd/NiHT1 and Pd/NiHT3 catalysts showed higher TCE conversion (> 80 %) than the Pd/NiHT2 catalyst which scored < 60% conversion. This can be accounted by the metal-metal interaction and metal-support phenomenon. The higher TCE conversion observed for Pd/NiHT1 catalyst could be related to its higher hydrogen uptake capacity resulting from the Pd-Ni interaction. Hence, the near existence of Pd and Ni over the catalyst surface is influential in HDC reaction. Moreover, since Ni has the ability to hydrodechlorinate, an increase in Ni content should also influence in the catalytic activity despite the lower reducibility of NiMgAl support at this temperature as shown by the H_2-TPR.

At the same time, increasing the Mg content inside the support showed an improved catalytic activity as shown for Pd/NiHT3 catalyst. This can be explained by the metal-support cooperation where the higher basicity of the support resulting from the Mg species promotes Pd. As demonstrated in the previous section, the basicity of the support can also influence the HDC catalytic activity. In general the catalytic conversion follow a trend of Pd/NiHT1>Pd/NiHT3>Pd/NiHT2. Moreover, Pd/NiHT1 catalyst is associated with better stability.

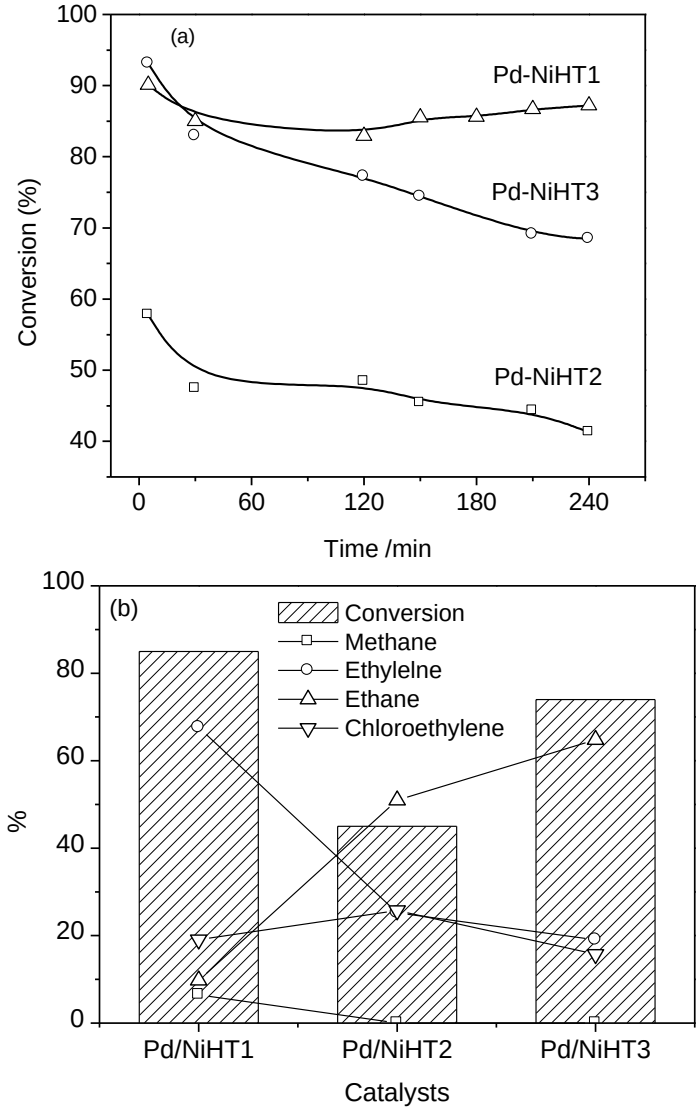

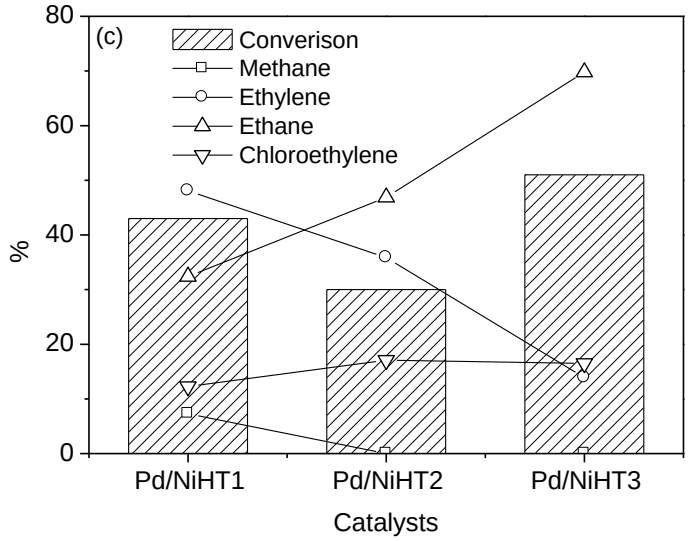

Fig. 6 (a) Catalytic activity of Pd/NiHT catalysts (with different NiMgAl molar ratios reduced at 623K), (b) product distribution at end of reaction (c) selectivity at lower conversion level.

The product distributions of these catalysts at end of reaction and at low conversion level are shown in fig. 6b and fig. 6c, respectively. During the catalytic reaction, ethylene, ethane and chloroethylene were the main products even though methane, 1,1-dichloroethylene and 1,2-dichloroethylene were detected. At end of the reaction, higher ethylene selectivity was observed for PdNiHT1 catalysts. On the other hand, Pd/NiHT3 catalyst with higher Mg content showed higher selectivity towards ethane. Fig. 6c summarizes the catalytic selectivity of Pd/NiHT at 623 K at lower initial conversion levels. Reduced catalytic conversions were achieved by increasing 3 times the space velocity with out affecting the H_2/TCE molar ratio. It was observed that the Ni rich Pd/NiHT1 catalyst favored mainly formation of ethylene (47%). The secondary products observed are methane, ethane (32%), vinyl chloride and traces of dichloroethylene. While the Mg rich Pd/NiHT3 catalyst mainly produced ethane (66%) as principal product while ethylene (13%) and chloroethylene as a secondary product. In general, the selectivity of the catalysts towards ethylene follows a trend: Pd/NiHT1 > Pd/NiHT2 > Pd/NiHT3. The HDC of TCE by Ni catalysts favors the formation of ethylene whereas over Pd

catalysts produces ethane. The presence of more metallic Ni species on the surface enhances the formation of ethylene, the lower the Pd/Ni ratio the higher ethylene selectivity. In contrast increasing the Pd/Ni ratio, literally more metallic Pd is enriched on the surface, then higher the ability of the catalyst to form ethane as a final product. Based on the product distribution on Fig. 6, as the metallic Pd/Ni ratio in the samples increased, higher amount of ethane was obtained (clearly seen for Pd/NiHT3 catalyst). Observing the above results a significant amount of ethane (>30%) was formed on Pd/NiHT1 catalyst despite the low Pd/Ni metal ratio on the surface. This implies that the very small amount of Pd(0.5%) employed is probably being masked by metallic Ni species, inhibiting the hydrogenation of ethylene to ethane when compared to the other catalysts. However, the results also demonstrate the involvement of metallic Pd species in the hydrodechlorination reaction. The main reason for this behavior could be accounted by the degree of the NiO reducibility from the NiMgAl surface. From H_2-TPR analysis, no reduction of NiO was initiated at temperature lower than 700 K. This suggests that the Pd/NiHT catalysts reduced at 623K is mainly composed of metallic Pd species and small amount of surface metallic Ni species. Consequently, their catalytic activity is mainly dominated by the noble metal which is responsible for hydrogenation of the ethylene to ethane. Since the reducibility of NiO in the synthesized catalysts increases from NiHT3<NiHT2<NiHT1, the Pd/NiHT1 is expected to involve more metallic Ni species accounting the difference in ethylene selectivity among different supports. As a result the higher metallic Ni the higher selectivity to ethylene as observed for Pd/NiHT1 catalyst. From the above selectivity results we can observe that little involvement of metallic Ni catalyst in the HDC reaction. In order to have better Pd-Ni interaction in the Ni rich catalyst, higher catalyst reduction temperature was employed.

2.2.2. Effect of reduction temperature

The effect of catalyst reduction temperature was investigated for the gas phase HDC reaction of TCE. The TPR and CO-FTIR profiles demonstrated the difficulty NiO reduction at lower reduction temperature and absence of Pd-Ni interaction. This suggests that the Pd/NiHT catalyst reduced at 623 K is mainly composed of metallic Pd species. Consequently,

their catalytic activity is mainly governed by the noble metal which is responsible for hydrogenation of the ethylene to ethane.

Further catalytic test were employed over NiHT1 and Pd/NiHT1 catalysts in order to investigate the effect of reduction temperature for HDC reaction. Fig.7 reports the catalytic behavior of the NiHT1 catalyst reduced at 623 K, 723 K and 823 K in flowing hydrogen. The catalyst reduction temperature has a significant effect on the catalytic performance of the catalysts. As shown in Fig. 7a, increasing the reduction temperature from 623 K to 823 K for NiHT1 catalysts raised the initial catalytic conversion from 32% to 63% respectively. NiHT1 catalysts reduced at 723 K have a conversion of 57%. Improvement of the catalytic behavior at higher reduction temperature is probably due to generation of more metallic Ni species from the mixed oxide structure.

The product distribution of NiHT1 catalysts at different reduction temperatures at end of the reaction are shown in Fig. 7b. Methane, ethylene, CE and traces of DCE were detected. The production of ethylene and methane increases with increasing the reduction temperature. In fact, the increase in methane production is associated with the property of Ni for the C-C bond cleavage at high temperatures. On contrary, at lower catalyst reduction temperature a slight increase to vinyl chloride formation was observed. Here it is important to note that ethane was noticed only when the catalyst was treated at higher reduction temperature. Indeed, during HDC of TCE, the three processes are able to occur over the Ni surfaces. Nickel is generally known for its ability to catalyze hydrogenation, hydrognolysis and hydrodechlorination processes. After hydrodechlorination of TCE, the ethane can be formed by hydrogenation of ethylene and further suffer hydrogenolysis to form methane. The changes in selectivity observed for NiHT catalysts when the reduction temperature is increased may be attributed to the migration of Ni atoms from the bulk to the surface of the catalyst. Hydrodechlorination of C-Cl bond may require large Ni ensembles. The reduction treatment may generate a number sufficiently large Ni cluster suitable for the C-Cl bond scission. The hydrogenolysis property of NiHT catalysts for C-C bond cleavage (formation of methane) seems to be also induced by the reduction temperature. Additionally it cannot be ruled out the possibility Ni atoms being boarding on the edges and steps at the surface

with reduction temperature. The hydrogenolysis of C-C bond by hydrogen is well known to be structure sensitive. As also observed by UV-Vis reflectance spectroscopy, the surface exhibited by the NiMgAl mixed oxide after reduction is similar as the bulk reduced NiO species, showing the enrichment of Ni species over the surface. The C-C bond cleavage reaction (hydrogenolysis) is mainly activated at higher reaction temperature, which also explains the lower selectivity to methane with respect to ethylene.

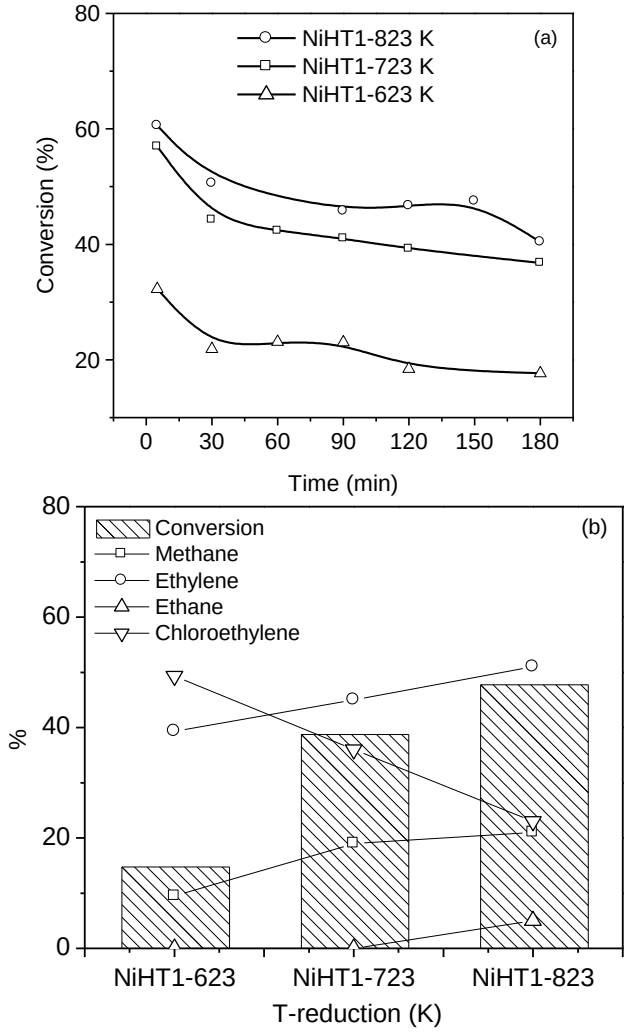

Fig. 7 Effect of reduction temperature on the catalytic behavior of NiHT1 catalysts (a) conversion, (b) product distribution at steady state

HDC of TCE was further studied on Pd impregnated catalyst, Pd/NiHT1, reduced at 623 K and 723 K as shown in Fig. 8. Reduction of this catalyst at a temperature higher than 823K was not employed in order to minimize effect of Pd sintering. As the reduction temperature increased from 623 K to 723 K, the catalytic activity also increased from 90% to 100% (shown in fig. 11a). Addition of small amount of Pd over the NiHT catalyst significantly modified the catalytic behavior

The product distributions of these catalysts were investigated at low conversion level as shown Fig. 8. The Pd impregnated catalysts tend to form ethane, ethylene and vinyl chloride. As shown in the Fig. 8, Pd/NiHT1 catalysts reduced at 723 K results higher selectivity towards formation of ethylene (70%) than catalyst reduced at 623 K (50%). In addition, selectivity towards ethane formation declined with increasing reduction temperature. Slight increase in methane formation was also noticed as the reduction temperature increased. Moreover trace amounts of Chloroethylene and dichloroethylene were detected for these reactions. In general, higher catalytic activity with significant selectivity towards ethylene is achieved by increasing the reduction temperature. The increase in ethylene formation and decrease in ethane production is probably due to the involvement of more Ni species in which the Ni rich environment dilutes and interacts with the noble metal inhibiting further hydrogenation of ethylene and/or facilitating C-C cleavage. Here we cannot rule out the presence of isolated Pd species and Pd-Ni alloy over the surface of the catalyst.

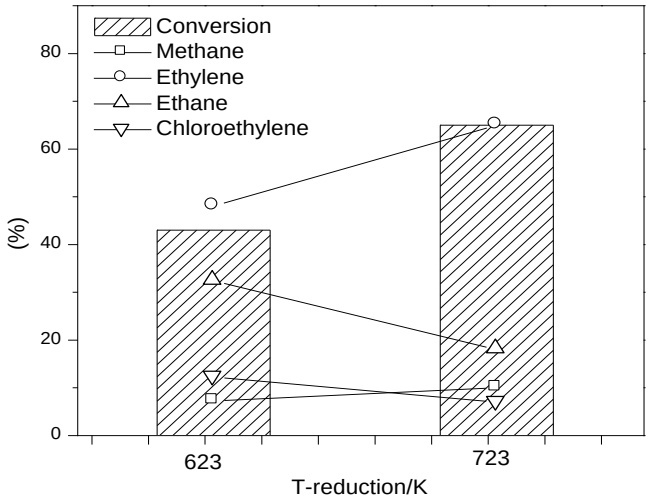

Fig. 8 Effect of reduction temperature on the catalytic behavior of Pd/NiHT1 catalysts reduced at 623 K and 723 K and product distribution.

2.2.3. Effect of synthesis protocol

In order to minimize surface Pd sintering and the covering of Pd by the bulk support during high temperature treatment, different synthesis protocol was employed. The synthesis protocol allows the evaluation of the effect of metal-metal cooperation between palladium-nickel on the surface. In the synthesis protocol, palladium with different weight loading was impregnated over previously reduced (823 K) NiHT1 catalyst. This catalyst was further dried and calcined at 623 K for 2h. Higher reduction temperature (823K) was employed in order to induce the migration of the Ni species from the bulk of the mixed oxide to its surface.

Powder X-ray diffraction patterns recorded for the Pd/NiHT are shown on the Fig 1 indicating the presence of NiO phase (JCPDS 00-044-1159). On the other hand the diffraction profile for Pd/rNiHT catalysts (Fig. 9) showed distinct peaks corresponding to metallic Ni species (JCPDS- 03-065-2865) and/or periclase (JCPDS-87-0653) or NiO (JCPDS-00-044-1159) phases. This is probably due to the high temperature employed during

reduction of the NiHT1 (823 K). Diffraction pattern corresponding to Pd or Pd-Ni alloy species are not observed either due to the small metallic loading or due to high dispersion over the surface of the rNiHT1 catalyst which can also be masked by the metallic Ni presence.

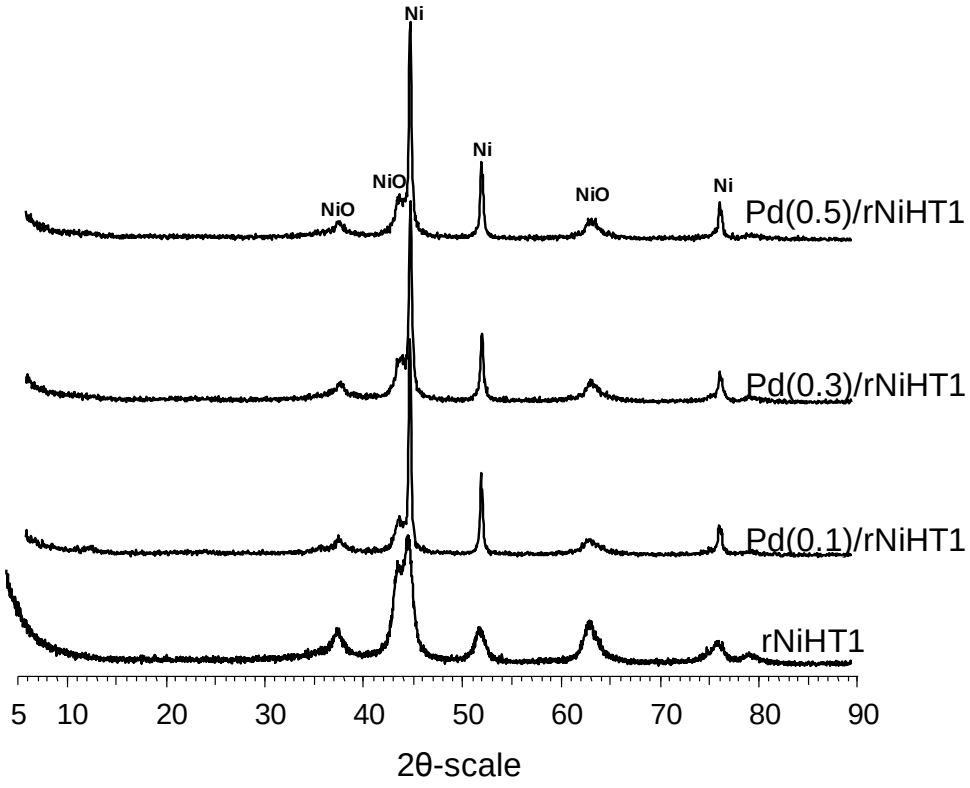

Fig. 9 X-ray diffraction patterns for the different rNiHT1-823K and Pd(*x*)/rNiHT1 catalysts where *x* represents Pd wt %.

Low-magnification high-resolution transmission electron microscopy (HRTEM) images of samples with 0.1%, 0.3% and 0.5% wt/wt of Pd are shown in fig. 10a, 10b and 10c, respectively. All samples are very similar and comprised by small particles of about 5-15 nm in size, as expected for NiHT oxides derived from NiMgAl hydrotalcites. Fig. 10d corresponds to a HRTEM image of sample with 0.3% wt% of Pd along with the corresponding Fourier Transform (FT) image. Rings at 1.49, 2.11 and 2.43 Å match exactly the (220), (200) and (111) crystallographic planes of MgO, respectively. In addition, spots at 1.76 Å correspond well to the (200) spacing of metallic Ni. The location of MgO and Ni in the image has been

indicated with appropriate labels. In this sample, as well as in the sample with 0.1 wt% of Pd, Pd or Pd-bearing particles are elusive, possibly due to the low amount of Pd. Therefore, more effort has been invested in the analysis of the sample with the highest Pd loading (0.5 wt %). In this sample, metallic Ni as well as Ni-Pd particles has been identified (see figs. 10e and 10f). Fig. 10e shows a crystallite with lattice spacing at 2.04 Å, which corresponds to the (111) crystallographic planes of metallic Ni. Lattice fringes are perfectly defined and no defects are detected. In contrast, fig. 10f shows another particle with a particular microstructure, as deduced from the accurate analysis of its lattice fringes. Different contrast areas are identified in the HRTEM image with different lattice fringes, as revealed by their profile analysis. Areas with lattice fringes at 2.16 Å alternate with brighter areas with lattice fringes at 2.04 Å. As explained above, lattice fringes at 2.04 Å correspond to (111) crystallographic planes of metallic Ni, but the new lattice fringes at 2.16 Å are intermediate of (111) planes of Ni at 2.04 Å and (111) planes of Pd at 2.25 Å. Taking into account that both metallic Ni and Pd exhibit the Fm3m crystallographic structure, it is likely the formation of an Ni-Pd alloy.

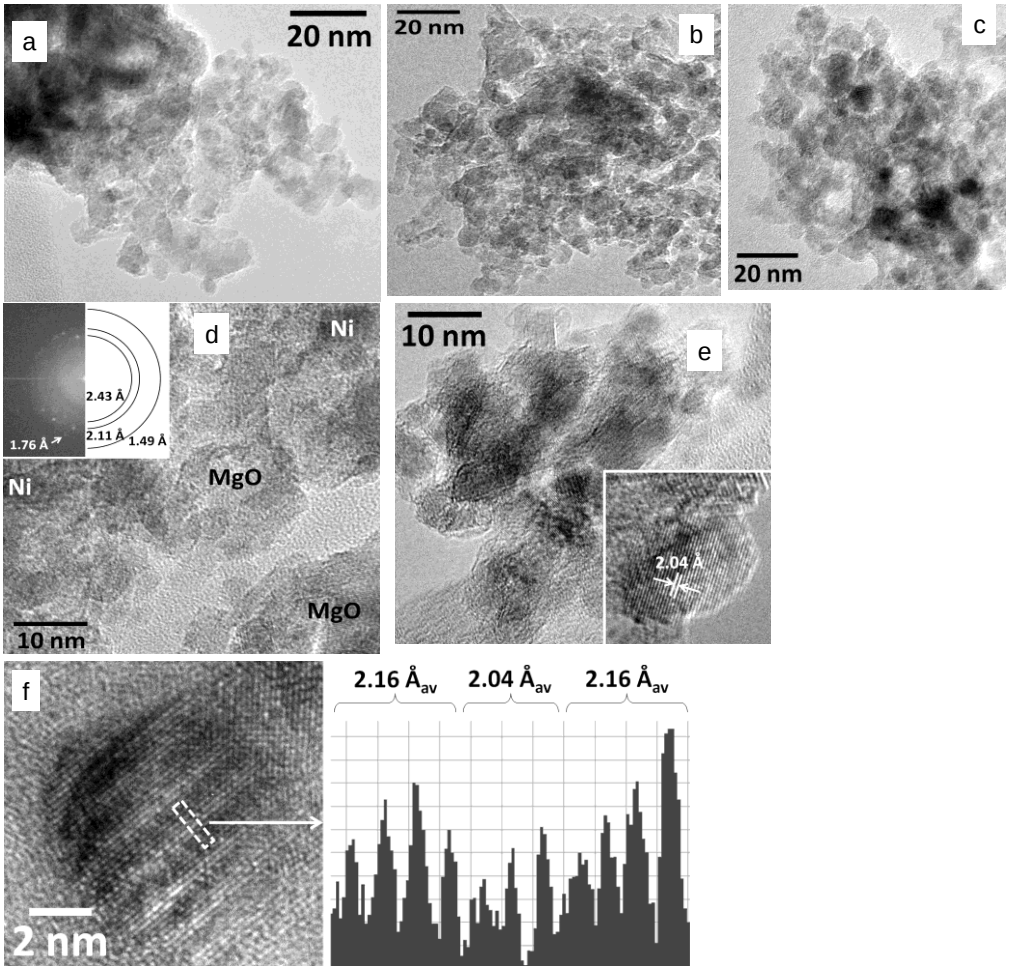

Fig. 10 low and high magnification of HRTEM images for Pd/rNiHT1 catalysts.

The HDC of TCE was conducted in a flow reactor maintaining similar conditions as stated above. Fig. 11a comparatively displayed the catalytic activities of Pd(*x*)/rNiHT1 samples and Pd/NiHT1-723K catalyst. HDC of TCE over Pd/NiHT1-723K catalyst resulted in 100% conversion at stoichiometric H_2/TCE molar ratio and 573K. The different protocol or treatment used to immobilize Pd over the NiHT surface resulted in lower catalytic activity as shown in the figure. The Pd(0.5)/rNiHT1, Pd(0.3)/rNiHT1, Pd(0.1)/rNiHT1 catalyst scored an initial activity of 89%, 87% and 82% respectively. Pd(0.1)/rNiHT1 catalyst is associated with rapid deactivation than the others, probably due to its lower Pd loading.

In general the higher activity achieved by Pd/NiHT-723K than Pd(0.5)/rNiHT1 catalyst can be explained by the basic properties of the supports. The rNiHT-823K sample which was treated at higher temperature should possess lower basic property when compared with the rNiHT1-723K. This difference in basicity could reflect the different in the catalytic activity between Pd/NiHT1-723 and Pd(0.5)/rNiHT1 catalyst.

Fig. 11b and 11c represent the catalytic selectivity at initial and end conversions respectively. The main products observed during HDC of TCE were methane, ethylene, ethane and chloroethylene. Traces of dichloroethylene were also observed through time of reaction. As shown in figure, the selectivity of ethylene at initial and end conversions for Pd/NiHT1-723 catalyst is around 67% and 54% respectively. Slight decrease in ethylene selectivity and increase in ethane selectivity was observed throughout the reaction. While almost similar selectivity to ethylene as Pd/NiHT1-723 was observed for Pd(0.5)/rNiHT1 catalyst (about 66%) at initial conversion level as shown in fig. 11b. Previous works [127] reported that with this synthesis protocol a better metal-metal interaction are more likely to occur. Since the palladium was added after the support is treated at high temperature (823 K), it is highly possible that the resultant surface of the Pd/rNiHT1 catalyst surface was better promoted by the Pd species introduced. Higher ethylene selectivity, at initial conversion, achieved by Pd(0.5)/rNiHT1 catalyst shows that the surface is probably enriched by metallic Ni in cooperation with Pd-Ni alloy which its existence was detected by HRTEM. As a result due to the presence of higher quantity of Ni species, the importance of Pd-Ni alloy would be activating the Ni species by providing active hydrogen for the HDC reaction to proceed. However at end of reaction a drastic decrease in ethylene selectivity (23%) and an increase in ethane (64%) formation was observed for Pd(0.5)/rNiHT1 catalyst. In general at end conversion lower selectivity to ethylene was observed for Pd(0.5)/rNiHT1 catalyst. The reason for the increase in hydrogenation degree of Pd(0.5)/rNiHT1 through time of reaction could be related to the metallic states of Pd and Ni after reaction. The ethane is formed probably over segregated Pd species from catalyst since Pd is nearer to the surface.

In a bimetallic system the component that interacts more strongly with the ambient gas could diffuse and reach the surface. In the case of Pd-Ni

system Ni has higher surface free energy (2.426 J/m^2) than Pd (2.043 J/m^2). As a result during the reduction of the catalyst, hydrogen is strongly adsorbed on Pd surface. Thus, this fact may favor the enrichment of the surface with Pd. This process, at the beginning of the reaction was negligible, since higher enrichment of surface metallic Ni which shows higher selectivity to ethylene. However at the end of reaction, since Pd is more near to the surface, Pd or Pd-Ni alloy segregates from the catalyst to the surface and involve directly in the reaction forming ethane. In case of Pd/NiHT-723 catalyst, since the reduction is employed in the presence of Pd, higher interaction of the bulk with Pd is expected. This implies the mobility of Pd from the bulk to the surface is unlikely to occur inhibiting the formation of ethane.

To improve the selectivity to ethylene with time on stream, while maintaining the higher catalytic activity of Pd/rNiHT1 catalysts, lower the Pd loading was employed. Since Pd is responsible for hydrogenation of ethylene to ethane, lowering its amount could favor ethylene production. As expected the initial catalytic activity of Pd/rNiHT1 slightly decreases as the Pd amount decreased. However, as shown in Fig. 10b and 10c, lowering the Pd loading to 0.3% drastically increased the ethylene selectivity (80%) at the same time maintaining initial conversion level as that of 0.5Pd/rNiHT1 catalyst. At the end of catalytic test the selectivity of ethylene is maintained constant. This shows that the Pd(0.3)/rNiHT1 catalyst has resulted in better catalytic activity and selectivity towards ethylene selectivity. Further lowering the Pd content to 0.1 wt% lowers the catalytic activity to 82 % but showed good selectivity to ethylene. At end of reaction these catalyst showed an increase in methane and chloroethylene formation. In general the catalysts selectivity towards ethylene at initial conversion follows trend as: Pd(0.3)/rNiHT1 > Pd(0.5)/rNiHT1 ≈ Pd/NiHT1-723K > Pd(0.1)/rNiHT1.

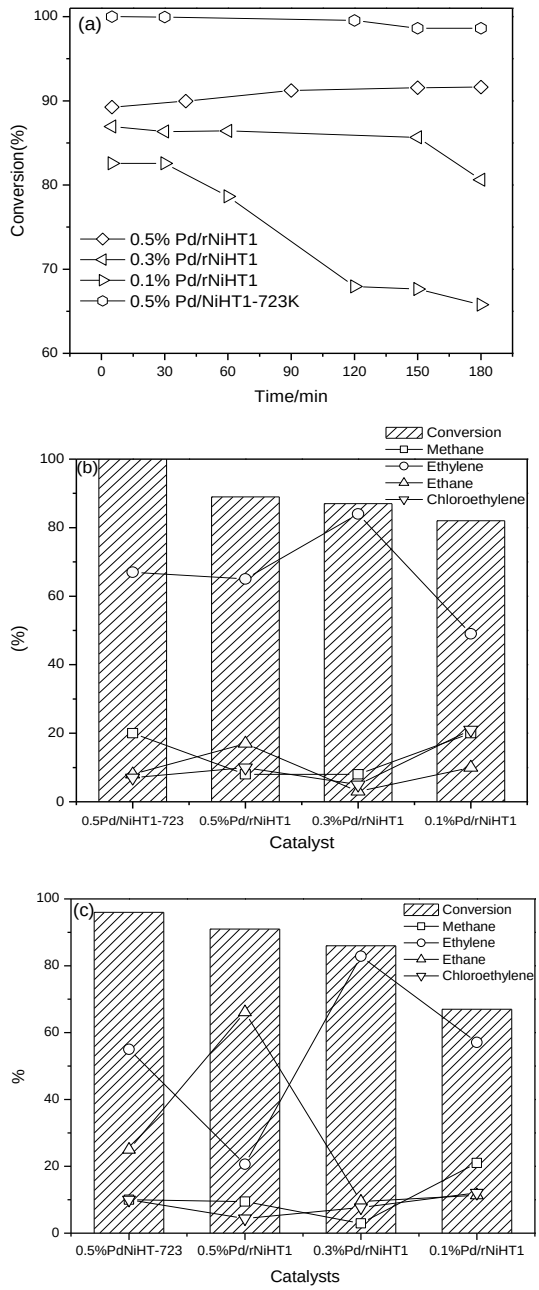

Fig. 11 Catalytic conversion Vs time of reaction for Pd/rNiHT1 and Pd/NiHT1-723 catalysts (a), product distribution at beginning o reaction (b), and product distribution at the end(c).

3. Discussion

The type and molar composition of a support and active metal, method of preparation protocol and catalyst activation determines the physico-chemical properties of a catalyst and its behavior towards a catalytic reaction. For instance, N_2-physisorption result for the Pd/NiHT catalysts suggests the difference in molar composition between Ni, Mg and Al affects the textural property of the catalyst. The increase in the Ni content inside the NiHT mixed oxide lowers the BET surface area as shown for Pd/NiHT1 catalyst. The XRD profile also demonstrated that the high crystalline property of this material as compared with the other catalysts. The higher cystallinitiy and hence the lower BET surface area for Pd/NiHT1 catalysts is probably due to the segregation of NiO phase of the mixed oxide. In contrast, the increase in Mg content slightly decreases the BET area which is shown for PdNiHT3 catalyst due to the high interaction between MgO species and NiO. No peaks correspondent to palladium particles in the XRD profiles were detected probably due to small Pd particle sizes that are beyond on the limit of detection of the diffractometer. Further characterization using FFT integrated HRTEM analysis for PdNiHT samples (Fig 2) illustrate the nature of the Pd particle size and NiHT support morphology in the Pd/NiHT samples after reduction at 623 K. The palladium particles appeared as small dark spherical particles with mean diameter around 5 nm dispersed in the mixed oxide support with platelet-like morphology. Almost similar Pd particle size was observed for all catalysts. The Pd and Ni interaction, as a form of alloy or else, at 623 K reduction temperature is not clear as the HRTEM picture depicts only isolated Pd particles.

The Pd-Ni interaction was further studied by the H_2-TPR analysis (Fig 3) for both the NiHT mixed oxide and Pd promoted NiHT catalysts. As shown in fig. 3, for the Pd promoted catalysts, the NiO phase inside the NiHT tends to reduce at higher temperatures (> 800 K) in contrast to PdO phase which reduces at lower temperatures (< 500 K). This implies the Pd-Ni interaction, or formation of metallic Ni at 623 K is impossible unless higher reduction temperatures are applied. This is due to the high stability against reduction and interaction of NiO phase incorporated inside the mixed oxide structure. However the existence of Pd on the surface of the NiHT

increases/facilitates the reducibility of the NiO species as well as its hydrogen uptake capacity. Furthermore the TPR analysis depicts that increasing the Ni content modifies the reducibility and the hydrogen uptake capacity. This is probability due to the high surface enrichment of NiO for the Pd/NiHT1 catalyst. In contrast, the TPR profile showed that increasing Mg content in the NiHT catalysts lowers NiO reducibility and total hydrogen uptake. The shift towards higher temperatures reduction peak of the nickel species in the presence of Mg is well documented in the literature [178] and it was associated to the formation of NiO-MgO solid solution in which Ni ions are stabilized against reduction and sintering by the MgO type matrix. Apart from the temperature shift, the decrease in hydrogen uptake capacity is related to some covering of NiO by the MgO in the vicinity. The decoration effect was clearly demonstrated by the H_2-chemisorption results. As shown in table 1, the Pd/NiHT3 catalyst scored the lowest hydrogen uptake capacity as compared to Pd/NiHT2 catalyst which possesses similar Ni content. Based on these results, it appears that as the amount of magnesium species in the support increases, the uptake of hydrogen decreases probably due to some decoration effect by the mixed oxide.

Apart from instrumental characterization techniques, the TCE HDC catalytic activity depicts the metallic states and mechanisms. In general depending on the degree of metal-metal or metal-support interaction the HDC catalytic activity and selectivity towards formation of ethylene or ethane can be modulated. For instance in HDC reaction of TCE by noble metals, like Pd, tends to convert trichloroethylene to fully hydrogenated products like ethane. In contrast, mild hydrogenation catalysts like Ni form ethylene or other unsaturated products but with low conversion. Bimetallic catalysts can achieve both enhanced catalytic activity and selectivity towards ethylene formation. As a result, the catalytic activity of Ni can be modified by addition of small amount of Pd. The Pd has ability to break molecular hydrogen and providing active hydrogen (spillover) for the reaction to continue while Ni is engaged in the HDC process. Consequently, the Ni particles that are located near Pd species are probably highly active. As shown in Fig. 6, even though the three catalysts are able to form different HDC products, Pd/NiHT1 catalyst with higher amount of Ni, scored the best catalytic performance and attained relatively higher selectivity to ethylene. This implies that catalyst containing small amount of Pd deposited over a

surface enriched with Ni, favors the formation of olefinic products during HDC of TCE at 573K. Ni has also the ability to break the C-C bond (hydrogenolysis) forming methane as final product. The hydrogenolysis of C-C bond is considered as structure sensitive process where the higher the ensemble the higher activity. As shown for a catalyst containing higher Ni content, such as Pd/NiHT1, methane was observed apart from ethane and chloroethylene. Another observation of Pd/NiHT catalysts, with different Ni/Mg/Al and reduced at 623K, resulted in significant formation of ethane apart from ethylene and other chlorinated hydrocarbons. The formation ethane is likely to be favored over the surface of Pd despite its low metal loading. This signifies that in the HDC of TCE, metallic Pd species are highly involved in direct HDC of TCE, hydrogenating part of the ethylene formed to ethane.

Higher reduction temperatures were employed for NiHT1 and Pd/NiHT1 catalysts to induce the formation of more metallic Ni species on the catalyst. Pd/NiHT1 catalyst, with higher Ni content, was chosen due to its higher catalytic performance than the others. Application of higher catalyst reduction temperature resulted in better catalytic activity. As shown in Fig. 7 and Fig. 8 increasing the metallic Ni phases by increasing the reduction temperature, modified the catalytic behavior for both the NiHT1 and Pd/NiHT1 catalysts. In case of NiHT1 catalyst methane, ethylene and some chlorinated products were produced. Ethane was not detected. However, the formation of methane increased with the catalyst reduction temperature treatment. The mechanism of HDC of TCE over reduced NiHT surface is displayed in scheme 1a based on a hypothesis that the ethane that is formed is rapidly transformed to methane. This can be further supported by two possible explanations. Since the activation energy required for hydrogenation of a double bond in the unsaturated hydrocarbons is higher than that for the cleavage of a C–Cl bond [61], the dechlorination reaction over Ni catalysts might be faster than the further hydrogenation of ethylene in the hydrodechlorination of TCE. The second explanation is associated with rapid dissociation of ethane to methane molecule at 623 K. The ethane produced by hydrogenation of ethylene could further hydrogenate breaking the C-C bond to form methane.

Lower reduction temperature employed for the Pd/NiHT-623K resulted in higher selectivity to ethylene. However a significant amount of ethane was observed. This could be due to the existence of surface Pd metals that are directly involved in the reaction. The mechanism of the reaction over metallic Pd enriched surfaces of Pd/NiHT1-623K catalysts is displayed in scheme 1b. As shown in scheme 1b the TCE hydrodechlorinates finally to ethylene and chloroethylene, then consequently the ethylene formed is hydrogenated to ethane by the Pd enriched sites. The higher catalyst reduction temperature (723 K) applied for Pd/NiHT1 catalyst to create better Pd-Ni interaction modified both activity and selectivity. TCE conversion of 100% was achieved at normal operating conditions; however the product distributions were compared at reduced conversion levels. As shown in Fig. 8 as the reduction temperature increased, ethylene and methane formation increased whereas ethane is decreased. This is due to the involvement of more metallic Ni species formed by the higher reduction temperatures employed. The changes in selectivity induced by the catalyst reduction temperature treatment may be related to the migration of Ni atoms from the bulk of the mixed oxide to the surface of the catalyst. Hydrodechlorination of C-Cl bond may require large Ni ensembles. The reduction treatment may generate a number sufficiently large Ni cluster suitable for the C-Cl bond scission. Surfaces usually exhibit unique compositions or structures that can deviate significantly from the bulk. The surface of a bimetallic system is enriched with a component with lower surface free energy. Surface segregation is one mechanism by which the material tries to lower its overall surface energy. Considering that the surface free energy of Pd is lower than that of Ni, Pd preferentially enriches the surface. Another parameter that may affect the surface composition is the selective chemisorption of a gas on the components of the bimetallic system. The component which interacts more strongly with the ambient gas could diffuse and enrich the surface. In the case of Pd-Ni bimetallic system both parameters lead to enrichment of the surface with Pd. However both Pd/NiHT1-723 and Pd/rNiHT1 catalysts in general presented higher selectivity of ethylene compared to the NiHT1.

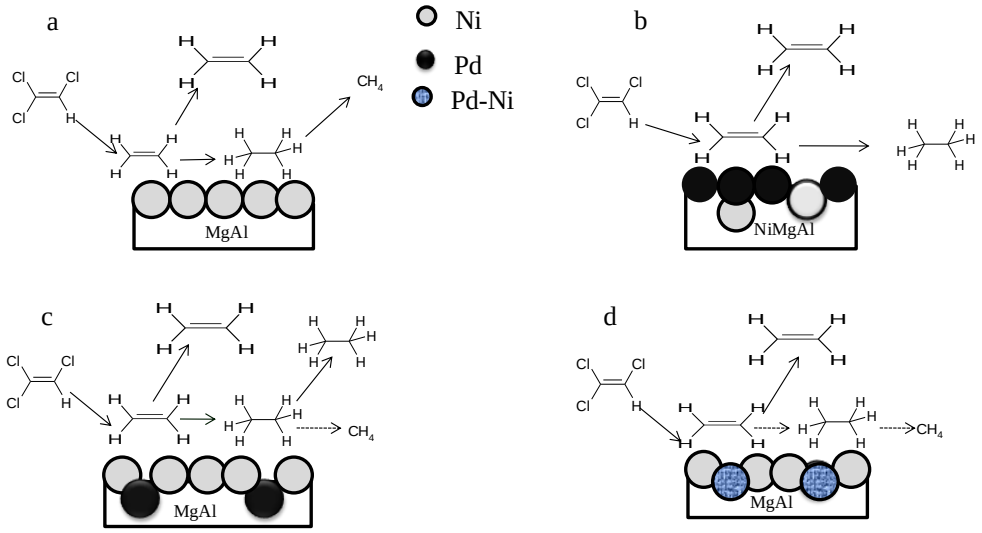

Scheme 1 Mechanism of ethylene conversion over Pd-Ni surfaces (dashed arrow represent less favoured pathway).

It is clear that the presence of metallic Pd modified the conversion of TCE probably by providing active hydrogen and activating the Ni. However the effect of Pd and Pd-Ni alloy, on the selectivity for the Pd/NiHT1 seems to be masked by the highly enriched Ni surface when compared with Pd/rNiHT1-723 samples. It can not be rule out the effect of higher temperature reduction of Pd/NiHT1 catalyst promote more severe Pd metal sintering as well as diffusion of Pd far from the surface. The fate of ethylene over for Pd/NiHT1-723 catalyst surfaces is displayed in scheme 1c. The existence of significant amount of ethane and other species demonstrates the hetrogenity of the surface. Apart from isolated metallic Ni, isolated Pd and can be formed even though under high temperature reduction, Pd masked by the bulk could dominate.

A better Pd-Ni interaction on the surfaces seems to be obtained by the Pd/rNiHT1 catalyst particularly Pd(0.3)/rNiHT1. The synthesis protocol for this samples minimized effects of palladium sintering and masking. As already shown in fig. 9, in this case the XRD profiles metallic Ni species were observed. The UV-Vis reflectance spectroscopy also depicted also that after reduction of the NiHT1 catalyst at 823 K, the absorption band is similar as the bulk reduced Ni. This fact can also indicate the formation of large ensembles of metallic nickel species. These domains are favourable for the

C-Cl hydrodechlorination. Further deposition of palladium resulted in a better mixed Pd-Ni domains. The Ni particles that are promoted by the nearby metallic Pd-Ni alloy as observed by HRTEM, improved the performance of the HDC reaction as observe by the increase in ethylene formation. The mechanism of ethylene hydrogenation over this catalyst is depicted in scheme 1d, where higher ethylene selectivity was obtained on the surface of metallic Ni that is promoted by the Pd-Ni alloy. A summary of catalytic activities are shown in Fig. 12, where Pd(0.3)/rNiHT1 catalyst resulted in good selectivity towards ethylene formation.

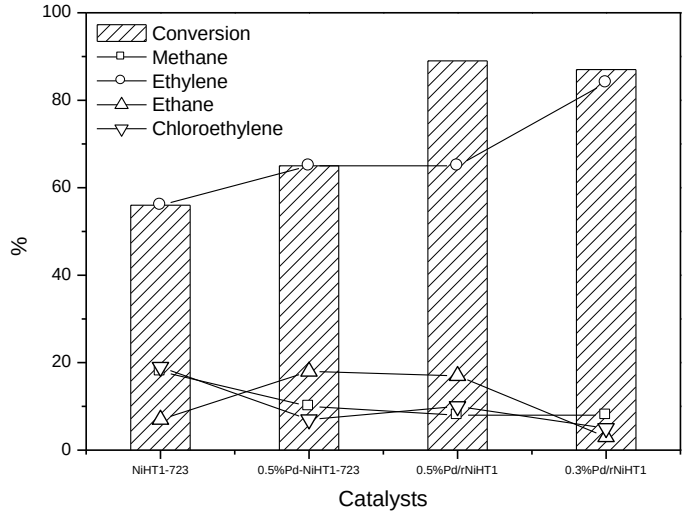

Fig. 12 Comparison of catalytic activities at the beginning of the reaction.

Conclusion

Hydrotalcite derived NiMgAl mixed oxide (NiHT) catalysts with different NiMgAl molar ratio were synthesized for selective gas-phase HDC of TCE to ethylene. The mixed oxide was further promoted by Pd (0.5 wt %) in order to obtain Pd/NiHTl catalysts. The catalysts were characterized by using different characterization techniques. The catalysts performances for

hydrodechlorination of trichloroethylene depend on Ni/Mg/Al molar ratio, temperature of reduction, and method of noble metal incorporation protocol. The higher Ni amount the higher the HDC catalytic activity and ethylene selectivity. Introduction of Pd helps to increase the HDC catalytic activity. However, at lower reduction treatment a mixture of ethane, ethylene and chloroethylene were formed signifying direct involvement of metallic Pd on the surface. The selectivity towards ethylene formation for Pd/NiHT1 catalyst was modified when increasing the surface metallic Ni species during high temperature reduction treatment. A better Pd-Ni interaction on the surfaces was obtained by employing different Pd incorporation protocol for Pd(0.3)/rNiHT1 catalyst. Higher ethylene selectivity (80%) was attained when Pd(0.3%) was introduced after reduction of NiHT mixed oxide. The higher selectivity was associated to metallic Ni that is promoted by Pd-Ni alloy, which its existence was detected by HRTEM.

Hydrotalcite derived NiMgAl mixed oxide (NiHT) catalysts with different NiMgAl molar ratio were synthesized for selective gas-phase HDC of TCE to ethylene. The mixed oxide was further promoted by Pd (0.5 wt %) in order to obtain Pd/NiHTl catalysts. The catalysts were characterized by using different characterization techniques. The catalysts performances for hydrodechlorination of trichloroethylene depend on Ni/Mg/Al molar ratio, temperature of reduction, and method of noble metal incorporation protocol. The higher Ni amount the higher the HDC catalytic activity and ethylene selectivity. Introduction of Pd helps to increase the HDC catalytic activity. However, at lower reduction treatment a mixture of ethane, ethylene and chloroethylene were formed signifying direct involvement of metallic Pd on the surface. The selectivity towards ethylene formation for Pd/NiHT1 catalyst was modified when increasing the surface metallic Ni species during high temperature reduction treatment. A better Pd-Ni interaction on the surfaces was obtained by employing different Pd incorporation protocol for Pd(0.3)/rNiHT1 catalyst. Higher ethylene selectivity (80%) was attained when Pd(0.3%) was introduced after reduction of NiHT mixed oxide. The higher selectivity was associated to metallic Ni that is promoted by Pd-Ni alloy, which its existence was detected by HRTEM.

4.5.

Nanoparticle synthesis and application in HDC of trichloroethylene

1. Introduction/Overview

1.1. Polyol mediated synthesis of nanoparticles

Nanoparticles (NPs) have unique physical and chemical properties different from bulk materials. They are particles that have one dimension with 100 nanometers or less in size bridging the gap between bulk materials and individual atoms or ions. Extremely high surface areas and high ratios of metal atoms occupying positions on or close to the surface and presence of various types of active sites make such nanoparticles ideal candidates as key components of catalytic systems. Nanoparticle atoms have lower coordination numbers than in the bulk and as a consequence are expected to exhibit greatly enhanced activity to all manner of substrates. Greater accessibility to all constituent (surface) atoms and enhanced activity because of the low coordination number they exhibit makes nanoparticle interesting in many reactions. Moreover, the transition metal nanoclusters also serve as a bridge between homogeneous and heterogeneous catalysts and provide new opportunities for catalysis [179]. This is typically because nanoparticles have a greater surface area per weight than larger particles; this causes them to be more reactive to certain molecules [180]. Striking novel catalytic properties including greatly enhanced reactivity and selectivity have been reported for NP catalysts as compared to their bulk counterparts [181]. The catalytic behaviors of nanoparticles depend on different factors like, particle size, morphology, alloying, surface groups. Therefore, nanoparticle preparation of practical realization requires the solution of extremely challenging issues of applied technology, e.g. control the geometry, the particle size, the morphology of nanoparticles and their assembly into structures performing specific functions and delivering specific effects. Among various transition metal particles, copper nanoparticles have attracted considerable attention because of its unique catalytic, optical and electrical conducting properties. Several methods have been developed for the preparation of copper nanoparticles, via physical and chemical methods. The physical synthesis method includes thermal reduction, sono-chemical reduction, metal vapor synthesis, vacuum vapor deposition, radiation methods and laser ablation [182, 183]. The common industrial production process for particles of size approximately 100 nm or slightly below is the physical vapour synthesis: a

precursor metal is heated up and releases vapors that are then cooled with a gas and condense into liquid molecular clusters. Most of the physical NP synthesis methods use an oxygen-free environment to synthesize copper as it easily oxidizes in air. The chemical synthesis methods involve chemical reduction of copper in aqueous or non aqueous solutions [184, 185]. Although, the chemical reduction in aqueous phase presents a fast reaction rate, it results agglomeration and non uniform copper nanoparticles. Hence the preparation of copper nanoparticles avoiding these is a challenge in this research field. The polyol process is one of widely applied technique using non-aqueous liquid (polyol) both as a solvent and reducing agent for nanoparticle preparation [185]. The use of non-aqueous solvents has an advantage of minimizing surface oxidation and agglomeration. Polyol mediated nanoparticles synthesis allows flexibility of controlling the size and shape of nanoparticles. This method can also be applied during large-scale nanoparticle production. In this process, additional stabilizing agents are employed in order prevent the nanoparticle from agglomeration, oxidation or precipitation of the particles. Furthermore a stabilizing agent determines the shape, size and uniformity of the resulting nanoparticles [186-188], related with the [stabilizing agent]/M^{2+} molar ratio. The most widely used polymer includes poly-vinylpyrrolidone, (PVP). Recently Zhu et al. [189] show this effect, preparing well-dispersed nanoparticles with controllable shapes (rods, needles, etc) adjusting the composition of the reaction system. Other synthesis parameter that is able to determine the shape and size of the nanoparticle is the type of stabilizing agent. There has been few quantity of work based on the use of long-chain alkylamine as stabilizing agents during polyol synthesis.

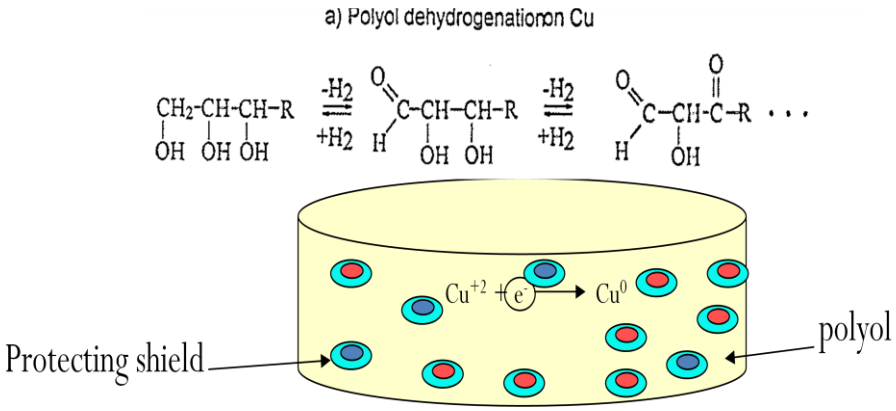

Fig. 1 Preparation of metal nanoparticles in homogeneous solution by chemical method

The long chain alkylamine are successfully employed as capping and phase-transferring agents in phase-transfer synthesis of several nanoparticles in aqueous phase. Phase transferring process involves the movement of aqueous metal nanoparticles which are capped by the alkylamine, into non-polar organic solvents. The alkylamines can form stable amine complex with transition metals, which result in small and stable nanoparticles. In a polyol process, V. Tzitzios et. al. depicted that the use of mixtures of Oleic acid and oleylamine during polyol synthesis of hexagonal close-packed Ni particles favors higher solubility of the nanoparticles in non-polar solvent [190]. Shen et. al. successfully synthesized the alkylamine capped gold nanoparticles by ethanol (polar) reduction under microwave irradiation [191]. In the same way Fe, Co and Ni nanoparticles were prepared using dodecylamine as stabilizing agents by microwave assisted polyol synthesis [192, 193]. The authors demonstrated narrower size distributions could be obtained with longer chain length such as octadecylamine. The distribution of particle size obtained using the commonly used poly vinyl pyrodaniline (PVP) are large for further application in fields like catalysis.

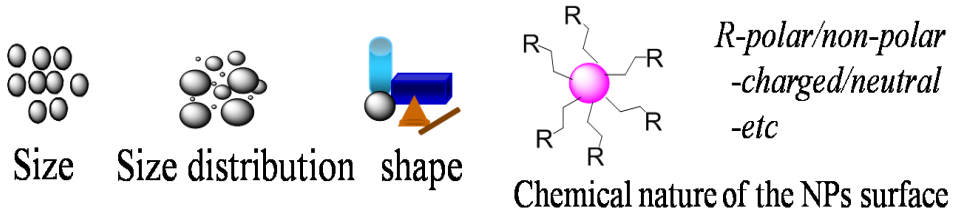

Fig. 2 Different configurations of nanoparticles

Based on this view, the use of the long chain alkylamine template during polyol process of nanoparticle fabrication could result highly dispersed small nanoparticles than that of PVP, which usually the average reported size includes 20-500 nm. Here we report a procedure developed for synthesis of 1-hexadecylamine (HDA) capped metal Cu nanoparticles (HDA-M) using polyol method. The metal nanoparticle complex can be recovered from the solution by polyol-organic phase-transfer techniques. In this way different HDA protected Pd, Cu, Au mono and bi metallic nanoparticles were synthesized by polyol process aiming their catalytic application.

1.2. Hydrodechlorination of TCE over bimetallic catalysts

TCE is one of widely distributed pollutant with carcinogenic and mutagenic property. It can selectively undergo hydrodechlorination to more valuable products like ethylene by using appropriate catalytic system. Noble metals have been reported to have high activity for this reaction due to the capacity for hydrogenolysis of C-Cl bonds. However the problem associated with noble metal catalyzed HDC reaction of TCE is the formation of unsaturated products like ethane due to complete hydrogenation of the double bond. Ethane is less desired commercial product when compared to ethylene. HDC over noble metal surfaces tend to rapidly hydrogenate the olefin formed as a primary product in the presence of H_2. In addition, the monometallic catalysts tend to deactivate rapidly with time on stream.

Monometallic Cu or Ag can catalyze the reaction to form selectively ethylene, however these metals are associated with low activity [125]. In addition, according to the study of Fung and Sinfelt [126] concerning the hydrogenolysis of methyl chloride CH_3Cl on metals, metals from Group IB, such as Ag and Cu, are able to form a metal–chlorine bond, as demonstrated

by the existence of stable chloride showing rapid deactivation. Surface chlorine atoms could not be removed easily due to lack of surface hydrogen. In this case, noble metals like palladium, with high hydrogen chemisorption capacity, could be needed to provide an abundant source of dissociated hydrogen, to reduce surface CuCl species and form HCl. In addition, the modification of supported Pd noble metal catalysts by the addition of a second metal changes the catalytic performance for vicinal chloro-carbon dechlorination. Higher olefin selectivity can be attained as demonstrated by Pd catalysts doped with second transition metals like Ag [118], Cu [117, 127] or Sn [128]. Comparable catalytic activity can be obtained by Pd-Cu alloys as monometallic noble metal catalysts, showing minimal deactivation.

Several possible theories have been reported in the literature to explain the reasons for high olefin selectivity in hydrodechlorination using bimetallic catalysts from the point of view of the noble metal. The effect of an electronic modification of Pt on the ethylene selectivity of the Pt–Cu/SiO2 catalysts in1,2-dichloroethane hydrogen-assisted dechlorination reaction has been investigated [129]. The electronic state of Pt was probed by CO adsorption. It was shown that Pt in the Pt–Cu/SiO_2 catalysts is modified electronically, but this modification does not control the selectivity toward ethylene [117]. To explain the high ethylene selectivity of the Pt–Cu catalysts for the dechlorination of 1,2-dichloroethane, Vadlamannati et. al. suggested that the C–Cl bond dissociation on Pt is a structure-sensitive or size-demanding elementary step [119]. If the dissociative adsorption of 1,2-dichloroethane requires large ensembles, the dilution of Pt with Cu splits such ensembles and suppresses the activity of Pt in the dechlorination reaction. Kovalchuk et al [117] proposed that the governing factor for the high olefin selectivity of bimetallic catalysts in hydrogen-assisted dechlorination of chlorocarbons is the low adsorption energy for olefins on active sites, which consist of isolated noble metal atoms in a matrix of the modified catalyst's surface. Thus, adjusting the chlorocarbon to H_2 ratio in the reaction feed could be an effective means to control the hydrogenation activity of the catalysts for hydrogen-assisted dechlorination of vicinal chlorocarbons.

From the point of view of the modifiers, the mechanism of 1,2-dichloroethane hydrodechlorination studied by Heinrichs et. al. for Pd-Ag catalysts suggested that the mechanism over alloys is based on the sequence

of elementary steps, which suggests a process of chlorination of the silver surface by 1,2-dichloroethane followed by a hydrodechlorination of that surface by hydrogen adsorbed on palladium. Used alone, silver deactivates rapidly due to its covering by chlorine atoms. However palladium present in the alloy supplies hydrogen atoms for the regeneration of the chlorinated silver surface into metallic silver [125, 130]. A study for 1,2-dichloroethane hydrodechlorination over Pt–Cu/SiO_2 catalysts also proved that the addition of CO into the $CH_2Cl–CH_2Cl + H_2$ reaction mixture at 473 K to block Pt sites only results in an improvement in the ethylene selectivity of the bimetallic catalysts at the expense of ethane. These observations were consistent with the idea that with Pt–Cu catalysts, ethylene forms on Cu sites that were not blocked by carbon monoxide [131]. Barrabes et. al. [127] presented a reaction scheme similar to what was proposed by the groups of Heinrichs [125] and d'Itri [131] for hydrogen-assisted dechlorination of dichloroethane on PdCu catalysts where, adsorption of TCE on the Cu phase leading to dechlorination reaction producing ethene is proposed. The main role of the noble metal forming the alloy is the regeneration of the Cu-Cl_x species by spillover of hydrogen. On the alloyed particles a high selectivity to ethene is obtained. However, on catalysts containing copper and the noble metal in separate form the dehalogenation reaction occurs on the copper surface whereas on the surface of the noble metal a deep hydrogenation to ethane is taking place [127]. The catalytic performance, however, depends on the modifier to noble metal ratio, and reaction condition [128]. Supported bimetallic Pd-Cu catalysts are one of the most widely studied for HDC of TCE to ethylene.

Catalyst synthesis protocol can also influence the catalytic activity by controlling uniformity metal-metal interaction. Most of the methods used to prepare bimetallic catalysts are based on co-impregnation, sequential impregnations, co-exchange with the salts of the two metals or redox reaction. As a result the above protocol was adopted to prepare several monometallic Pd and bimetallic Pd-Cu nanoparticles with different Pd/Cu molar ratios (Pd_1Cu_1, $Pd_{1.6}Cu_{1.2}$, Pd_1Cu_5). Pd1Au1 catalysts were also prepared and employed for HDC of TCE. In previous work, Barrabés *et. al.* prepared Pd–Cu bimetallic catalysts supported on alumina by several preparation methods expecting different surface chemistry such as metal-metal interaction, isolated phases, alloy formation. In this way surface redox

reaction (Controlled surface reaction), sequential impregnation (SI and S reduction I) and co-impregnation (COI) protocols have been employed in order to study the effect of the method of preparation on the activity and selectivity in gas phase hydrodechlorination of TCE reaction [119].

2. Experimental

2.1. Preparation techniques

2.1.1. Synthesis of nanoparticles

Synthesis of copper nanoparticles

Copper nanoparticles were synthesized by polyol method, using long chain alkyl amine as protecting agent. Analytically pure $Cu(NO_3)_2.2H_2O$, 1-hexyldecylamine (HDA) and ethylene glycol were used as the starting materials without further purification. In a typical synthesis procedure, 100 ml of 0.05 M ethylene glycol (Eg) solution of $Cu(NO_3)_2.2H_2O$ was mixed with an appropriate amount of HDA in a round-bottom flask equipped with a magnetic stirrer, refluxing device and thermometer. The mixture was mixed thoroughly at 333 K to achieve a complete homogeneous solution. The solution was then heated up rapidly to 413 K and kept there for 16 h. The previous transparent blue solution rapidly turned into intense blue, green turbid, then to brown solution of CuO, which later changed into an intense red mixture of Cu_2O. Finally the mixture started to turn into brown-black turbid. After the reaction, the solution was then cooled rapidly to room temperature. Toluene (40 ml) was added to the cooled mixture and stirred for 15 min. Phase separation between the polar solvent Eg and non-polar solvent toluene was achieved by centrifugation. The copper nanoparticles trapped in the toluene were separated and washed several times with ethanol to remove other non polar organic compounds, and stored under Ar atmosphere. Following this procedure copper nanoparticles were synthesized with HDA/Cu molar ratio of 3 and 1. The nanoparticles are readily soluble in toluene or any non-polar solvent. Following similar protocol PVP capped copper nanoparticles were synthesized using PVP/Cu molar ratio of three.

Synthesis of Pd, Au and Pd-Au nanoparticles

Modified procedure of the above protocol was adopted in order to prepare HDA capped Pd, Au and Pd-Au nanoparticles. Analytically pure Pd acetyl acetonate ($Pd(AcAc)_2$) and Gold salt $HAuCl_4$ were used as the starting materials without further purification. In a typical synthesis procedure, 100 ml of 0.05 M ethylene glycol solution of the respective metal was mixed with an appropriate amount of hexadecylamine (HDA) in a round-bottom flask equipped with a magnetic stirrer, refluxing device and thermometer. The mixture was mixed thoroughly in an ice bath to prevent rapid reduction of the noble metals in ethylene glycol and HDA solutions at room temperature. The solution was then heated rapidly to 333 K and kept there for 3 h. Pd/Au nanoparticles with different Pd/Au molar ratio were prepared using the same protocol. The nanoparticles were synthesized maintaining HDA/metal molar ratio of three.

Synthesis of Pd-Cu nanoparticles

The bimetallic Pd-Cu nanoparticles were prepared similar protocol as the Pd nanoparticle synthesis but after mixing the appropriate amount of Pd and Cu the temperature was raised to 413 K for 12 h. Different proportions of Pd/Cu molar ratio were synthesized.

2.1.2. Synthesis of Alumina support nanoparticle catalysts

The Pd and Pd-Cu nanoparticles prepared in ethanol/toluene solution were impregnated over γ-Alumina. After evaporation of the solvent in rotavapor the catalyst was dried overnight at 373 K, calcined in air at 623 K for 2h and reduced by flowing hydrogen at 573 K for 2h prior to reaction. The different catalysts synthesized are labeled as Pd/Al_2O_3, $Pd1Cu1/Al_2O_3$, $Pd1Cu5/Al_2O_3$, and $Pd1.6Cu1/Al_2O_3$. For instance $Pd1Cu1/Al_2O_3$ represents 1%Pd and 1%Cu metal with nanoparticle precursor.

2.1.3. Synthesis of Alumina support bimetallic catalysts

$PdCu/Al_2O_3$ (Pd/Cu molar ratio=1) catalysts were prepared following different synthesis protocol in order to achieve different Pd/Cu interactions by Barrabés *et al*. [127]. Monometallic Pd/Al_2O_3 catalysts was prepared by cationic exchange between the metallic complex and the alumina surface in

an aqueous solution at pH=11 obtained by the addition of ammonia. After evaporation of the aqueous phase, the catalyst was dried at 393 K and calcined in air at 723 K. After that, the monometallic Pd catalyst was directly impregnated with the copper salt (SI-sequential impregnation) or reduced under hydrogen flow at 673K for one hour before impregnation with the copper salt solution (sequential reduction impregnation), or introduced to an aqueous solution containing a copper nitrate salt under hydrogen flow (control surface reaction). The COI catalysts (co-impregnated) were prepared by direct impregnation with a solution containing the two metals ($Pd(NO_3)_2 \cdot 2H_2O$ and $Cu(NO_3)_2.3H_20$). Then the samples were dried and calcined at 573 K for 2h, and finally reduced at 673 K under hydrogen flow for 1h.

2.2. Characterization technique

2.2.1. Nanoparticle characterization

The main characterization of copper, Palladium and gold nanoparticles in solution was investigated by transmission electron microscopy. TEM operated at 100 kV (JEOL JEM-2000 EX II) was taken to analyze the morphology and dispersion of nanoparticles. Samples were dispersed in alcohol/toluene mixture bath and a drop of suspension was poured onto a holey carbon-coated grid and dried completely before the measurements were taken. Uv-Vis spectra of ethanol solution alkylamine capped copper nanoparticles were carried out at ambient temperature using UV-Vis spectrophotometer by scanning wavelengths between 200-820 nm. FTIR spectra for copper nanoparticle were adopted in order to study surface species that bound with copper.

2.2.2. Supported catalysts characterization

The chemical composition of the samples was determined by ICP-OES with a Perkin-Elmer Plasma 400 instrument. The oxidation state and crystallinity of the supported catalyst after calcination was investigated using X-ray diffraction, Siemens D5000 diffractometer (Bragg-Bentano for focusing geometry and vertical θ-θ goniometer) fitted with a grazing incident (ω: 0.52º) attachment for thin film analysis and scintillation counter as a detector. TEM operated at 100 kV (JEOL JEM-2000 EX II) was taken to analyze the morphology and dispersion of Pd/Al_2O_3 catalyst. High-

Resolution Transmission Electron Microscopy (HRTEM) was carried out at 200 kV with a JEOL JEM 2100 instrument equipped with a LaB_6 source. About 90 individual particles were used in each sample for particle size determination.

The temperature programmed reduction studies were performed in a ThermoFinnigan (TPORD 110) apparatus equipped with a thermal conductivity detector (TCD). The samples were then purged with argon flow before the TPR analysis. The analysis was carried out using a 3% H_2/Ar gas flowing at 20 ml min^{-1} by heating from room temperature to 1173 K with a ramp of 15 K min^{-1}. Prior to analysis the catalysts were pretreated in air for an hour, at 393K. Water produced during TPR was trapped in CaO + Na_2O (Soda lime) before reaching the TCD. The characterization results were used to interpret their catalytic behaviors.

2.3. Catalytic activity

The catalysts were tested for gas-phase hydrodechlorination reaction of trichloroethylene (TCE) using a continuous fixed-bed glass reactor described previously as the reaction conditions [127]. The gas feed is obtained by flowing an inert gas (He) and hydrogen through a saturator kept at 298 K by a thermostat, containing trichloroethylene (TCE) in liquid phase. The TCE partial pressure of 92 mbar was achieved. The molar ratio of H_2/TCE (related to the chloride species) was maintained at stoichiometric amount. The gas flows are adjusted by mass flow controllers (Brooks Instrument 0154) and introduced into the reactor, which is placed in a furnace coupled with a temperature controlling system. The outlet of the reactor is connected by a six-way valve to a gas chromatograph (HP 5890 series II, HP Poraplot column, FID). Catalytic conversion and selectivity were calculated by analyzing the peak areas of TCE and the respective products.

3. Results and discussion

3.1. Characterization results

3.1.1. Copper nanoparticles

The color of the nanoparticles usually can explain the oxidation states of the respective nanoparticles. The solution of the copper nanoparticles synthesized using the amine and PVP stabilizer show brown-black color indicative of copper nanoparticles and the capping agent. Indeed, XRD analysis of brown powders prepared by either methods, confirmed formation of metallic copper in the end product as shown in fig. 3. Bragg's reflections for Cu nanoparticles are observed in the XRD pattern at 2θ value of 43.6^{o}, 50.7 ^{o} and 74.45 ^{o} representing (1 1 1), (2 0 0) and (2 2 0) planes of fcc crystal structures of bulk copper. Copper nanoparticles prepared using PVP stabilizer and Cu/HDA 1:1 possess crystalline peaks when compared with HDA capped copper nanoparticle, which is typical property of large particles as shown in Fig 3a. While copper nanoparticle prepared by using HDA/Cu molar ratio of 3 resulted also an intense copper peak but with much lower intensity as comparde to the others as shown in fig 3b.

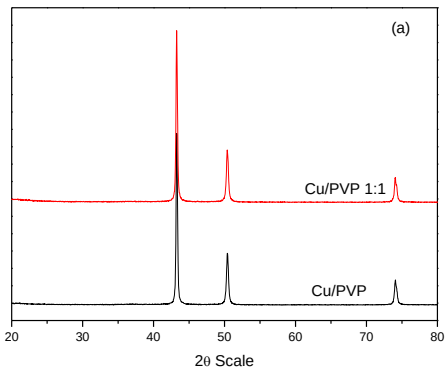

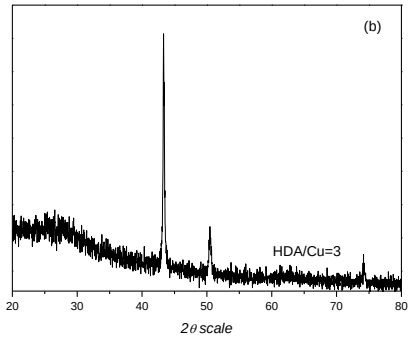

Fig. 3 XRD profile of copper nanoparticles synthesized using HDA and PVP (Stabilizer/Cu molar ratio of 3).

Fig. 4 shows broad UV-Vis absorption spectra of copper nanoparticles capped by the HDA dispersed in toluene solution. HDA capped copper nanoparticles showed a two main UV-absorption peak at around 410 nm and 571 nm respectively as shown in Fig. 4. The first absorption peak can be assigned to small separated Cu nanoparticle complexes of amines. This peak was also observed by Aslam et. al. [9]. The second absorption peak (571 nm) could represent absorption of copper nanoparticles. The typical surface Plasmon resonance for copper nanoparticles is at around 600 nm. The blue shift of the absorption edge for the prepared copper nanoparticles (480 nm) relative to that of bulk copper could suggest the existence small Cu nanoparticles.

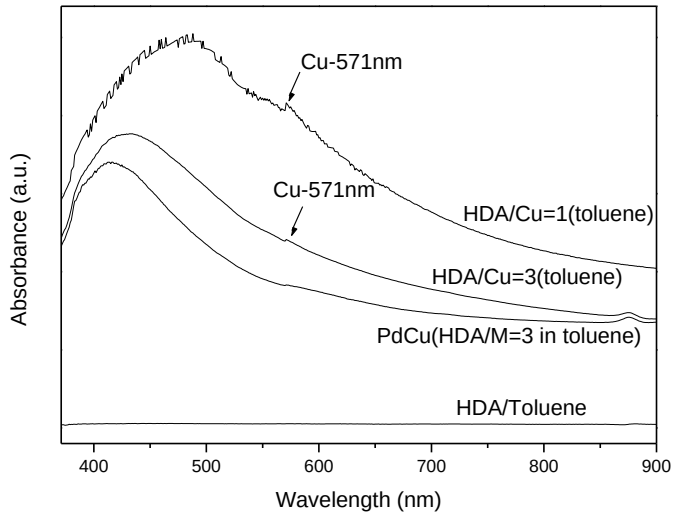

Fig. 4 UV-Vis spectra of HDA capped copper nanoparticles (HDA/Cu=3).

In order to investigate the existence of some capping agents bound to the surface of the cleaned copper nanoparticles, FTIR spectrum was measured. In the present case it is applied to find out whether there are any peaks due to the amines and alkanes in the final copper nanoparticle from the stabilizers. Fig. 5 displays the FTIR profiles for copper capped copper nanoparticles. It can be clearly observed that the FTIR spectrum of HDA-capped copper is associated to different C-H and N-H streching and bending bands. As shown in the profile the C-H stretching and bending modes are also observed at 2955 cm^{-1} and 1487 cm^{-1} respectively. Besides, the N-H in NH_2 stretching and bending bond is observed at 3394 and 706 cm^{-1} respectively. This implies that even after cleaning the Nps several times, organic species (HDA) are bound to the nanoparticles protecting it from oxidation.

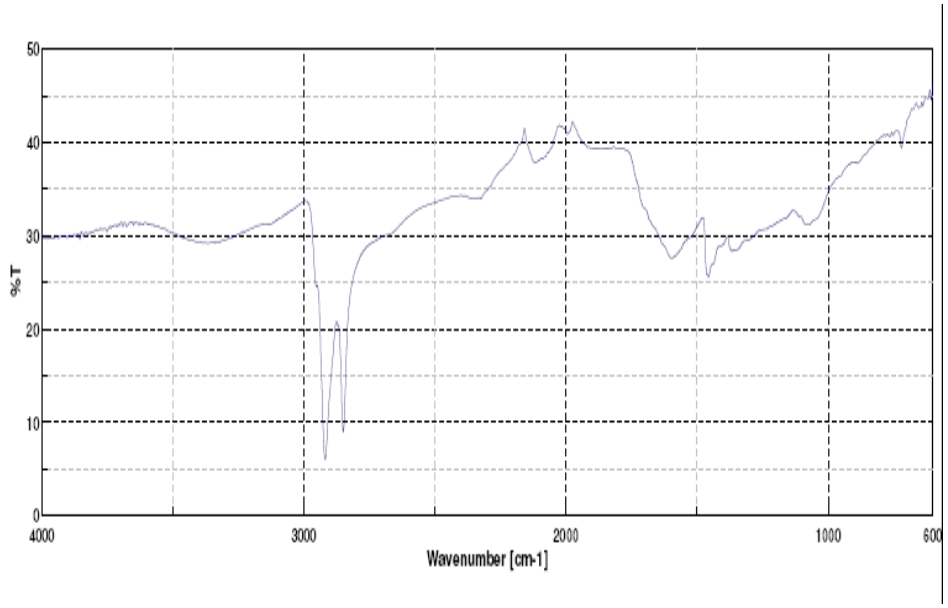

Fig. 5 FTIR spectra of HDA capped copper with HDA/Cu molar ratio 3.

Since HDA is coordinated with the copper through its amine group, a decrease in the intensity of the NH_2 band in the HDA capped copper nanoparticle is observed. This observation is further reinforced by proton nuclear magnetic resonance (NMR) study as shown in Fig. 6, where the free

-NH_2 band has disappeared, despite techniques limitation towards magnetic materials.

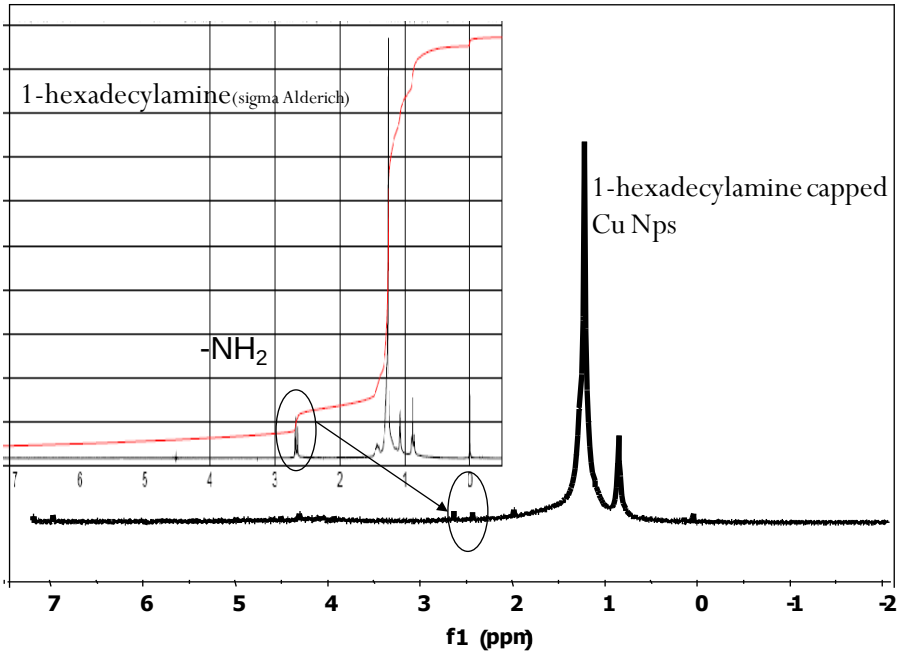

Fig.6 Proton NMR spectra of HDA capped copper (Inset-pure HDA molecule with free NH_2 groups).

Therefore in the process, the copper solution at the start could coordinate with 1-hexadecylamine with the amine extension while the long alkyl chain sterically inhibits further particle growth and agglomeration as shown in scheme 1.

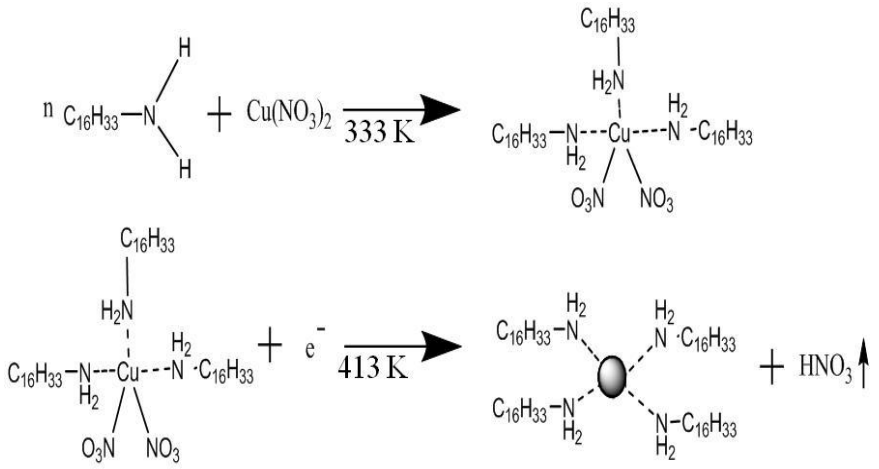

Scheme 1 Schematic representation of copper nanoparticles with HDA.

Copper nanoparticles in toluene solution were further characterized using transmission electron microscopy (TEM) as shown in Fig. 7. The PVP stabilized copper is characterized by large particles with polyhedron like structures as shown in Fig. 7a. In contrast, the HDA capped Cu nps shown in Fig. 7b, prepared with similar HDA/Cu molar ratio, showed small transparent spherical nanoparticles. This shows that the HDA is more viable stabilizer than the PVP in the preparation of Cu nanoparticles at these operating conditions.

TEM pictures, shown in Fig. 7b and Fig. 7c, confirm the difference in the particle size related with the HDA/Cu molar ratio employed during the polyol synthesis method. As molar ratio between HDA/Cu increased the particles size decreased from an average of 20 nm to 8 nm as shown in Fig. 7. The stabilizing agent also affected the shape configuration. In case of lower molar ratio, polyhedrons were obtained with rod, hexagonal and triangular like structures, whereas using higher HDA/Cu molar ratio resulted in transparent like spheres with narrow particle size distribution. Fig. 7 also shows the size distributions of copper nanoparticles. The copper nanoparticle prepared using HDA/Cu molar ratio of 2 has large size distribution between 10 nm to 80 nm as shown in Fig. 7c. While Cu NPs prepared at higher Cu/HDA molar ratio has a narrow size distribution between 2-20 nm.

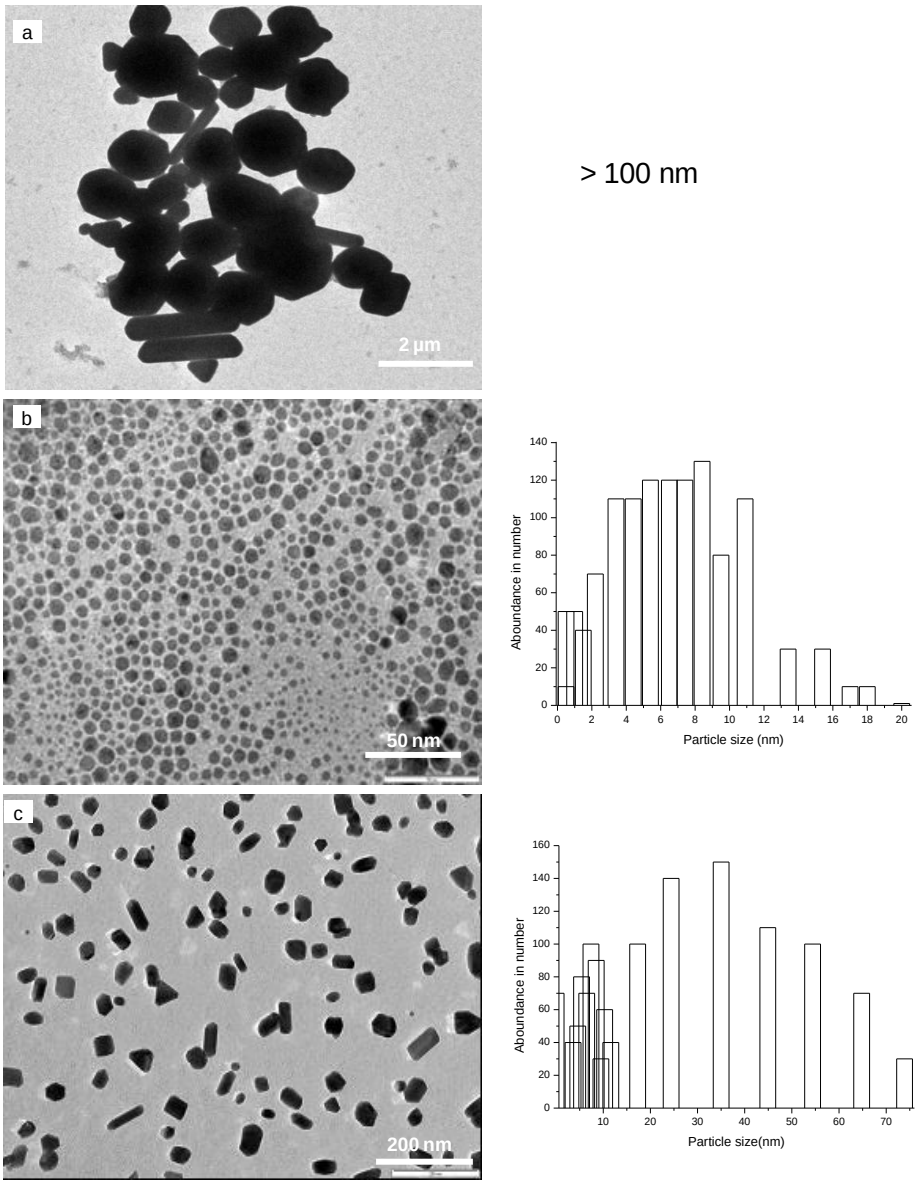

Fig. 7 TEM images of the alkylamine capped copper nanoparticles. The particle size distributions are shown in the form of histograms alongside the TEM images. (a) PVP/Cu molar ratio of 3. (b) HDA/Cu molar ratio of 3. (c) HDA/Cu molar ratio of 2.

3.1.2. Pd, PdCu and Pd-Au nanoparticles

The TEM profiles of palladium and gold nanoparticles prepared are comparatively shown in Fig. 8a. The TEM profile presents average particle size of 4 nm and 15 nm for Pd and Au respectively. These particles are characterized by a uniform size distribution and self-assemble property of Pd and Au nanoparticles on 1-hexadecylamine template.

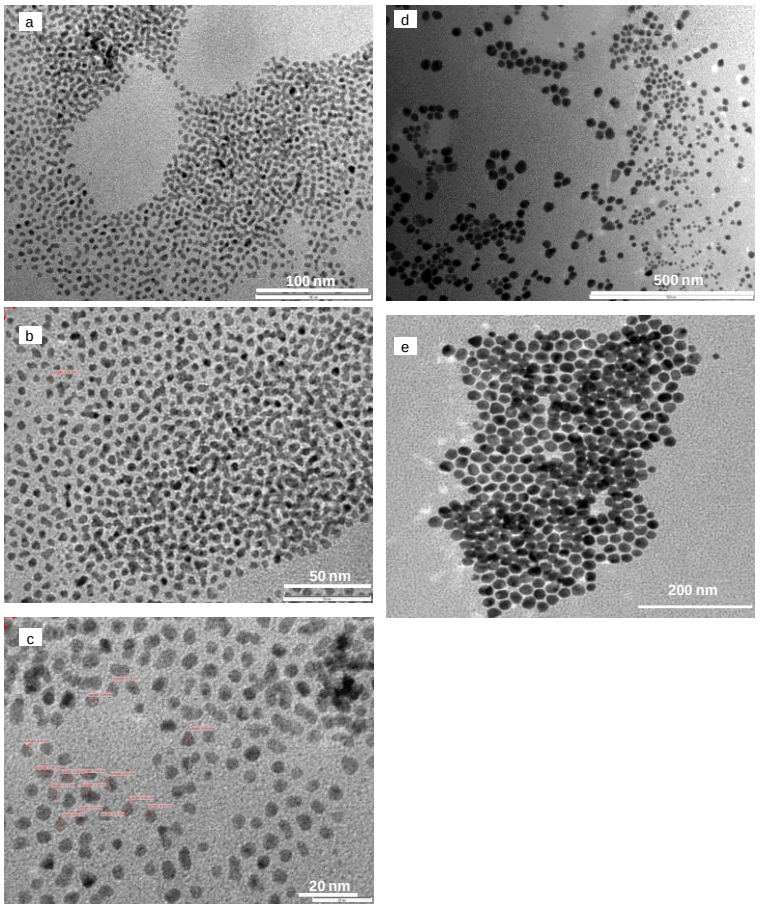

Fig. 8a TEM pictures of HDA stabilized palladium (a,b,c) and gold (d,e) nanoparticles, (HDA/Metal molar ratio of 3.

The TEM profiles of Pd-Au nanoparticles prepared with different PdAu molar ratio of 1 and 5 are comparatively shown in Fig. 8b. The TEM profile in both cases presents particle size between 1-10 nm. The average

particle sizes for Pd5Au1 and Pd1Au1 are 3 nm and 5 nm respectively. These particles like the monometallic Pd and Au, are characterized by a uniform size distribution and self-assemble property of PdAu on on 1-hexadecylamine template.

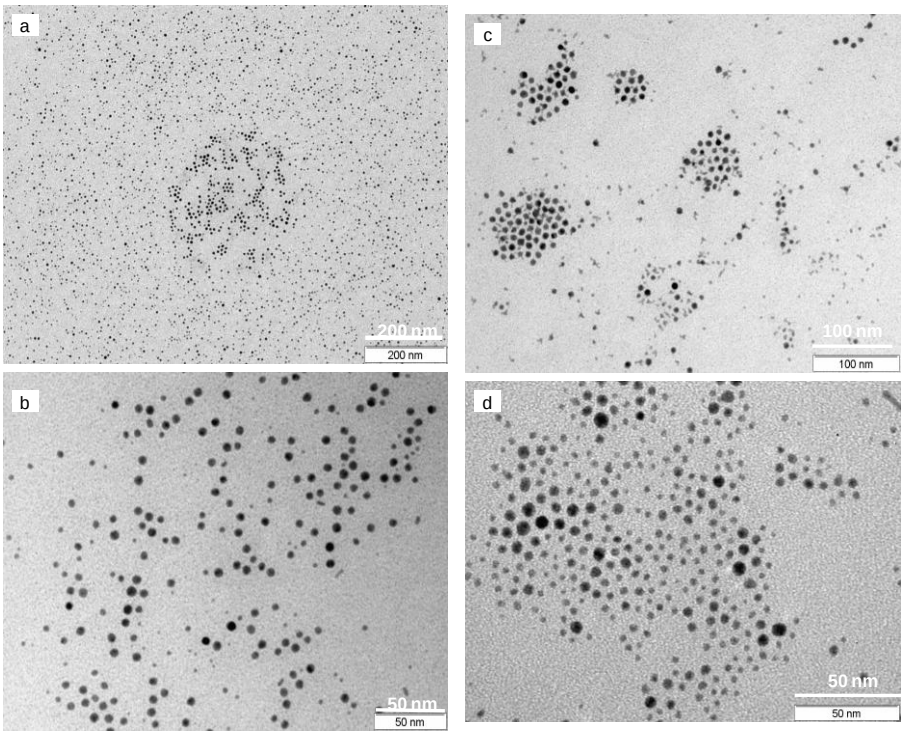

Fig. 8b TEM pictures of HDA stabilized palladium Pd1Au1 (a and b), Pd5Au1(c and d) nanoparticles, (HDA/Metal molar ratio of 3.

3.1.3. Supported Pd, Pd-Cu catalysts

For a long time it has been known that a bimetallic surface can exhibit chemical and catalytic properties that are very different from those of the surfaces of the individual metals. The nanoparticle synthesis protocol was adopted to prepare different supported materials for catalytic application. We have focuses on synthesis of Pd-Cu nanoparticles as they show high selectivity to ethylene during HDC of trichloroethylene. The molar compositions of the metals were investigated using ICP-OES, spectroscopy. The results are summarized in Table 1.

Table 1. Physical characteristics of Pd-Cu nanoparticles

Catalysts	Metal loading			Particle size (nm) TEM
	Pd (wt%)	Cu (wt%)	Atomic ration (Pd:Cu)	
Pd/Al_2O_3	0.8	-	-	10
$Pd1Cu1(i)/Al_2O_3$	0.7	0.8	0.5	-
$Pd1Cu1/Al_2O_3$	0.9	1.1	0.5	15
$Pd1Cu5/Al_2O_3$	0.9	4.7	0.1	-
$Pd1.6Cu1/Al_2O_3$	1.6	1	1	15

The presence of crystalline Pd or/and Cu containing phases within calcined Pd-Cu/γ-Al_2O_3 samples was investigated by XRD as shown in Fig. 9a and 9b. The pure alumina support shows the typical pattern of transitional alumina, characterized by γ-Al_2O_3 (JCPDS-01-079-1558). This pattern is evedent in all samples. Broad and diffuse diffraction lines of the support sample indicate poor crystallinity of γ-alumina. In agreement with the previously reported results, it is confirmed that low to moderate total metal loading on high surface area Al_2O_3 support calcined gives highly dispersed Cu and Pd species which are difficult to be detected by X-ray diffraction [194]. However the total Pd and Cu loading influences the intensity of alumina, the peak position between to 30-50°, due to the diffusion of Cu and Pd atoms into the γ-alumina lattice as shown in Fig. 9. In order to clarify the existence of peaks related to Pd and Cu species, the XRD profiles were magnified in scale between 30-50°as shown in fig. 9b. In Pd/Al_2O_3 catalyst, apart from the alumina species, PdO phases (JCPDS-00-043-1024), around 34.4°, 42°, 55° were observed. The PdO species are clearly observed for bimetallic catalysts. Additional metallic Pd (JCPDS-01-087-0641) diffraction peak was observed for $Pd1.6Cu1/Al_2O_3$ catalyst at 40.5° and 47.3°. The characteristic peak of CuO phases were not clearly visible in all bimetallic catalysts probably due to an overlap with the diffraction peak of alumina at around 40°. However

there is a clear distortion of the alumina diffraction line around 37.8^{o} probably due to the existence of some CuO species.

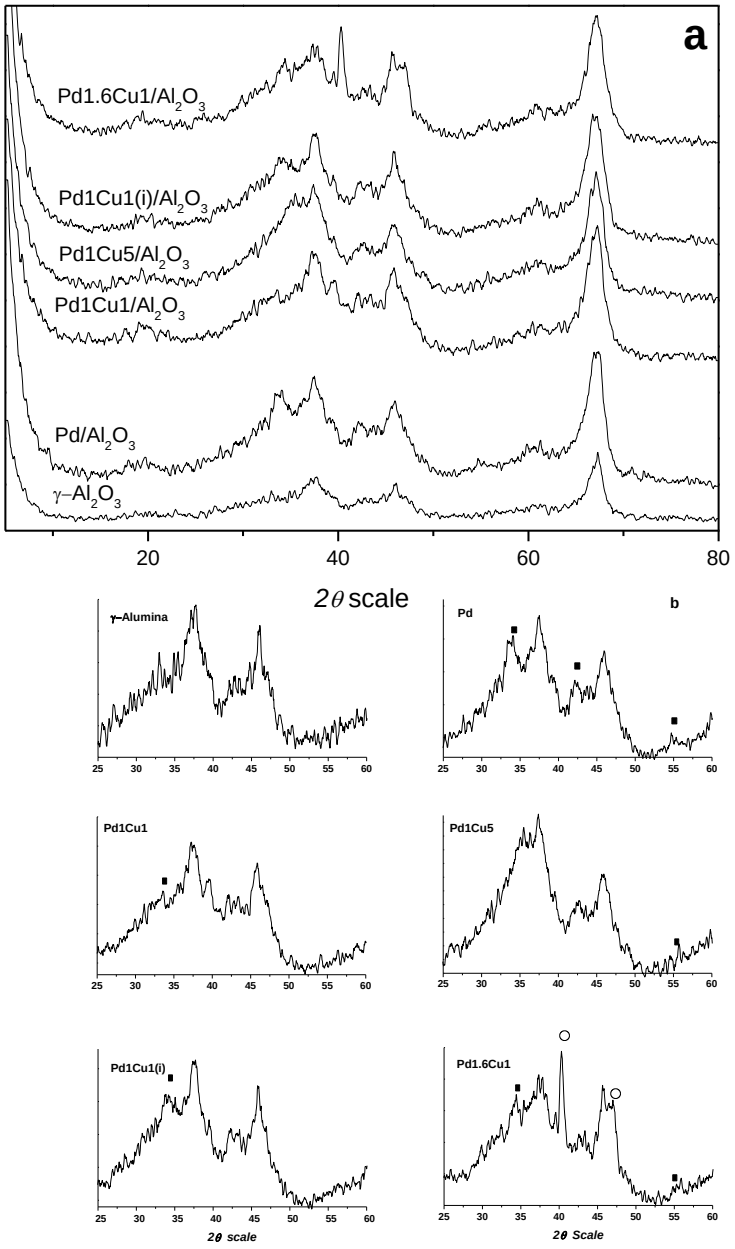

Fig. 9 XRD profiles of γ-alumina supported Pd and PdCu nanoparticles (a) complete diffractogram (b) magnified (25-60^{o}), ■ PdO, ○-metallic Pd.

The degree of Pd-Cu interactions was further investigated by H_2-Temperature programmed reduction analysis as shown in Fig. 10. The consumption of hydrogen and reducibility of supported metal catalysts depends on metal-support interaction, metal-metal interaction, particle size distribution. The TPR profile for Pd/Al_2O_3 catalyst showed major reduction peak at around maximum of 380 K. The reduction peak at around 333 K that is related to the decomposition of Pd β-hydride was not observed, which may indicate that Pd is well dispersed on the support with small particle size or prior calcination employed for this catalyst. The bimetallic catalysts feature resulted in different TPR profiles which are assigned tentatively. This difference could be due to different degree of interaction the particles exhibit towards the support or each other. As shown in the fig. 10, the $Pd1Cu1(i)/Al_2O_3$ catalyst prepared by impregnation, with Pd/Cu molar ratio of 0.5, showed a main reduction peak at around maximum of 424 K that can be assigned to the reduction of CuO, promoted by the near presence of the Pd. Small reduction peak at around 274 C is assigned to the reduction isolated copper species far from the noble metal ensemble.

The main reduction peak for this catalyst shifted to high temperature when compared to the Pd/Al_2O_3 catalyst. The decrease in the reduction temperature of supported copper in bimetallic catalysts induced by the presence of palladium indicates that a close proximity between copper and palladium species was achieved. The TPR profile for $Pd1Cu1/Al_2O_3$ catalyst is characterized by broad peaks around 342 K, 401 K, and 523 K respectively. The peaks around 342 K is probably due to the reduction of isolated PdO species. The main reduction peak located at maximum of 401 K is probably related to the reduction of Pd-Cu oxide species that are in close vicinity, probably alloys before calcination. The lower reduction temperature for the bimetallic PdCu phase could depict the surface is enriched with Pd species. The broad peak located > 450 K can be assigned for the reduction of isolated CuO species and spillover. The existence of different reduction peaks shows the heterogeneity of the surface species based or particle size and or Pd-Cu interaction. The TPR profile for $Pd1Cu5/Al_2O_3$ catalyst in general shows a uniform broad peak at maximum around 470 K. No peak related to the reduction of isolated PdO species at lower temperatures was detected for this catalyst. The reduction peak at 470 K is related to reduction of CuO species. These species could be affected by the presence of Pd as they reduce at lower

temperatures. Small reduction peaks located at 573 K and 647 K are associated with isolated CuO far from the noble metal ensemble.

The TPR profile for $Pd1.6Cu1/Al_2O_3$ catalyst did not reveal a uniform reduction peak showing the existence of different surface species. The profile consists of distinct peaks located around 369 K, 396 K and 478 K. As expected the first shoulder like peak at 369 K is associated to the reduction of isolated PdO species, which presents similar profile as Pd/Al_2O_3 catalyst. The main reduction peak located at maximum around 396 K is assigned tentatively to Pd-Cu oxide species that are in close vicinity to each other. While the high temperature reduction peak at 478 K is related to reduction of isolated CuO species as observed also for $Pd1Cu5/Al_2O_3$ catalyst. The different TPR reduction peaks relates that the bimetallic catalyst prepared using the polyol synthesis protocol did not result in uniform alloy formation. Instead isolated Cu and Pd and Pd-Cu alloy exist on alumina surface. While the $PdCu(i)/Al_2O_3$ catalysts relatively forms a uniform reduction peak associated to the PdCu species.

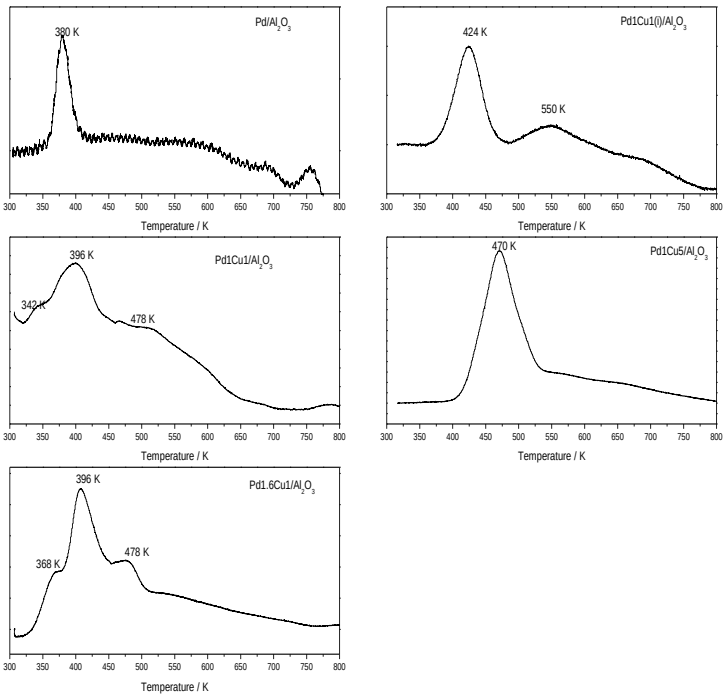

Fig. 10 H_2-TPR profiles for monometallic Pd and bimetallic $PdCu/Al_2O_3$ catalysts.

Selected catalysts which are characterized by HRTEM and TEM techniques are shown in the Fig. 11 and 12. The TEM profiles for Pd/Al_2O_3 catalyst after reduction are shown in Fig. 11. Palladium particles that are clearly visible as dark contrasts are uniformly dispersed on the surface of support with an average particle size of 10 nm. The Pd nanoparticles prepared before impregnation were characterized by small particle size with average diameter of 4 nm. As expected the increase in particle size in Pd/Al_2O_3 catalysts is probably due to the heat pretreatments used during calcination.

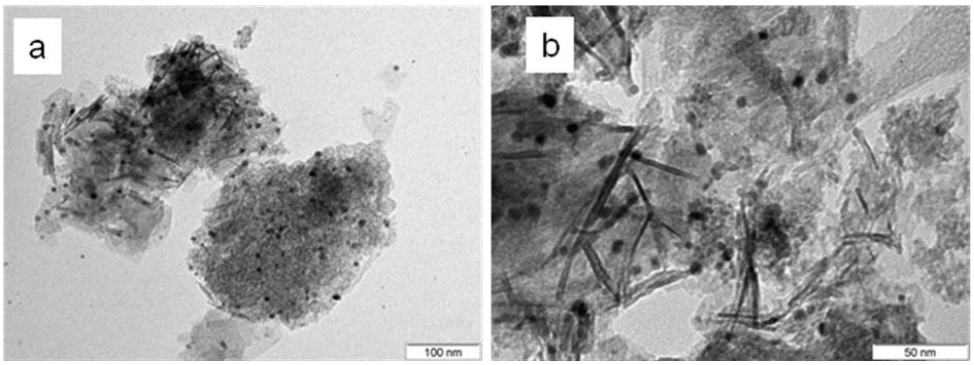

Fig. 11 TEM pictures of Pd/Al_2O_3 catalysts.

The bimetallic $Pd1.6Pd1/Al_2O_3$ and $Pd1Cu1/Al_2O_3$catalysts were characterized using TEM and HRTEM integrated with Fourier transform technique, as shown in Fig. 12. $Pd1.6Cu1/Al_2O_3$ sample is comprised by particles with very different size. As a general trend, there are large particles of about 100 nm in diameter along with smaller particles, varying between 10 and 20 nm. Fig. 12a and 12b show bright-field TEM images at low magnification, where both types of particles are easily recognized. They are supported over Al_2O_3 with a much smaller particle size. High-resolution TEM (HRTEM) cannot be performed over the large particles because they are too thick for lattice-fringe analysis, Fig. 12c and 12d therefore correspond to HRTEM images of the small particles. The particle depicted in Fig. 12c shows a lattice spacing at 2.62 Å, as deduced from Fourier Transform (FT) analysis (inset). This correspond to (110) planes of Cu_3Pd alloy. The structure of pure Pd and Cu is cubic ($F_{m\text{-}3m}$). The same symmetry is found for the CuPd alloy, but the Cu_3Pd alloy is tetragonal (P_{4mm}) and, for that reason, can be easily recognized. Fig. 12d shows another HRTEM image

for another particle. In this case, the particle shows two domains, indicated in the figure with labels “a” and “b” with the FT analyses of both domains attached. Domain “a” shows spots at 2.62 and 2.76 Å. Again, crystallographic planes at 2.62 Å can only be ascribed to (110) planes of Cu_3Pd alloy. The spots at 2.76 Å in domains “a” and “b” correspond to (110) planes of pure Pd. The coexistence of Pd and Cu_3Pd phases is commonly encountered in the sample.

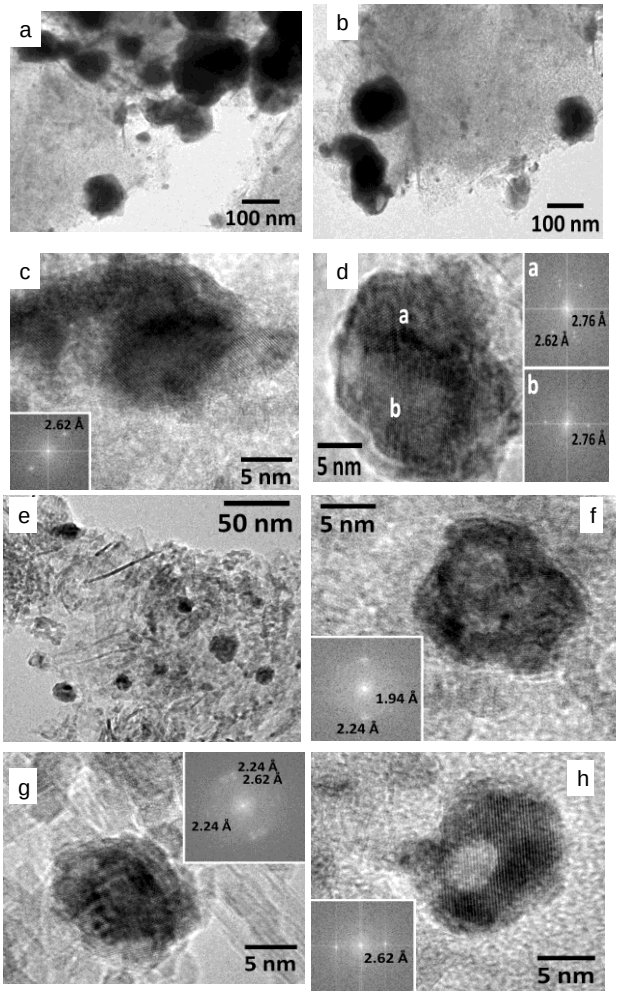

Fig. 12 HRTEM profile for $Pd1.6Cu1/Al_2O_3$ (a-d) and $Pd1Cu/Al_2O_3$ (e-h)samples.

A low-magnification view of $Pd1Cu1/Al_2O_3$ catalyst is shown in Fig. 12e. In this case, the particle size distribution spans from 10 to 25 nm in

diameter, being the mean particle size centered at about 14-15 nm. A careful lattice fringe analysis of these particles carried out with HRTEM is shown in Fig.12f, 12g and 12h. In Fig. 12f, the FT analysis shows the occurrence of spots at 1.94 and 2.24 Å, which correspond to (200) and (111) planes of pure Pd metal, respectively. Another representative particle is shown in Fig. 12g, along with its FT analysis. In this case, several spots at 2.24 and 2.62 Å are recognized in the FT image, which are ascribed to (111) crystallographic planes of Pd and (110) planes of Cu_3Pd, respectively. The coexistence of these two phases in the particle induces structural stress, which is observed as poor-defined lattice fringes in the HRTEM image. Finally, Fig. 12h shows an individual Cu_3Pd alloy particle exhibiting lattice fringes at 2.62 Å, corresponding to (110) crystallographic planes.

3.2. Catalytic activity

Hydrodechlorination of TCE over nanoparticle impregnated catalysts

Investigations of supported bimetallic Pd–Cu catalysts for gas-phase HDC of TCE provide evidence that the catalytic behavior depends on the Pd:Cu molar ratio, preparation procedure and the nature of support and particle size which have a great impact on the surface atomic arrangements and the formation of bimetallic particles.

Catalysts prepared from Pd-Cu nanoparticles supported on Al_2O_3 were tested in the TCE hydrodechlorination reaction. Fig. 13 shows the catalytic activities of the catalysts vs. time on stream. The monometallic Pd/Al_2O_3 catalysts scored initial conversion of 55 % then rapidly deactivates through the course of reaction. After 180 min of reaction the conversion drops to 20 %. The bimetallic catalysts showed slightly lower catalytic performances than the monometallic Pd/Al_2O_3 catalyst. The catalytic behaviors of Pd-Cu bimetallic catalysts with different Pd/Cu weight loading are comparatively displayed. All the Pd-Cu catalyst follow similar trend as the monometallic Pd catalysts through time of reaction. They all possess higher initial catalytic activity; however the conversion drops as the reaction continues. Higher initial catalytic activity was observed for $Pd1.6Cu1/Al_2O_3$ catalysts with initial conversion of 70% due to probably the higher high metal loading. $Pd1Cu1/Al_2O_3$, $Pd1Cu1(i)/Al_2O_3$, and $Pd1Cu5/Al_2O_3$ catalysts showed moderate catalytic activity 52%, 48% and 46% of initial conversion

respectively. After 3 h of reaction the conversion drop is about 35% for Pd1Cu1/ Al_2O_3, 66% for Pd1Cu1(i)/Al_2O_3, 37 % for Pd1Cu5/Al_2O_3, and 38% for Pd1.6Cu1/Al_2O_3. The PdCu(i)/Al_2O_3 catalyst prepared by bulk impregnation method shows high rate of deactivation. The deactivation of the Pd1.6Cu1/Al_2O_3 and Pd1Cu1/Al_2O_3 bimetallic catalysts prepared by nanoparticle synthesis route is slower as compared to monometallic Pd/Al_2O_3 catalyst. From the conversion results, the higher the Pd loading the higher the catalytic activity as observed for Pd1.6Cu1/Al_2O_3 catalysts. While comparing catalysts containing 1% Pd loading, all the catalyst possesses almost similar initial conversion with slight slope for the monometallic catalyst. However through time of reaction the bimetallic Pd1.6Cu1/Al_2O_3 and Pd1Cu1/Al_2O_3 catalyst showed better performance.

Palladium-on-gold nanoparticles (Pd/Au NPs) have recently been shown to catalyze the hydrodechlorination of trichloroethene in water, at room temperature, and in the presence of hydrogen, with the most active Pd/Au material found to be >70 times more active than Pd supported on alumina on a per-Pd atom basis [195, 196]. The Pd1Au1/Al_2O_3 catalysts prepared by the Polyol method showed very high rate of reaction achieving almost 90 % initial conversion as shown in Fig. 13.

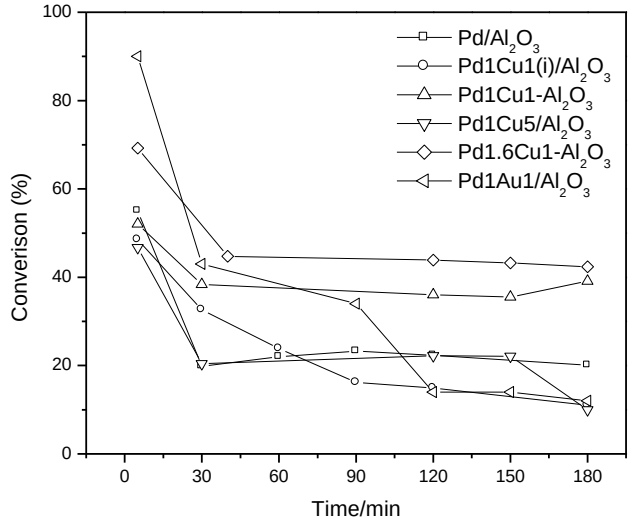

Fig. 13 HDC activity of monometallic Pd and PdCu monometallic catalysts against time on stream.

Selectivity of catalysts towards Ethylene

The selectivity of the catalysts are compared at 5 min and 180 min time of reaction as shown in Fig. 14a and 14b respectively. Ethylene, Ethane, and chloroethylene are the main products observed even though traces of dichloroethylenes were detected. The monometallic Pd/Al_2O_3 catalyst has resulted in the formation of ethylene, ethane and chloroethylene compounds. Surprisingly higher selectivity towards ethylene was obtained by this catalyst. As shown in Fig. 14a, 70 % and 28 % selectivity to ethylene and ethane was obtained at initial time of reaction respectively. The selectivity to ethylene increases with time on stream as shown in fig. 14b, where 87% of ethylene and 20% of ethane are observed at end of reaction. A hypothesis is proposed to explain the catalytic behavior of the Pd nanoparticle. The high selectivity of the monometallic catalyst towards ethylene, unlike previous reported monometallic noble metal catalysts, could be explained owing to the nanoparticles unique nature towards adsorption where the decrease in adsorption energy of ethylene on the Pd nanoparticle surface occurs. Considering the mechanism proposed by S.Ordonez et. al, where the dechlorination of TCE to occur first then hydrogenation of the double bond, the ethylene formed over the surface of the Pd nanoparticles can desorbs faster avoiding further hydrogenation. The adsorption energy of ethylene was given as a possible mechanism for higher selectivity to ethylene over Pt-Cu catalysts during HDC of 1,2-dichloroethane. This explanation could be due to prior passivation of the Pd surface possibly by organic species during the nanoparticle preparation. The existence of some organic phases as part of the nanoparticle could dilute the catalysts. Consequently, if the dissociative adsorption of TCE requires large ensembles, the dilution of Pd with the organic species, the same as the bimetallic catalysts, splits such ensembles and suppresses the activity of Pd in the hydrogenation of ethylene to ethane. Another possiblility could be the hydrogen uptake capacity of the Pd nanoparticles. Boudart *et. al.* showed that small particles possess low capacity towards hydrogen dissociation (lower hydrogen uptake capacity)[159]. Consequently the ability of Pd nps to hydrogenate ethylene to ethane is lower as justified by the higher selectivity of the Pd catalyst to ethylene. With time on stream a decrease in ethane formation, shown in fig. 14b, was observed probably due to chloride poisoning. Chloride atoms co-adsorbed on the catalyst surface do affect hydrogenation ability of the Pd and favor the formation of olefinic products [117]. The selectivity's of the bimetallic Pd-Cu

catalysts depend on total metal loading and the Pd/Cu molar ratio. As shown in Fig. 14a, the Pd-Cu bimetallic catalysts containing similar Pd content with different copper molar ratios has shown distinct selectivity. Pd1Cu1/Al_2O_3 and Pd1Cu5/Al_2O_3 catalysts showed total selectivity towards ethylene formation at initial conversion level respectively. PdCu catalysts prepared by simple impregnation of the Pd and Cu salts, Pd1Cu1(i)/Al_2O_3, resulted in 80% selectivity to ethylene. 10% selectivity to ethane and 4 % chloroethylene formed over Pd1Cu1(i)/Al_2O_3 catalyst shows the existence of isolated Pd species probably (big particles) over the alumina surface. The total selectivity of ethylene achieved by Pd1Cu1/Al_2O_3 and Pd1Cu5/Al_2O_3 shows that the Pd is totally alloyed with the copper and/or exists in close vicinity with Cu. This shows that the nanoparticle catalyst is efficient in this reaction than the conventionally co-impregnated PdCu catalyst. The selectivity of ethylene and ethane over Pd1.6Cu1/Al_2O_3 catalyst is 89% and 10% respectively. At end (180min) of reaction 100% ethylene selectivity was obtained for Pd1.6Cu1/Al_2O_3 catalyst. With time of reaction increases the selectivity of towards the formation ethylene increases. The dissociative adsorption of 1,2-dichloroethane requires large ensembles, the dilution of Pt with Cu splits such ensembles and suppresses the activity of Pt in the dechlorination reaction [117]. It is likely that ensembles of Cl atoms on the catalyst surface favor olefin selectivity [117]. In general for samples, Pd1.6Cu1, Pd1Cu1 and Pd1Cu5, increasing copper content in bimetallic catalysts results in an increase in ethylene selectivity. Similar observation was found by Lamberat *et. al.* [175]. Pd1Cu1 catalyst, despite the presence of isolated Pd species, resulted in total selectivity to ethylene.

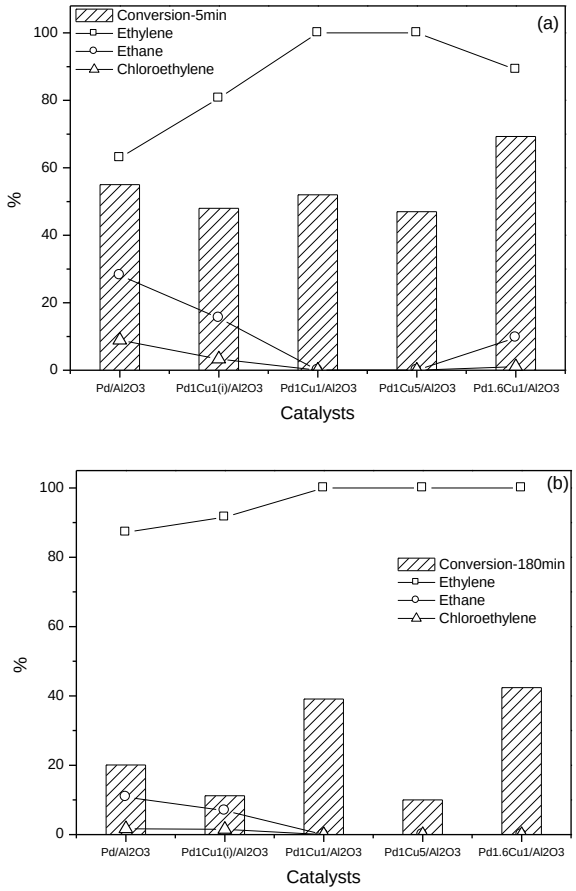

Fig. 14 HDC activity of monometallic Pd and PdCu catalysts and product distribution (a) at initial catalytic activity (b) at 180 min of reaction.

Conclusion

We have synthesized copper nanoparticles in ambient atmosphere by a polyol method. The obtained copper particles were confirmed to be phase-pure crystalline copper with face centered cubic (fcc) structure on the basis of XRD analyses. It has been demonstrated that uniform, nanosized, spherical copper nanoparticles were obtained using 1-hexadecylamine as

protective agents in polyol method. High molar ratios of alkylamine/copper favor production of small and spherical copper nanoparticles. TEM results showed smaller average particle size (8 nm) using the alkylamine as protecting agent. Palladium and Gold prepared in similar way showed a uniform particle size distribution with an average particle size of 4 nm and 15 nm and self-assembly property.

The $PdCu/Al_2O_3$ catalysts were tested for gas phase HDC of trichloroethylene. Their catalytic activity mainly depends on the amount of the noble metal and the selectivity by the amount of copper. It was demonstrated that the $Pd1.6Cu1/Al_2O_3$ with high amount of Pd possesses good catalytic activity. The monometallic Pd/Al_2O_3 catalysts showed comparable initial catalytic conversion as the bimetallic $Pd1Cu1/Al_2O_3$ catalysts. However the later was associated with 100% selectivity towards ethylene. Higher amount of copper decreases the catalytic activity achieving total selectivity to ethylene. Higher ethylene selectivity by the monometallic Pd/Al_2O_3 catalyst observed was associated with the particle size effect (structure sensitivity) or due to passivation of the nanoparticle by the organic species.

UNIVERSITAT ROVIRA I VIRGILI
HYDRODECHLORINATION OF CHLORINATED ORGANIC WASTES OVER PD SUPPORTED MIXED OXIDE CATALYSTS
Beteley Tekola Meshesha
DL: T.1347-2011

5.

Conclusion

Environmental pollution by polychlorinated aromatic (PCA) and aliphatic (PCAl) species is of great concern. They are distributed widely throughout the world due to their diverse use. Despite their wide application they are classified as carcinogenic and mutagenic chemicals that undergo bioaccumulation in fatty tissues. They can be released into water, soil and air from household or industrial facilities. The options of their disposal related to incineration, pyrolysis, biological treatment and catalytic oxidation are associated with drawbacks of high toxic emissions such as dioxins, low rate of reaction and high energy cost.

Catalytic hydrodechlorination reaction is an efficient technique for safe disposal of chlorinated organic wastes (COCs). It involves selective removal of the chloride from the COCs forming non or less toxic hydrocarbons which can be recycled or burned without toxic emission. This research work focuses to study hydrodechlorination reactions of two families

of COCs: 1,2,4-Trichlorobenzene (chlorinated aromatic compound) and (chlorinated aliphatic compound trichloroethylene). The first part of the thesis related to the HDC of 1,2,4-trichlorobenzene, aims at increasing the reactivity of C-Cl bond in poly chlorinated aromatic compounds. While the second part aims at increasing the selectivity of ethylene during HDC of trichloroethylene. This was achieved by preparing Pd catalysts basing the mechanistic aspects of each compound in HDC reaction. The characterization of the catalysts was achieved in order to correlate the chemical and physical properties with the catalytic behaviors.

HDC of chloroaromatic compounds proceeds through an electrophilic attack of the C-Cl bond by the active hydrogen. Hence, electron donating species (basicity) can facilitate the reaction by donating electrons to the aromatic ring and by providing suitable environment spillover hydrogen to activate C-Cl bond. One way of inducing basicity in the catalytic system is utilization of basic supports, like Mg/Al mixed oxide derived from hydrotalcite, with tunable basic property. In the first part a series of palladium (1 wt/wt%) catalysts supported on several Mg/Al hydrotalcite derived mixed oxide with Mg/Al molar ratio of 2, 3, 4 were prepared, characterized and studied in the hydrodechlorination of 1,2,4-trichlorobenzene. The fresh catalysts were characterized using ICP-OES, XRD, N_2-physisorption, H_2-chemisorption, TPR and TEM. It has been observed that the activity, stability and selectivity of the catalysts in the hydrodechlorination reaction of 1,2,4-trichlorobenzene were strongly dependent on the Mg/Al molar ratio in the Mg(Al)O support. It has been shown that palladium catalyst supported on calcined hydrotalcites with higher Mg/Al ratio showed a total conversion of 1,2,4-trichlorobenzene toward benzene at 473K. The sample with Mg/Al ratio of 4 exhibited the highest stability and selectivity toward total hydrodechlorination reaction giving benzene. The catalytic activity and selectivity follow a trend Pd/HT41>Pd/HT31>Pd/HT21. Further rehydration of the calcined Pd hydrotalcite catalyst (Pd/HT41) resulted in an enhancement of the hydrodechlorination performance. The rehydration was related to the generation of more strong basic OH^- groups characterized by bronsted type of basic sites that promoted the catalytic behavior than the Lewis type of O-basic sites. The spent samples were characterized by TPO-MS, TGA and ESEM-EDS techniques. Instrumental characterizations of the spent catalysts

operated at 473K revealed that the deactivation is mainly due to coke deposition on the surfaces and not from the HCl product. The stabilities of the catalysts were also strongly dependent on the Mg/Al of the support. Additionally activation of the Pd-Mg(Al)O sample with Mg/Al molar ratio of 4 by rehydration enhanced both the catalytic activity and stability. Finally these results indicated the feasibility of hydrotalcite-like and derived materials as catalyst support in the hydrodechlorination reaction of 1,2,4-trichlorobenzene.

Another way inducing basicity in the catalyst is by promotion of the catalyst surface using basic additives like alkali-metal oxides. With this view, the best performing Pd/HT catalyst with Mg/Al molar ratio of 4 was further modified by using different alkali metals. Alkaline-metal-modified Pd/HT catalysts were synthesized for the HDC reaction of 1,2,4-trichlorobenzene. The catalysts were modified by addition of alkaline nitrates (ANO_3) and alkaline hydroxides (AOH) precursors. The alkaline-metal-modified Pd/HT catalysts showed lower BET surface area, H_2-uptake capacity (mainly for Cs and Na catalysts) and crystallinity than the unmodified Pd/HT catalyst. However, the average size of Pd particles was quite similar for all the catalysts. On the other hand, depending on the alkali precursor Pd/HT modified catalyst presented some differences in basic strength with respect to the Pd/HT catalyst. The total number of basic sites followed the trend: Pd/HT(AOH) > Pd/HT(ANO_3) > Pd/HT. In general, the modified catalysts showed higher activity (expressed in mmol of 1,2,4-TCB consumed per exposed Pd surface), stability and selectivity than the Pd/HT unmodified catalyst. The hydrodechlorination reaction of 1,2,4-trichlorobenzene was strongly dependent on the type of alkaline additives (Li, Na or Cs) and alkaline precursors (OH^- or NO_3^-) used. The basic properties of the catalysts showed a predominant role in activity, selectivity and stability of the catalysts. Furthermore the HDC catalytic activity is highly dependent in the intrinsic property of alkali metal species where catalyst doped with Cs>Na>Li regardless of the precursor used. The basicity of the alkaline metals is considered responsible for the higher activity of the modified catalyst. The main products obtained were *o*-dichlorobenzene and benzene. In general, higher selectivity to benzene was recorded for the alkali-modified catalysts, particularly for alkali nitrate modified catalysts. However, the poor selectivity to benzene of the CsOH and NaOH modified

catalysts than the nitrate ones may be due to the harsh alkaline impregnating solution, which affects the hydrogen chemisorption capacity (limiting the accessible Pd surface). Characterization of the spent catalyst by XPS, HRTEM and EDX showed that affinity of the chloride produced during the reaction to the strong basic alkali surface contributes for the higher stability of the alkali-modified catalyst. Calcination-reduction and reduction treatments were employed to regenerate the catalyst. The initial catalytic activity was recovered when the used sample was regenerated by reduction treatment. The regeneration of the catalysts modifies the active metal site, alkaline promoter and support material probably that was poisoned by the chloride species.

One of the advantage of using the hydrotalcite derived mixed oxide is its diverse surface property when calcined, rehydrated or intercalated with other anions that is manifested on the catalytic behavior of the supported metal. Under calcination at different temperature the mixed oxide can possess different surface groups and hence different interaction with Pd metal. In this view, several Pd catalysts supported Mg/Al mixed oxide (HT31), where the support was calcined at 623K, 723K , 923K and 1123K, were synthesized, characterized and tested for HDC of 1,2,4-Trichlorobenzene. Interesting observations have been made in this study. The highest surface area was observed for Pd/HT723 and Pd/HT923 catalysts. While at calcination > 923K results a decrease in surface area due to pore destruction and increase in crystallinity. Upon calcination of HT support, different structural evolution was observed by the XRD analysis. At 623K a more amorphous type of periclase structure was noticed. Increasing the calcination temperature at 723 K and 923 K the more crystalline peaks of periclase structure was obtained. However calcination at 1123 K resulted in segregation of the mixed oxide into MgO and spinel phases, increasing its crystalline nature. It was demonstrated that the basicity of the mixed oxide support decreases as the calcination temperature increases. Pd/HT623 catalysts possess higher basicity both in strength and in number probably due to the existence of strong surface OH^- groups. As the calcination temperature increase the Bronsted type of basic sites kept decreasing emerging the Lewis type of basic sites from the Metal-O species. As a result Pd/HT1123 is associated with poor basic property. Pd catalytic behavior towards HDC of 1,2,4-trichlorobenzene depends on the HT structure. The calcination mainly

affects the catalytic conversion while slight difference was observed for the selectivity. Pd impregnated over HT calcined at lower temperature resulted in higher activity and stability for HDC of 1,2,4-trichlorobenzene, in contrast lower catalytic activity was achieved for Pd/HT1123 catalyst.

The second part deals with the hydrodechlorination of TCE. Although supported noble metal catalysts particularly Pd exhibit good catalytic activities and stability during HDC of TCE at mild conditions, it mainly produce ethane, which is much less desired product, than ethylene [30, 117, 118]. Other cheaper but active transition metal includes nickel, which is able to catalyze HDC of vicinal aliphatic chlorinated carbons. There are reports that they possess lower selectivity towards the formation of the less desired ethane product during HDC of TCE. However, the major disadvantage of using Ni catalysts is that it requires high temperature (>473K) or high hydrogen pressure to reach significant activity and rapid catalyst deactivation. Promotion of Ni rich catalysts using small amount of noble metals like Pd, increases its catalytic activity for HDC reaction. In this view, different Pd/NiMgAl catalysts were prepared for gas phase HDC of TCE. The catalysts were activated using different catalyst reduction temperature. Our findings demonstrate NiMg(Al)O supported palladium catalysts are effective for the gas phase hydrodechlorination of trichloroethylene. The catalysts performance for the hydrodechlorination was significantly affected by the Ni/Mg/Al molar ratio, temperature of reduction, and method of noble metal deposition protocol in the support. Both Mg and Ni promote the reaction. The former due to induction of basicity to the surface while the later is associated to its HDC ability. However, best performance and good ethylene selectivity was achieved by a catalyst containing higher amount of Ni. The selectivity towards ethylene formation is modified by increasing the surface metallic Ni species during high temperature reduction (>723K). Introduction of 0.5% of Pd helps to increase the catalysts activity (100%) as in Pd/NiHT1. The method of Pd deposition affected the catalyst ability towards the formation of ethylene. Impregnation of Pd over previously reduced NiMgAl catalyst, so as to achieve better Pd-Ni interaction, modifies the catalyst selectivity towards ethylene formation.

Owing to the poor ethylene selectivity of Pd, there are reports that higher olefin selectivity can be attained by doping it with different transition metals like Ag [118], Cu [117, 127] or Sn [128]. For instance, supported bimetallic

Pd-Cu is cited to selectively hydrodechlorinate TCE to ethylene. However, the catalytic performance depends on the bimetallic molar ratio, synthesis protocol, reaction conditions. The synthesis protocol used during the preparation of bimetallic catalysts determines the particles size and distribution and metal-metal interaction (alloys or isolated) presenting different catalytic behaviors. Synthesis of nanoparticles of Cu and Pd can affect the metallic properties and their behavior towards the reaction. Here we report a procedure developed for synthesis of 1-hexadecylamine (HDA) capped metal Cu nanoparticles (HDA-M) using polyol method. The use of the long chain alkylamine template during polyol process of nanoparticle fabrication could result highly dispersed small nanoparticles than that of PVP, which usually the average reported size includes 20-500 nm. The metal nanoparticle complexes were recovered from the solution by polyol-organic phase-transfer techniques. The obtained copper particles were confirmed to be phase-pure crystalline copper with face centered cubic (fcc) structure on the basis of XRD analyses. It has been demonstrated that uniform, nanosized, spherical copper nanoparticles were obtained using 1-hexadecylamine as protective agents in polyol method. High molar ratios of alkylamine/copper favor production of small and spherical copper nanoparticles. TEM results showed smaller average particle size (8 nm) using the alkylamine as protecting agent. Palladium and Gold prepared in similar way showed a uniform particle size distribution with an average particle size of 4nm and 15 nm and self-assembly property. The $PdCu/Al_2O_3$ catalysts were tested for gas phase HDC of trichloroethylene. Their catalytic activity mainly depends on the amount of the noble metal and the selectivity by the amount of copper. It was demonstrated that the $Pd1.6Cu1/Al_2O_3$ with high amount of Pd possesses better catalytic activity. The monometallic Pd/Al_2O_3 catalysts showed comparable initial catalytic conversion as the bimetallic $Pd1Cu1/Al_2O_3$ catalysts. However the later was associated with 100% selectivity towards ethylene. Higher amount of copper decreases the catalytic activity but achieved total selectivity to ethylene as for $Pd1Cu5/Al_2O_3$ catalyst. Higher ethylene selectivity by the monometallic Pd/Al_2O_3 catalyst observed was associated with the particle size effect (structure sensitivity) or due to passivation of the nanoparticle by the organic species (during Nps preparation).

References

[1] EuroChlor, *http://www. eurochlor. org/*.

[2] M. A. Keane, **2005**, *J. Chem. Technol. Biot., 80*, 1211.

[3] R. J. Farrauto, R. M. Heck, **2000**, *Catal. Today, 55*, 179.

[4] Euro chlor-1,2,4-Trichlorobenzene Risk Assessment for the Marine Environment OSPARCOM Region - North Sea, **2002**, *Eurochlor*.

[5] M. Rossberg, W. Lendle, G. Pfleiderer, et.al, *Chlorinated Hydrocarbons*, Wiley-VCH Verlag GmbH & Co. KGaA, **2000**.

[6] L. Magos, J. K. Fawell, S. Hunt, **1989**, *J. Appl. Toxicol., 9*, 285.

[7] Regulatory toxicology and pharmacology, **1997**, *Int. J. Toxicol., 16*, 67.

[8] F. Milton, F. J. Christian, *Field Manual of Wildlife Diseases; General Field Procedures and Diseases of Birds*, U.S. Department of the Interior; U.S. Geological Survey**1999**.

[9] G. W. Gribble, **1994**, *Environ. Sci. Technol., 28*, 310A.

[10] W. J. Hayes, E. R. Laws, *Handbook of pesticide toxicology*, John Wiley & Sons, Ltd.**1991**.

[11] C. Menini, C. Park, E. Shin, G. Tavoularis, M. A. Keane, **2000**, *Catal. Today, 62*, 355.

[12] D. F. Laine, I. F. Cheng, **2007**, *Microchem. J., 85*, 183.

[13] K. Jiang, L. Li, Y. Chen, J. Jin, **1997**, *Chemosphere, 34*, 941.

[14] G. McKay, **2002**, *Chem. Eng. J., 86*, 343.

[15] H. Huang, A. Buekens, **2001**, *Chemosphere, 44*, 1505.

[16] S. A. Villalobos, M. J. Anderson, M. S. Denison, D. E. Hinton, K. Tullis, I. M. Kennedy, A. D. Jones, D. P. Chang, S. J. Gregg, **1996**, *Environ. Health Perspect., 104*, 734.

[17] Eds: B. Gori Gio, Sc D., MPH, ATS Vol. 20, Gio, B. Gori; D., Sc.; MPH; ATS**1994**, S960-S1029.

[18] F. Alonso, I. P. Beletskaya, M. Yus, **2002**, *Chem. Rev., 102*, 4009.

[19] R. A. Hites, **1990**, *Acc. Chem. Res., 23*, 194.

[20] S. Sakai, M. Hiraoka, N. Takeda, K. Shioxaki, **1996**, *Chemosphere, 32*, 79.

[21] W. L. Kranich, R. B. LaPierre, G. Laszlo, A. H. Weiss, in *Disposal and Decontamination of Pesticides*, Vol. 73 (Anonymous), American Chemical Society**1978**, 24-34.

[22] A. D. Harley, M. T. Holbrook, D. D. Smith, M. D. Cisneros, L. N. Ito, C. B. Murchison, US Patent 08/227,812, **1995**.

[23] F. Kopinke, K. Mackenzie, R. Koehler, A. Georgi, **2004**, *Appl. Catal. A: Gen., 271*, 119.

[24] L. Calvo, M. A. Gilarranz, J. A. Casas, A. F. Mohedano, J. J. Rodríguez, **2009**, *J. Hazard. Mater., 161*, 842.

[25] Y. Ukisu, T. Miyadera, **1997**, *J. Mol. Catal. A: Chem*, *125*, 135.

[26] E. R. Ritter, J. W. Bozzelli, A. M. Dean, **1990**, *J. Phys. Chem., 94*, 2493.

[27] E. Shin, M. A. Keane, **2000**, *J. Chem. Technol. Biot., 75*, 159.

[28] B. Coq, G. Ferrat, *et al* F. Figueras, **1985**, *Reaction Kinetics and Catalysis Letters, 27*, 157.

[29] I. L. Simakova, V. A. Semikolenov, **1991**, *Kinet. Catal., 31*, 892.

[30] S. Kovenklioglu, Z. Cao, D. Shah, R. J. Farrauto, E. N. Balko, **1992**, *AICHE J., 38*, 1003.

[31] E. N. Balko, E. Przybylski, F. Von Trentini, **1993**, *Appl. Catal. B: Environ., 2*, 1.

[32] C. A. Marques, M. Sleva, P. Tunfo, **1996**, *Gazz. chem. Ital, 126*, 317.

[33] H. R. Buser, **1979**, *Chemosphere, 8*, 251.

[34] C. M. King, R. Bruce King, N. K. Bhattacharyya, M. Gary Newton, **2000**, *J. Organomet. Chem., 600*, 63.

[35] L. Lassová, H. K. Lee, T. S. A. Hor, **1999**, *J. Mol. Catal. A: Chem, 144*, 397.

[36] L. LassovÃ¡, H. K. Lee, T. S. A. Hor, **1998**, *J. Org. Chem., 63*, 3538.

[37] S. H. Tabaei, C. U. Pittman, **1993**, *Tetrahedron Lett., 34*, 3263.

[38] Y. Zhang, S. Liao, Y. Xu, **1994**, *Tetrahedron Lett., 35*, 4599.

[39] M. Stiles, **1994**, *J. Org. Chem., 59*, 5381.

[40] J. Hagen, *Industrial Catalysis: A practical approach*, Vol. 1, 2nd edn., Wiley-VCH Verlag GmbH & Co. KGaA**2006**.

[41] J. Chen, J. Zhou, R. Wang, J. Zhang, **2009**, *Ind Eng Chem Res, 48*, 3802.

[42] A. H. Weiss, S. Valinski, G. V. Antoshin, **1982**, *J. Catal., 74*, 136.

[43] A. R. Suzdorf, S. V. Morozov, N. N. Anshits, S. I. Tsiganova, A. G. Anshits, **1994**, *Catal. Lett., 29*, 49.

[44] E. Shin, M. A. Keane, **1998**, *Appl. Catal. B: Environ., 18*, 241.

[45] Y. Cesteros, P. Salagre, F. Medina, J. E. Sueiras, **1999**, *Appl. Catal. B: Environ., 22*, 135.

[46] K. V. R. Chary, C. S. Srikanth, V. V. Rao, **2009**, *Catal. Commun., 10*, 459.

[47] V. Felis, C. De Bellefon, P. Fouilloux, D. Schweich, **1999**, *Appl. Catal. B: Environ., 20*, 91.

[48] J. B. Hoke, G. A. Gramiccioni, E. N. Balko, **1992**, *Appl. Catal. B: Environ., 1*, 285.

[49] B. Coq, G. Ferrat, F. Figueras, **1986**, *J. Catal., 101*, 434.

[50] J. M. Moreno, M. A. Aramendía, A. Marinas, J. M. Marinas, F. J. Urbano, **2005**, *Appl. Catal. B: Environ., 59*, 275.

[51] F. J. Urbano, J. M. Marinas, **2001**, *J. Mol. Catal. A: Chem, 173*, 329.

[52] S. Ordonez, H. Sastre, F. V. Diez, **2003**, *Appl. Catal. B: Environ., 40*, 119.

[53] E. López, S. Ordóñez, F. V. Díez, **2006**, *Appl. Catal. B: Environ., 62*, 57.

[54] Y. Hashimoto, A. Ayame, **2003**, *Appl. Catal. A: Gen., 250*, 247.

[55] M. A. Aramendía, V. Boráu, I. M. García, C. Jiménez, A. Marinas, J. M. Marinas, F. J. Urbano, **2003**, *Appl. Catal. B: Environ., 43*, 71.

[56] K. A. Frankel, B. W. Jang, J. J. Spivey, G. W. Roberts, **2001**, *Appl. Catal. A: Gen., 205*, 263.

[57] S. Ordóñez, F. V. Díez, H. Sastre, **2001**, *Appl. Catal. B: Environ., 31*, 113.

[58] M. A. Aramendía, V. Boráu, I. M. García, C. Jiménez, J. M. Marinas, F. J. Urbano, **1999**, *Appl. catal. B: Environ., 20*, 101.

[59] M. Öcal, M. Maciejewski, A. Baiker, **1999**, *Applied Catalysis B: Environmental, 21*, 279.

[60] J. Tsuji, **2005**, *Journal of synthetic organic chemistry*, *63*, 539.

[61] B. Coq, J. M. Cognion, F. Figueras, D. Tournigant, **1993**, *J. Mol. Catal. A: Chem*, *141*, 21.

[62] J. Estelle, J. Ruz, Y. Cesteros, R. Fernandez, P. Salagre, F. Medina, J. Sueiras, **1996**, *J. Chem. Soc. , Faraday Trans.*, *92*, 2811.

[63] B. F. Hagh, D. T. Allen, **1990**, *AICHE J.*, *36*, 773.

[64] J. Frimmel, M. Zdrazil, **1997**, *J. Catal.*, *167*, 286.

[65] P. Bodnariuk, B. Coq, G. Ferrat, F. Figueras, **1989**, *J. Mol. Catal. A: Chem*, *116*, 459.

[66] R. Gopinath, K. Narasimha Rao, P. S. Sai Prasad, S. S. Madhavendra, S. Narayanan, G. Vivekanandan, **2002**, *J. Mol. Catal. A: Chem*, *181*, 215.

[67] N. Lingaiah, M. A. Uddin, A. Muto, T. Iwamoto, Y. Sakata, Y. Kusano, **2000**, *J. Mol. Catal. A: Chem*, *161*, 157.

[68] V. I. Simagina, V. M. Mastikhin, V. A. Yakovlev, I. V. Stoyanova, V. A. Likholobov, **1995**, *J. Mol. Catal. A: Chem*, *101*, 237.

[69] T. Lim, B. Zhu, **2008**, *Chemosphere*, *73*, 1471.

[70] K. V. R. Chary, K. S. Lakshmi, M. R. V. S. Murthy, K. S. R. Rao, M. Papadaki, **2003**, *Catal. Commun.*, *4*, 531.

[71] K. V. R. Chary, K. S. Lakshmi, P. V. R. Rao, K. S. R. Rao, M. Papadaki, **2004**, *J. Mol. Catal. A: Chem*, *223*, 353.

[72] K. V. R. Chary, P. V. R. Rao, V. Vishwanathan, **2006**, *Catal. Commun.*, *7*, 974.

[73] Y. Cesteros, P. Salagre, F. Medina, J. E. Sueiras, **2000**, *Appl. Catal. B: Environ.*, *25*, 213.

[74] Y. Cesteros, P. Salagre, F. Medina, J. E. Sueiras, **2002**, *Catal. Lett., 79*, 83.

[75] Y. Cesteros, P. Salagre, F. Medina, J. E. Sueiras, D. Tichit, B. Coq, **2001**, *Appl. Catal. B: Environ., 32*, 25.

[76] E. Shin, A. Spiller, G. Tavoularis, M. Keane A., **1999**, *Phys. Chem. Chem. Phys., 1*, 3173.

[77] J. M. Moreno, M. A. Aramendía, A. Marinas, J. M. Marinas, F. J. Urbano, **2007**, *Appl. Catal. B: Environ., 76*, 34.

[78] M. A. Keane, **2004**, *Appl. Catal. A: Gen., 271*, 109.

[79] D. H. Lenz, W. C. Conner, J. P. Fraissard, **1989**, *J. Mol. Catal. A: Chem, 117*, 281.

[80] U. Roland, R. Salzer, T. Braunschweig, F. Roessner, H. Winkler, **1995**, *J. Chem. Soc. , Faraday Trans., 91*, 1091.

[81] F. Roessner, U. Roland, **1996**, *J. Mol. Catal. A: Chem, 112*, 401.

[82] U. Roland, T. Braunschweig, F. Roessner, **1997**, *J. Mol. Catal. A: Chem, 127*, 61.

[83] W. Wu, J. Xu, **2004**, *Catal. Commun., 5*, 591.

[84] S. Zinovyev, A. Shelepchikov, P. Tundo, **2007**, *Appl. Catal. B: Environ., 72*, 289.

[85] M. A. Aramendía, R. Burch, I. M. García, A. Marinas, J. M. Marinas, B. W. L. Southward, F. J. Urbano, **2001**, *Appl. Catal. B: Environ., 31*, 163.

[86] M. A. Aramendía, V. Boráu, I. M. García, C. Jiménez, F. Lafont, A. Marinas, J. M. Marinas, F. J. Urbano, **2002**, *J. Mol. Catal. A: Chem, 184*, 237.

[87] P. Kim, Y. Kim, H. Kim, I. K. Song, J. Yi, **2005**, *J. Mol. Catal. A: Chem*, *231*, 247.

[88] B. M. Choudary, S. Madhi, N. S. Chowdari, M. L. Kantam, B. Sreedhar, **2002**, *J. Am. Chem. Soc.*, *124*, 14127.

[89] A. Cwik, Z. Hell, F. Figueras, **2006**, *Advanced Synthesis & Catalysis*, *348*, 523.

[90] F. Figueras, **2004**, *Topics in Catalysis*, *29*, 189.

[91] S. Abelló, F. Medina, D. Tichit, J. Pérez-Ramírez, X. Rodríguez, J. E. Sueiras, P. Salagre, Y. Cesteros, **2005**, *Appl. Catal. A: Gen.*, *281*, 191.

[92] A. Corma, R. M. Martín-Aranda, **1993**, *Applied Catalysis A: General*, *105*, 271.

[93] M. J. Climent, A. Corma, S. Iborra, J. Primo, **1995**, *J. Mol. Catal. A: Chem*, *151*, 60.

[94] M. J. Climent, A. Corma, S. Iborra, K. Epping, A. Velty, **2004**, *J. Catal.*, *225*, 316.

[95] S. Velu, C. S. Swamy, **1994**, *Applied Catalysis A: General*, *119*, 241.

[96] Y. Hashimoto, Y. Uemichi, A. Ayame, **2005**, *Appl. Catal. A: Gen.*, *287*, 89.

[97] F. Cavani, F. Trifirò, A. Vaccari, **1991**, *Catal. Today*, *11*, 173.

[98] X. Duan, D. G. Evans, *layered double hydroxides: structure and bonding*, Vol. 119, Springer-Verlag, berlin **2006**.

[99] V. Rives, M. Angeles Ulibarri, **1999**, *Coord. Chem. Rev.*, *181*, 61.

[100] J. I. Di Cosimo, V. K. Díez, M. Xu, E. Iglesia, C. R. Apesteguía, **1998**, *J. Catal.*, *178*, 499.

[101] D. Tichit, B. Coq, **2003**, *CATTECH, 7*, 206.

[102] G. Zhang, B. Coq, L. Charles de Ménorval, D. Tichit, **1996**, *Appl. Catal. A: Gen., 147*, 395.

[103] Y. Z. Chen, C. W. Liaw, L. I. Lee, **1999**, *Appl. Catal. A: Gen., 177*, 1.

[104] V. Rives, F. M. Labajos, R. Trujillano, E. Romeo, C. Royo, A. Monzón, **1998**, *Appl. Clay. Sci., 13*, 363.

[105] F. M. Cabello, D. Tichit, B. Coq, A. Vaccari, N. T. Dung, **1997**, *J. Mol. Catal. A: Chem, 167*, 142.

[106] H. Matsuhashi, M. Oikawa, K. Arata, **2000**, *Langmuir, 16*, 8201.

[107] H. Matsuhashi, K. Arata, **1995**, *J. Phys. Chem., 99*, 11178.

[108] G. Yuan, M. A. Keane, **2004**, *J. Catal., 225*, 510.

[109] F. Prinetto, M. Manzoli, G. Ghiotti, M. d. J. Martinez Ortiz, D. Tichit, B. Coq, **2004**, *J. Catal., 222*, 238.

[110] V. B. Kazansky, V. Y. Borovkov, A. I. Serykh, F. Figueras, **1997**, *Catal. Lett., 49*, 35.

[111] S. Ordóñez, H. Sastre, F. V. Díez, **2000**, *Appl. Catal. B: Environ., 25*, 49.

[112] C. G. Schreier, M. Reinhard, **1995**, *Chemosphere, 31*, 3475.

[113] S. Ordóñez, F. V. Díez, H. Sastre, **2002**, *Ind Eng Chem Res, 41*, 505.

[114] M. Martino, R. Rosal, H. Sastre, F. V. Díez, **1999**, *Appl. Catal. B: Environ., 20*, 301.

[115] W. Nishijima, Y. Ochi, T. Y. Tsai, Y. Nakano, M. Okada, **2004**, *Appl. Catal. B: Environ., 51*, 135.

[116] E. Diaz, S. Ordonez, R. F. Bueres, E. Asedegbega-Nieto, H. Sastre, **2010**, *Appl. Catal. B: Environ.*, *99*, 181.

[117] V. I. Kovalchuk, J. L. d'Itri, **2004**, *Appl. Catal. A: Gen.*, *271*, 13.

[118] B. Heinrichs, F. Noville, J. Schoebrechts, J. Pirard, **2003**, *J. Catal.*, *220*, 215.

[119] N. Barrabés Rabanal, **2009**, *Thesis URV, T-1539-2009/ 978-84-692-4557-6*.

[120] P. Kim, H. Kim, J. B. Joo, W. Kim, I. K. Song, J. Yi, **2006**, *J. Mol. Catal. A: Chem*, *256*, 178.

[121] A. Śrębowata, W. Juszczyk, Z. Kaszkur, J. W. Sobczak, L. Kępiński, Z. Karpiński, **2007**, *Appl. Catal. A: Gen.*, *319*, 181.

[122] D. I. Kim, D. T. Allen, **1997**, *Ind Eng Chem Res*, *36*, 3019.

[123] Y. H. Choi, W. Y. Lee, **2001**, *J. Mol. Catal. A: Chem*, *174*, 193.

[124] Y. Choi, W. Lee, **2000**, *Catal. Lett.*, *67*, 155.

[125] B. Heinrichs, J. Schoebrechts, J. Pirard, **2001**, *J. Catal.*, *200*, 309.

[126] S. C. Fung, J. H. Sinfelt, **1987**, *J. Catal.*, *103*, 220.

[127] N. Barrabes, D. Cornado, K. Foettinger, A. Dafinov, J. Llorca, F. Medina, G. Rupprechter, **2009**, *J. catal.*, *263*, 239.

[128] W. D. Rhodes, K. Lázár, V. I. Kovalchuk, J. L. d'Itri, **2002**, *J. Catal.*, *211*, 173.

[129] L. S. Vadlamannati, D. R. Luebke, V. I. Kovalchuk, J. L. d'Itri, in *Studies in Surface Science and Catalysis*, Vol. 130 (Anonymous), Elsevier**2000**, 233.

[130] B. Heinrichs, F. Noville, J. Schoebrechts, J. Pirard, **2000**, *J. Catal., 192*, 108.

[131] V. Y. Borovkov, D. R. Luebke, V. I. Kovalchuk, J. L. d'Itri, **2003**, *J. Phys. Chem. B, 107*, 5568.

[132] B. Aristizábal, C. A. González, I. Barrio, M. Montes, C. Montes de Correa, **2004**, *J. Mol. Catal. A: Chem, 222*, 189.

[133] A. Śrębowata, W. Juszczyk, Z. Kaszkur, Z. Karpiński, **2007**, *Catal. Today, 124*, 28.

[134] V. Simagina, V. Likholobov, G. Bergeret, M. T. Gimenez, A. Renouprez, **2003**, *Appl. Catal. B: Environ., 40*, 293.

[135] B. T. Meshesha, R. J. Chimentão, F. Medina, J. E. Sueiras, Y. Cesteros, P. Salagre, F. Figueras, **2009**, *Appl. Catal. B: Environ., 87*, 70.

[136] N. Barrabes, K. Foettinger, J. Llorca, A. Dalinov, F. Medina, J. Sa, C. Hardacre, G. Rupprechter, **2010**, *J. Phys. Chem. C, 114*, 17675.

[137] Y. Cesteros, P. Salagre, F. Medina, J. E. Sueiras, **2000**, *Catal. Lett., 67*, 147.

[138] Cullity B.D., S. R. Stock, *Elements of X-ray diffraction*, 3rd edn., Prentice Hall, New jersey **2001**.

[139] W. Clegg, *Crystal structure determination*, Oxford University Press, New York **1998**.

[140] L. H. Schwartz, J. B. Cohen, *Diffraction from materials*, 2nd edn., Springer-Verlag, New York **1987**.

[141] D. B. Williams, C. B. Carter, *Transmission electron microscopy :a textbook for materials science*, Plenum Press, New York etc. **1996**.

[142] G. Lawes, A. M. James, Acol, *Scanning electron microscopy and x-ray microanalysis*, Published on behalf of ACOL, Thames Polytecnic, London, by Wiley, Chichester etc. **1987**.

[143] R. F. Egerton, *Physical principles of electron microscopy :an introduction to TEM, SEM, and AEM*, Springer Science+Business Media, New York **2005**.

[144] Y. Amenomiya, R. J. CvetanoviÄ, **1963**, *J. Phys. Chem.*, *67*, 2705.

[145] M. Anpo, S. Dzwigaj, M. Che, in *Advances in Catalysis*, Vol. Volume 52 (Ed: Bruce C. Gates and Helmut Knözinger), Academic Press**2009**, 1-42.

[146] M. Anpo, M. Che, in *Advances in Catalysis*, Vol. Volume 44 (Ed: Werner O. Haag,Bruce C.Gates and Helmut Knözinger), Academic Press**1999**, 119-257.

[147] H. G. Timothy, in *Encyclopedia of Analytical Chemistry* (Anonymous), John Wiley & Sons, Ltd, Chichester **2000**, 9209.

[148] Kolasinski K.W., *Surface Science: Foundations of Catalysis and Nanoscience*, 2nd edn., John Wiley & Sons Ltd, England **2008**.

[149] S. Brunauer, P. H. Emmett, E. Teller, **1938**, *J. Am. Chem. Soc.*, *60*, 309.

[150] W. W. Russel, **1944**, *J. Chem. Educ.*, *21*, 52.

[151] S. J. Gregg, K. S. W. Sing, *Adsorption, surface area and porosity*, Academic Press, London etc. **1967**.

[152] S. Brunauer, L. S. Deming, W. E. Deming, E. Teller, **1940**, *J. Am. Chem. Soc.*, *62*, 1723.

[153] J. H. de Boer, B. C. Lippens, **1964**, *Journal of Catalysis*, *3*, 38.

[154] E. P. Barrett, L. G. Joyner, P. P. Halenda, **1951**, *J. Am. Chem. Soc.*, *73*, 373.

[155] Y. Amenomiya, R. J. Cvetanovic, **1963**, *J. Phys. Chem., 67*, 144.

[156] S. B. Halligudi, B. M. Devassay, A. Ghosh, V. Ravikumar, **2002**, *J. Mol. Catal. A: Chem, 184*, 175.

[157] J. S. Valente, F. Figueras, M. Gravelle, P. Kumbhar, J. Lopez, J. -. Besse, **2000**, *J. Catal., 189*, 370.

[158] P. Claus, H. Berndt, C. Mohr, J. Radnik, E. Shin, M. A. Keane, **2000**, *J. Catal., 192*, 88.

[159] M. Boudart, H. S. Hwang, **1975**, *J. Catal., 39*, 44.

[160] M. A. Keane, G. Pina, G. Tavoularis, **2004**, *Appl. Catal. B: Environ., 48*, 275.

[161] L. Calvo, M. A. Gilarranz, J. A. Casas, A. F. Mohedano, J. J. Rodríguez, **2006**, *Appl. Catal. B: Environ., 67*, 68.

[162] P. Marécot, A. Akhachane, C. Micheaud, J. Barbier, **1998**, *Appl. Catal. A: Gen., 169*, 189.

[163] F. Figueras, F. Gomez, M. Primet, **1973**, *Adv. Chem. Ser., 121*, 480.

[164] T. Huang, B. Kang, **1995**, *J. Mol. Catal. A: Chem, 103*, 163.

[165] C. Marta, E. Motti, F. Faccini, R. Ferraccioli, **2005**, *Pure and Applied chemistry, 77*, 1243.

[166] L. F. Liotta, G. A. Martin, G. Deganello, **1996**, *J. Mol. Catal. A: Chem, 164*, 322.

[167] S. Fujita, B. M. Bhanage, D. Aoki, Y. Ochiai, N. Iwasa, M. Arai, **2006**, *Appl. Catal. A: Gen., 313*, 151.

[168] G. Del Angel, J. L. Benitez, **2001**, *J. Mol. Catal. A: Chem, 165*, 9.

[169] N. M. Rodriguez, S. G. Oh, R. A. Dalla-Betta, R. T. K. Baker, in *Studies in Surface Science and Catalysis*, Vol. Volume 88 (Ed: B. Delmon and G.F. Froment), Elsevier**1994**, 417-424.

[170] H. Chul Choi, S. H. Choi, O. B. Yang, J. S. Lee, K. H. Lee, Y. G. Kim, **1996**, *J. Mol. Catal. A: Chem, 161*, 790.

[171] A. H. Padmasri, A. Venugopal, V. Siva Kumar, V. Shashikala, B. M. Nagaraja, P. Seetharamulu, B. Sreedhar, B. David Raju, P. Kanta Rao, K. S. Rama Rao, **2004**, *J. Mol. Catal. A: Chem, 223*, 329.

[172] L. B. Kong, J. Ma, H. Huang, **2002**, *Mater Lett, 56*, 238.

[173] V. K. Díez, C. R. Apesteguía, J. I. Di Cosimo, **2003**, *Journal of Catalysis, 215*, 220.

[174] S. Narayanan, K. Krishna, **1997**, *Chem. Commun.*, 1991.

[175] S. Lambert, F. Ferauche, A. Brasseur, J. Pirard, B. Heinrichs, **2005**, *Catal. Today, 100*, 283.

[176] A. Davidson, J. F. Tempere, M. Che, H. Roulet, G. Dufour, **1996**, *J. Phys. Chem., 100*, 4919.

[177] V. Rives, S. Kannan, **2000**, *J. Mater. Chem., 10*, 489.

[178] K. Schulze, W. Makowski, R. Chyzy, R. Dziembaj, G. Geismar, **2001**, *Appl. Clay. Sci., 18*, 59.

[179] L. N. Lewis, **1993**, *Chem. Rev., 93*, 2693.

[180] Y. Wang, J. Ren, K. Deng, L. Gui, Y. Tang, **2000**, *Chem. Mater., 12*, 1622.

[181] B. R. Cuenya, **2010**, *Thin Solid Films, 518*, 3127.

[182] Z. Liu, Y. Bando, **2003**, *Adv Mater, 15*, 303.

[183] N. A. Dhas, C. P. Raj, A. Gedanken, **1998**, *Chem. Mater., 10*, 1446.

[184] X. Song, S. Sun, W. Zhang, Z. Yin, **2004**, *J. Colloid Interface Sci., 273*, 463.

[185] B. K. Park, S. Jeong, D. Kim, J. Moon, S. Lim, J. S. Kim, **2007**, *J. Colloid Interface Sci., 311*, 417.

[186] C. Lu, M. Wey, Y. Fu, **2008**, *Appl. Catal. A: Gen., 344*, 36.

[187] H. Zhang, X. Ren, Z. Cui, **2007**, *J. Cryst. Growth, 304*, 206.

[188] R. J. Chimentão, N. Barrabés, F. Medina, J. L. G. Fierro, J. E. Sueiras, Y. Cesteros, P. Salagre, **2006**, *J. Exp. nanosci., 1*, 399.

[189] J. Zhu, Y. Wang, X. Wang, X. Yang, L. Lu, **2008**, *Powder Technol, 181*, 249.

[190] A. M., G. G.L., *et al*V. W., **2002**, *J. Colloid Interf. Sci., 255*, 12.

[191] M. Shen, Y. Du, N. Hua, P. Yang, **2006**, *Powder Technol, 162*, 64.

[192] A. Tzitzios, G. Basina, *et al*D. Petridis, **2006**, *Nanotechnology, 17*, 3750.

[193] K. Sridhar, et al, **2004**, *Journal of Physics: Condensed Matter, 16*, S1305.

[194] J. Batista, A. Pintar, J. P. Gomilsek, A. Kodre, F. Bornette, **2001**, *Appl. Catal. A: Gen., 217,* 55.

[195] K. N. Heck, M. O. Nutt, P. Alvarez, M. S. Wong, **2009**, *J. catal., 267*, 97.

[196] M. O. Nutt, K. N. Heck, P. Alvarez, M. S. Wong, **2006**, *Appl. Catal. B: Environ., 69*, 115.

Publication

Articles

B.T. Meshesha, R.J. Chimentaõ, F. Medina, J.E. Sueiras, Y. Cestros, P. Salagre, F.Figueras. Catalytic hydrodechlorination of 1,2,4-trichlorobenzene over Pd/Mg(Al)O catalysts. *Applied Catalysis B; Environmental*, 87(1-2):70-77, 2009.

B.T. Meshesha, R.J. Chimentaõ, A. M. Segarra, J. Llorca, F. Medina, B. Coq, J.E.Sueiras. Performance of alkali modified Pd/Mg(Al)O catalysts for hydrodechlorination of 1,2,4-trichlorobenzene. *Applied catalysis B; Environmental*, 105 (3-4): 361-372, 2011.

Submitted article

B.T. Meshesha, N. Barrabés, R.J. Chimentaõ, K. Föttinger, F. Medina, G. Rupprechter, J.E. Sueiras. Gas-phase Hydrodechlorination of trichloroethylene over Pd/NiMgAl catalysts *Journal of Molecular catalysis A*, submitted, 2011.

Contributions to proceeding journal (isiknowledge)

B. T. Meshesha, N. Barrabés, F. Medina, and J. E. Sueiras. Polyol mediated synthesis and characterization of Cu Cu nanoparticles: effect of 1 hexadecylamine as stabilizing agent. *In Proceedings of the 1st WSEAS international Conference on Nanotechnology, Cambridge, UK*, 87: 91, 2009.

Publications under preparation

N. Barrabés, **B.T. Meshesha**, K. Föttinger, F. Medina, G. Rupprechter, J.E. Sueiras. Study of the PdCu interaction: effect of the synthesis protocol on the hydrodechlorination TCE. *Catalysis communication*, to be submitted, 2011.

B.T. Meshesha, N. Barrabés, K. Föttinger, F. Medina, G. Rupprechter, J.E. Sueiras. Polyol mediated synthesis of Pd-Cu nanoparticle and application in

hydrodechlorination of trichloroethylene. *Journal of nonmaterial*, to be submitted, 2011.

B.T. Meshesha, R.J. Chimentaõ, J. Llorca, F. Medina, J.E. Sueiras. Hydrodechlorination of 1,2,4-trichlorobenzene over Pd/Mg(Al)O catalysts; Effect of support calcination temperature. *Catalysis communication*, to be submitted, 2011.

Conference Contributions

N. Barrabés, **Beteley Meshesha**, Karin Föttinger, Jordi Llorca, Anton Dafinov, Günther Rupprechter, Francisco Medina. Bimetallic (PdCu) catalysts on alumina for selective hydrodechlorination of TCE. Effect of synthesis protocol. *XXII CICAT -Congreso Iberoamericano de Catálisis*, August 2010.

B.T. Meshesha, N. Barrabés, J. Llorca, K. Föttinger, F. Medina, G. Rupprechter. Gas phase hydrodechlorination of Trichloroethylene over Pd/NiMgAl catalyst. *Poster: the* 10*th Pannonian International Symposium on Catalysis; 08-29-2010-09-02-2010; in: "Proceedings of the* 10*th International Symposium on Catalysis", ISBN: 978-83-929430-4-4; 177-179, Kraków, Poland*, August 2010.

N. Barrabés, **B.T. Meshesha**, Karin Föttinger, Jordi Llorca, Anton Dafinov, Günther Rupprechter, Study of the PdCu interaction: effect of the synthesis protocol on the hydrodechlorination TCE. *Talk:* 10*th Pannonian International Symposium on Catalysis;08-29-2010 - 09-02-2010; in: "Proceedings of the* 10*th International Symposium on Catalysis", (2010), ISBN: 978-83-929430-4-4; 53 - 54, Kraków, Poland*,August 2010.

B.T. Meshesha, Noelia Barrabés, F. Medina, K. Föttinger, G. Rupprechter. Hydrodechlorination of trichloroethylene over Pd/NiMgAlO catalysts: Effect of support composition. *European catalysis society (Europacat IX) Salamanca, Spain*, September, 2009.

B. T, Meshesha, A. M. Segarra, F. Medina, J.E. Sueiras. Alkali metal modified Pd-MgAlO catalyst for hydrodechlorination of chloro-aromatic pollutants: activity and reactivation study. *5th International Conference on Environmental Catalysis, Belfast, N. Ireland*, August 2008.

B.T. Meshesha, F.Medina, Y. Cesteros,P. salagre, J.E. Sueiras. Hydrodechloricion 1,2,4-trichlorobenzene encima de pd catalizador. 20*th Spanish catalyisis society (SECAT) Bilbao, Spain*, June 2007.

Other Contributions

Beteley T. Meshesha, F. Medina, J.E. Sueiras, Y. Cesteros, P. Salagre. Catalytic hydrodechlorination of 1,2,4-trichlorobenzene over Pd/MgAlOx catalyst. 7*th PhD Poster Exhibition of URV, Tarragona, Spain*, 2007.

Beteley T. Meshesha,Noelia Barrabés, Karin Fottinger, Jordi llorca, Francesc Medina and Gunther Rupprechter. Synthesis of Pd and Pd/Cu nanoparticles by Polyol route for selective hydrodechlorination of Trichloroethylene. 10*th PhD Poster Exhibition of URV, Tarragona, Spain*, 2010.

UNIVERSITAT ROVIRA I VIRGILI
HYDRODECHLORINATION OF CHLORINATED ORGANIC WASTES OVER PD SUPPORTED MIXED OXIDE CATALYSTS
Beteley Tekola Meshesha
DL: T.1347-2011